Author:
Sofi, Roba R

Title:
In search for new therapeutic approaches for glioblastoma multiforme

In Search for New Therapeutic Approaches for Glioblastoma Multiforme

Roba A. Sofi

A dissertation submitted to the University of Bristol in accordance with the requirements for award of the degree of Doctor of Philosophy in the Faculty of Life Sciences

School of Physiology, Pharmacology and Neuroscience

Faculty of Life Sciences

June 2021

Word count: 41,404

Abstract

Glioblastoma Multiforme (GBM) is a very aggressive type of primary brain cancer with poor prognosis. According to the WHO classification of CNS tumours, GBM is a high-grade infiltrating glioma (grade IV). The introduction of "Stupp protocol" in 2005 was a major milestone towards improving quality of life and clinical outcome for GBM patients. However, since then and up until now, the expanding knowledge about the molecular basis of the disease has only led to small advancement in the therapy and prognosis of GBM, which remains abysmal. This is mainly due to the tremendous heterogeneity of molecular abnormalities between GBM and within GBM. Non-conventional therapeutic approaches, such as photodynamic therapy (PDT) and drug repurposing, could help to speed up the progress in our fight against this deadly disease. PDT is the concept of using a molecule, a photosensitizer (PS) that is not inherently toxic, to induce toxicity selectively on cancer cells after illumination. Drug repurposing is defined as the use of an existing approved drugs for treatment of other diseases than the indicated target disease. Six different primary human GBM cell lines were used in the project and normal rat astrocytes served as a reference. In the first part of the project, the molecular heterogeneity of my GBM cohort was evaluated by Sanger sequencing. RNA samples were extracted from all 6 GBM cell lines, followed by reverse transcription for cDNA synthesis. Next, PCR was done using primers for 4 commonly mutated genes implicated in gliomagenesis, including IDH-1, p53, PTEN, and EGFR. In the second part, the feasibility and efficiency of utilizing Tetramethylrhodamine methyl ester (TMRM), as a novel PS was assessed. TMRM was originally develop as dye to assess mitochondrial membrane potential. The properties of TMRM as a PS, and the efficacy of TMRM-PDT were evaluated. Possible synergy with other pharmacological agents was also examined. Finally, based on pre-existing literature, efficacy of antidepressants (AD) for treatment of GBM was re-evaluated. ADs were assessed for their toxicity towards GBM cells, and their effect on some cellular biological functions.

Different molecular prints were documented among the 6 GBM cell lines, including mutations in p53 and EGFR genes. Future work should include functional gene studies to correlate these molecular profiling of GBM with their sensitivity to different therapeutic

models. TMRM-PDT showed promising results on GBM cell lines. Future modification of treatment protocol should aim to enhance efficacy and selectivity of this treatment modality. Finally, ADs were effective in inducing GBM death, however, the required concentrations for this effect were high and poor selectivity towards cancer cells vs normal astrocytes was noted. This effect was associated with mitochondrial depolarization rather than cAMP activation, contrary to some previous reports.

Acknowledgement

First and foremost, I would like to thank my supervisors Professor Sergey Kasparov and Dr Anja Teschemacher for their invaluable advice and continuous support and dedication through my PhD. They guided me with their immense knowledge and vast experience, and I am very grateful and privileged to have been their student. I am very grateful to my sponsor King Abdulaziz University, Jeddah, Saudi Arabia, for granting me this huge opportunity to pursue my dream of achieving this academic degree. I would like to also thank professor G. Pilkington from the University of Portsmouth, and Dr S. Smith and Dr R. Rahman from the University of Nottingham for providing me with the GBM cells that were the core of my project. Thank you also to Prof Kees Jalink from Van Leeuwenhoek Centre of Advanced Microscopy, Amsterdam, The Netherlands, for providing the Epac-based FRET cAMP sensor. Thank you to the staff at Wolfson bioimaging facility for helping me with the microscope work. I would like to express my gratitude to Dr Beihui Liu, Dr Valentina Mosienko, and Lesley Arberry for sharing their knowledge with me, and advising me during my laboratory work. I am also very grateful to Dr Barbara Vaccari Cardoso and Dr Iliana Barrera who were always there to help and offer academic and emotional support when most needed. I gratefully acknowledge input from A. Vasilev, an academic visitor from I. Kant University (Russia), on the methodology of TMRM-PDT. A very special thanks to my mom, my sisters, and my brother for their unconditional love and support. Thanks to my daughters Laila and Nadia for the love that kept me going. My deepest gratitude to my husband Mohammad, I would have never accomplished this without his most appreciated support. Finally, I dedicate this work to my father whose blessings I feel in everything I do.

Declaration

I declare that the work in this dissertation was carried out in accordance with the requirements of the University's Regulations and Code of Practice for Research Degree Programmes and that it has not been submitted for any other academic award. Except where indicated by specific reference in the text, the work is the candidate's own work. Work done in collaboration with, or with the assistance of, others, is indicated as such. Any views expressed in the dissertation are those of the author.

SIGNED: Roba Sofi DATE: 24 June 2021

Table of content

List of Figures

List of Tables

Related abstracts and publications

Alex Vasilev, Roba Sofi, Li Tong, Anja G. Teschemacher, and Sergey Kasparov. In Search of a Breakthrough Therapy for Glioblastoma Multiforme. **Neuroglia 2018**, 1, 292–310; doi:10.3390/neuroglia1020020. https://www.mdpi.com/2571-6980/1/2/20

R. Sofi, A. Vasilev, A. G. Teschemacher, S. Kasparov. In Search of Alternative Therapies for Glioblastoma Multiforme. **Poster communication in: XIV European Meeting on Glial Cells in Health and Disease, 2019, Porto.**

Vasilev A, Sofi R, Rahman R, Smith SJ, Teschemacher AG, Kasparov S. Using Light for Therapy of Glioblastoma Multiforme (GBM). **Brain Sci. 2020**;10(2). https://www.mdpi.com/2076-3425/10/2/75.

List of abbreviations

5-ALA 5-aminolevulinic acid
AC Adenylate cyclase
AD Antidepressants
ALT Alternative lengthening of telomeres
AMPA α-amino-3-hydroxy-5-methyl-4-isoxazolepropionic acid receptor
ATRX α-thalassemia/mental retardation syndrome X-linked protein
BBB Blood brain barrier
BPD Benzoporphyrin derivatives
cAMP Cyclic adenosine monophosphate
CAN Copy number alteration
CDK Cyclin dependent kinase
CL Clomipramine
CNS Central nervous system
CREB cAMP response element binding protein
CSC Cancer stem cell
CSF Cerebrospinal fluid
CT Computed tomography
CTC Circulating tumour cell
CYP Cytochrome P450 family
db-cAMP di-butyryl cyclic AMP
DMEM Dulbecco's Modified Eagle Medium
DMSO Dimethyl sulfoxide
dNTP deoxynucleotide triphosphate
EGFR Epidermal growth factor receptor
Epac Exchange protein directly associated with cAMP
FACS Florescence-activated cell sorting
FBS Foetal Bovine Serum
FDA Food and drug administration
FGS Fluorescence guided surgery
FLX Fluoxetine
fMRI Functional magnetic resonance imaging
FRET Förster Resonance Energy Transfer
FSK Forskolin
PDE Phosphodiesterase enzyme
PDGFR Platelet derived growth factor receptor
PDT Photodynamic therapy
PFS Progression free survival
GBM Glioblastoma multiforme
GF Growth factor
GFAP Glial fibrillary acidic protein
GPCR G-protein coupled receptor
GSC Glioma stem cell
GSEA Gene set enrichment analysis
HDAC Histone deacetylase
HGG High grade glioma
HP Hematoporphyrin
HPD Hematoporphyrin derivatives
IDH Isocitrate dehydrogenase
IL-4 Interleukin 4
IMS Inner mitochondrial space
IMM Inner mitochondrial membrane
IM Imipramine
iPDT Interstitial photodynamic therapy
KPS Karnofsky performance status
LDH Lactate dehydrogenase
LGG Low grade glioma
MAP1-LC3 or LC3 Microtubule associated protein light chain 3
MGMT O6-methylguanine-DNA methyltransferase
MPTP Mitochondrial permeability transition pore
miRNA micro-RNA
MMP or Δψm Mitochondrial membrane potential
MRI Magnetic resonance imaging
mtDNA Mitochondrial DNA
NF-1 Neurofibromatosis 1
NSC Neural stem cell
OMM Outer mitochondrial membrane
OPC Oligodendrocyte precursor cell
oPDT or cPDT Open cavity photodynamic therapy
OS Overall survival
OXPHOS Oxidative phosphorylation

PI3K Phosphatidylinositol-3-OH-kinase
PKA Protein kinase A (PKA)
PPIX Protoporphyrin IX
pRB Retinoblastoma protein
P/S penicillin/ streptomycin

PS Photosensitiser
PTEN Phosphatase and tensin homolog
RA Rat astrocytes
RB Retinoblastoma gene
ROS Reactive oxygen species
RT Radiotherapy
RTK Receptor tyrosine kinase
RWD relative wound density
SNV Single nucleotide variant
SSRI Selective serotonin reuptake inhibitors
TCA Tricyclic antidepressants
TCGA The Cancer Genome Atlas
TERT Telomerase reverse transcriptase
TMRM Tetramethylrhodamine methyl ester
TMZ Temozolomide
TTF Tumour treating fields
VEGF Vascular endothelial growth factor
WHO World health organization

Chapter 1: Introduction

1.1 An Overview of GBM

1.1.1 Definition and origin

Gliomas are tumours of glial cells arising in the CNS (1). Glial cells are the type of cells responsible for structural support and maintenance of homeostasis in the CNS. Glial cells are classified into astrocytes, oligodendrocytes, microglia, and ependymal cells (2).

Glioblastoma multiforme (GBM) is the most aggressive type of gliomas. 2016 WHO classification of brain tumours describes GBM as the highest grade (grade 4) diffuse infiltrative glioma (3). The term multiforme implies that this disease is heterogenous in nature, with different cellular phenotypes, mutational profile, and molecular and clinical trajectories (4). Glial cells have long been thought of as electrically silent despite their known major role in modulating synaptic transmission (2). Bergles et al. were among the first groups who documented synaptic communication between neurons and non-neuronal glial cells (5). Stimulation of excitatory axons in the hippocampus elicited an inward current detected from oligodendrocyte precursor cells (OPCs) and mediated by AMPA receptors (5). These synapses are believed to regulate growth and differentiation in the developing brain. Regarding malignant brain tumours, GBM in particular, synapses between neurons and glioma cells (neuron-to-glioma synapses) were recently identified using electron microscopy (6). These synapses were predominantly found in the infiltrative zone of the tumour and were electro-physiologically functional (6). In addition, the neuronal factor neuroligin-3, which is known to promote glioma progression in a paracrine fashion (7), is found to stimulate the expression of synaptic genes and enhance neuron-to-glioma synapse formation (6). These findings strongly suggest a role of neuron-to-glioma synapse in regulating glioma progression and infiltration. Moreover, synaptic gene enrichment was chiefly found in subpopulation of glioma cells resembling OPCs, and the postsynaptic current in them was mediated by glutamate AMPA receptors (8). This highly suggests a role

of these synapses in regulating proliferation of tumour cells, because of the similar properties they share with the normal neuron-to-glia synapses. In fact, glioma cells are known for their ability to hijack growth promoting mechanisms of the normal brain for their own benefit (8).

There are many theories about the cell of origin in glioma tumours, all of them perhaps could prove to be true at least to some extent. The most recognized candidates for glioma origin are astrocytes, OPCs, and neural stem cells (NSCs) (9). One of the key studies on this topic was carried out ~20 years ago (10). Induction of the expression of oncogenic mutations in a cell specific manner in astrocytes and NSCs, utilizing tissue specific promoters, was performed. Holland et al. induced activating mutations of Ras and Akt in astrocytes and NSCs of genetically engineered mice using viral vectors and assessed them for GBM-like tumour formation. They found that co-expression of these two activating mutations was sufficient to induce glioma tumours in mice only if expressed in NSCs but not in mature astrocytes (10). This finding is one of those, supporting the notion that neural stem cells are the origin of glioma tumours. On the other hand, Lindberg et al. have done similar work on genetically modified mice models inducing oncogenic mutations, but this time in OPCs (11). They found that oncogenic mutation in OPCs was sufficient to induce glioma-like tumour formation, concluding that OPCs, in particular, are the cells of origin of glioma (11). However, some recent studies have provided strong evidence that some subpopulations of astrocytes can be precursors of malignant cells (12).

A number of studies identified subpopulations of cells within GBM tumours with stem cell-like properties, known as cancer stem cells (CSCs) or, more precisely, glioma stem cells (GSCs) (13). They have been implicated in tumour initiation, progression, therapy failure, and recurrence. These cells are identified by expression of stemness markers such as nestin, SOX1/2, CD44, and CD133 and reside in niches within tumour microenvironment (TME), around vascular or necrotic foci (13). Among the first studies which identified these markers in primary brain tumours is Singh et al. (14). These authors identified CD133 expression in subpopulations of cultured astrocytoma cells. These cells lacked the expression of neural differentiation markers and had a high capacity for proliferation and self-renewal, which correlated with tumour aggressiveness (14). GSCs or GBM cells can lose or gain stemness markers and stem cell-like properties depending on signals from the TME (14), making their

accurate identification and classification difficult. Moreover, a sub-population of fibroblast-like cells called glioma-associated stem cells (GASC) has also been described (15). GASC had some stem cell-like properties such as anchorage-independent growth, but they are not tumorigenic (15). These cells are suggested to reside within the TME and modulate its cellular components to support the growth of the tumour and the aggressiveness of GCS in-vitro by releasing exosomes (15).

The three universally accepted models about the mechanism of initiation and maintenance of tumour growth are illustrated in **Figure 1.1.** The clonal evolution model (stochastic model) states that the accumulation of genetic mutations or epigenetic alterations, inherited or acquired, can potentially cause differentiated cells to become tumour cells (16). These mutations produce clones of cells with stem-like properties. Stronger clones with evolutionary growth advantages expand to form a tumour bulk that houses multiple clones of stem-like cells with tumorigenic potentials **(Figure 1.1 a)** (17). On the other hand, the stem-cell model (hierarchical model) states that mutations in embryonic stem cells or NSCs give rise to CSC with self-renewal and tumorigenic capacities, and only these CSCs can give rise and sustain tumour growth (17). CSCs divide symmetrically to expand the pool of stem cells, and asymmetrically to generate the bulk of the tumour **(Figure 1.1 b)** (17). The third model, the plasticity model, suggests that the previous two models are not mutually exclusive, and that any cell of the tumour bulk has the potential to de-differentiate and form a CSC with stem cell properties and growth potentials **(Figure 1.1 c),** and this is suggested as one of the mechanisms responsible for tumour heterogeneity (17, 18).

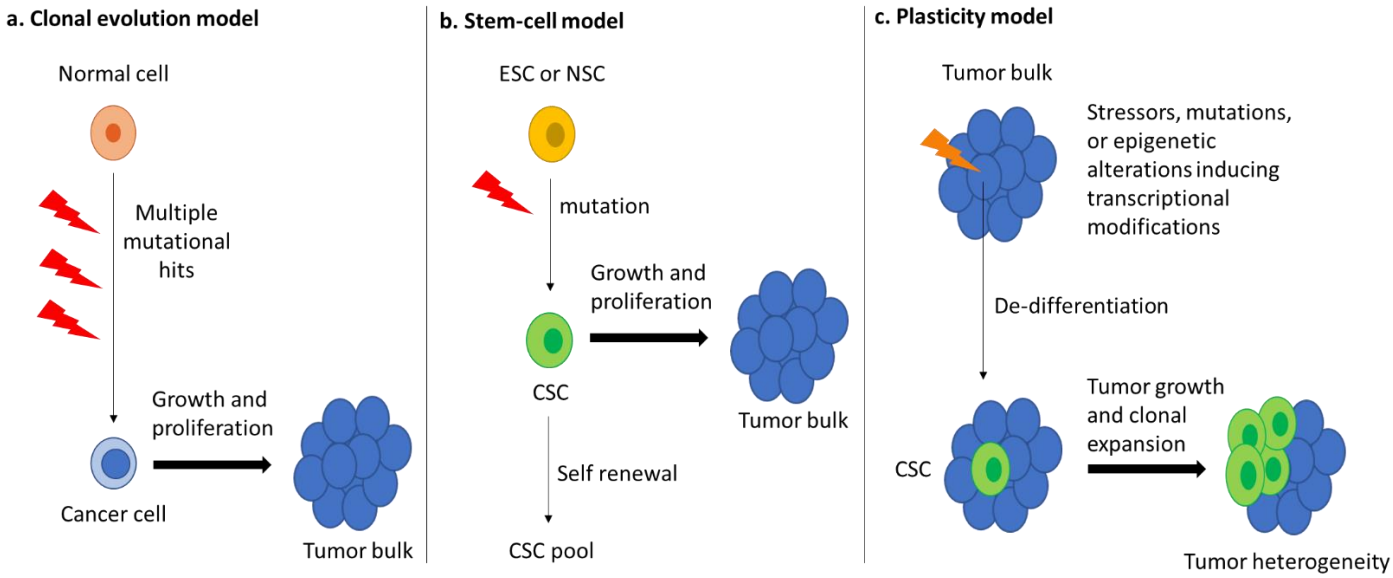

Figure 1.1. Models of cancer origin and maintenance.

1.1.2 Epidemiology and risk factors

GBM is the most lethal and the most frequently diagnosed primary malignant CNS tumours (80%) (4, 19). GBM accounts for 56.6% of all gliomas (20). It also accounts for 60% of all brain tumours diagnosed in adults (19). The average survival rate after diagnosis is 12 months and the 5-year survival rate is less than 5% (21). Different reports of incidence rates of glioma vary significantly according to country, age group, gender, and histological definitions (22). According to the Central Brain Tumour Registry of the USA statistical report published in 2018, the overall age and population-adjusted incidence rates range from 4.67 to 5.73 per 100 000 population for all gliomas and from 0.59 to 3.69 per 100 000 population for GBM (20, 22). For all primary CNS tumours, the median age at diagnosis is 60 years (20). GBM incidence rates are higher among elderly, reaching the peak at age 85 years or more (83.75 per 100,000 population) (20).

Primary malignant CNS tumours have an average annual mortality rates ranging from 0.72 per 100,000 population in children to 9.01 per 100,000 population in 40+ year-old individuals (20). More than 95% of GBM occur in cerebral hemispheres (19). Of all gliomas

diagnosed in the USA during 2011-2015, 23.9% occurred in the frontal lobe, 17.5% occurred in the temporal lobe, 10.4% occurred in the parietal lobe (20).

Thousands of epidemiological studies have been performed to understand the risk factors for GBM. However, few of them showed consistent results and of those, only few have shown strong association (23). Exposure to ionizing radiation is one of the risk factors that have strong association with increased risk of glioma (23). In contrast to some other cancers, alcohol and cigarette smoking have not been linked to increasing GBM risk (23), and neither have been dietary factors or environmental exposure to chemicals (19). In regard to the alleged risk of mobile phone use, an international case-control study INTERPHONE has found no association between phone use and risk of glioma (24).

Surprisingly, there is a strong epidemiological evidence (mostly case-control studies) that asthma and other allergic conditions are associated with reduced risk of glioma (22, 25-29). A recent meta-analysis of 19 studies included a total of 8435 cases and 118,719 controls has also concluded that allergies, general or specific to particular antigens, are "protective" against glioma (25). Whether this association is due to the hyper-reactive immune system causing allergic disease itself, or the use of anti-inflammatory or antihistamine medications is yet to be established. Moreover, IgE, commonly associated with the allergic reaction seem to be somehow protective against glioma. At least, it was found that higher glioma risk is associated with lower serum IgE levels (26, 30). Aggressive gliomas with higher expression of stemness marker CD133 were found to have lower expression of 80% of 919 genes related to allergy and inflammation (31).

An important inflammatory mediator negatively associated with glioma risk is interleukin-4 (IL-4). Several attempts have been made to develop therapeutic approaches aimed to increase IL-4 levels, and they were to some extent successful in inhibiting GBM tumour growth or prolonging animal survival (28). For example, in one study U87 glioma cells and engineered interleukin 4-secreting cells were co-transplanted into nude mice (32). This has resulted in decreased tumour size and improved survival of mice withn mixed transplants compared to control mice which received U87 glioma cells and negative control cells only (32). Moreover, some studies are focusing on the expression of IL-4 receptor (IL-

4Ralpha) which is found to be higher in GBM cells compared to normal cells, and makes a plausible target for immunotherapy (33).

Micro-RNAs (miRNA) are known to be crucial onco-modulators, and expression of some miRNAs was thought to be a factor of risk for (e.g. miR-221, miR-222) or protective against (e.g. miR-17-5p, miR-19) the development of GBM (34). However, although extensively researched, no strong or conclusive association between these miRNAs and the risk of GBM has been proven (34).

Some inherited genetic disorders are strongly associated with increased risk of developing gliomas (22). Familial adenomatous polyposis (APC gene mutation), melanoma-neural system tumour syndrome (mutations in CDKN2A), mismatch repair deficiency syndrome (DNA mismatch repair genes), Li–Fraumeni syndrome (mutations in p53 gene), retinoblastoma (mutations in Rb1), and neurofibromatosis 1 (mutations NF1), are examples of hereditary cancer syndromes associated with high glioma risk (35). This is not surprising since these mutations all cause or promote genetic instability and/or loss of control of cell cycle. Nevertheless, these diseases does not noticeably contribute to the overall risk of GBM, due to their rarity (23). 5-10% of glioma patients have relatives, most commonly siblings, who have the disease (23). This familial clustering of glioma cases may suggest a distinct genetic aetiology, or may point toward shared environmental exposure as well (23).

1.1.3 Classification of glioma

The latest WHO revision for classification of tumours of the central nervous system was published in 2016 (36). It integrates histopathological features with molecular signatures for more precise diagnosis. It also recognized for the first time the diagnostic and prognostic importance of Isocitrate dehydrogenase (IDH) mutational status. Histological grading is based on: anaplasia, nuclear pleomorphism, proliferative activity (mitotic cells), necrosis, and neovascularization (3). This classification broadly stratifies gliomas into non-proliferating low grade gliomas (grade I) and infiltrating high grade gliomas (grade II- IV) (36). GBM is considered high grade (grade IV) diffuse infiltrative glioma. These grades are further classifies according to presence or absence of common mutations found in gliomas

such as IDH mutation status, p53 mutation status, 1p19q co-deletion status, O6-methylguanine-DNA methyltransferase (MGMT) promoter methylation status, α-thalassemia/mental retardation syndrome X-linked protein (ATRX), telomerase reverse transcriptase (TERT) promoter, and Epidermal growth factor receptor (EGFR) (36).

Since then, advances and discoveries of new molecular markers and gene signatures have led to the formation of a scientific platform called: Consortium to Inform Molecular and Practical Approaches to CNS Tumor Taxonomy – not officially WHO (cIMPACT-NOW). This platform has further refined the WHO classification based on newly discovered data on the role and interplay of different molecular markers, and came up with recommendations that are more clinically relevant (37).

According to cIMPACT, IDH mutation remains a major classifying factor. IDH-mutant gliomas with ATRX mutation are now called IDH-mutant astrocytoma with or without 1p/19q codeletion (38). IDH-mutant astrocytoma may correspond to grade II, III, or IV of the WHO classification, with CDKN2A homozygous deletion as a marker for the highest grade (38). IDH-wildtype tumors with TERT promoter mutation, EGFR amplification, and/or chromosome 7 or 10 abnormalities are classified as IDH-wildtype glioblastoma (37). A new entity of IDH-wildtype glioblastoma has been proposed as grade IV diffuse hemispheric gliomas exhibiting histone 3.3 G34- mutations (37). This refined classification is important for accurate prediction of clinical behaviour and assignment of appropriate treatment plan (37).

1.1.4 Histological features of GBM

Macroscopically, GBM appears as an irregular heterogenous mass , with multiple haemorrhagic spots, cystic formations, and foci of necrosis (19). Histologically, these tumours are anaplastic, pleomorphic, poorly differentiated cells displaying high mitotic activity, high nucleus/ cytoplasm ratio, and glomeruloid structures indicative of neovascularization (newly formed blood vessels) (19). Pseudo-palisading necrosis is a hallmark for glioblastoma (39). It consists of crowded palisade-like alignment of pleomorphic nuclei around an irregularly shaped centre of necrosis (39). Neovascularization

classically appear as glomeruloide tufts, with multi-layered endothelial cells, smooth muscle cells and pericytes (19).

GBM are histologically heterogenous but predominantly resemble astrocytes. Therefore, the expression of glial fibrillary acidic protein (GFAP), the well accepted marker of astrocytes, along with the presence of fine fibrillary processes are important diagnostic features of GBM tumours (4). Different histopathological variants of GBM have been described in the literature. They represent the spectrum of phenotypic heterogeneity, associated with fairly specific molecular fingerprint. These variants include small cell glioblastoma, giant cell glioblastoma, granular cell glioblastoma, epithelioid glioblastoma, glioblastoma with primitive neuronal component, and gliosarcoma (36, 40, 41). Small, giant, and granular cell glioblastomas appear under the microscope with minimal pleomorphism and as their names suggest: small, big, and granular macrophage-like, respectively (36, 41). Small cell glioblastoma is associated with Epidermal growth factor receptor (EGFR) amplification in 70% of the cases (42), and PTEN/10q mutations in 100% (41). Epithelioid glioblastoma cells look large and eosinophilic, with prominent nucleoli and rhomboid-like component (36). They are associated with BRAF mutations in 50% of the cases (42). Glioblastoma with primitive neuronal component are diffuse nodular astrocytomas that can spread into the craniospinal fluid (36). Gliosarcomas are tumours with both glial and mesenchymal components (41). Epithelioid, giant cell glioblastoma, as well as gliosarcoma are almost always genotypically IDH-wildtype (36). Each of these histological variants are further clinically classified into primary (IDH-wildtype) or secondary (IDH-mutant) GBM. This molecular diversity will be discussed later in more details.

1.1.5 Clinical presentation and diagnosis

Gliomas occur most commonly in the frontal lobe, then overlapping more than one lobe, and less likely in the temporal or parietal lobes (43). 95% of GBM tumour arise in the supratentorium, and only rarely gliomas are found in the brain stem, cerebellum, or spinal cord (4). These atypical locations are more prevalent, but still rare, in younger patients (43).

The time from the onset of symptoms until the diagnosis of GBM is typically weeks or months depending on the severity of symptoms, which reflects the aggressiveness of the tumour (44). Mostly, symptoms arise from increased intracranial pressure, or pressure from the tumour mass affecting nearby neurological structures depending on the location of the tumour (44). Seizures, headache, and/or neurological deficits (cognitive, motor, or sensory) are the most common presenting symptoms in GBM (45). Fatigue, drowsiness, aphasia, and confusions are also common but more prevalent as symptoms of advanced disease (45).

Provisional diagnosis of GBM is routinely made based on radiographic imaging with computed tomography (CT) scans or magnetic resonance imaging (MRI) (44). These imaging modalities are usually supplemented with anatomical, functional, and/or metabolic contrast imaging techniques in order to aid the diagnosis, differentiating glioma from non-glioma tumours or non-neoplastic lesions, outline tumour extension, and delineate its relationship to the surrounding brain structures (44). A stereotactic biopsy can be taken from the tumour preoperatively with radiographic guidance, and it is often enough to establish the diagnosis of GBM, but more precise diagnosis is made with tumour tissue samples acquired intraoperatively (46). Microscopic histopathological examination of tumour sample frozen sections is the golden standard in GBM diagnosis (46). Degree of anaplasia, extent of tumour infiltration, and signs of necrosis are all considered in the examination and classification of glioma tumours (47).

1.1.6 Molecular hallmarks of GBM

Advancements in molecular and genetic testing have led to expansion in our knowledge about driver genetic mutations for gliomagenesis and other molecular changes associated with its progression. The Cancer Genome Atlas (TCGA) study published in 2008 has identified main signalling abnormalities involved in the development of GBM, including [1] activation of growth signals by activating receptor tyrosine kinase (RTK) pathways involving growth factors (GF), [2] activation of phosphatidylinositol-3-OH-kinase (PI3K) pathway, and [3] mutations of p53 and retinoblastoma (Rb) tumour suppressor pathways (48). A summary of the molecular hallmarks in GBM is presented in **Figure 1.2.**

RTK and growth factors. RTKs are transmembrane glycoprotein receptors for numerous ligand types such as growth factors, hormones, or cytokines (49). When activated, RTKs' downstream signals are mediated by several effectors including Ras/MAP kinase pathway, PI3K pathway, Phospholipase C and others (49). These pathways regulate cell proliferation, response to apoptosis signals, inflammation, and cell migration (49). RTK signalling is dysregulated in 70% of GBM cases and either an RTK or one of its effector pathways is altered in 90% of GBM cases (50). Epidermal growth factor receptor (EGFR) is the most frequently affected RTK in cancers and accounts for 45-55% of RTK abnormalities in GBM (50). The most common type of alterations involving EGFR signalling is EGFR gene amplification resulting from structural rearrangement of EGFR gene, namely in-frame deletion in exon 2-7 affecting the extracellular ligand-binding domain (51). This variant is called EGFRvIII, and the product of it is a constitutively active growth receptor which signals downstream regardless of the availability of the ligand (49, 51). Other alterations include defective gene inactivation, increase copy number, EGFR single nucleotide variants (SNVs), or ligand (Endothelial Growth Factor) overproduction (51). Other RTKs related to glioma development or progression are vascular endothelial growth factor receptor (VEGFR) and platelet derived growth factor receptor (PDGFR) (49). VEGFR and its ligand VEGF are the master regulator of angiogenesis and neovascularization in cancer cells and are commonly overactivated in GBM in areas adjacent to necrosis (4). PDGFR and the ligand PDGF are important for cellular differentiation and migration (49). PDGFR or PDGF gene overexpression is only detected in 13% of GBM patients (49). Any of these abnormal RTKs along with their ligands are capable of creating a growth-promoting autocrine loop, stimulating uncontrollable growth in the GBM (4, 49).

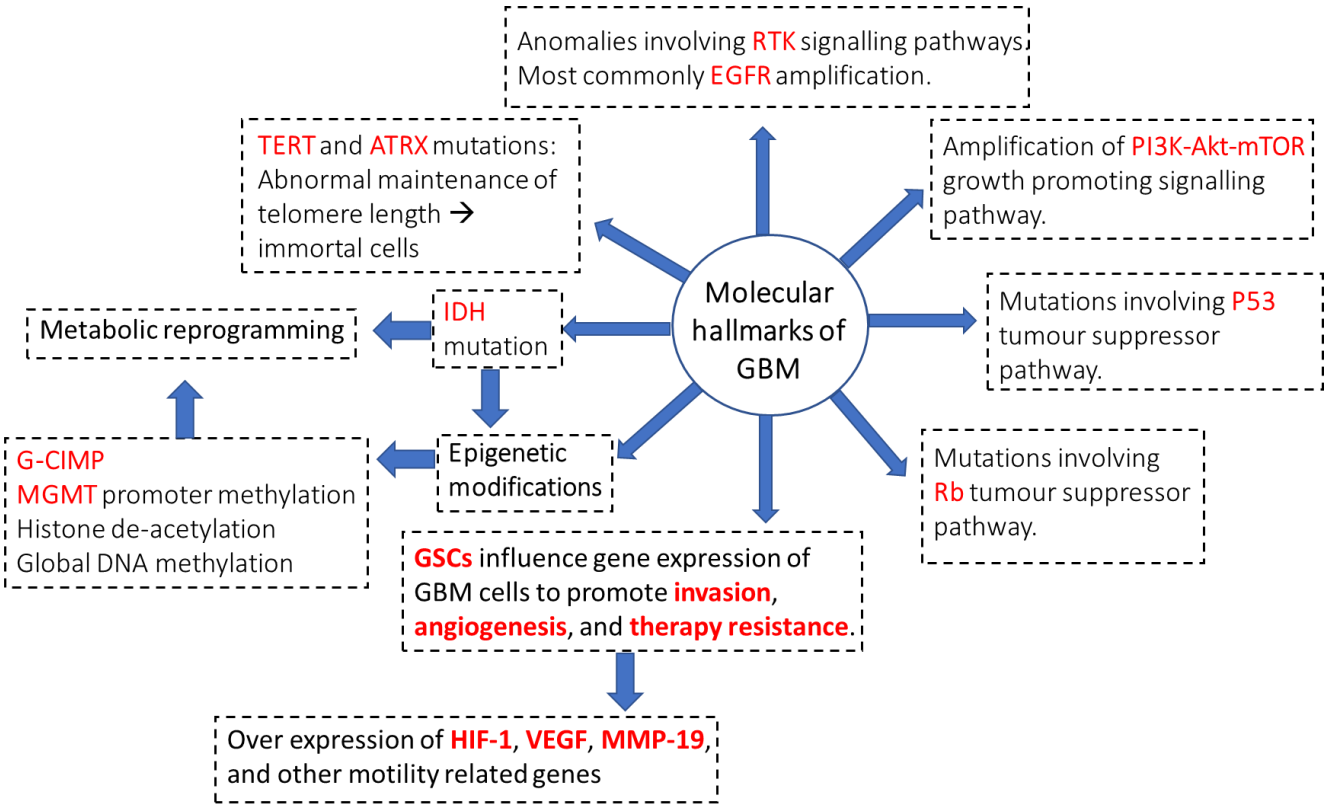

Figure 1.2. Molecular aberrations commonly seen in GBM.

PI3K-Akt-mTOR pathway. PI3K is an enzyme that interacts with RTK or GPCR and delivers signals to cellular pathways controlling growth, apoptosis, and motility (52). It consists of two subunits: regulatory and catalytic (4). Gene amplification of the catalytic subunit (p110α) is reported 4 – 27% in primary GBM and is associated with poor prognosis (52). Under normal circumstances, activated RTK activates PI3K, resulting in the recruitment of Akt to its active site at the plasma membrane, which then phosphorylates downstream molecules such as mTOR and regulates protein synthesis (translation) and cell growth (52). PTEN inhibits the activation of Akt by interfering with its recruitment to this active site (52) thus limiting its signalling. Homozygous deletions or inactivating mutations in PTEN gene are detected in 40% of GBM patients (4). PI3K seems to be an obvious drug target and more than 50 different PI3K inhibitors have been tested for cancer therapy including GBM (52). However, only few of them have moved to phase I or II clinical trials (52). PI3K inhibitors, selective p110α inhibitors, dual PI3K/mTOR inhibitors have shown some initial promising results in GBM research (52). However, activation of compensatory pathways and severe

side effects limiting their tolerable doses have proven difficult to avoid, leading to failures in clinical trials (52).

P53 and Rb tumour suppressor pathways. In normal cells, there is always a balance between mitogenic stimuli and cell cycle suppressors such as p53 and Rb (4). In GBM, disturbances of p53 and Rb tumour suppressor pathways are common and are among the main molecular drivers, responsible for gliomagenesis (48). In fact, p53 tumour suppressor pathway is the most commonly mutated pathway in cancer in general (53).

Cellular stressors (DNA damage, hypoxia, etc.) induce different kinases and mediators of p53 tumour suppressor pathway, resulting in activation of p53 tumour suppressor protein by post-translational modifications at different amino acid residues (54). Different types of stressors uniquely modify different amino acids residues, which is followed by modulation of specific effectors and transcription factors leading to inhibition of cell cycle progression and induction of DNA repair or apoptosis (54).

MDM2 is a negative regulator of p53, blocking its function and resulting in progression of cell cycle. P53 activity activates MDM2 creating a negative feedback loop between the two molecules as illustrated in **Figure 1.3.** Protein ARF, on the other hand, exerts its tumour suppressor effect by inhibiting MDM2 activity, thus supporting the activity and function of p53 pathway (54).

A study on 34 different human glioma cell lines has shown a high incidence of mutations in p53 tumour suppressor pathway among these cell lines (94.1% of glioma cell lines) (55). More recently, TCGA study has revealed that ARF-MDM2-p53 pathway is dysregulated in 84% of GBM tumours (48). The most common mutation in p53 pathway is homozygous deletion of the CDKN2A/ARF locus, seen in about 60% of GBM cases, followed by missense mutation of p53 gene, and MDM2 amplification (56). P53 pathway mutations are more associated to secondary GBM than primary (56).

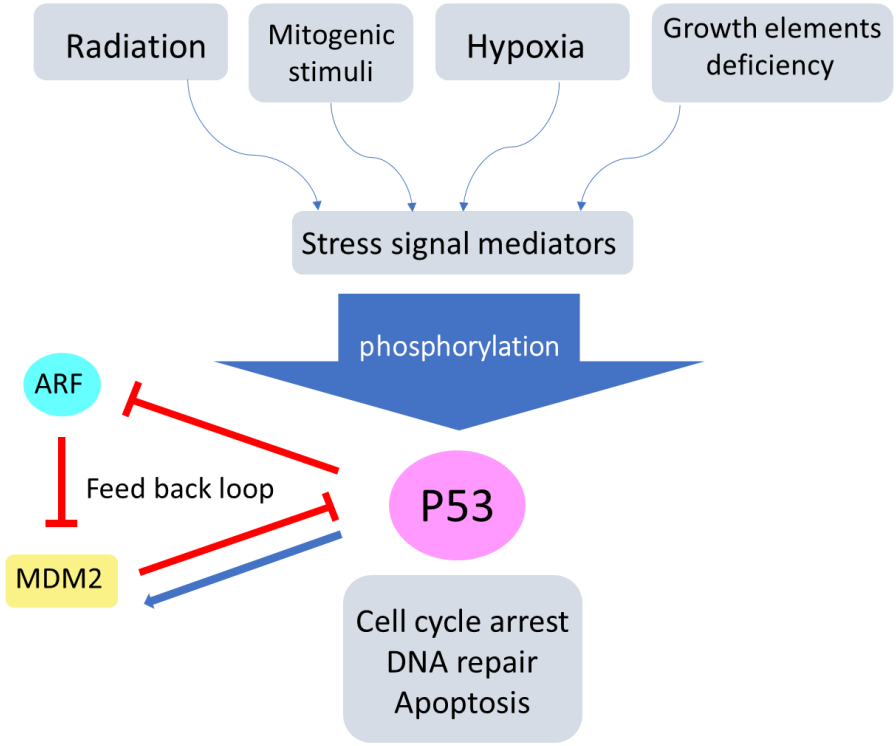

Figure 1.3. Activators and feedback loop of p53 tumour suppressor pathway.

RB (retinoblastoma pathway) is a tumour suppressor pathway involving cyclins, cyclin dependent kinases (CDKs), retinoblastoma protein (pRB), and E2F family of transcription factors. Normally, pRB is dephosphorylated and active. When active, it attaches to E2F and blocks it from stimulating transcription of genes required for cell cycle progression (**Figure 1.4**). The result is cell cycle arrest at G1/S phase and induction of cell differentiation (57). CDKN2A/B is a key regulator of Rb pathway. As shown in **Figure 1.4**, it blocks CyclinD/CDK4-6 dependent phosphorylation (inactivation) of pRB. When phosphorylated, pRB can no longer form a complex with E2F, which is now released from the block and actives transcription of cell cycle E2F-dependent genes (57). RB pathway anomalies found in GBM include CDKN2A/B deletions or inactivating mutations (40%), RB1 gene deletions or inactivating mutations (40%), or Cyclin/CDK4 -6 amplification (15%) (4).

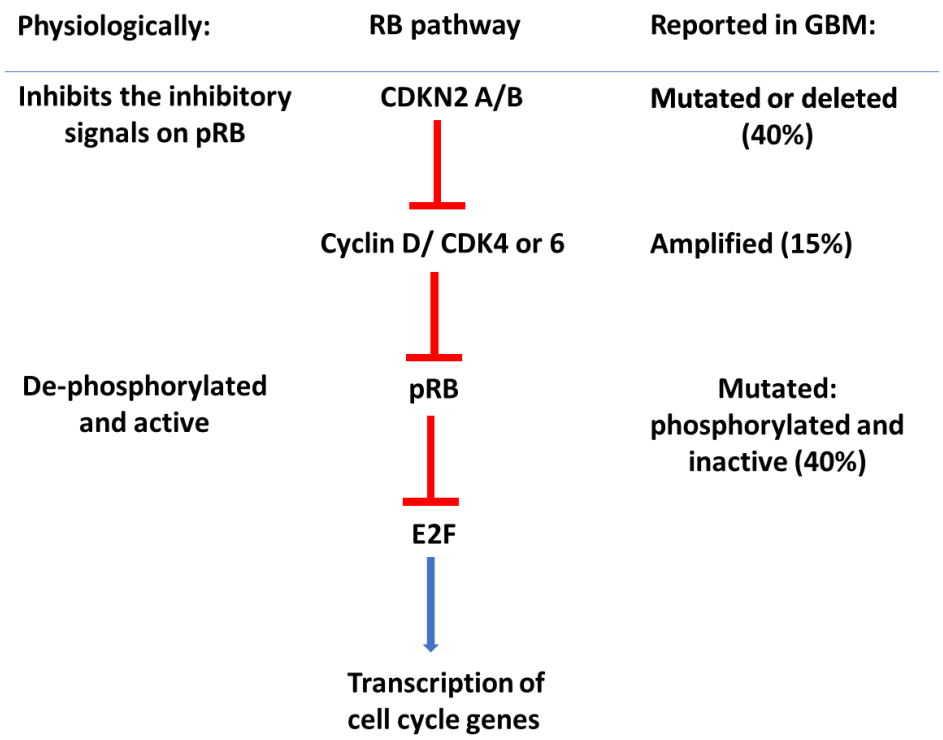

Figure 1.4. RB tumour suppressor pathway.

Angiogenesis. Growth of solid tumours is tightly associated with angiogenesis, which is the formation of new blood vessels (58). Neovascularization is typically stimulated by hypoxia. One of the key molecules sensing hypoxia is Hypoxia inducible factor (HIF), which increases production of VEGF, which then initiates sprouting of old blood vessels, building of an endothelial lining, and remodelling of the extracellular matrix to form new tumour vasculature (59). Within TME there are niches of GSC, neoplastic infiltrating cells, reactive astrocytes, fibroblasts, endothelial cells, and immune cells such as tumour associated macrophages and T-cells (42). Components of TME synergise to promote invasion, angiogenesis, and therapy resistance (60). GCSs have been hypothesised to mediate the recruitment of tumor-associated endothelial cells to angiogenic foci (13). It has also been suggested that neovascularization in GBM involves differentiation of tumour stem cells into endothelial cells (59) although this idea needs further proof.

The new vasculature of GBM is distorted with leaky and poorly organised vessels, which do not meet the tumour's growing need for oxygen and nutrients, thus creating a

feedback loop of hypoxia-mediated stimulation of angiogenesis, which renders GBM tumours extensively vascular (58). The degree of hypoxia and acidosis correlates to GBM aggressiveness and poor patient survival (61). HIF were found to be highly expressed in GSCs (60). Activation of HIF enhances the expression of multiple genes related to angiogenesis and cell migration (60). For that reason HIF is suggested as yet another target for therapy and this has even been tested in GBM xenograft models (58).

VEGF is found to be overexpressed in GSCs compared to non-stem cells, suggestive of increased angiogenic properties of these cells (58). Bevacizumab, a monoclonal anti-VEGF antibody, was developed with the aim to cut the blood supply to the tumour and has indeed shown promising results in pre-clinical research (58). However, in phase II clinical trials there was only minimal survival advantage in GBM treatment arm compared to control arm (58). This is now believed to be a consequence of a tumour adaptive process to hypoxia mediated by HIFs. The result of such adaptation is enhancement of stemness characteristics of the tumour and further vascularization rather than induction of apoptosis (58).

Invasion. Presence of fibrillary cellular extensions is a distinctive feature of astrocytic tumours and is more prominent in aggressive tumours such as GBM (62). GBM does not metastasize to other organs but it is highly invasive within the brain (4). Invading cells detach from neighbouring tumour cells, and migrate along vessels, dendrites, or fibres of the white matter in fine streaks (4). Their migratory behaviour resembles that of neural progenitor cells during development, suggesting a role for modulators of developmental neural cell migration in tumour cell invasion (4). Migrating tumour cells can infiltrate beyond the margins of resectable tumour and serve as an origin of recurrence, which almost always happen within the borders of the previously resected tumour directly at the wall of the surgical cavity (63). In a study concerning patterns of recurrent GBM, 17 out of 20 patients (85%) had the recurrent tumour within 2.5 cm from the resected tumour edge despite having had complete resection of the contrast-enhanced tumour, indicating the presence of infiltrative cells not identified radiographically (64).

By using high resolution time-lapse intravital imaging techniques, Alieva et al. were able to provide reliable images and analysis for the dynamics of cell invasion (63) in mice. They implanted GSCs derived from IDH-wildtype GBM tumours and stably expressing neural

marker (H2B-Dendra2) into the brains of immunodeficient mice. The images obtained have shown two distinctive invasion patterns in GBM tumours: (a) protruding multicellular edge from the tumour core into the surrounding tissue, creating an 'invasive edge pattern', (b) no defined protrusions but instead individual 'scout cells' diffusely infiltrating the surrounding tissue and creating a 'diffuse infiltration pattern' (63). Measurements of cell velocity revealed that cells in the tumour core and cells at well-defined borders are much less motile than cells at the diffuse infiltrative margins (63).

Smith et al. have also documented differential expression of some genes in fresh surgical samples taken during fluorescence guided surgery (FGS) from the core compared to samples obtained from the infiltrating margins (65). Analysis of RNA sequencing data obtained from these different samples revealed significantly different gene expression profiles for metabolism and extracellular matrix components (65). Invasive cells had an overall pre-inflammatory and anti-apoptotic gene print (65). Moreover, two of the differentially expressed genes, VEGFα and Matrix metalloproteinase-19 (MMP-19) were particularly involved in migration and invasion process (65). This differential expression is possibly the reason why therapies targeted against these two molecules failed in clinical trials. RNA sequencing also identified SERPINE1 gene (also known as plasminogen activator inhibitor 1, PAI-1) as a candidate for anti-invasion targeted therapy, due to its increased expression in infiltrating cells (65).

Invasion occurs early in GBM progression (63). It is thought to be initiated by different autocrine and paracrine factors that regulate the activity of number of cell surface proteins. Key players in glioma invasion are: Rho family GTPases; which mediate receptor-mediated invasion signals, integrins; which mediate interactions with extracellular matrix components, cell adhesion molecule CD44 and proteolytic enzymes; such as ADAMs and MMPs (66).

TERT and ATRX mutations. Telomeres are repetitive guanine-rich non-coding DNA elements that cap the ends of a linear chromosome to protect coding regions from terminal sequence loss (67). Telomere shortening is a normal phenomenon that accompanies cell division and is accountable for cell senescence, when cells have exhausted their replicative potential but are still metabolically active (67). Telomerase is a specialized reverse

transcriptase responsible for maintaining telomere length. It is inactivated in most non-dividing cell types by silencing the telomerase reverse transcriptase (TERT) gene encoding its catalytic domain (67). This physiological silencing of TERT is an important tumour suppressor mechanism to ensure that old cells which most probably have accumulated DNA damage and might have escaped DNA repair mechanisms do not enter mitotic cycle.

Activating mutations of TERT are detected in more than 90% of all human cancers (68). TERT promoter mutations are found in more than 50% of primary adult GBM, or up to 80% in some reports (41, 68). Cells with activating TERT promoter mutations become immortal due to high expression of telomerase which maintains long telomeres.

Another type of mutation that leads to maintenance of telomere length is inactivating mutation of α-thalassemia/mental retardation syndrome X-linked protein (ATRX). ATRX mutation does not lead to overexpression of telomerase; it rather induces telomere lengthening by a mechanism known as alternative lengthening of telomeres (69). This type of mutation is associated more with secondary GBM, and paediatric and lower grade gliomas, with strong correlation with IDH mutations (41, 69).

Epigenetic modifications. Epigenetic modifications modify gene expression without affecting the DNA sequence, and could potentially also be targeted for anti-GBM therapy (70). The most important epigenetic modifications in GBM are histone acetylation and DNA methylation (70). Chromatin is the structure formed by the organization of DNA molecule around histone proteins (70). Histone acetylation is the addition of acetyl group to amino acid lysine of histone H3 or H4 molecule (70). This modification causes chromatin remodelling in a form that makes DNA more accessible to transcription factors, which enhances gene expression (70). Histone deacetylases (HDAC) are commonly over-expressed in GBM (71). HDAC inhibitors have been developed and pre-clinical studies reported promising results for this class of drugs, including inhibition of tumour growth, improvement of radiosensitivity (71), or induction of metabolic re-programming in GBM cells (72).

DNA methylation is a silencing modification which compacts the chromatin and makes it inaccessible for transcriptional machinery (70). DNA methylation occurs mainly in CpG islands (CG rich regions of the DNA) which typically belong to promoter regions of genes

(70). GBM genome, like other cancers, is generally hypomethylated which leads to pathological enhancement of gene expression and genomic instability (70). This phenomenon is observed in 80% of GBM (70).

Glioma-CpG island methylator phenotype (G-CIMP) was first identified in 2010 as a unique subset of GBM (73). G-CIMP is usually found in younger patients and is associated with IDH-1 mutations and better prognosis (73). In fact, IDH-1 mutation is believed to cause this hypermethylated phenotype (74). Induction of IDH-1 mutation in astrocytes resulted in hypermethylated genome, with identical distribution of methylation marks to G-CIMP IDH-mutant glioma (74). CpG methylation marks were found to be differently distributed among gene sets in new tumours compared to recurrent ones (75). Kraboth et al. examined the methylome of primary and recurrent GBM tumours and reported that hypomethylation of gene sets associated with neuronal differentiation, synapse organization, and endothelial cell proliferation could be implicated in tumour development (75). They also found that gene families which regulate cellular communication and neurotransmitter release were significantly more methylated in recurrent GBM samples (75) which perhaps reflects their progressive de-differentiation.

O6-methylguanine-DNA methyltransferase (MGMT) is a nuclear dealkylating enzyme important in repairing DNA mismatches that occur spontaneously during DNA replication, or due to the impact of mutagens, environmental pollutants or alkylating drugs (76). MGMT gene status has a significant role in chemotherapy resistance in GBM patients. When overexpressed, MGMT enzyme corrects the intentional base mispairing produced by alkylating chemotherapeutic agents such as temozolomide (TMZ) (76). This will ultimately result in tumour cells escaping apoptosis and death and resistance (76). MGMT gene is located on chromosome 10q26.3 and its expression is highly regulated by different mechanisms including transcription factors such as NF-κB and CREBP, which are known to activate its transcription (76). Epigenetic regulation of MGMT plays an important role in development of resistance in GBM (76). Histone acetylation in MGMT promoter region is associated with active transcription of MGMT gene and higher expression of MGMT promoting the resistance (77). Histone deacetylase inhibitors (77) in xenograft models promoted a hyperacetylated chromatin status, induced MGMT expression, and aided the development of TMZ resistance (77). On the contrary, MGMT promoter methylation is

associated with silencing of MGMT gene and downregulation of MGMT enzyme level, which negatively affects DNA repair and enhances the response to anti-cancer alkylating agents (76). In a study involving 109 GBM patients, surgically obtained samples were examined for MGMT promoter methylation (78). These patients also received chemotherapy and radiotherapy after the surgery. MGMT promoter methylation was documented in 53.2% of patients, and it positively correlated to progression-free survival (PFS) and overall survival (OS) (78). Intratumour heterogeneity in MGMT methylation status was also documented in ~14% of the cases where different methylation status was found in different samples (78).

1.1.7 Classification of GBM based on transcriptional profile

There is more than one way to classify GBM. These classifications, either clinical, histological or molecular, overlap and complement each other in describing each case of GBM individually to help in making decisions regarding therapy and prognosis.

IDH-1 or 2 mutations are found in almost all secondary gliomas and are considered 'core mutations' essential for the secondary transformation of lower grade tumours to high grade infiltrative ones (79). Primary GBM rarely have IDH mutations. IDH is an enzyme that has 5 isoforms, IDH-1 to -5. They play roles in citric acid cycle, glutamine metabolism, and most importantly regulation of redox status by providing NADH/ NADPH and maintaining cellular levels of reduced glutathione (80). Mutations of IDH-1 or -2 found in GBM are monoallelic point mutation and are considered gain-of-function mutations resulting in neomorphic enzyme activity, where IDH-1 or -2 enzymes gain the ability to catalyse a reverse reductive carboxylation reaction that leads to accumulation of the oncometabolite 2-hydroxyglutarate (2-HG) and exhaustion of cellular NADPH (80). NADPH is important in cellular antioxidant defence system. Accumulation of 2-HG promotes epigenetic changes associated with abnormal expression of many genes, including activation of oncogenes and silencing of tumour suppressor genes (81-83). Moreover, 2-HG can inhibit key dioxygenases (80), and diminish complement system activation (84), affecting many elements of cellular signalling and immunity. Accumulating 2-HG destabilizes HIF-1 (85), which will negatively affect angiogenic capabilities of tumour cells and this perhaps could explain observations of

less necrosis and less vascularity associated with IDH-mutant GBM. The impact of IDH mutation on cellular functions is summarized in **Figure 1.5.**

IDH-mutant and IDH-wild type gliomas behave differently in terms of treatment response and prognosis. IDH-mutant GBM cells were found to be more sensitive to oxidative damage from chemotherapy and radiotherapy than IDH-wildtype GBM cells (86-88), most probably caused by inability of cells to buffer radiation-induced reactive oxygen species due to reduced cellular NADPH (89). In general, GBM with IDH-1 or -2 mutations have better prognosis and longer progression free survival than IDH-wildtype (83). Concurrent CDKN2A homozygous deletion was found to be a reliable predictor of poorer prognosis and shorter overall survival in IDH-mutant GBM (79, 90). **Table 1.1** summarizes the main differences between primary and secondary GBM in terms of clinical and molecular profile.

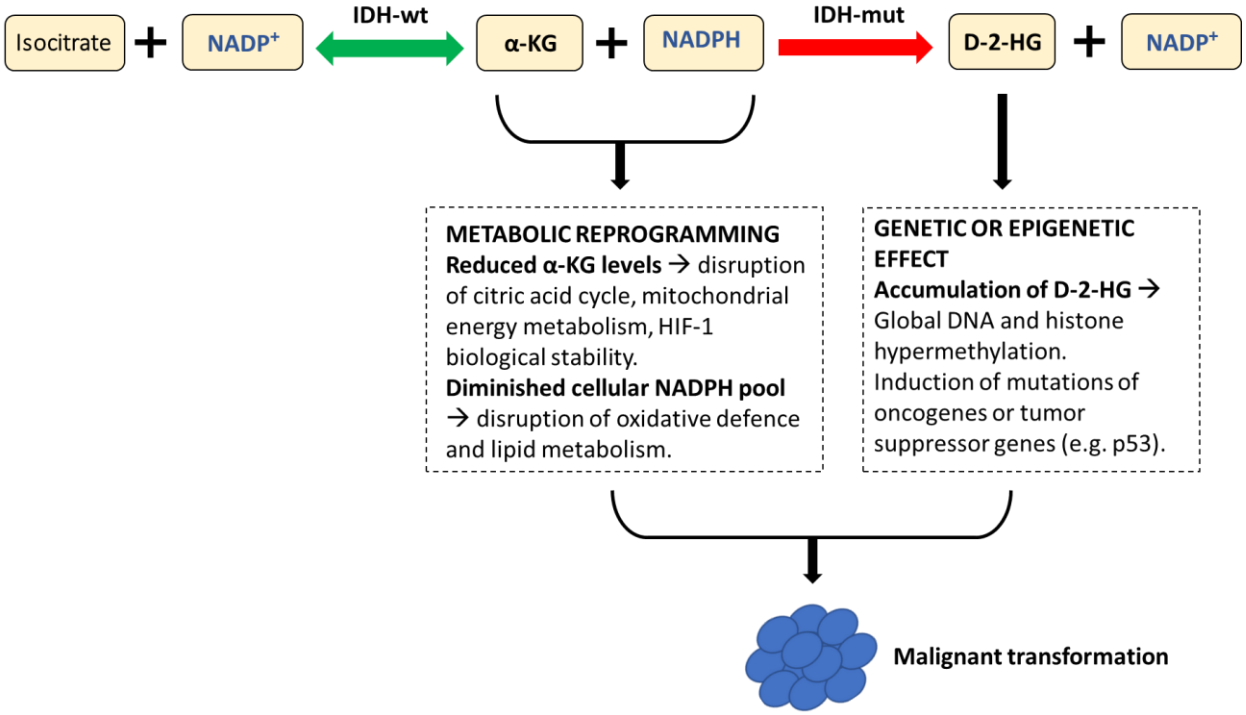

Figure 1.5. The impact of mutant IDH neomorphic enzyme on cellular mechanisms. IDH-wt: IDH wildtype, IDH-mut: mutant IDH, α-KG: α-ketoglutarate, D-2-HG: D-2-hydroxyglutarate, HIF-1: hypoxia inducible factor-1. Adapted from (91).

Verhaak et al. have described a molecular classification of GBM based on gene profile (gene expression, patterns of somatic mutations, and DNA copy number alterations) (92). Advanced gene analysis technology and software were used to analyse data derived from TCGA project, to try to find specific clustering of gene aberrations that can define a distinct GBM class. 1,740 genes (further filtered to 840 classifying genes) were found to be consistent within clusters but highly variable between them. Accordingly, four different molecular GBM classes are defined: Classical GBM, Proneural GBM, neural GBM, and mesenchymal GBM (92).

Classical GBM is characterised by chromosome 7 amplification, loss of chromosome 10, and EGFR amplification, distinctly paired with CDKN2A deletion affecting RB pathway, plus lack of IDH-1 and p53 mutations. Classical GBM highly express neural stem cell markers NES and Notch.

Proneural GBM is defined by abnormalities in PDGFRA and point mutations in IDH-1. Other features include higher expression of oligodendrocytic development gene OLIG2 as well as neural development gene SOX, plus p53 mutations.

Neural GBM is the least defined of the four GBM classes. It expresses neuron markers such as NEFL (an axo-skeleton gene) and GABRA1. It also shows similar expression pattern to normal oligodendrocytes and astrocytes.

Mesenchymal GBM is characterised by NF1 and PTEN co-mutations. This class of GBM is associated with higher degree of necrosis and inflammation. Expectedly, genes of tumour necrosis factor super family pathway (e.g. TRADD) and genes of NF-κB immune pathway are highly expressed in mesenchymal GBM. They also express Schwann cell markers and microglial markers.

Table 1.1. Comparing clinical behaviour and molecular profiles of primary and secondary GBM. Reference (40, 41).	
Primary GBM (de novo); IDH-wild type - Comprises 90% of all GBM cases. - Aggressive tumours with more pronounced necrosis and angiogenesis. - Older age at diagnosis. - Lower overall survival rate (11-15 months). - Clinical subtype: Proneural, neural, mesenchymal, or classical.	Secondary GBM; IDH-mutant - Comprises 10% of all GBM cases. - Less aggressive, less necrosis, and less angiogenesis. - Younger age at diagnosis. - Better overall survival rate (31 months). - Clinical subtype: Proneural.
- IDH mutations are rare. - Amplification of EGFR signalling. - PTEN mutations. - TERT mutations. - Monosomy 10.	- IDH mutations are very common (85%). Thought of as a driver mutation for development of secondary GBM from lower grade tumours. - P53 and Rb mutations. - PDGFR mutations. - ATRX mutations. - 1p/19q co-deletion. - MGMT promoter methylation.

1.1.8 Standard treatment for GBM

"Stupp" protocol has been the standard protocol for treatment of newly diagnosed GBM since 2005 (93). A 2-year multi-centre phase III randomized clinical trial, supported by the European Organisation for Research and Treatment of Cancer (EORTC) and the National Cancer Institute of Canada Clinical Trials Group (NCIC) (93), was followed by a 5-year analysis (94). After maximal safe resection (complete in 40%, partial in 45%, or biopsy in 15%), 573 patients were randomized to receive radiotherapy alone or radiotherapy with concomitant and adjuvant chemotherapy (93). Radiotherapy was delivered as fractional focal irradiation with a total dose of 60 Gy divided as 2 Gy daily for 5 days/ week for 6 weeks (93). Concomitant TMZ was given at low continuous dose of 75mg/ cm^2/day daily during the radiotherapy period (93). This dosing schedule was expected to eventually exceed the capacity of the DNA repair mechanisms (mainly the MGMT enzyme) and was found to be well tolerated by patient in a pilot phase II trial (93). Adjuvant TMZ was given after a 4-week break after radiotherapy and concomitant chemotherapy, with the approved conventional

dose of 150-200mg/cm^2/day for 5 successive days in a 28-day cycle, for 6 cycles (93). OS was 14.6 months for combined-therapy arm versus 12.1 months for the radiotherapy-alone arm. In the two year follow up, 26.5% of the patient in the combined-therapy arm were alive compared to 10.4% in the other group (93). Regarding toxicity, about half of the patients in the combined-therapy arm developed grade 3 or 4 adverse effects (mainly haematological) at any point during the trial, either during the concomitant TMZ period (17%) or the adjuvant TMZ period (35%) (93). In addition, 33% of the patients reported moderate to severe tiredness in the combined-therapy arm compared to 26% in the radiotherapy-alone arm (93). In the 5-year follow up analysis, the overall survival at 3 and 5 years was 16% and 9.8%, respectively, in the combined-therapy arm compared to 4.4% and 1.9% in the radiotherapy-alone arm (94). Thus, a clear survival advantage for concomitant and adjuvant TMZ therapy over radiotherapy alone in GBM patients was established (94) and became the standard of care across the world to this day.

TMZ is an oral alkylating prodrug that can cross the BBB (95). After oral administration, TMZ has a 100% bioavailability and a short half-life of 1.8 hours (95). It undergoes rapid non-enzymatic conversion to the active metabolite 5-(3-methyltriazen-1-yl) imidazole-4-carboxamide (MTIC) (95). MTIC methylates guanine bases in the DNA (95). At therapeutic doses, DNA repair mechanisms fail to correct for the DNA damage induced by TMZ and apoptosis signalling is initiated (95). Myelosuppression is not uncommon with TMZ treatment (95). The risk of potentially irreversible haematological toxicity such as aplastic anaemia and sever thrombocytopenia is small but significant, and must be addressed in research and discussed with patients (95).

The standard protocol for GBM therapy now consists of maximum safe surgical resection, followed by radiotherapy plus concomitant chemotherapy with TMZ, followed by adjuvant chemotherapy with TMZ (96). Gross total resection whenever feasible improves survival outcome regardless of age or molecular profile of the tumour (96).

More recently a method of fluorescence-guided surgery (FGS) was developed. This method is based on the use of 5-aminolevulinic acid (5-ALA). 5-ALA accumulates preferentially in GBM cells due to their high proliferative metabolic signature and helps surgeons to better visualize the tumour boundaries and to achieve maximum safe tumour

resection (97). This increases the extent of safe resection and improves survival in GBM patients compared to conventional surgery (96). Corticosteroids are sometimes used to reduce peritumoral oedema preoperatively or to control the side effects of radiotherapy, although their impact on overall survival is controversial (98). Radiotherapy for GBM helps in local control of the disease and improve survival.

For recurrent GBM, re-surgery is used to relieve intracranial pressure symptoms if present (99). At this stage treatment aims to slow down the progress of the disease and improve quality of life (99). TMZ is still an option although resistance is common at this point. Other alkylating agents might be used including carboplatin or lomustine (99). A slow-release chemotherapy wafers containing the alkylating agent carmustine (Gliadel wafers) could be placed inside the tumor bed intraoperatively for local release of the drug. Although FDA approved, this therapy carries a risk of serious side effects (99). A retrospective analysis of 6 clinical trials involving a total of 44 patients who received local carmustine plus chemoradiotherapy reported grade 3 or 4 adverse effects in 19/44 patients, including wound healing problems, intracranial abscesses, and seizures (100). In a literature analysis of 8 retrospective analyses (including the previously mentioned one), 2 Phase I/II clinical trials, and 1 observational study a survival advantage was documented for the use of carmustine wafers. However, the treatment caused grade 3 or 4 adverse effects in ~22% of the cases, including problems of surgical wound healing and neurological deficits (101).

In 2011 the US FDA approved yet another treatment modality for recurrent GBM and in 2015 it was approved for treatment of newly diagnosed GBM (102). This treatment modality is called tumour treating fields (TTF) (103). It consists of a device with number of electrodes connected to the patients' scalp delivering low intensity intermediate frequency alternating electrical fields to the tumour (103). This electrical current is meant to disturb the architecture of mitotic spindles in proliferating cells and induce mitotic arrest and cell death (104).

Despite the growing volume of research on GBM, the addition of TTF to the treatment protocol for GBM was the only major advancement during the past 15 years. Some molecular targeted drugs have shown promising results in preclinical research but have failed to improve progression free survival or overall survival in clinical trials. Examples

include an EGFR inhibitor gefitinib ((105), a selective integrin inhibitor cilengitide (106) and an mTOR inhibitor everolimus (107). The controversial results of molecular therapy are most likely due to intertumour/ intratumour heterogeneity, failure to reach therapeutic concentrations inside the brain or the presence of compensatory signalling pathways (51).

As mentioned above, bevacizumab, a monoclonal antibody against VEGF-A has only shown minimal survival advantage in clinical trials (108, 109), although was approved by the FDA for treatment of recurrent GBM (109). Attempts to combine it with other modalities are not very successful, since they lead to high rates of toxicity. One example is a phase II clinical trial (110) where combination therapy with TMZ resulted in no improvement of clinical outcome, quite the contrary, combination therapy resulted in serious haematological side effects in 33% of the cases including one death due to haemorrhage from severe thrombocytopenia, as well as neurological deficits in 86% of the cases (110). Other examples include combining bevacizumab with a PI3K inhibitor (111) or an HDAC inhibitor (112) and both combinations were ineffective and poorly tolerable.

Immunotherapy involves the utilization of the patient's immune system to fight the cancer (99). One way to accomplish this is by triggering an immune response against a specific tumour marker which is lacking in normal cells (99). An example of immunotherapy in GBM is the vaccine rindopepimut targeting the EGFR variant EGFRvIII that is expressed uniquely in GBM cells (99). The vaccine was successful in phase II clinical trials in inducing immunity against EGFRvIII positive GBM cells and eliminating them (99). More advanced clinical testing is needed to confirm its efficacy and safety.

Oncolytic viruses, suicide gene therapy, and immunomodulatory gene therapy are viral vector mediated therapeutic modalities that can be developed for GBM therapy, this was recently reviewed by our laboratory (113). Clinical studies on viral vectors for GBM therapy are mostly concerning safety at this stage (113).

From the previous, it is clear how far we still are from the ideal treatment protocol for GBM. Available chemotherapeutic agents carry significant toxicity. Scientists are continuously developing older treatment modalities including surgical techniques and trying innovative ones such as electrical therapy and photodynamic therapy (PDT). GBM treatment

is particularly challenging due to the biological characteristics of the disease including the location, the unique brain microenvironment, and the presence of the BBB. It is believed that the future of GBM treatment is a multi-modal individualized treatment protocol with surgery remaining the cornerstone of GBM therapy, not forgetting the role of supportive and palliative treatment in improving the quality of life (96).

1.1.9 Challenges in GBM treatment

The diversity in genetic and epi-genetic alterations is huge, leading to GBM tumours that are heterogenous, yet receive almost similar standard treatment. Different studies have reported that different tumour samples derived from one patient could fall into different TCGA subtypes depending on the site from where the sample is obtained (114, 115). Tumours classified together often respond differently to chemotherapy or radiation, and molecularly targeted drugs have not been successful in clinical trials mainly due to intertumoral or intratumoral heterogeneity.

The introduction FGS in GBM surgeries has maximized the extent of safe resection and has improved patient survival (116). However, total surgical resection is in most cases impossible because of the critical location of the tumour and its infiltrative nature. Infiltrating cells may extend beyond the contrast-enhancing mass, and they are often left behind despite maximum surgical resection (117). Scientists have successfully cultured GBM cells from brain tissue acquired from sites as far as 4 cm away from the main resectable tumour mass (118). All of this will ultimately lead to inevitable recurrence. **Figure 1.6.** recaps the main aspects of this challenging war against GBM.

Resistance to therapy by TMZ commonly develops, mainly by MGMT enzyme expression, which mediates a one-step transalkylation DNA repair reaction (119). Interestingly, although MGMT promoter methylation is the most important predictor of good TMZ response in GBM (119), some patients methylated MGMT promoter still don't respond to TMZ, or develop resistance eventually (120).

There are various ways by which GBM evade the effects of drugs such as TMZ. One interesting mechanism of resistance is via regulation of alternative pathways by long non-coding RNA (lncRNA) (121). Pengfei et al. utilized RNA microarray to compare expression of lncRNA between TMZ-sensitive and TMZ-resistant GBM cells (121). This was a paired comparison as the TMZ-resistant cells were developed from TMZ-sensitive cells following TMZ desensitization protocol (121). They found that lnc-TALC was overexpressed in resistant cells (121). The expression of lnc-TALC correlated to the degree of phosphorylation (activation) of Akt and STAT3 molecules involved in growth signalling and are commonly activated in TMZ-resistant GBM (121).

Another example concerns dehydroepiandrosterone (DHEA), a circulating neurosteroid that protects cells from stress-induced apoptosis (122). High levels of DHEA were detected in serum of GBM patients and that correlated with poor treatment response (122). Moreover, DHEA attenuated DNA damage caused by TMZ in MGMT-deficient astrocytes, inducing TMZ resistance (122). This effect was mediated by specificity protein-1 (Sp1) which was activated in presence of DHEA presumably facilitating DNA repair mechanisms (122).

The role of GSCs in therapy resistance is very well recognized but not well understood. It could be due to upregulation of mechanisms or shutting down apoptosis signals (123). Resistance could also be acquired following exposure to antineoplastic therapy (123). The stress produced by chemotherapy or radiotherapy, on GBM cells or GSCs, promotes Darwinian clonal selection which leads to survival of the toughest cells with the best adaptive mechanisms against therapy, resulting in resistant, more aggressive tumours (123).

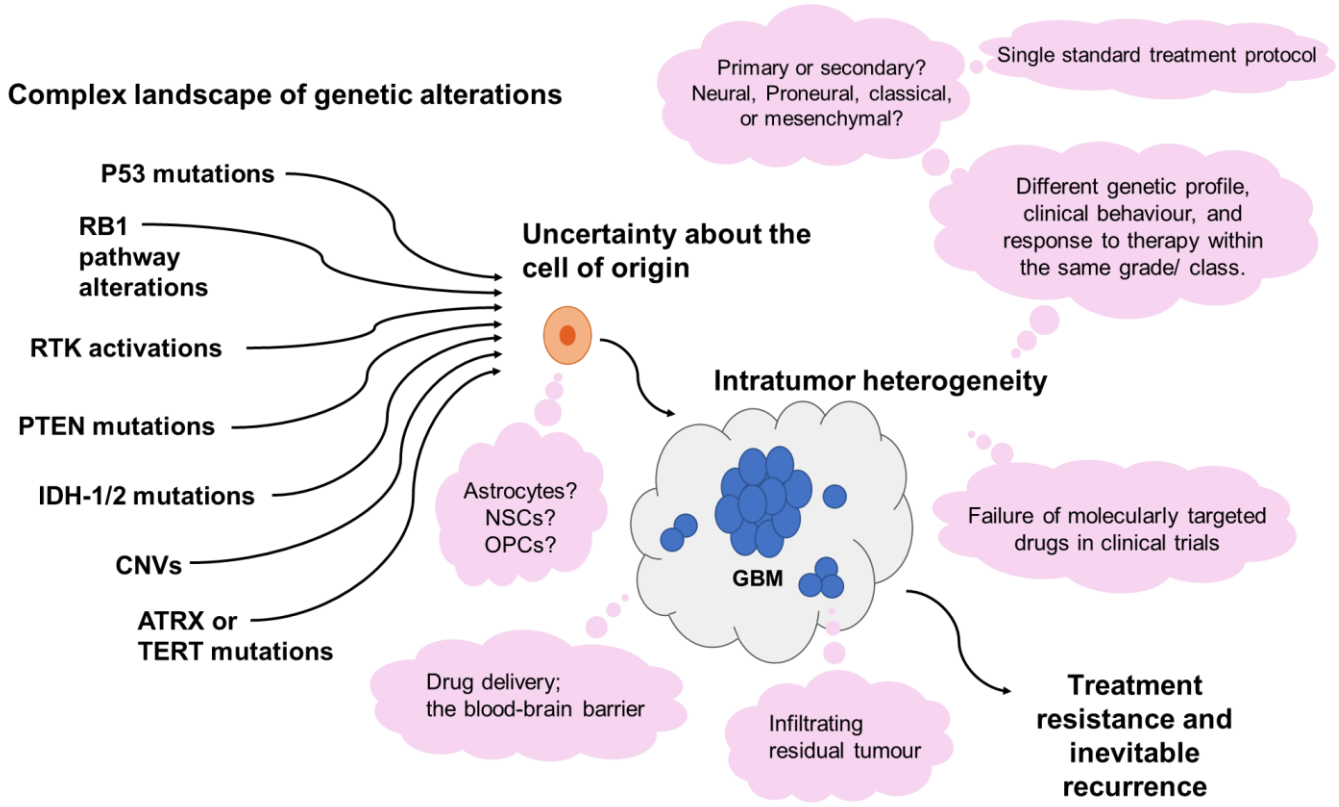

Figure 1.6. Challenges in GBM treatment.
CNV; copy number variation, NSC; neural stem cell, OPC; oligodendrocyte precursor cell.

Tumour heterogeneity is a complex problem that leads to recurrence and treatment failure. Genetic instability and the resultant tumour heterogeneity drive tumour adaptation allowing tumour cells to grow. Two models to explain tumour heterogeneity have been proposed (145). The Clonal evolution model supports the erratic genetic instability hypothesis, namely that during tumour progression, a cell micro-population acquires genetic or epigenetic modifications that are beneficial for its survival, these cells then proliferate and form a unique constituent of the tumour mass (145). Successive waves of similar incidents create a tumour mass containing subpopulations of cells with different molecular profiles and different biological behaviours (145). The other model, known as stem cell model, proposes that only CSCs can self-renew, proliferate, and initiate diverse subclones within the same tumour, which have different molecular profiles from the mother stem cell (145). Clonal evolution model correlates more to intratumour heterogeneity, while stem cell

model correlates more to intertumour heterogeneity (145). Clonal evolution is the key to the development of resistance. Unfortunately, the most powerful stressors to induce genomic or epigenetic alterations in tumour cells are surgery, chemotherapy, and radiotherapy (143). It follows that although we successfully destroy some of the cells by the therapy, those which survive are theoretically the toughest according to natural selection laws (143). These cells start a focus of recurrence, more aggressive and resistant to treatment than the initial tumour (143).

Comparative gene analysis of different GBM samples has been used to study GBM heterogeneity. Different cells obtained from the same tumour mass have shown different EGFR and PDGFRA gene profiles and responded differentially to ligand stimulation and chemical inhibition (124). A key study on intratumoural heterogeneity was published in 2013 by a group of scientists from the University of Cambridge (115). They used Florescence-Guided Multiple Sampling technique to extract 4-6 samples from the individual tumour from 11 different patients. Samples were at least 1 cm apart and were labelled according to the depth they were situated at in the tumour mass. Profiling of DNA copy number revealed copy number alterations (CAN) detected in some samples but not others from the same tumour mass (115). These CANs involved common GBM driver genes including EGFR, PDGFR, and PTEN. Moreover, heterogeneously altered genes were found to be related to the same biological process, suggesting that during tumour growth, a subset of cells experience some environmental challenges unique to them due to their location within the tumour and modify their DNA to survive and overcome these challenges.

A study by Smith SJ et al. evaluated expression of stemness markers, along with other parameters, in different samples taken from different tumor locations in 14 patients during FGS (125). Core samples were taken from the deep enhancing tumour, rim samples were taken from rim enhancement and invasive tumour samples were taken from 5-ALA-positive region beyond the tumour enhancement delineated by MRI (125). Array PCR studies revealed high variability of stem cell marker expression between different tumour sites suggestive of polyclonal heterogeneity and consistent high expression of certain markers in invasive samples, which is suggested to be functionally related to radio and chemoresistance (125).

Evolution and survival of cancer cells is influenced by their immediate microenvironment, which modulate gene expression patterns in cancer cells or CSCs, resulting in tumour heterogeneity (126). Gillies et al. described tumour heterogeneity as being either spatial or temporal (127). Different tumour cells encounter different microenvironmental stressors due to their different spatial relationship to the TME, resulting in subpopulation of cells, each one carrying a distinct genomic profile that ensure their survival against the type of stressor they have encountered (127). Temporal heterogeneity on the other hand is exemplified in recurrent tumours that exhibit different, often more aggressive, molecular profile than the initial tumor due to selection pressure on the residual cells induced by therapy (127).

Johnson et al. performed mutational analysis on initial tumours and compared them to matched recurrent tumors in 23 GBM patients (126). They reported that recurrent tumours had only 54% similarity with the parent tumour in the mutational profile (126). IDH-1, p53, and ATRX mutation statuses were found to be preserved in the two groups, suggesting a pivotal role for these mutations in the development of the tumour (126).

Drug delivery and retention at the tumour site is a major issue in neuropharmacology due to the presence of the blood brain barrier (BBB). Surprisingly, it was reported that less than 20% of plasma TMZ concentration is found in the brain tissue (128). On the other hand, gefitinib, a drug that has shown no success in clinical trials, had 30 times higher concentration in brain tissue than in blood (128). Thus, understanding drug distribution in the CNS is another complicating factor in GBM therapy leading to treatment failure.

In summary, modern medicine faces multiple very difficult problems which have to be addressed in order to improve the outcomes for GBM patients. Molecular diversity and biological features of GBM require application of novel strategies and ideas.

1.2 Photodynamic therapy in GBM

1.2.1 Definition of photodynamic effect

A photodynamic effect may be defined as an effect of light on the atomic dynamics of a chemical substance in the presence of oxygen, leading ultimately to the production of reactive chemical species (129). This effect can be used to induce damage to biological structures such as abnormal cells or microorganisms. This is a concept known as photodynamic therapy (PDT) (129). The ultimate goal of PDT in cancer treatment is to destroy cancer cells without significantly affecting the surrounding normal tissue. PDT involves the use of a non-toxic substance, called a photosensitiser (PS), that preferentially affects or accumulates in the target cells and only produce toxicity upon activation with light delivered to that specific area (130). Oxygen is a crucial requirement for the traditional photodynamic effect and the formation of reactive oxygen species (ROS) (130).

1.2.2 Development of the concept of photodynamic therapy

Since ancient civilizations, light has been used to treat skin disorders. The beginning of the 20th century demarcates the establishment of a scientifically founded case for the use of light for therapy (131). **Figure 1.7** illustrates the main developments in the photodynamic therapy field since the beginning of the 20th century to date. PDT naturally evolved from attempts to use light to treat skin diseases and malignancies. The development of Hematoporphyrin derivatives (HPD) in 1955 by Samuel Schwartz, and later the refinement of the molecule by Richard Lipson were considered a big step forward in PDT research (131). HPD, chlorin derivatives (e.g. temoporfin and talaporfin sodium), Benzoporphyrin derivative, and 5-ALA were later identified as photosensitisers and were used (and some are approved- see **Figure 1.7**) for diagnosis or treatment of many types of cancer including bladder cancer, oesophageal cancer, and GBM (131). Regarding GBM, the first attempt to use PDT against GBM date back to the 1970s, but there has been no major breakthrough in application of this technology until the utilization of 5-ALA in FGS was approved in 2007 after proving effectiveness in improving surgical resection and OS (116). As for therapy, many in-vivo and clinical studies have utilized PDT for treatment of GBM but the results were controversial

due to technical matters or occurrence of toxicity (132). This will be discussed more in the following sections.

1.2.3 Mechanisms of photodynamic induced toxicity

During light application, PS molecules absorb light and transform from the ground state to the excited singlet state (129). This state is short lived and soon the electrons excited within the molecule go back to ground state and the energy is released as florescence or heat as shown in **Figure 1.8**. Sometimes, randomly, molecules transform into an excited triplet state (129). This state is relatively longer-lived than the excited singlet state. The excited triplet PS molecule can **either** directly react with the surrounding cellular organic substrates to form reactive radicals that can themselves react with oxygen and generate ROS, namely, superoxide anions or hydrogen peroxides, **or** transfer its energy to oxygen and excite it to form the highly reactive singlet oxygen (129). These two possibilities are known as type I and type II photodynamic reactions, respectively **(Figure 1.8)**. The ROSs produced by both types of reactions have detrimental effects on cellular health and commonly leads to apoptosis. Both types of photodynamic reactions can occur simultaneously, the overall direction of the reaction depends on many intermingled factors such as the type of PS, the site of its accumulation, availability of oxygen and others (130).

Photodynamic reactions induce cell toxicity in one of three ways: induction of necrosis or apoptosis in cells by direct interaction between reactive species and cell components, indirect induction of necrosis or apoptosis as a result of local hypoxemia produced by local vascular constriction or thrombus formation (induction of coagulation), or indirect induction of necrosis or apoptosis due to activation of intense local inflammatory response and infiltration by immune cells (133). Because the photo-induced oxygen species are highly reactive, they react instantaneously with organic substances (e.g. amino acids, lipids, or DNA molecules) that are in close proximity to their site of production (130). Therefore, they have ultra-short half-lives of nanoseconds to microseconds (132). This is advantageous for clinical PDT application, since the toxic effect is expected to be confined to a radius of less than 20 nm from the site of PS generation (130).

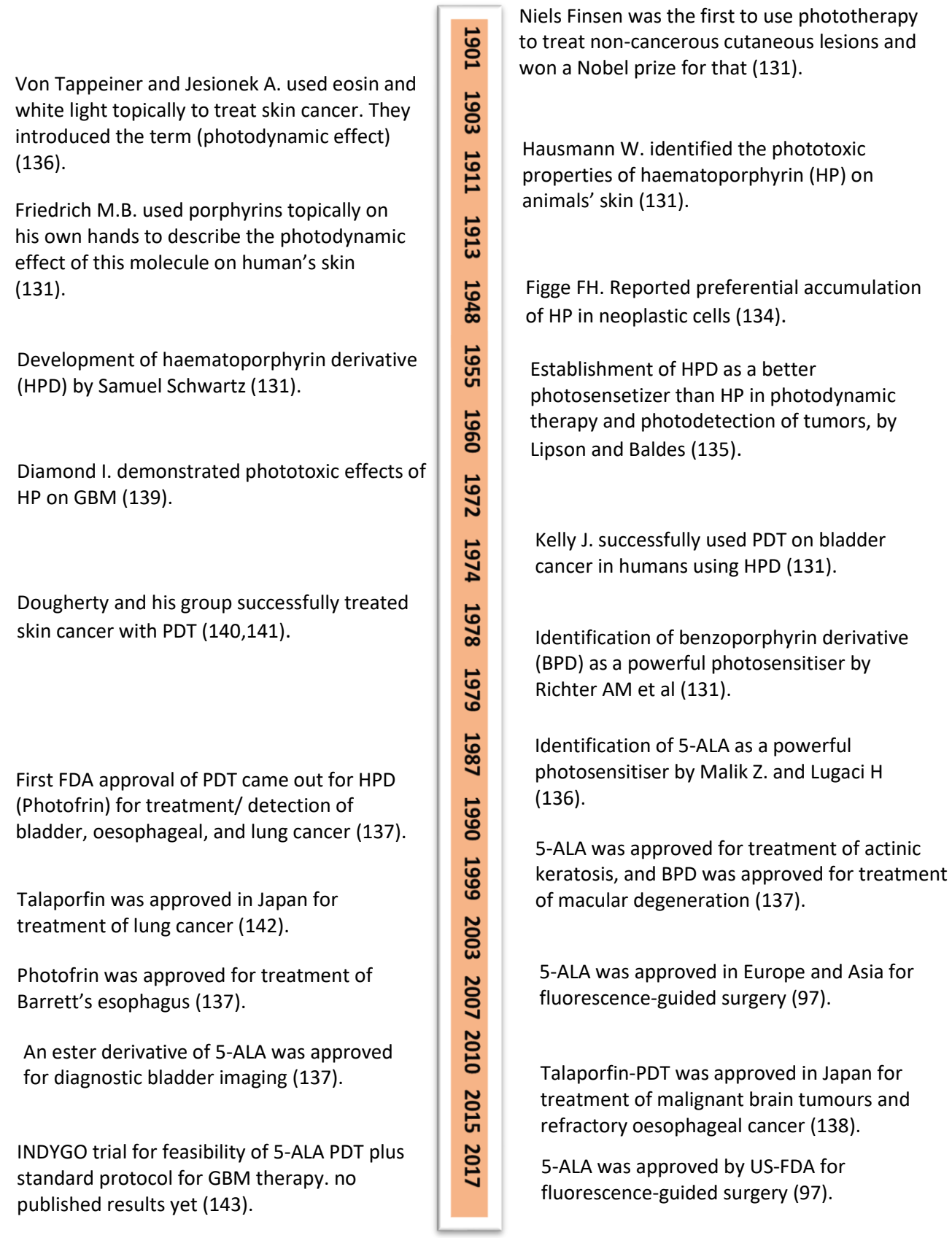

Figure 1.7. Timeline of the most important milestones in the development of PDT for cancer. References (97, 131, 134-143)

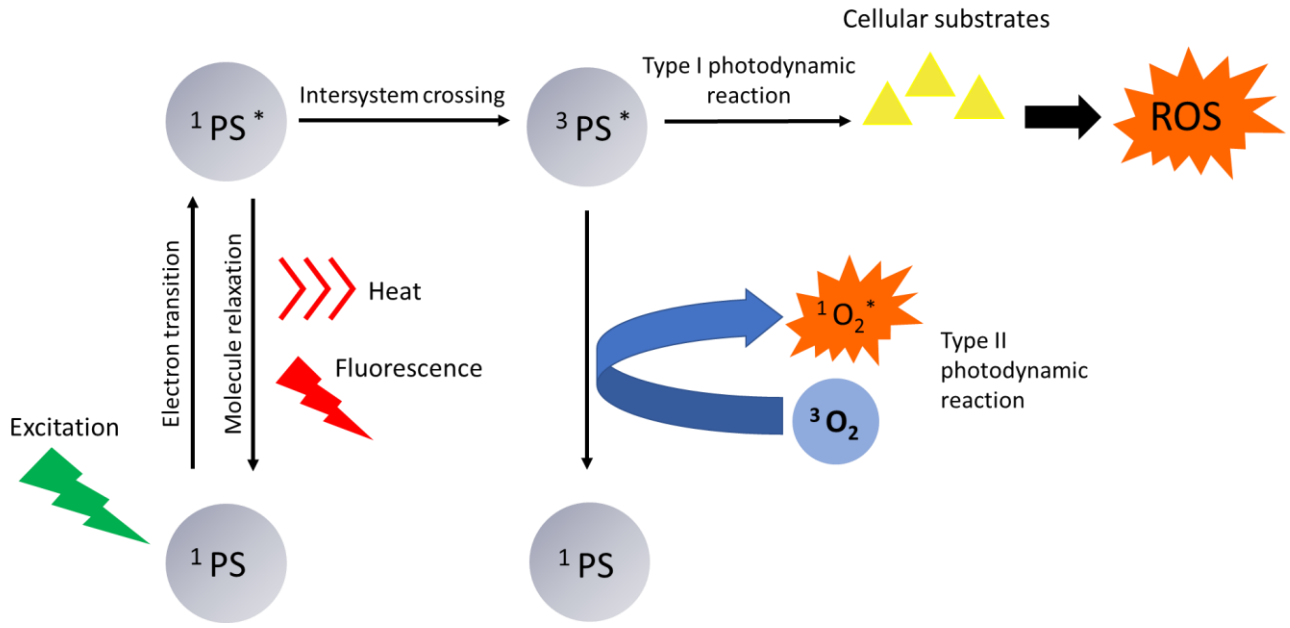

Figure 1.8. Graphical representation of the basic mechanism of Photodynamic reactions. ^{1}PS: PS molecule in ground singlet state, $^{1}PS^{*}$: PS molecule in excited singlet state, $^{3}PS^{*}$: PS molecule in triplet excited state, $^{3}O_2$: triplet ground oxygen, $^{1}O_2^{*}$: singlet excited oxygen. Adapted from (132).

1.2.4 Elements of PDT: photosensitizers and light sources

For successful PDT 3 principal elements are required: a photosensitizer, light source, and oxygen. It starts with the administration of a non-toxic PS that should localize and accumulate inside target cells. PS needs to be illuminated by light at specific wavelength from a light source. When the absorbed light photons excite the PS, ROS are generated via either one of two photodynamic reaction (see **Figure 1.8**). The ideal PS must [1] be naturally occurring and easily purified or easily synthesized, [2] be easily administered, stable and soluble in tissue fluids, [3] specifically target cancer cells, [4] have no toxicity on cells except when light is applied, [5] have high ROS yield, [6] have an excitation wavelength that has a good tissue penetration property (137). Some of the problems of the currently used PSs arise from their lipophilic nature and their consequent tendency to form hydrophobic aggregates in aqueous solutions, which compromises their distribution and delivery to target sites, hinders their effectiveness by reducing the quantum yield of ROS, and

complicate their use in clinical practice (144). On the other hand, highly hydrophilic PS will not penetrate the cell membrane and will not accumulate inside target cells. Therefore, an ideal PS must be amphiphilic with both hydrophilic and hydrophobic moieties for better solubility and diffusion (144).

Most of PS used in research and diagnostics are naturally occurring substances (or their derivatives) that have tetrapyrrole aromatic centre in their chemical structure (130). Some non-tetrapyrrole naturally occurring dyes ,like curcuminoids, are known for anti-microbial rather than anti-cancer PDT (130).

PS may be classified into first, second, and third/ new generation PS (137, 145). First generation PS are Hematoporphyrin (HP) and its derivatives HPD. The best known HPD is Porfimer sodium (Photofrin®). HPD have high ROS quantum yield, and they are the first group of photosensitizers to be studied in research. However, apart from the presence of hematoporphyrin oligomers, the exact chemical structure of the side chains is still not clear (130). Moreover, this group of PS have poor selectivity to cancer cells, prolonged half-life causing long-lasting skin sensitivity where they accumulate (130). All these drawbacks prompted the need to develop PS with better characteristics.

Second generation PS are a big category which includes chlorins and benzoporphyrin derivatives (e.g. Talaporfin sodium, BPD-MA, and temoporfin), pheophorbides, bacteriopheophorbides (e.g. Tookad), phthalocyanines, texaphyrins, and protoporphyrin IX (PpIX) inducing compounds (e.g. 5-ALA), plus other molecules designed around a porphyrin or chlorin core (137, 145). They are theoretically superior to first generation PS. In general, they have improved chemical purity, better localization, and less skin photosensitivity. In clinical studies, they are often excited with red light at ~630 nm (132). This wavelength might be better penetrating in brain tissue, but long wave photons carry much less energy than green or blue and very inefficient in exciting the most commonly used PS, 5-ALA, as the optimum excitation wavelength for these PS is between ~400-440 nm (116). On the other hand, red photons easily release their energy as heat, thus predisposing the surrounding normal tissue to heat injury and necrosis (132).

Third generation is an emerging category of PS. They were developed be conjugating first or second generation PS with a carrier for targeted delivery (144). Researchers have been trying conjugation with different carriers such as albumin, liposomes, and nanoparticles to prevent aggregation of the PS, and to ensure better delivery and accumulation in target tissue (129, 145). Engineered multifunctional nanoparticles that can recognize specific GBM-related surface moieties, which might increase PS concentration in target cells, and/or increase production of ROS have been successfully developed and tested with promising results (144). However, most of the development of potential PS for GBM was performed in-vitro using one particular GBM cell line, U87-MG (144). This is a very old line with a huge burden of de-novo mutations and unclear degree of similarity to the in situ GBM cells in a human brain. Taking into consideration the intertumoural and intratumoural GBM heterogeneity, future work must include more cell lines, primary GBM cells, and most importantly *in-vivo* models.

Light in the PDT protocols may be delivered by two approaches. In interstitial PDT (iPDT) optic fibers are inserted with radiographic guidance into the tumour mass itself, thus, light is applied directly into the tumour tissue in cases where the resection is not an option. In other cases “open” or “cavity” illumination (oPDT or cPDT) is employed, when the light illumination is carried out after surgical resection either directly into the resection cavity or via an inflatable cavity balloon filled with light diffusing solution (117, 146). iPDT is developed as a therapy option for unresectable tumours, and to overcome the problem arising from poor penetration of light in brain tissue, by directly applying light into the tumour mass. The use of multiple cylindrical light diffusers in iPDT is thought to further improve light delivery to tumour areas and was implemented on non-resectable GBM tumours for photodynamic therapy with 5-ALA (147, 148). These studies suggested a possible therapeutic effect of this treatment modality, although outcome depended largely on initial 5-ALA accumulation which was heterogenous across patients. A laser device have been developed, by Modulight (Finland), with the aim to ensure even distribution of light inside tumour mass via the use of multiple optical fibres which emit light laterally. Multiple channels could be arranged according to the tumour size. The same device can also be used to monitor fluorescence of the tissue and even temperature.

Light sources can be either non-coherent (e.g. light emitting diodes; LED) or coherent (e.g. laser light) (132). The type of light source per se does not affect the outcome of PDT, yet laser light is superior to LED because it can be delivered through fine optic fibers which can be inserted into the brain tissue for iPDT (132). The most important factors related to the use of light, which can affect the outcome of PDT are, excitation wavelength and the total dose of light (149). Longer wavelengths tend to penetrate deeper in the tissue reaching for deeply situated tumour cells (149). A range of wavelengths from 400-800 nm is usually studied for PDT (149). Wavelengths of less than 400 nm should be avoided for their poor tissue penetration, while wavelengths of more than 800 nm bare a huge risk of strong thermal effect (132). As mentioned before, for the sake of further tissue penetration, many of previously tested PS were excited with wavelengths between 600-700 nm (145). Yet when 5 different wavelengths were tested for their singlet oxygen yield, It was found that the quantum yield of singlet oxygen is the greatest at wavelengths 488, 510, and 532 nm, and very low at 578 and 630 nm (150). Thus, higher efficacy of shorter wavelengths could compensate for the poorer penetration. In the majority of biological tissues, light energy drops very rapidly, being only a small fraction of the initial power at 5 mm of depth, and essentially zero at 1 cm (149). It follows that the optimum wavelength for excitation might be somewhere in between the far red and deep blue light in the green part of the spectrum (530-560 nm) but the type of tissue and the mode of delivery of the PDT (iPDT or o/cPDT) also need to be taken into account (132).

1.2.5 Photodynamic therapy in the management of GBM: diagnostic and therapeutic applications

The use of advanced imaging techniques, like magnetic resonance imaging (MRI) or positron emission tomography (PET), has a major role in the diagnostics and pre-surgical evaluation of GBM cases (44). FGS is one of the relatively recent imaging techniques used intra-operatively to facilitate maximum tumour resection (149). It is unique for being simple in application yet very efficient in delineating the tumour territories and allowing real-time tracking of the tumour margins at macro level. The use of 5-ALA for FGS has been popular in clinical practice especially after the results of the randomised phase III clinical trial by

Stummer and his group were published in 2006 (116), which led to its approval by the FDA in 2007 in Europe and later in USA in 2017 (97). With the help of 5-ALA guided surgery, total resection was achieved in 65% of GBM patients, which significantly improved their progression-free survival (116). Up to date, PDT for GBM treatment is still in clinical trials. INDYGO is an example of a clinical trial addressing the feasibility and efficacy of intraoperative cavity PDT, after tumour resection (143). PDT is planned to be delivered using a cavity illumination with an inflatable balloon, filled with a diffusing solution, to house multiple light diffusers for more uniform light distribution within the resection cavity (143, 146). The trial is in the active phase now and no results are published yet. The main 4 PSs under investigation are: hematoporphyrin derivative (porfimer sodium or Photofrin©), 5-ALA (Levulan© or Gleolan©), talaporfin sodium (NPe6 known also as Laserphyrin©), and meta-tetra(hydroxyphenyl) chlorin (mTHPC known also as temoporfin or Foscan©) (144).

Porfimer sodium (Photofrin©) is a first-generation PS derived from hematoporphyrin by acid purification (151). It is injected intravenously and has a strong excitation at wavelength 400 nm (152). Post-operative photofrin-PDT with cavity illumination proved to be tolerable for glioblastoma patients, however, this series of studies and clinical trials conducted by Muller and Wilson did not report any survival benefits in test arm compared to surgical resection alone (153). They suggested that this might be due to low illumination light power and suggested the use of higher light dose in future. Nevertheless, consequent research have shown poor qualities of photofrin as a photosensitiser, such as poor chemical purity, nonspecific accumulation in normal cells, and prolonged skin sensitivity (117, 145, 154, 155), and the focus has shifted towards the radio-sensitizing property of the molecule in radiodynamic therapy rather than its photodynamic effect (151).

5-ALA (Levulan© or Gleolan©) is a pro-drug that is not florescent itself. It is the natural precursor of protoporphyrin (PpIX) in the heme synthesis pathway. After the administration of 5-ALA, PpIX accumulates preferentially in GBM cells due to their deficiency in the enzyme ferrochelatase that converts PpIX into heme. PpXI is florescent and it may act as a PS. It absorbs light in the range of 375-440 nm and emits light in the range of 640-710 nm (156). 5-ALA carries the advantage of being orally administered with high bioavailability (149). It is also very convenient to carry out 5-ALA PDT right after 5-ALA FGS, which is now a well-established practice in GBM surgeries (149). In a recent study by Schipmann et al., 5-

ALA FGS was combined with 5-ALA PDT in 20 recurrent GBM patients (154). This treatment approach, although well tolerable, resulted in no improvement in PFS, which was reported to be 6 months (154), while the expected survival in recurrent GBM is 5-7 months (157).

Three small scale clinical studies were conducted to evaluate the efficacy and safety of 5-ALA mediated iPDT in non-resectable GBM (147, 148, 158). They have utilized mathematical modelling software to design their illumination protocols. Authors reported adequate illumination of the tumour mass by using several fiber-based laser light diffusers that were stereotactically placed inside the tumour mass and emitted light at a wavelength of 633 nm (147, 148, 158). As mentioned above, PpXI, which is the product of 5ALA conversion, absorbs photons best in the deep blue part of the spectrum (420-430 nm), and the use of 633 nm laser light seems odd. In fact, photons of long wavelengths carry much less energy which inevitably makes them less efficient in triggering photochemical reactions. This might explain the lack of clear survival advantage reported in these studies.

One of the three studies utilized their protocol to evaluate intertumour heterogenous uptake of 5-ALA during 5-LAL-iPDT (148). Live intraoperative spectroscopic measurements of 5-ALA fluorescent intensity were obtained before and after photoactivation, and at least three tissue samples were taken from each patient from different tumour areas before photoactivation to measure 5-ALA tissue concentration (148). Results revealed high pre-illumination fluorescent intensity coinciding with high tissue concentration of 5-ALA in three patients, low fluorescent intensity occurring despite high 5-ALA tissue concentration in one patient, and low florescent intensity coinciding with low tissue concentration in one patient (148). Photoactivation was carried out for all patients regardless of the fluorescent intensity. The three patients who exhibited higher florescent intensity survived longer (at least two years) than the other two patients who died after 3 or 9 months from the time of the procedure (148). Even though this suggest some benefit, the sample size was much too small to draw any conclusions. Nevertheless, the sample was sufficient to demonstrate three different patterns of 5-ALA uptake among GBM tumours. This heterogeneity in 5-ALA uptake could explain the variability in treatment response to PDT.

5-ALA was successfully implemented in purifying infiltrating GBM cells from the margins of the tumour by developing 5-ALA-based metabolic cell sorting (65). Smith et al.

have obtained samples from different tumour regions from a total of 11 GBM patients who underwent 5-ALA FGS. Samples were taken from the central 5-ALA enhancing region (core samples), the peripheral 5-ALA and gadolinium-enhancing areas (rim samples), and from 5-ALA enhancing tumour peripheries that are beyond gadolinium enhancing regions (invasive zone) (65). Invasive samples were then stratified using FACS against 5-ALA fluorescence into 5-LAA enriched true infiltrative cells and 5-ALA negative cells (65). This method of isolating infiltrative GBM cells from non-neoplastic parenchyma is novel and valuable in representing true molecular profile of infiltrative cells which are important targets in molecular therapy (65). In fact, the study group have reported a significant difference in expression of 78 genes between the 5-ALA enriched and 5-ALA negative cells (65).

Talaporfin sodium (Laserphyrin®) is a second-generation PS derived from chlorin structure with peak excitation wavelength at 412 nm (159). In a phase II clinical trial (160) involving 22 patients with primary malignant brain tumours, 13 of whom where GBM cases, subjects received intravenous talaporfin 1 day prior to surgery. Next day, they were treated with intraoperative cavity PDT carried out after maximal safe tumour resection and followed by standard treatment protocol. 100% of the GBM study cohort were free of recurrence at 6-month follow up and survived for at least one year after talaporfin-PDT combined therapy (160). The PFS and OS were 12.0 and 24.8 months, respectively (160). This was interpreted as a promising outcome and talaporfin-PDT was approved in Japan for treatment of primary brain tumour as an adjuvant therapy (138). A follow up analysis of the long-term outcome of the previous trial was published in 2019 (138). This analysis also included GBM patients who enrolled in the post-therapy surveillance, increasing the total sample size to 30 cases. The results of talaporfin-PDT were compared to 164 control cases diagnosed and treated with standard treatment protocol during the same period of the trial (138). PFS was 19.6 months in PDT group compared to 9 months in control group, and the OS was 27.4 months in PDT group compared to 22.1 months in the control group (138). Thus, it is possible that this protocol, if developed further could increase the quality of life of patients which had to undergo GBM surgical removal.

Meta-tetra(hydroxyphenyl) chlorin (temoporfin or Foscan®) is a second generation PS with significant cell specificity to tumor cells (145). It has a peak excitation wavelength at 400-440 nm (161), and was extensively studied for treatment of head and neck tumours,

colorectal cancer, and dermatological diseases (145). In two independent small clinical trials including newly diagnosed and recurrent GBM cases, temoporfin-PDT was delivered in form of intraoperative cavity irradiation after tumour resection (162, 163). Post operatively, all groups of patients (treatment and control) received the standard chemotherapy and radiotherapy. Results of the two studies are conflicting. One reported a significant improvement of overall survival by 5.5 months in treatment compared to control arm (162), the other reported weak evidence of survival advantage (wide range for confidence interval) (163). Moreover, some serious PDT-related adverse effects (including two deaths) were reported in one of the two studies (163).

In conclusion, a key factor for GBM recurrence are infiltrating GBM cells, and PDT could be a promising modality to locally destroy these residual cells. PDT for GBM is a work in progress and the development of good PS is a cornerstone of its success. Studies have reported what looks like promising clinical outcomes using second-generation PS, however, the small sample size, the development of toxicity, and some technical issues related to light illumination make it hard to draw clear conclusions as to the feasibility and effectiveness of current PDT protocols tested against GBM. I hypothesize that TMRM – a dye commonly used to visualize mitochondria- is a safe and effective photosensitizer in inducing death in GBM cells, and that it has better spectral properties than other photosensitizers used in the field.

1.3 Repurposing of Antidepressants for GBM Therapy

1.3.1 Concept and examples of drug repurposing in GBM

The idea of drug repurposing implies the use of the existing FDA-approved drugs for new applications (164). It is related to the concept of poly-pharmacology which is defined as use of a drug for multiple diseases rather than one drug for one disease (165). These concepts are based on the fact that most, if not all drugs have multiple cellular and molecular targets and affect a variety of biological pathways (165). The development of new therapies is desperately required to tackle GBM and drug repurposing might be a fast-track strategy.

There is epidemiological evidence supporting the statement that the use of antidepressants decrease the risk of many types of cancers including colon cancer (166), hepatocellular carcinoma (167), and GBM (168). A very interesting in-silico study matched the molecular classification of GBM to the best candidate drugs for repurposing, based on the genetic and phenotypic profile of GBM and the drugs' known molecular targets (169). Using artificial intelligence programs, antipsychotics were identified as best candidates for repurposing in classical, proneural, and mesenchymal subtypes, but second to best in neural subtype. Blood lowering drugs were among the top 5 drug candidates for repurposing in all subtypes except mesenchymal GBM. Antidepressants and protein kinase inhibitors were among the top 5 ranked candidates in all four GBM subtypes. The study has also uniquely prioritized imipramine as a candidate drug for repurposing in proneural GBM. A more recent study used a robotic platform to perform concentration/ response analysis of the effect of 167 FDA approved drugs with variable molecular targets and good brain tissue penetration, on the growth of GSCs (170). Twenty-two candidate drugs were identified which led to a concentration-dependent growth inhibition on GSCs, 4 of which were neuropsychiatric drugs. The list included anti-psychotics Divalproex and Brexpiprazole, an anti-migraine drug Rizatriptan, and the anticholinergic Alzheimer's medication Trihexyphenidyl (170). These drugs (except the last) are already in different stages of clinical or pre-clinical research as candidates for repurposing for GBM therapy (170).

The blood lowering drug metformin, the lipid lowering drug mevastatin, and the antimalaria drug chloroquine, along with antipsychotics and antidepressants, are among the most notable drugs in GBM repurposing research literature (164). Although these drugs have been reported to be effective against cloned GBM cells in vitro, the research methodology of these studies are criticised for using much higher, than biologically relevant concentrations, using old commercially available cell lines, rather than those obtained recently from patients and/or the lack of well-matched controls (164). Moreover, different research groups propose different mechanisms of action to explain the anti-GBM effect of the same drug, which further weakens the scientific argument.

1.3.2 Repurposing of Antidepressants for GBM treatment

As mentioned in the previous section antipsychotics and antidepressants have been suggested as potential drug classes for re-purposing (164, 169, 170). These drugs have well-studied pharmacokinetics including ability to cross BBB and an already established safety profile (164). Moreover, these medications are anyway being prescribed to some patients against depression or anxiety, which are common co-morbidities with cancer, especially very aggressive forms such as GBM.

In 2005, Barak et al. have found significantly lower incidences of cancer among schizophrenic patients compared with the general population (171). This has opened the door for other epidemiological studies to examine the correlation between psychiatric illnesses and the development of cancers in general, and brain cancer in particular. Two matched case-control studies, with minimal differences in methodologies, have reported an inverse association between the use of tricyclic antidepressants (TCAs), but not selective serotonin reuptake inhibitors (SSRIs), and the risk of development of glioma tumours including GBM (168, 172). Although this association was not proven to be statistically significant, there was a trend in both studies towards decreasing glioma incidence with prolonged exposure to TCAs.

Two well-known antidepressants are imipramine (IM) and clomipramine (CL), which chemically are tertiary amines. IM has been approved for treatment of depression long time

ago. Although it is no longer the first line for treatment of depression, it is still used to treat severe melancholic and psychotic depressions, nocturnal enuresis in children, and neuropathic pain (173). Antidepressant effect of IM is usually ascribed to the blockade of the reuptake of monoamines (e.g. serotonin and noradrenaline), thus increasing their extracellular concentration or enhancing signalling via their cognate receptors. IM also blocks some ''off-target'' receptors (e.g. histamine and muscarinic receptors) producing anti-histaminic and anti-cholinergic side effects (173). On the other hand, CL is approved for the treatment of anxiety and obsessive-compulsive disorder (OCD) and is the most potent of all TCAs in terms of blocking serotonin reuptake (174). CL has been reported to have a pro-apoptotic effect on cancer cells via its action on mitochondria (175). A study by Z Xia et al. published ~ 20 years ago, reported reactive oxygen species (ROS) accumulation, caspase 3 activation, and induction of apoptosis in acute myeloid leukaemia cells following IM and CL treatment (175), and studies on GBM cells have come to similar conclusions (see **Table 1.2**). Imipramine's toxicity to GBM cells is believed to be mediated by induction of autophagy rather than apoptosis (176).

Fluoxetine (FLX), a specific serotonin reuptake inhibitor (SSRI), is an FDA approved drug for treatment of depression, obsessive compulsive disorder, panic disorders, and bulimia (177). Fluoxetine rather selectively blocks reuptake of serotonin, increasing serotonin mediated signalling (177). The anti-cancer effect of fluoxetine is usually explained by 'induction of apoptosis', following cellular calcium overload and mitochondrial disfunction. Fluoxetine is thought to increase intracellular calcium by activating α-amino-3-hydroxy-5-methyl-4-isoxazolepropionic acid (AMPA; ionotropic glutamate receptors which are over expressed in GBM cells), or by triggering endoplasmic reticulum stress response (178, 179). Fluoxetine has also demonstrated synergy with TMZ and radiotherapy (179-181).In contrast, a negative effect of imipramine treatment on sensitivity of GBM cells to TMZ has been described (182). Fluoxetine treatment successfully reversed concomitant neuropsychological problems, such as depressive behaviours and anxiety, in GBM mouse models following radiotherapy and chemotherapy (183, 184). A number of studies where the effect of antidepressants on GBM cells was studied are summarized in **Table 1.2.**

Table 1.2. summary of studies on the effect of antidepressants IM, CL, and FLX treatment on GBM. RT: radiotherapy, h: hours. Study findings irrelevant to the topic are not discussed in the table.

Drug	Cell type	Treatment plan	Key findings	Reference
IM and FLX	C6 rat glioma cells	1 or 5 µM for 1 or 5 days	Induction of a DNA fragmentation pattern related to apoptosis.	(Spanova et al., 1997) **(185)**
IM, CL, and FLX	C6 rat glioma cells	100 nM for 48h followed by 10 µM serotonin	↑ serotonin-dependant intracellular calcium mobilization. (FLX did not show similar results).	(Muraoka et al., 1998) **(186)**
CL and FLX	C6 rat glioma cells	6-50 µM for 4 or 24h	Detection of fragmented apoptotic DNA. ↑ caspase 3 and cytochrome c. (IM did not show similar results). Effective concentration: CL 25 µM, FLX 50 µM.	(Levkovitz et al., 2005) **(187)**
CL	Primary GBM cells	1-228 µM for duration range 1h-24h	↓ Oxygen consumption (inhibition of cellular respiration). ↑ caspase 3 activity. Effective concentration: starting at 114 µM	(Daley et al., 2005) **(188)**
CL	5 different primary GBM cell lines	20-100 µM for 6 hours	More apoptotic cells detected by Annexin V/ flowcytometry. Induction of intrinsic apoptosis pathway. Suggestions of calcium involvement. Effective concentration: staring at 60 µM.	(Peregrin K and Pilkington GJ, 2006) **(189)**
CL	HGG cell line (at passages 46-50)	250, 500, 750, and 900 µM OR dexamethasone pre-treatment + 500 µM	↓ Oxygen consumption rate indicating inhibition of cellular respiration (OCR was measured in different time points in the 20 minutes following addition of treatment). Effective concentration starting at 250 µM	(Higgins SC and Pilkington GJ, 2010) **(190)**
IM	U-87MG and C6 glioma cells	60 µM for 24h	Cell death and decreased clonogenicity. Inhibition of Akt-mTOR signalling. Induction of autophagy, but not apoptosis. ↑ LC3 expression (marker of autophagy). Autophagy is Beclin-1 dependent.	(Jeon SH et al., 2011) **(191)**
FLX	C6 rat glioma cells	10 µM for 24 or 72h	Gene profile suggestive of increased cAMP signalling: upregulation of Gsα and downregulation of Gαi2 gene expression. Upregulation of Bcl-xL gene expression indicating apoptosis inhibition.	(Choi MR et al., 2011) **(192)**
FLX	C6 rat GBM and U87MG, GBM8401, and Hs683 human GBM cell lines	0-30 µM for 24h	↑ transmembrane calcium influx associated with AMPAR activation. Induction of intrinsic apoptosis pathway. ↓ tumour growth in nude mice. Effective concentration: 25 µM in-vivo Effective dose in-vivo: 10 mg/kg	(Liu KH et al., 2015) **(178)**
IM	*In-vitro:* LN71, LN229, and LN443 human GBM cell line *In-vivo:* gliomagenesis mice models	*In-vitro:* 20 or 40 µM for 24, 48, or 72h *In-vivo:* 40 mg/kg/day	Induction of autophagy. ↑ LC3 expression (marker of autophagy). Associated with ↑ cAMP. Prolonged survival of treated tumour-bearing animals. Less expression of proliferation marker Ki67 in tumour samples. Effective concentration: 40 µM.	(shchors et al., 2015) **(176)**

	(defective p53 and HRas)			
FLX	T98G, U138, SF767, and U251 glioma cell lines, with high MGMT expression	1-30 µM for 6, 12, 24, 48h +/- TMZ	Reduction of MGMT expression with 1 µM FLX. FLX sensitized glioma cells to TMZ: no inhibition of colony formation when given at 10 µM except in combination with TMZ. Down regulation of NF-κB signalling.	(Song T et al., 2015) **(180)**
FLX	C6 rat glioma cells	10 or 20 µM for 24h +/- TMZ	Inhibition of growth. Induction of apoptosis via endoplasmic reticulum stress-induced apoptosis pathway. Synergy between FLX and TMZ. Effective concentration starting at 10 µM.	(Ma J et al., 2016) **(179)**
IM and FLX	T98G and U87 human glioma cell line	10 µM for 24h, in different hypoxia models.	↓ viability and mitochondrial activity. ↓ expression of stemness markers: CD44, nestin, and SOX1/2. Pro-survival effect on normal human astrocyte line. Results were seen with IM only, FLX did not show significant results.	(Bielecka-Wajdman AM et al., 2017) **(193)**
IM and FLX	T98G human GBM cell line	10 µM for 24h, in 2.5 or 20% oxygen.	↓ MMP and mitochondrial volume. ↑ ROS production. ↓ lactate release. ↓ expression of nuclear factor κB (NF- κB) gene.	(Bielecka-Wajdman AM et al., 2018) **(194)**
IM	*In-vitro:* U87MG and GBM8401 human GBM cells *In-vivo:* athymic BALB/c nu/nu mice	*In-vitro*: 20-80 µM for 24 or 48h *In-vivo*: 10 mg/kg/day for 21 days	↓ cell viability, migration, and invasion abilities. Induction of apoptosis via both extrinsic and calcium mediated intrinsic pathways. ↓ tumour progression via inhibiting ERK/NF-κB signalling. Suppression of growth of U-87MG tumour xenograft in vivo. Effective concentration: 20 µM	(Hsu FT et al., 2020) **(195)**
FLX	U-87MG glioma cells	5-60 µM for 2 or 3 days OR 10 µM for 24h +/- RT	↓ proliferation, ↓ survival fraction of U-87 colonies with FLX + RT compared to RT alone. ↑ apoptotic cells with FLX + RT compared to RT alone. Effective concentration: 10 µM.	(Hosseinimehr SJ et al., 2020) **(181)**
FLX	U87 and U251 GBM cells, and other non-glioma cells (colon cancer and breast cancer)	10, 20, 40, 80, and 160 µM for 72 h	Among different drugs tested for induction of cell death, FLX induced strong toxicity in all cell lines IC50 ~20 µM FLX treatment disrupted MMP and increased the lysotracker stain for autophagosome-lysosomes in breast cancer cells, at 5 µM.	(Varalda M. et al., 2020) **(196)**

There is no obvious universal mechanism to explain how antidepressants may be effective against GBM. One of the ideas proposed relatively recently implicated cyclic adenosine monophosphate (cAMP). cAMP may play a role in the antidepressant action of TCA and SSRI (197). Classical ADs are believed to increase the central concentration of monoamines by blocking their reuptake, which in theory should increase their signalling via their cognate receptors some of which are coupled to adenylate cyclase (AC) and therefore can lead to cAMP production. Some of the studies suggested that an increase in cAMP production can explain their suppressant effect on the tumour cell lines, while others proposed anti-GBM mechanisms revolving around mitochondrial damage and induction of apoptosis or autophagy (see **Table 1.2**).

1.3.3 Cyclic adenosine monophosphate signalling pathway as a target for anti-GBM therapy

Physiology of cAMP signalling pathway

cAMP is a key second messenger in intracellular signalling and the first ever discovered molecule to mediate this type of signalling. It is essential in regulating many cellular functions, including inflammation, immunity, growth, differentiation, transcription and protein expression (198). In a classic scenario transmembrane G-protein coupled receptors (GPCR) coupled to AC activate production of cAMP from ATP (198). Upon activation of GPCR by its ligand, the type of Gα subunit of the GPCR determines the downstream consequences. Gαs-coupled receptors, when activated, increase intracellular cAMP, while Gi coupled reduce cAMP production. Downstream effectors of cAMP include protein kinase A (PKA), exchange protein directly associated with cAMP (Epac) and cyclic nucleotide gated ion channels found at some locations (199). Phosphodiesterases (PDE) are responsible for the hydrolysis of cAMP and the termination of its signalling (198).

cAMP signalling in astrocytes

Astrocytes are among the cells often mentioned as the key progenitors for the GBM. Differentiation of cortical precursor cells through astroglial linage and maturation of

astrocytes are thought to be triggered by cAMP (200). Mature astrocytes, the most abundant glial cells in the human brain, express various GPCRs that can up or down regulate astrocytic cAMP, which plays a major role in executing homeostatic functions of astrocytes such as glycogenolysis, glutamate uptake, K^+ buffering, and lactate-pyruvate shuttle (201). A differential effect of cAMP on astrocytes versus neurons has been reported. cAMP was found to stimulate MEK1/2 and ERK growth pathways in neurons ,which have high expression of B-RAF, while in astrocytes, which have lower expression of B-RAF, cAMP decreased the activity of MAPK, thus, inhibited growth and proliferation (202). More effects on astrocytes were observed with experimentally elevated cAMP including decreased reactive gliosis (203), cell cycle arrest due to downregulation of Cyclin G1 (204), and increased stellation (205), all seen as signs of terminal differentiation. In cultured astrocytes activation of AC by chemicals such as forskolin results in a switch to a phenotype closely resembling postnatal differentiated quiescent astrocytes in situ (206).

Gene Ontology analysis was conducted to study the effect of cAMP elevation on functional gene expression profile of mouse cortical astrocytes (206). Paco et al. found that cAMP upregulated the expression of genes associated with mature homeostatic non-reactive astrocyte, and down regulated genes that are usually up regulated in reactive astrocytes (206). Among the most up regulated functional categories are genes responsible for antioxidant defence, ions and neurotransmitter transporters, and genes of metabolic functions, where down regulated genes included genes responsible for cell cycle and apoptosis, and genes of cytoskeleton and motility (206). Thus, overall, cAMP pathway seems to be directing astrocytes towards a resting, fully differentiated phenotype and away from the proliferative and reactive state.

cAMP signalling in GBM as a potential molecular target for therapy

Dysfunction of cAMP signalling pathways is known to contribute to cancer progression (207). For instance, CREB which is a transcription factor downstream of cAMP regulates the expression of 2 important proteins implicated in cell cycle, c-Jun and cyclin D1 (207). Depending on the cancer cell type and the nature of the underlying molecular defects, pathological or experimental induction of intracellular cAMP or downstream PKA in cancer cells can have either tumour-suppressor (reported in GBM) or tumour-promoting effect

(reported in lung cancers) (207). Four times lower cAMP levels have been found in brain cancer cells compared to normal cells (208). In 1975, Sato et al. have successfully induced differentiation of GBM cells to astrocyte-like cells by adding cAMP analogue di-butyryl cyclic AMP (db-cAMP) to the culture medium (209). Following that, researchers have tried different means for elevating intracellular cAMP in GBM cells. For example, U87MG glioma cell line was exposed to db-cAMP for 6 days resulting in decreased proliferation and invasiveness (210). Elevating cAMP also decreased the angiogenic properties of U87MG cell line, evident by reduced angiogenic transformation of co-cultured peripheral endothelial cells (210).

One of the ways to increase cAMP is to inhibit PDE and PDE inhibitors are among candidates for GBM therapy (211). Higher expression of PDE is documented in GBM, correlating to tumour aggressiveness (211, 212). Elevating intracellular cAMP in primary GBM cells, using a novel small molecule PDE4 inhibitor, resulted in growth arrest and induced neural differentiation of the CSCs sub-population, which was associated with upregulation of p53 protein expression (213). In another study, using an AC activator forskolin (FSK) +/- a non-selective PDE inhibitor (IBMX) to stimulate elevation of intracellular cAMP has resulted in growth inhibition of some GBM cell lines but not the others (214). That study identified low MAPK activity and high CD44 expression as predictors of GBM sensitivity to cAMP treatment (214).

Exposure to db-cAMP for 48 hours have induced morphological changes in different GBM cell lines and their differentiation into a mature astrocyte-like phenotype (215). Global gene expression profile and gene set enrichment analysis (GSEA) found a significant effect of cAMP elevating treatment on the expression of genes related to mitochondria, especially those involved in oxidative phosphorylation (215). Measurements of metabolism such as oxygen consumption rate, extracellular acidification rate, and uptake of florescent glucose have all indicated a shift in metabolism of db-cAMP treated cells to oxidative phosphorylation rather than glycolysis, a phenomenon described by the authors as “anti-Warburg” effect (215). Furthermore, treatment with db-cAMP inhibited tumour growth in-vivo, and prolonged survival of GBM-xenografted nude mice (215). The authors hypothesized that cAMP elevation modified the expression profile of mitochondrial genes which resulted in mitochondrial biogenesis and enhanced mitochondrial functions, which in

turn caused a shift in the metabolic state of the tumour cells from glycolysis to oxidative phosphorylation. Thus, db-cAMP has forced GBM cells to exhibit features of differentiated healthy glial cells (215).

In another study, treatment of Nestin/CD133-positive GSCs with FSK plus IBMX resulted in inhibition of growth and induction of apoptosis in one of the two cell lines tested, although both cell lines have increased expression of phosphorylated CREB protein as a result of the treatment (216). Inhibiting MAPK pathway pharmacologically increased the sensitivity of the non-responsive GSC line to FSK/ IBMX-induced growth inhibition (216).

From the studies cited above, it is clear, that elevation of cAMP is disadvantageous to GBM cells, and therefore, therapies aimed for rising cAMP might be a good novel strategy in GBM therapy. As discussed earlier, there is an opinion that some currently used antidepressants may be able to do that.

This concept, namely that the anti-tumour effect of antidepressants is due to their ability to increase intracellular cAMP has been strongly argued by Shchors et al. (176). The study reports the therapeutic effect of IM on genetically modified mice with p53 loss, known to reproducibly develop high grade gliomas (176). Tumour bearing animals were reported to survive longer, and to exhibit less proliferation and lower histological grades after IM treatment compared to the control cohort (176). The mechanism of this effect was investigated, and it was reported that the tumour tissue collected from IM-treated animals had higher expression of microtubule associated protein light chain 3 (MAP1-LC3), which is an indicator of autophagy activation, whose expression correlates with the number of autophagosomes in the cell (176). The induction of autophagy was associated with increase in intracellular cAMP levels (176). Similar effects were seen on human GBM cell lines. The authors concluded that the mechanism of anti-tumour action of IM is via stimulating AC and cAMP-Epac signalling pathway leading to induction of autophagy (176). However, the authors failed to explain how IM could engage a cAMP-dependent signalling *in vitro*, in the absence of any monoamines which, in theory could then act on Gs-coupled receptors to stimulate cAMP production. Even *in vivo* such scenario appears rather unlikely because the tumour cells lack properly organised innervation by monoaminergic axons from the nuclei in the brainstem, and therefore should not have the biological substrate from which

noradrenaline and/or serotonin can be released or into which monoamines should be taken up. In fact, clear evidence for the ability of antidepressants to elevate cAMP in astrocytes of GBM cells in vivo is lacking altogether, in spite of the presence of some Gs-coupled receptors for noradrenaline and serotonin on these cells.

If this effect is not mediated by an increased signalling of noradrenaline and/or serotonin, what are the alternatives? One current hypothesis suggests a direct action on the lipid rafts within cells membrane. Chronic treatment of C6 glioma cells with AD (desipramine and fluoxetine) was reported to enhance the translocation of Gαs from the lipid rafts to associate more with AC, increasing intracellular cAMP (217). Similarly, chronic treatment using other AD such as escitalopram and fluoxetine was found to cause re-distribution of Gαs protein away from lipid rafts, increasing the receptor's availability, thus increasing cAMP signalling (218). Imipramine has also shown the same Gαs-translocating effect (219). The three studies cited above utilised C6 glioma cells as a model while focusing on an alternative mechanism of action of antidepressants. C6 is a common cell line for studying signalling mechanisms *in vitro* or *in-vivo,* as xenografts (220, 221). Thus, if antidepressants can elevate cAMP via a mechanism independent of the monoamines, that would be one potential explanation for the results of the study by Shchors et al. (176) discussed above.

Altogether, at first glance antidepressants seem like a promising drug for repurposing for GBM therapy, but there is obviously a need to further explore their efficacy. Possible mechanisms of the anti-tumour effects of antidepressants are also not clear. Published evidence points towards two main possibilities: antidepressants could act by increasing the level of cAMP (176, 192), and by some toxic effect on GBM mitochondria (188, 190, 194). There is also a need to conduct tests on primary human GBM cells of relatively low passage from a range of recent patients, ideally from the invasive margin, rather than commercially available cell lines some of which have been passaged over 30 years *in vitro* or even more. In contrast, most- if not all- of the studies mentioned earlier in this section and in **Table 1.2** utilised commercially available GBM cell lines, such as C6, U87MG, or U251. These cell lines have been used in research for decades and might have accumulated numerous mutations which make them poor representatives of the real GBM.

1.3.4 Mitochondria as a target for anti-GBM therapy

Our study is looking at novel/alternative strategies which could be used to tackle the formidable problem of GBM. Mitochondria attract a lot of attention in cancer research. They are numerous double-membrane cellular organelles responsible for energy production, regulation of cell metabolism and apoptosis signals (222). A mitochondrion consists of two membranes: inner and outer mitochondrial membranes (IMM and OMM), creating an intermembrane space (IMS) between them (222). The IMM encloses the mitochondrial matrix which holds the mitochondrial DNA (mtDNA) (222). Cristae form from folding of the IMM and serve to increase the surface area of the IMM and enhance the efficiency of electron transport chain and ATP production (222). Brain cells extract essentially all their energy from glucose, which first undergoes glycolysis, followed by utilization of pyruvate in the citric acid cycle, and finally the production of ATP on the inner mitochondrial membrane, in a process called oxidative phosphorylation (OXPHOS) (222). Mitochondrial redox reactions create a proton gradient (ΔpH^+), and an electrical gradient called the mitochondrial membrane potential ($\Delta\Psi m$ or MMP) across the inner mitochondrial membrane (223). MMP is maintained in certain range to ensure the continuity of normal mitochondrial functions and is the key indicator of mitochondrial ability to generate ATP.

In cancer cells, metabolic reprogramming results in decrease reliance on OXPHOS for ATP synthesis. Instead, cancer cells consume 5-10 times more glucose than normal cells and use it for glycolysis, producing copious amount of lactate (222). This metabolic shift from OXPHOS to aerobic glycolysis regardless of oxygen availability is called the Warburg effect. Inhibitors of glycolysis are extensively studied for their role as anti-cancer therapy (224), although up to this day we do not know exactly why Warburg effect is so characteristic to cancers. Nevertheless, it is a generally accepted fact that mitochondria in cancers are different to their counterparts in healthy cells.

Mitochondria are also linked to cancer development or progression via their fundamental role in regulating apoptosis (222). Apoptosis can be triggered by one of two pathways, an extrinsic pathway (death receptor pathway originating from signals at the plasma membrane), and the intrinsic pathway (release of relevant apoptotic trigger molecules from the mitochondria) (222). In a classic scenario for the extrinsic pathway, a

ligand binds to the cell tumor necrosis factor (TNF) receptor, this leads to assembly of the death-inducing signalling complex and subsequent activation of initiator caspases (222). The intrinsic apoptosis pathway can be initiated by opening of the mitochondrial permeability transition pore (MPTP) and the release of cytochrome C and mitochondria-derived activator of caspase (Smac) into the cytoplasm (222). The release of these molecules triggers the formation of apoptosome and the activation of the apoptotic protease activating factor-1 (APAF-1), which in turn activates executioner caspases 3 and 9 (222).

It is important to realise that evolution resulted in the loss of the vast majority of the mitochondrial genes required for the synthesis of mitochondrial proteins and their translocation into the nuclear genome. As few as 13 key mitochondrial proteins are still encoded by the circular chromosomes residing in the organelle, but the rest are supplied by the main cellular genome either as ready-made proteins or as mRNAs which are locally translated in the mitochondria (222). This creates a unique situation where the two independent genomes must coordinate their activity very tightly because any mismatch in the expression of the proteins involved in OXPHOS is detrimental to the electron transport chain. The process of coordination of the activity of nuclear and mitochondrial genomes is poorly understood but is fundamental to the efficiency and health of these organelles and the cell as a whole.

Dysregulation of mitochondrial functions can be either a result of nuclear DNA aberrations (mutations or epigenetic dysregulation) or mtDNA mutations (222). mtDNA is highly susceptible to mutations, mainly due to lack of histone structure, poor DNA repair mechanisms, and proximity to ROS production sites at the IMM (222).

Cancer genome and particularly of GBM, is extremely unstable and gain or loss of function mutations are common. Thus, the fine tuning of expression of mitochondrial genes is almost always absent in cancer cells, resulting in dysregulation of mitochondrial functions and metabolic disturbances (225). Identifying these differences in mitochondrial function between cancer and normal cells and utilizing them as targets for anti-GBM therapy is a developing and promising field of research (225).

Compromising GBM energy supply and triggering apoptosis seem to be the two plausible strategies in targeting mitochondria for GBM therapy. Three connected groups of scientists examined the ability of some antidepressants, particularly CL and FLX, to activate the intrinsic (mitochondrial) apoptotic pathway in GBM (187-189). They have all reported some evidence of apoptosis in GBM following CL or FLX treatment, including increase apoptotic cell count, and activation of caspase 3 and cytochrome C. One of these studies uniquely reported a decrease in oxygen consumption and MMP indicating an injury to the mitochondria, however, this injury was induced only with exceedingly high concentration of CL (114µM) (188). The other study has suggested that the apoptosis-inducing effect of CL is mediated by Ca^{+2} overload which can stimulate intrinsic apoptotic cascade (189). Two other independent groups have reported mitochondrial calcium overload following FLX treatment in GBM and non-GBM cells, which consequently resulted in activation of the intrinsic apoptosis pathway (178, 226). In GBM cells, this effect was induced by direct binding of FLX to glutamate receptor-1 (GluR-1) subunit of AMPA receptor, which is highly expressed in gliomas (178). On the other hand, FLX at lower doses (10µM compared to 25 µM or 50 µM in the previous studies) was not effective in inducing mitochondrial damage in two GBM cell lines, unlike IM, which significantly inhibited mitochondrial oxidation of NADPH, compromising mitochondrial metabolic function, and inducing cell death (193). This is surprisingly incompatible with other studies which reported effectiveness of FLX but not IM in inducing apoptosis (187). It is worth notice that AMPA receptor is the key excitatory receptor mediating glutamatergic transmission in the mammalian CNS and from the biological perspective the idea that FLX “overexcites” AMPA receptors looks implausible.

Treatment with db-cAMP was reported to induce mitochondrial biogenesis, increase oxygen consumption, and decrease extracellular acidification in commercially available and patient derived GBM cell lines (215). This was associated with enhanced expression of mitochondrial OXPHOS genes (215). The authors called it anti-Warburg effect to describe the shift in metabolic state of GBM cells from glycolysis to OXPHOS following cAMP stimulation, which is also reported to induce differentiation of GBM cells to more mature phenotype (215).

Possibly, mitochondria could be targeted with the aim to sensitize GBM cells to conventional chemotherapy with TMZ. TMZ-resistant GBM were found to have better

mitochondrial coupling capacity associated with higher expression of cytochrome c oxidase, which enhances the OXPHOS capabilities of TMZ-resistant cells and is associated with disease progression and poor prognosis (227). Oliva et al. identified chlorpromazine (the anti-psychotic) as mitochondrial cytochrome oxidase inhibitor and reported its growth inhibiting effect on TMZ-resistant GBM cells (228), as well as GSCs (229).

In summary, the evidence presented in this section suggests that the dysregulated mitochondria could be one of the few universal “weak spots” of the cancer cells, including GBM. Some of the cited studies reported that TCA and SSRI might have anti-cancer effects via targeting the mitochondria, although in most cases the concentrations used seem to be physiologically irrelevant. Moreover, there is inconsistency between the different groups regarding proposed mechanisms of action, which further complicates any conclusions. Nevertheless, I believe that targeting mitochondria in GBM is a strategy worth of further investigation and exploration. I hypothesize that ADs are effective in inducing GBM cell death via disrupting mitochondrial functions rather than cAMP elevation.

1.4 Project outlines

Motivated by the urgent need for more innovative, effective, and less invasive therapy modalities for GBM, my project aims to explore PDT and drug repurposing as novel therapeutic approaches for GBM therapy, inspired by the recent findings in the field. I used 6 different patient derived primary GBM cells. The first part of my project was dedicated towards exploring the molecular heterogeneity in my GBM sample in regard to TMZ sensitivity and mutational profile. I used Sanger sequencing technique to sequence 4 common genes involved in GBM development and progression in my GBM cells. In the second part, I explored the possibility of utilizing a dye, previously used to estimate mitochondrial membrane potential, as a novel PS to be used for PDT of GBM. I examined its localization in cells, safety, and efficacy in PDT against GBM cells, and I explored possible synergy between TMRM-mediated PDT and two pharmacological agents, NKH477 and clotrimazole. In the final part, I re-evaluated the efficacy some of the classical antidepressants IM, CL, and FLX, proposed for repurposing for treatment of GBM. I examined their toxicity to GBM cells and investigated into the mechanism of action behind that toxic effect, specifically whether it is mediated through cAMP rise or mitochondrial depolarization. Different treatment outcomes were observed within my GBM cohort throughout the project.

Chapter 2: Experimental Materials and Methods

2.1 The source and handling of cell cultures

2.1.1 Source and description of GBM cells

All GBM cell lines used in my experiments are primary cultures of human GBM cells obtained from patients during surgical resection, typically before TMZ treatment (not known in all cases). UP007 and UP029 GBM cells were received via collaboration from professor G. Pilkington (University of Portsmouth). GIN GBM cells (GIN8, GIN27, GIN28, and GIN31) were kindly donated by Dr S. Smith and Dr R. Rahman (University of Nottingham). While the exact location from which UP glioma cell lines were derived is unknown, GIN glioma cells were specifically extracted from the infiltrating cells taken from the tumor edge. The protocol for isolating GIN cells is described in Smith et al. paper (65). Briefly, surgical samples were obtained from multiple tumour regions. Invasive samples were obtained from areas of 5-ALA enhancement that are beyond the gadolinium enhancing tumour bulk or rim on fMRI (65). These cells were then sorted using Florescence-activated cell sorting (FACS) against 5-ALA florescence (65). GIN lines are derived from these FACS-sorted 5-ALA positive "true" infiltrating cells (65).

2.1.2 Preparation of cultured rat astrocytes

In my work normal rat astrocytes (RA) obtained from neonatal pups served as reference. It is important to state that these astrocytes may not be seen as equal to the mature human astrocytes, especially from older people. In fact, rats are born with brain much less developed than humans and their neonatal astrocytes are closer to the embryonic mid-term human astrocytes (230). For example, they still divide, something

which only rarely happen with astrocytes in the postnatal human brain (230). This factor is important to keep in mind when comparing them to the GBM cells. However, there are no better models available at the moment. This includes stem-cell-derived glia which cannot be equated to mature postnatal cells. I attempted to use human embryonic astrocytes (Lonza, #CC-2565), but the results were unreliable and are not presented here.

The preparation of primary dissociated RA was adapted from Marriott, Hirst & Ljungberg protocol published in 1995 (231). The protocol was modified as per previous publications from our laboratory (232, 233). All procedures followed directions of the Animal Scientific Procedures Act 1986 and current guidance of the UK Home office.

Two solutions were needed for the preparation of the cultures: DNase I solution and trypsin solution, and they were prepared fresh before the prep. DNase I solution contained 3mg/ml bovine albumin serum (Sigma A3294) and 0.04mg/ml Deoxyribonuclease I (Sigma D5025) diluted in 40ml Hank's Balanced Salt Solution (Invitrogen 14175-129). Trypsin solution was made by adding 15 ml of the DNase I solution to 0.25mg/ml trypsin (Sigma T9935). Neonate (P2) Wistar rat pups were overdosed with 5% isoflurane before decapitation. The head was immediately transferred into cold HBSS and to the laminar flow hood. In a petri dish, the skin was removed, and the skull was exposed and dissected to allow the collection of the brain tissue. Tissue was minced using a sharp scalpel and then submerged in trypsin solution for 15 minutes with constant gentle shaking at room temperature. After that Dulbecco's Modified Eagles Medium (DMEM) containing 10% foetal bovine serum (FBS, Invitrogen, 10108-165) was added to deactivate trypsin and the suspension was centrifuged for 5 minutes at 2000 rpm. The supernatant was removed, and the pellet was resuspended in DNase I solution. The cell-containing suspension was let to settle so the debris can sink at the bottom and the upper part containing cells was collected into a new falcon tube. The cell suspension was filtered through a 40 µm cell filter and centrifuged for 5min at 2000rpm. Finally, the pellet was resuspended in DMEM supplemented with 10% FBS and 1% Penicillin/ Streptomycin (P/S, at 10,000 U/mL, Invitrogen, 15140-122), and contents were transferred into T75 cell culture flask and incubated in a cell culture incubator at 37°C and 5% CO_2 for 7 days to allow astrocytes to attach and grow. To eliminate microglia and oligodendrocyte contamination, flasks were gently shaken overnight in a shaking chamber at 37°C. The media containing non-astrocytic

cells were replaced with fresh media and the flask was put back in the incubator. Astrocyte cultures prepared in this way were used in experiments for up to 3 weeks.

2.1.3 Maintenance and handling of GBM cell lines and astrocytes

UP GBM cell lines and normal RA were grown in Dulbecco's Modified Eagles Medium (DMEM) with GlutaMAX™ (Invitrogen, 61965-059), supplemented with 10% FBS and 1% P/S. GIN GBM cell lines were grown in low-glucose DMEM with L-Glutamine supplemented with 1% P/S and 10% or 15% FBS (15% for GIN8 and GIN27, and 10% for GIN28 and GIN31, as advised by the providers of these lines). All media and supplements were purchased from Gibco®. In all my experiments, the passage number of cells was always 30 or less, except for GIN31 where it was 32 or less.

For passage, cells were harvested when they were 70-80% confluent. First, flasks were washed with sterile phosphate buffer solution (PBS), then Trypsin-EDTA (Gibco®) was added to cover the bottom of the flask, which was then incubated at 37°C for 2-3 minutes to allow cells to detach. After incubation, sufficient amount of complete media was added to deactivate trypsin, then cell suspension was centrifuged at 1000 rpm for 5 minutes. The supernatant was discarded, and the pellet was resuspended in 2-3 ml of fresh full media. Finally, cell suspension was either sampled for measuring cell concentration and then used for experiments or sub-cultured in a new flask with the addition of fresh media. Flasks were carefully labelled and returned into the incubator. Cell handling was done in a sterile laminar flow hood to guarantee aseptic environment. Cell incubator was set to maintain temperature at 37°C and 5% CO_2, referred to as standard culture conditions hereafter. Sterile conditions were strictly followed at all times.

To achieve consistency in cell density between experiments, cells were counted using Neubauer Haemacytometers. This cell counting tool consists of a glass slide with a calibrated chamber and a glass cover. When the glass cover is placed over the glass slide a narrow chamber is created with a capillary action that allows a sample of previously diluted cell suspension to be loaded for counting. Cells occupying the outer 4 squares of the

calibrated chamber are counted. Considering the volume of a single square of the calibrated chamber (0.1mm^3 or 10^{-4} ml), cell concentration is calculated using the following formula:

Cell concentration (cells/ml) = (number of cells counted/ 4) x dilution factor x 10^4

2.1.4 Coating of glass coverslips with rat tail collagen

Whenever imaging of cells required plating them on glass coverslips, type 1 rat tail collagen (Sigma C3867) was used to coat the coverslip at working concentration of 0.25 mg/ml to promote cell attachment. Stock was diluted with 0.2M acetic acid. Glass coverslips were incubated with 300µl collagen for 15 minutes at room temperature. Collagen was then re-collected for re-use and coverslips were washed twice with PBS. Coated coverslips were made fresh before each experiment.

2.1.5 Production of stable EGFP-expressing GBM lines

One of the objectives of my project was generation of GBM cell lines stably expressing enhanced green florescent protein (EGFP) in order to track their behaviour in complex systems, such as cultured slices, in real time. This was achieved using lentiviral vectors (LVV) which permanently integrate their transgenes into the genomes of the target cells. This LVV was available in the laboratory and generated previously. An LVV where EGFP is expressed under the control of a stable and potent mammalian EF1-α promoter was used to produce stable lines of GFP-tagged GBM cells. GBM cells were seeded in 6-well plates at density of 10^5 cells/ 2 ml/ well, in order to achieve 80% confluency at time of transduction. Next day, LVV was introduced to cells in the presence of 8 µg/ml Polybrene (Hexadimethrine bromide, Sigma H-9268) to facilitate the transduction. The viral stock concentration was 5.1x10E10 pfu/ml, which was diluted to achieve MOI of 10, 20, 50, 70, and 100. For UP glioma cell lines, MOI of 30 was sufficient to transduce all cells, while for GIN cells MOI of 50 for GIN8 and GIN28, 70 for GIN31, and 100 for GIN27 were used. The following day (24 hours after introduction of the virus), polybrene containing media was replaced by fresh media. 48

hours after transduction, cells were checked for GFP expression. Since all visible cells were fluorescent green, not cell sorting was used. Cells were then transferred into cell culture flask to allow sufficient growth for cryopreservation.

2.1.6 Cryopreservation of cell lines

Whenever needed, cryopreservation was carried out as following: cells were grown in 175 cm^2 cell culture flask, trypsinized and collected for centrifugation. The cell pellet was then resuspended in adequate volume of freezing solution, consisting of FBS plus 10% dimethyl sulfoxide (DMSO). Finally, the cell solution was aliquoted in clearly labelled cryotubes and kept in -80°C freezer for future use.

2.1.7 Staining nuclei for counting using 4',6-Diamidine-2'-phenylindole dihydrochloride (DAPI) florescent dye

For cell counting, images of fluorescent nuclear stain DAPI were obtained using ZOE™ Fluorescent Cell Imager. ImageJ (Fiji) software was used to count the number of stained nuclei. DAPI is a dye that selectively binds to nuclear DNA and form a florescent complex (234). DAPI is more specific and photostable than other nuclear stains (234). It requires fixation of cells or permeabilization of cell membranes before the staining (234). Briefly, cells were washed with PBS and fixed using 4% paraformaldehyde (PFA) solution. After 15 minutes incubation with PFA, cells were washed with PBS then DAPI was added at working concentration of 1µg/ml and left to stain for 5-10 minutes. Finally, DAPI was removed and cells were washed and kept in PBS ready for imaging.

2.2 Exploring molecular diversity of our GBM sample

It was noted that different lines of GBM differ in their responses to the treatments that have been investigated. This was not surprising as GBM tumours are known to be heterogenous. It was reasonable to expect differences in TMZ sensitivity as well. Therefore, an initial enquiry into TMZ sensitivity among GBM cell lines was made. It is also well known that differences in treatment sensitivity are related to heterogeneity of molecular profiles of the tumours. Accordingly, I investigated the mutational status of four different known GBM driver genes (IDH1, EGFR, p53, and PTEN) using sequencing of the products obtained by RT-PCR of the mRNAs isolated from these genes.

2.2.1 Evaluating the toxicity of TMZ on GBM cell lines

The effect of TMZ was tested to evaluate TMZ sensitivity among the different GBM cell lines. It can also serve as a reference for other treatments tested in this project. TMZ is a first line chemotherapy in GBM treatment and has been described in chapter 1.

TMZ toxicity was assessed using PrestoBlue™ viability reagent (Invitrogen A13261). The basis of this assay is that only viable cells can convert the blue cell-permeable active ingredient, resazurin, into a red and florescent metabolite. This red colour and/ or florescent intensity are then measured. The more viable cells there are, the darker the red colour is in the culture media, and the more intense the florescence is. In my experiments, I measured colour absorbance in the culture media of the cells.

Cells were seeded in 96-well plates at 6,000 cells/ 100ul/ well for RA, and 5,000 cells/ 100ul/ well for GBM cells and incubated in standard culture conditions overnight. The next day, cells were treated with different concentrations of TMZ. Since TMZ needs to be dissolved in DMSO, for control I used solutions containing equivalent quantities of DMSO. Cells were incubated with TMZ for 9 days. Media containing drugs, negative controls, and DMSO controls were replaced with fresh ones every 3 days. After 9 days, a volume of PrestoBlue reagent was added to the final concentration of 10% of the total volume of culture media per well. Plates were returned into the incubators for 2 hours before reading

absorbance using the microplate reader. Absorbance was read at 570nm and normalized to 600nm (baseline).

2.2.2 RNA isolation

RNA purification from GBM cell lines was carried out using RNeasy Mini Kit from Qiagen. First, cells were detached from culture flasks using trypsin as mentioned previously in section 2.1.3. After centrifugation step the supernatant was removed, and the pellet was resuspended in 350 µl RLT lysis buffer. Equal amount of 70% ethanol was then added, and the mixture was loaded into a silica-membrane RNA-binding spin column, which was centrifuged at 8000 rpm for 15 seconds. The flow-through was discarded, and the spin column was placed back in the tube. Next, 700 µl of RW1 buffer was added to the spin column and the tube was centrifuged at 8000 rpm for 15 seconds. Again, the flow-through was discarded, and the spin column was placed back in the tube. Next, 500 µl of RPE buffer was added to the spin column and the tube was centrifuged again at 8000 rpm for 15 seconds. This step was then repeated with 2 minutes centrifugation instead of 15 seconds to dry the membrane out from any residual RPE buffer. Next, the column was placed in a clean microfuge tube and 30-50µl RNase-free water was added to the column and the tube was centrifuged for 1 minute at 8000 rpm to elute the RNA. RNA concentration was then measured using Nanodrop Spectrophotometer ND-1000.

2.2.3 Reverse transcription

Reverse transcription (RT) of RNA was carried out using QuantiTect Reverse Transcription kit from Qiagen, which consists of two main steps (1) elimination of genomic DNA (gDNA), (2) reverse transcription reaction. Briefly, RNA was incubated with gDNA wipe-out reagent in a water bath at 42°C for two minutes and placed in ice immediately. RT mixture was prepared on ice as well. It consists of reverse transcriptase, RT primer mix, and RT buffer. RT mixture was then added to the RNA isolated in the previous step and incubated for 15 minutes in water bath at 42°C. Finally, reverse transcriptase is inactivated by incubating at 95°C for 3 minutes. cDNA was either used directly or stored at -20°C.

2.2.4 Primer design and PCR for desired genes

Polymerase chain reaction (PCR) is a technique that allows in-vitro amplification of nanoscale quantities of DNA. It consists of cycles of thermally-driven enzymatic reactions: DNA denaturation, primer annealing, and extension (235).

Using IntOGen database of Oncogenomics, 4 driver genes implicated in the pathogenesis of GBM were selected and tested for mutations in my GBM cohort. Available information: https://www.intogen.org/search?cancer=GBM#driver-genes:plot .These genes are: IDH-1, p53, EGFR, and PTEN. PCR primers for those genes were designed using NCBI Primer-BLAST primer designing tool and ordered from Eurofins Genomics **(Table 2.1)**. Initially I planned to use Oxford Nanopore process for sequencing, which has no limit on the length of the sequenced nucleic acid fragments. However, because of the disruption caused by COVID pandemic I eventually chose to use Sanger sequencing. Sanger process is reliable for fragments of <700-800 nucleotides. However, in some cases I had to scan longer segments of the chosen genes. In these cases, more than one primer pair were designed with overlaps to cover the whole length of mRNA sequence. Primer pairs (forward and reverse) had Tm values not more than 4.1°C different from each other, with an average Tm of 59.3 ± 1.77 °C (mean ± SD) for all primer pairs. The average CG content was 54% ± 7.77 (mean ± SD).

PCR mixture was prepared as following: 2.5µl of forward primer, 2.5µl of reverse primer, 1µl (10mM) of dNTPs (New England Biolabs, N0447L), 0.5µl of DNA Polymerase, 10µl of Phusion High Fidelity Buffer (New England Biolabs, B0518S), and 31.5µl of nuclease-free water. Finally, 2µl of cDNA (the template) plus 48µl of the PCR mixture were added into a flat cap PCR tube (Starlab, I1402-8100) to the total volume of 50µl. PCR thermal cycler (G-Storm) was set as following: denaturation at 94°C for 20 seconds, annealing at variable temperatures according to the primers used ranging from 55.3-61.8°C for 30 seconds. When multiple samples with different primers were run simultaneously, annealing temperature was set at the average Tm. Annealing is followed by a 30-second extension step at 72°C (the optimum temperature for DNA polymerase enzyme activity). The cycle was repeated 35 times.

Table 2.1. List of primers used in PCR experiments.			
Gene of interest	**Sequence**		**Product length (bp)**
IDH1	Pair 1	**IDH1-fw:** GCGTCAAATGTGCCACTATCA **IDH1-rv:** CTCAGATACAAAGGCCAACCCT	416
EGFR	Pair 1	**EGFR-fw1:** TGCGACCCTCCGGGAC **EGFR-rv1:** TCACTGGGGGACTTGCCAC	688
	Pair 2	**EGFR-fw2:** GTGGCAAGTCCCCCAGTGA **EGFR-rv2:** AGGTTCTCAAAGGCATGGAGG	598
	Pair 3	**EGFR-fw3:** ACGGACCTCCATGCCTTTGA **EGFR-rv3:** TCTTAGGCCCATTCGTTGGAC	685
	Pair 4	**EGFR-fw4:** GGCCTAAGATCCCGTCCATC **EGFR-rv4:** TTGGCCAGCCCAAAATCTGT	685
	Pair 5	**EGFR-fw5:** ACACCGCAGCATGTCAAGAT **EGFR-rv5:** GACAGCTTTGCAGCCCATTT	637
PTEN	Pair 1	**PTEN-fw1:** TTCTTCAGCCACAGGCTCC **PTEN-rv1:** CTTGTGAAACAACAGTGCCA	615
	Pair 2	**PTEN-fw2:** AGTGGCACTGTTGTTTCACAAG **PTEN-rv2:** GCTGATCTTCATCAAAAGGTTCA	620
p53	Pair 1	**p53-fw1:** GTCCCCGGACGATATTGAACA p**53-rv1:** CGGATAAGATGCTGAGGAGGG	453
	Pair 2	**p53-fw2:** GCCCCTCCTCAGCATCTTATC p**53-rv2:** AGTCTGAGTCAGGCCCTTCT	616

2.2.5 Agarose gel electrophoresis

Agarose gel electrophoresis was used for identification and purification of target DNA fragment after the PCR step. PCR products, along with a DNA indicator ladder (New England Biolabs, N3200S), were loaded into freshly prepared 1% agarose gel containing 0.01% DNA-binding fluorophore (SafeView Nucleic Acid Stain, NBS Biologicals, NBS-SV1). Prior to loading, samples were mixed with a gel loading dye (Orange G; Sigma, O-3756) at a volume

ratio of 1:4. Electrical power supply was set to apply 110 volts for 20-30 minutes. Gels were placed in a transilluminating chamber to be visualized and photographed under UV light. Desired bands were then cut using clean scalpels and collected for DNA purification in 1.5ml microfuge tubes.

2.2.6 DNA purification

DNA extraction from gel bands was carried out using QIAquick Gel Extraction Kit from Qiagen. Buffer QG was added to obtain volume ratio 1:3 gel to buffer. The tube was then placed in 50°C water bath for 10 minutes to dissolve the gel. The mixture was then loaded into a filter column and centrifuged for 1 minute at 10,000rpm to trap the DNA in the filter. The flow through was discarded and 100% ethanol was added then the tube was centrifuged at 10,000 rpm for 1 minute. This was repeated with 750µl of buffer PE. Finally, Milli-Q water was added to elute DNA from the filter, which was then collected by centrifugation in a clean microfuge tube. Purified PCR products were then sent for sequencing. The sequencing sample was prepared by adding 2µl of one of the primers (either forward or reverse) to 15µl of DNA sample for a total concentration of 5ng/µl of the purified PCR product. Sanger sequencing was performed by Eurofin Genomics (UK).

2.3 Experiments with TMRM as a novel photosensitizer in photodynamic therapy for GBM

TMRM, the dye mentioned above, can be potentially used as an efficient photosensitiser. Upon illumination with moderate activity green light for fairly short periods of time (22 or 40 sec). TMRM led to strong depolarisation of mitochondria, manifested by the loss of fluorescence. It is generally believed that depolarisation of mitochondria may severely damage it, leading to release of pro-apoptotic molecules and cell death. Attempts were done to potentiate TMRM-PDT effect on GBM cells with AC activator NKH477 or glycolysis inhibitor clotrimazole.

2.3.1 TMRM as a photosensitizer

TMRM fluorescence decay dynamics after application of light was tested. The cells were plated at density of $5x10^4$ cells/ ml, on glass cover slips coated with type 1 rat tail collagen as previously described in section 2.1.4. Cover slips were placed inside small corning dishes. Dishes were incubated overnight under standard culture conditions. The next day, cells were loaded with 100nM TMRM for 1 hour. Before photoactivation of TMRM, baseline images were obtained as a sequence of 6 images, one every 10 seconds, for a total of one minute. This was followed by illumination with green light ($1.4mW/mm^2$ with x10 objective) for 30 seconds followed by a series of 20 images every 10 seconds, for a total of 3 minutes. Imaging was done using Leica DM IRB Inverted florescent microscope equipped with R6 Retiga digital camera and controlled by Micromanager software. Imaging parameters such as exposure time (200 msec) and light intensity were fixed throughout all imaging sessions. ImageJ (Fiji) software was used to process the images.

TMRM toxicity in absence of illumination was also evaluated. Cells were seeded in 96-well plates at density of 6,000 cells/100ul/well for GBM cells and 10^4 cells/100ul/well for RA. Next day, cells were loaded with different concentrations of TMRM ranging from 0 to 1600 nM for 1 hour, then media was replaced with fresh one, and the plates were incubated in standard culture conditions for 3 days. Measurement of toxicity was carried out using LDH assay as described in section 2.4.1.

2.3.2 Effect of photodynamic therapy on GBM cells' viability using TMRM as photosensitizer

Our protocol for photodynamic experiment consists of plating GBM cells, loading them with TMRM, photoactivation of TMRM using green light, and finally, an end point measurement of GBM cells' survival.

On day 1, a 4µl drop of cell suspension solution containing 350-400 cells was carefully placed in the centre of the well of 96-well plate **(Figure 2.1 left panel).** Cells were let to attach to the bottom of the plate for 45 minutes inside the incubator before topping up the

wells with 100µl fresh media. Cells were then allowed to grow in cell culture incubator overnight. This cell plating protocol was developed by my colleague Dr A Vasilev to ensure that the beam directed from the objective is able to illuminate all cells in the well **(Figure 2.1 middle panel).** This was important because in the preliminary experiments I found that the cells located at the margins of the wells and the walls do not receive sufficient density of light and therefore do not react to PDT. On day 2, media was replaced by 100µl fresh media containing 300nM TMRM. Cells were allowed to load for 45 minutes. After that, the centre of each well was illuminated by green light (~530-550 nm) using Leica EC3 florescent microscope with 5x objective at 1.06 mW/mm^2 for 22 or 40 seconds. Media was then removed, and cells were returned into the cell incubator. 3 days after photoactivation, PDT outcome was assessed by counting the number of visible nuclei in each well. This was done by staining nuclei with DAPI, according to DAPI staining protocol described in section 2.1.7, followed by obtaining florescent images for each well using Leica LASX live imaging fluorescent microscope with Leica DFC420C colour camera, with x5 objective to include all DAPI positive cells in one image for each well **(Figure 2.1 right panel)**. Number of DAPI-stained nuclei was counted using Fiji image processing software.

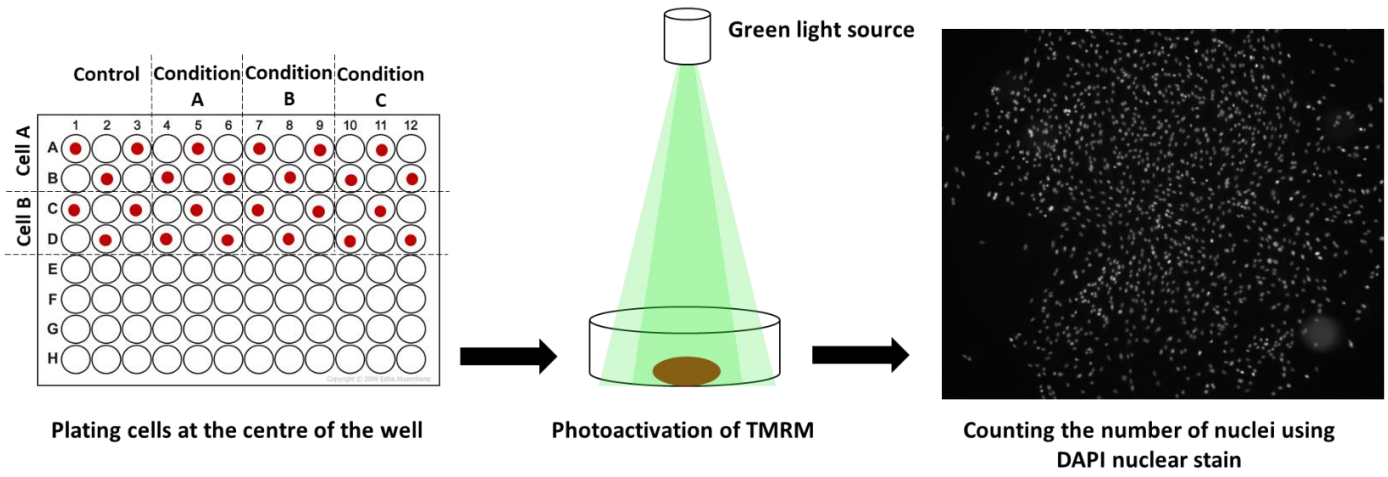

Figure 2.1. An illustration of the protocol used in TMRM-mediated PDT experiments. Plating of the cells, photoactivation of TMRM, and finally the measurement of outcome using cell counting as an estimation of toxicity in all experiments involving TMRM-PDT. Cell type, treatment conditions and durations, TMRM loading concentration, and light dose are unique to each experiment.

2.3.3 Using TMRM to assess the recovery of MMP after the PDT

Next to be tested was whether GBM cells would recover their normal MMP after photoactivation with TMRM. As mentioned above the insult caused by mitochondrial depolarisation may lead to irreversible consequences and cell death, however, it is possible that cells which are more resilient to treatment will recover their MMP.

Cells were treated with PDT initially as mentioned in the previous section. Briefly on day 1, cells were seeded using the special seeding protocol described previously. On day 2, cells were loaded with 300uM TMRM for 45 minutes, followed by photoactivation of TMRM with green light (1.06 mW/mm^2 for 40 seconds) using Leica EC3 florescent microscope and 5x objective, then cells were incubated with fresh media overnight. On day 3 of the experiment, cells were re-loaded with 300uM TMRM for 45 minutes. Images of TMRM-loaded cells were then obtained using ZOE™ Fluorescent Cell Imager. ImageJ (Fiji) image processing software was used to measure dye intensity to assess the recovery of MMP compared to baseline controls.

2.3.4 Potentiating the effect of photodynamic therapy on GBM cells

I investigated the possibility to enhance the effect of PDT with two pharmacological approaches, either an inhibitor of glycolysis (clotrimazole) or an activator of AC (NKH 477). Plating of cells was performed using the plating protocol described earlier in section 2.3.2. Milder TMRM-PDT conditions were used in these experiments, in order to easily reveal any additive or synergistic effects of the combined treatment. Specifically, 200nM TMRM was used to load the cells, instead of 300nM, and the duration of illumination was 17 seconds only. Leica EC3 florescent microscope was used to illuminate the cells with 5x objective lens and a light dose of 1.06 mW/mm^2 for 17 seconds.

To test whether NKH 477 can enhance TMRM-PDT, GBM cells were pre-incubated with 10 µM NKH 477 for 24 hours before TMRM-PDT was carried out. PDT outcome was evaluated on day 3 by cell counting using DAPI nuclear stain as previously described. I also tested whether I could potentiate the outcome of PDT with clotrimazole. 10µM of clotrimazole was added to the cells right after TMRM-PDT. Cells were incubated with

clotrimazole for three days before evaluating the outcome by cell counting using DAPI nuclear stain as previously described.

2.4 Re-evaluating the efficacy of antidepressants for GBM therapy

One of the objectives of this study was to re-evaluate the ability of antidepressant drugs to suppress GBM cells' growth and survival. The inspiration for this study came from several previously published studies where such effects were reported, and antidepressants were consequently proposed to be repurposed for cancer therapy **(Table 1.2).** However, the issue remains highly controversial. Here I re-evaluated the effect of several antidepressants on cell viability, proliferation and migration, intracellular cAMP level, and MMP.

The choice of IM and CL (TCA), and FLX (SSRI) was based on previously published work highlighted in **Table 1.2**. CL was also studied because it has a similar pharmacokinetic profile to, but is more potent than, imipramine (lower Ki for reuptake inhibition of serotonin) (2). I reasoned that this comparison might be useful in order to better understand the mechanisms of TCA effects on GBM.

2.4.1 Lactate dehydrogenase cytotoxicity assay

Lactate dehydrogenase (LDH) assay was used to determine the toxic action of antidepressants on GBM. LDH is an intracellular enzyme that is released from the cell upon disruption of the cell membrane or cell lysis (236). LDH is stable in the extracellular environment for 48 hours and its level in culture media reflects the degree of cytotoxicity induced by a stimulus (236). I used Thermo Scientific™ Pierce™ LDH Cytotoxicity Assay Kit (cat no. 88954) to measure LDH levels in the media. This is a colorimetric assay where a red product is generated in proportion to the LDH content of a sample **(Figure 2.2)**. Cells were plated in 96-well plates at density of 6,000 cells/100ul/well for GBM cells and 10^4 cells/100ul/well for normal RA. Plates were incubated overnight in standard culture conditions. On the next day, media was replaced with 100 µl fresh media containing different concentrations of IM, CL, or FLX. After three days of drug incubation, reaction

buffers provided with the kit were added and colour intensity in wells was measured using Infinite® 200 PRO microplate reader.

Toxicity was calculated based on levels of LDH in the media from wells (which reflects the amount of LDH released from dead or disintegrating cells as a direct effect of drug toxicity) and total levels of LDH obtained after lysis of the remaining cells (reflecting the LDH released from the remaining cells that were not affected by the treatment, this serves as internal control for each treatment condition). Ratio of both LDH levels were calculated as LDH in media/ LDH after lysis. Higher ratio means higher toxicity.

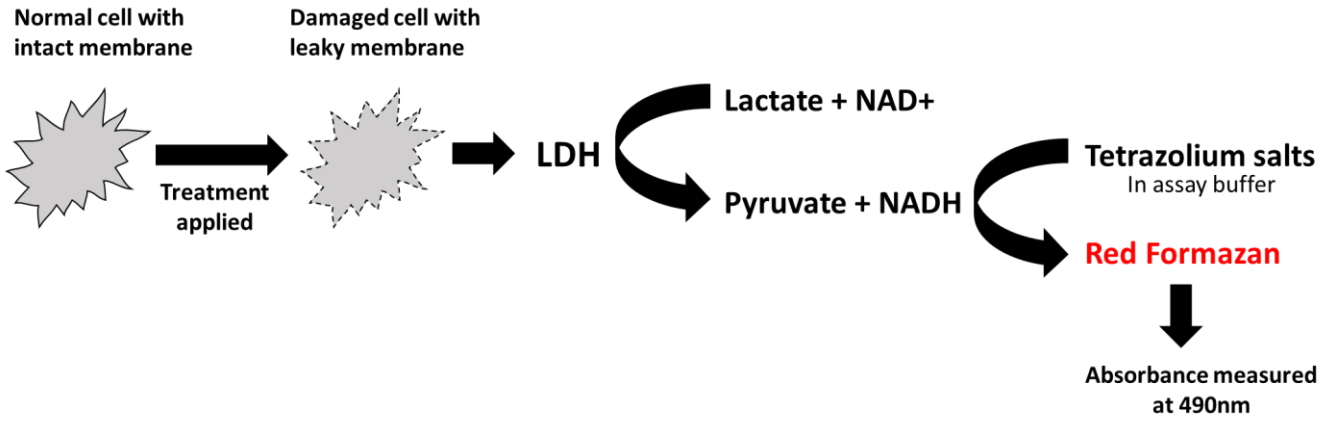

Figure 2.2. Schematic representation of the mechanism underlying LDH-mediated toxicity assay. Adapted from the assay manual.

2.4.2 Scratch wound healing assay

In-vitro scratch wound healing assay involves removing a streak of cells from a confluent cell monolayer and observing the proliferation and migratory behaviour of the cells into the barren area (237). It is an efficient method to study cell proliferation/ migration in-vitro.

Essen BioScience's IncuCyte™ 96-Well Scratch Wound Assay was used to evaluate the effect of drugs on GBM cells' proliferation/ migration. Cells were seeded in 96-well ImageLock plates (Essen BioScience 4379) at density of 30,000 cells/100ul/well for GBM

cells and 50,000 cells /100ul/well for normal RA and incubated in standard culture conditions for 24 hours to form a confluent cell monolayer. After 24 hours, identical micro-scratches were done in each well using WoundMaker™. Wells were washed twice using PBS to remove dislodged cells. Finally, media containing different concentrations of drugs were added and plates were incubated in IncuCyte ZOOM®. ZOOM software was set to obtain scans of the wound area every hour for 48 hours. ZOOM software was also used to analyse the images. **Figure 2.3** illustrates the principal steps in this assay. Confluency of wound area is compared between different time points and is expected to increase with time in physiological conditions as cells proliferate and migrate to close the wound gap. This measurement however is not very accurate, as it does not take into account the initial confluency of the monolayer or the confluency at the non-wound area. Relative wound density (RWD) is a more reliable measurement. It measures the density at wound area in relation to the density at the non-wound area at a given time. It Is calculated as follow:

$$\% \text{ RWD (t)} = 100 \cdot \frac{w(t)-w(0)}{c(t)-w(0)}$$

Where (t) means at a given time point, (0) means at time zero, (w) is the density at wound area, and (c) is the density at non-wound area. See **Figure 2.3** for reference.

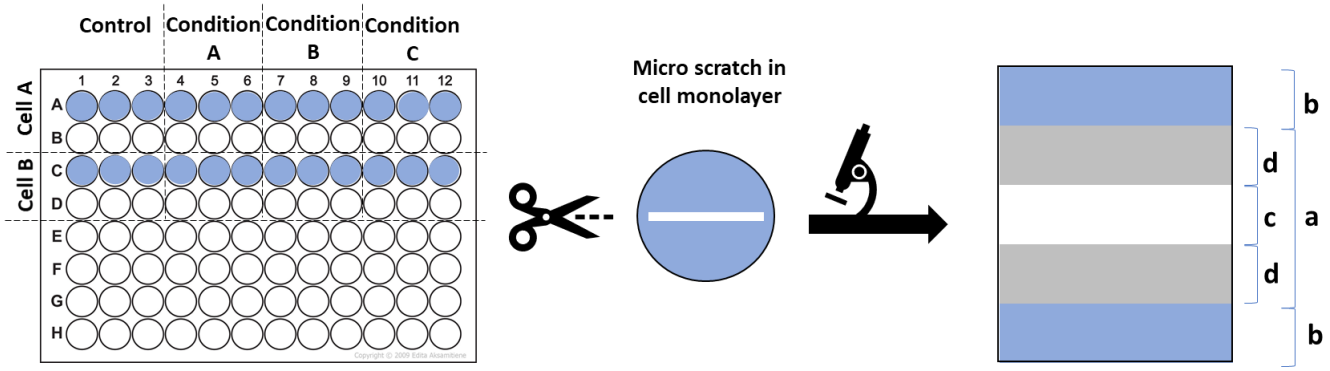

Figure 2.3. An illustration of the technical method of scratch wound healing assay. Cells are seeded to form a monolayer in a 96-well plate. A scratch wound is applied. Serial images are taken in time lapse mode to capture the process of wound healing for at least 48 hours after the scratch. a: initial wound area or wound width at time 0, b: non-wound area at time 0, c: wound area or wound width at time z,

d: wound confluency (fractional width of the initial wound occupied by cells at time z). Adapted from the assay manual.

2.4.3 Measurement of intracellular cAMP level changes in response to antidepressant drugs treatment using FRET Epac-based cAMP sensor

Föster resonance energy transfer (FRET) is the physical transference of light energy from one molecule, the donor to another, the acceptor (238). The efficacy of transfer depends on the proximity and geometrical interrelation of the two fluorophores (238). A typical FRET sensor consists of donor fluorophore, acceptor fluorophore, and ligand binding site. Upon binding of the ligand, the geometrical alignment of the two fluorophores changes. This affects the amount of energy transferred from the donor to the acceptor fluorophore (238). As a result, the relative quantities of photons emitted by donor and acceptor changes and this is what is registered by an optical instrument, such as a confocal microscope.

Measuring changes of intracellular cAMP level in GBM cells in response to drugs was carried out using Epac (Exchange protein directly activated by cAMP)-based FRET sensors kindly provided by Prof Kees Jalink (van Leeuwenhoek Centre of Advanced Microscopy, Amsterdam, The Netherlands) and described in (239). This sensor consists of donor cyan fluorophore (CFP), acceptor yellow fluorophore (YFP), and cAMP-binding domain based on the molecular structure of Epac (240). Physiologically, Epac protein binds cAMP and regulates the function of downstream proteins of cAMP pathway Rap-1 and Rap-2 (239). In a FRET experiment as in **Figure 2.4**, binding of cAMP to the Epac-based sensor causes conformational changes in the structure of the sensor, pulling the two fluorophores apart, and decreasing the amount of energy transfer (240). Hence, CFP fluorescence increases and YFP decreases.

cAMP EPAC sensor was delivered by plasmid transfection. On day 1, GBM cells were plated on glass coverslips coated with type I rat tail collagen as described in section 2.1.4, and placed inside 24-well plate, at density of roughly 3,000-4,000 cells/ 500µl/ well. Next day, plasmid transfection with mT2-Epac high aff-cpVcpV plasmid was carried out using TurboFect transfection reagent (Thermo Scientific R0531) to deliver the construct into GBM

cells. Transfection was carried out according to the manufacturer protocol using transfection reagent to DNA ratio 2:1. On day 3, media in wells were replaced with fresh media containing different concentrations of drugs (IM, CL, or NKH477). On day 4, 2 days post transfection, measurements were performed on Leica SP5 spectral confocal microscope. The readout is obtained by ratiometric measurement of CFP and YFP emissions as CFP/YFP ratio (channel 1/ channel 2), the higher ratio reflects higher intracellular cAMP level. Excitation wavelength was 458 nm, and emission was detected within 465-495 nm for CFP and within 515-560 nm for YFP. Parameters such as laser power, photomultiplier tube (PMT) sensitivity, pinhole and resolution were fixed throughout all imaging sessions. Images were analysed using Leica software quantifying tool.

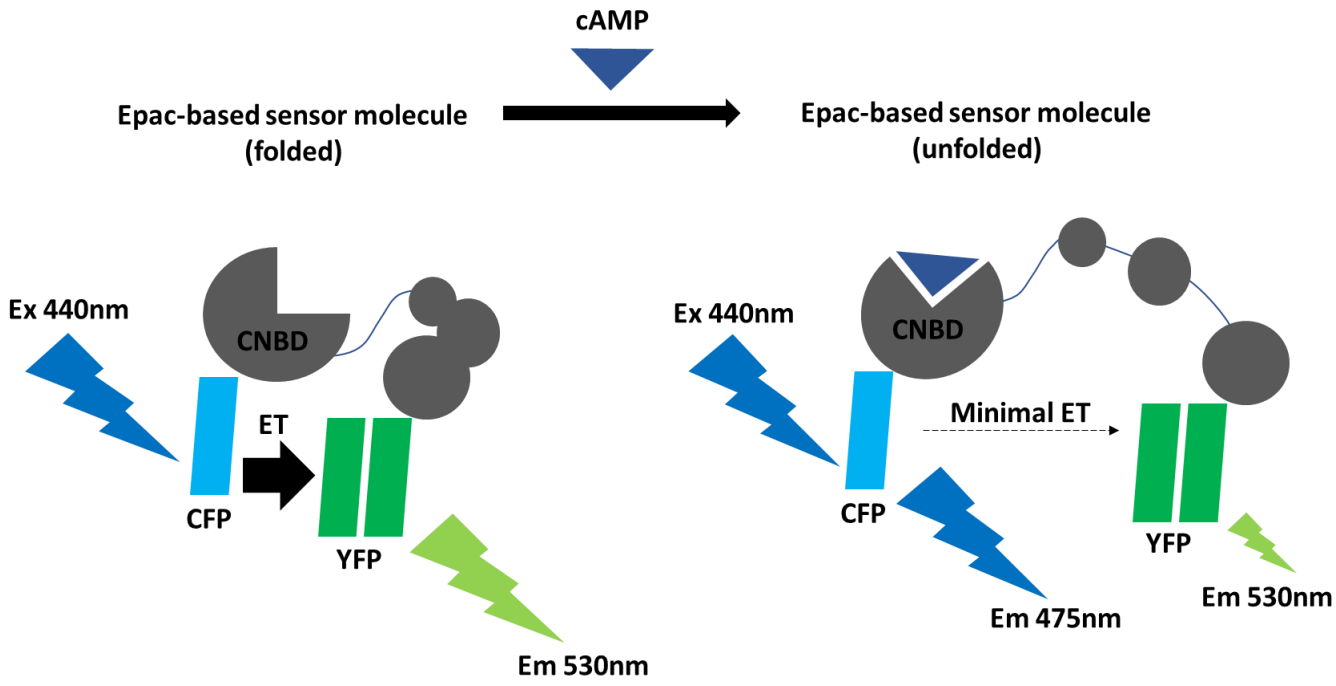

Figure 2.4. A schematic diagram of the Epac-based cAMP FRET sensor. CNBD: cyclic nucleotide binding domain, Ex: excitation wavelength, Em: emission wavelength, CFP: cyan fluorescent protein (donor fluorophore), YFP: yellow fluorescent protein (acceptor fluorophore), ET: energy transfer. Adapted from Ponsioen B, et al., 2004 **(240)**.

2.4.4 Assessment of Mitochondrial Membrane potential (MMP) in normal RA and GBM cells

Potential of the mitochondria is a critical determinant of mitochondrial ability to generate ATP and is also a signature of cell's metabolic status. One of the objectives of this project required evaluation of MMP in context of drug action and effects of photodynamic therapy. Therefore, an experiment was done to establish baseline MMP measurements for all untreated GBM cell lines as well as normal RA. This was achieved using Tetramethyl-rhodamine methyl ester (TMRM), which is a lipophilic cationic florescent dye that is potentially driven to specifically accumulate in the mitochondria in proportion to MMP. Therefore, TMRM is often used to estimate MMP and to assess mitochondrial integrity (223, 241, 242).

Cells were plated in a 96-well plate at density of 6,000 cells/ 100ul/ well. Plates were kept in the cell culture incubator at standard conditions overnight. Next day, culture media in each well was replaced with media containing 200nM TMRM and cells were incubated with the dye for 1 hour. After that, images were taken using ZOE™ Fluorescent Cell Imager. ImageJ software was used to measure dye intensity as an estimate for MMP.

2.4.5 Evaluation of antidepressants' effect on MMP of GBM cells and RA using JC-10 MMP assay

JC-10 method was used in conjunction with TMRM in experiments concerning MMP of GBM and RA. JC-1 (5,5',6,6'tetrachloro-1,1',3,3'-tetraethylbenzimidazole-carbocyanine) is a lipophilic fluorescent mitochondrial dye which can selectively enter the mitochondria driven by the MMP (243, 244). JC-10 Abcam® is a modified version of JC-1 mitochondrial probe with higher water solubility. According to the manufacturer guide, JC-10 monomers in the cytoplasm emit green florescence that can be detected at 520 nm. Upon entering the mitochondria, JC-10 monomers form aggregates and now emit orange/ red florescence that can be detected at 590 nm. The ratio between orange/ red to green florescence is used to estimate dye accumulation inside the mitochondria, which reflects the MMP.

On day 1, cells were plated in 96-well plates with black walls and clear flat bottom. Density of cells plated was 6,000 cells/ 100ul/ well for UP007 and UP029 GBM cells and 8,000 cells/ 100ul/ well for RA. Plates were kept in the incubator in standard conditions overnight. Next day, culture media in each well was replaced with fresh media containing different concentrations of drugs: from 0 to 50 µM IM, from 0 to 25 µM CL and FLX, 5 µM of mitochondrial un-coupler FCCP as a positive control, and 10 µM NKH477 (AC activator) for comparison. After 3 days of drug incubation, JC-10 assay was performed by adding 50 µL/ well of the dye-loading solution then incubating the plate in cell culture incubator at standard culture conditions for 1 hour. Next, 50 µL/ well of the assay buffer were added and the plate was kept at room temperature protected from light. After 15 minutes, measurements of fluorescence intensity at Ex/Em = 490/525 and 540/590 nm were obtained using Infinite® 200 PRO microplate reader set on bottom-reading mode.

Chapter 3: RESULTS-1

Identifying Heterogeneity in My GBM Sample

3.1 Heterogenous morphology of GBM cells

In my project I used a range of GBM cell lines obtained using different methods, from different areas of the tumours and from different patients. Images of GFP-tagged GBM cells were taken using upright Leica SP5 confocal laser scanning microscopes with 25x water immersion objective. **Figure 3.1** shows different morphology of these lines. For example, UP029 GBM cells were thin and elongated, similar to GIN8 and GIN28, and different from GIN27, which were obviously bigger and flatter. UP007 and GIN31 GBM cells' morphology was somewhere in between, cells being relatively large but also elongated. These GFP expressing stable cell lines were then cryopreserved and will be used for future work.

3.2 Differential effect of TMZ (standard drug of choice in GBM) on the 6 GBM cells

I decided to assess the effects of TMZ, as the standard of care drug, on GBM cells to examine for heterogenous sensitivity within my cohort of GBM cells. TMZ was applied for 9 days and control wells were supplemented with media containing the same amount of DMSO as used to dissolve TMZ. After 9 days, PrestoBlue assay was carried out as described in Methods section 2.2.1. This longer exposure time was chosen to simulate the clinical protocol of TMZ, which involves administration of TMZ in extended cycles with an intention to deplete cellular DNA repair mechanisms (95). Information about TMZ is presented in Chapter 1 section 1.1.8.

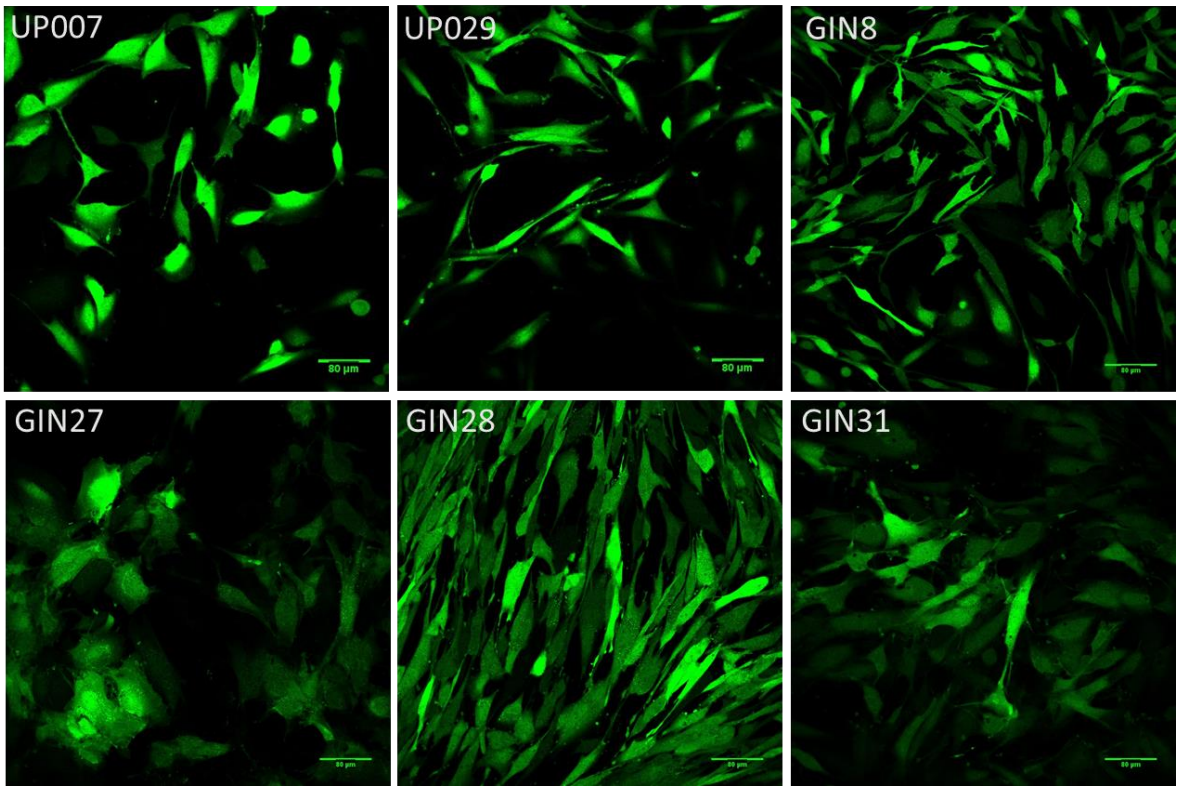

Figure 3.1. Confocal images of GFP-tagged GBM cells reveal heterogenous morphology. Scale bar: 80 µm.

The results of this analysis are rather surprising. It appears that RA which were used as control did not seem to be affected by TMZ more than by an equivalent concentration of DMSO **(Figure 3.2 a)**. UP007, UP029, and GIN28 exhibited sensitivity to TMZ **(Figure 3.2 b, c, and f)**, while GIN8, GIN27, and GIN31 were almost insensitive to it **(Figure 3.2 d, e, and g)**. In a previous publication, UP007 were also found to be sensitive to TMZ in-vitro in a concentration-dependent manner (245). Calculated EC_{50} values are: 41.46 µM for UP007, 149.9 µM for UP029, and 35.92 for GIN28. Here again, we see heterogeneity translated into different levels of sensitivity to therapy which is most probably linked to resistance mechanisms. GBM cells are known for their ability to evade chemotherapy and there are some reported mechanisms of this resistance discussed in chapter 1. It also appears that only 1 of the 4 cell lines derived from the leading edge of the GBM is sensitive to TMZ, possibly adding weight to the argument that infiltrating, fast migrating cells are equipped with survival mechanisms and are extremely aggressive.

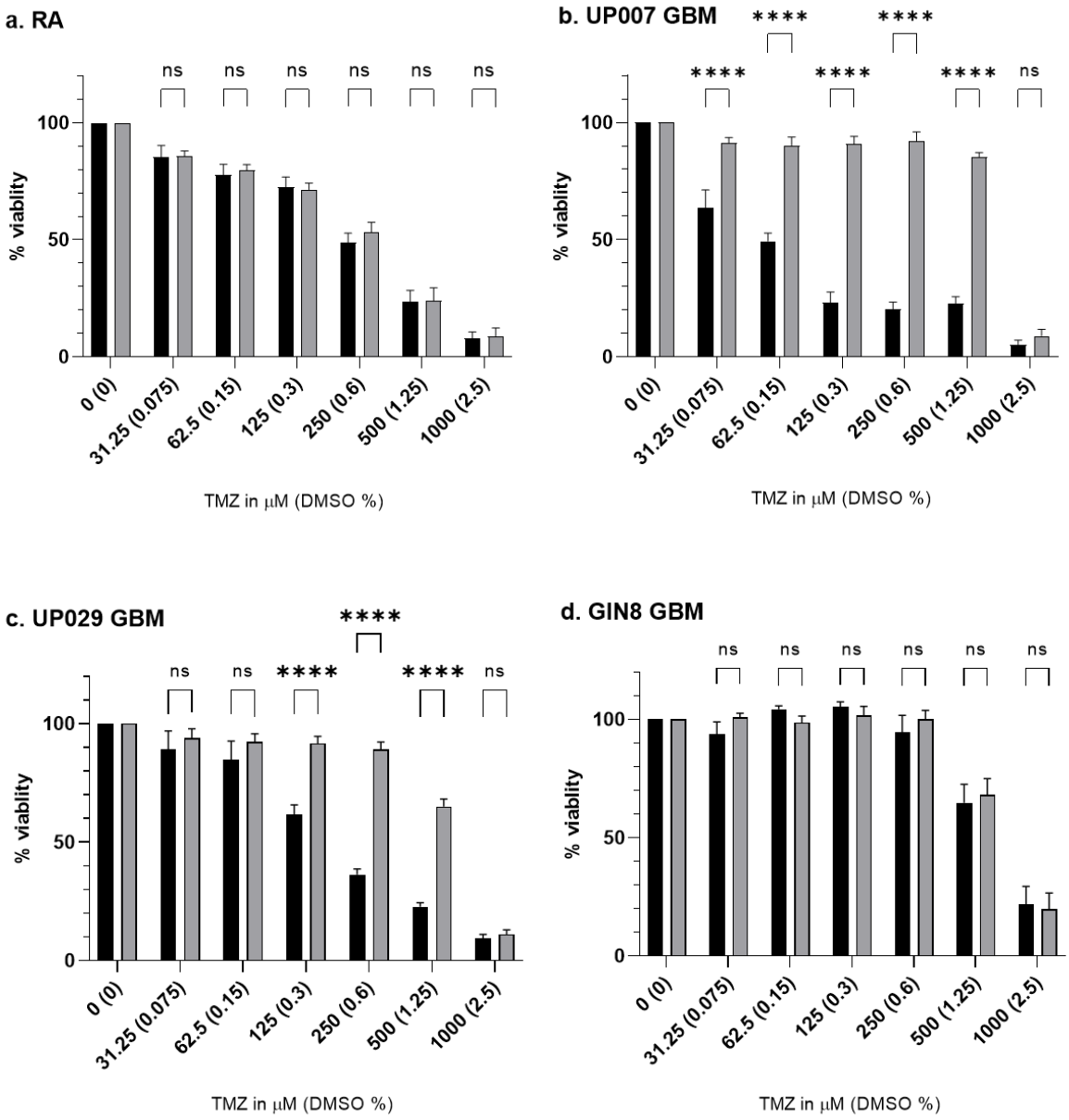
a. RA
ns
ns
ns
ns
ns
ns
100
50
0
% viability
0 (0)
31.25 (0.075)
62.5 (0.15)
125 (0.3)
250 (0.6)
500 (1.25)
1000 (2.5)
TMZ in μM (DMSO %)
b. UP007 GBM
****
****
****
****
****
ns
100
50
0
% viability
0 (0)
31.25 (0.075)
62.5 (0.15)
125 (0.3)
250 (0.6)
500 (1.25)
1000 (2.5)
TMZ in μM (DMSO %)
c. UP029 GBM
****
ns
ns
****
****
ns
100
50
0
% viability
0 (0)
31.25 (0.075)
62.5 (0.15)
125 (0.3)
250 (0.6)
500 (1.25)
1000 (2.5)
TMZ in μM (DMSO %)
d. GIN8 GBM
ns
ns
ns
ns
ns
ns
100
50
0
% viability
0 (0)
31.25 (0.075)
62.5 (0.15)
125 (0.3)
250 (0.6)
500 (1.25)
1000 (2.5)
TMZ in μM (DMSO %)

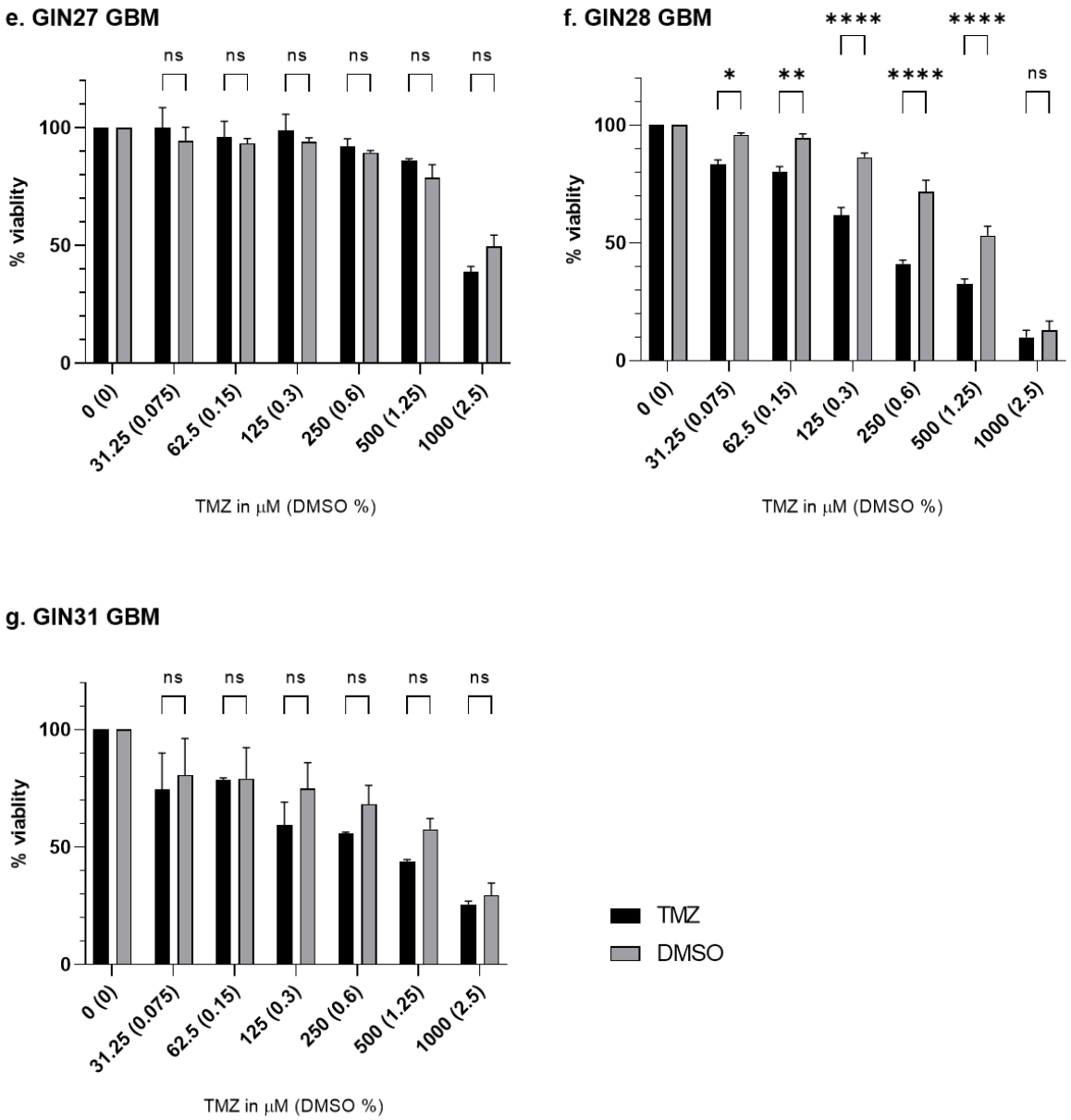

Figure 3.2. TMZ toxicity assessed using PrestoBlue assay. Effects of different concentrations of TMZ and the corresponding concentrations of DMSO were tested after 9 days of exposure. *(ns) p >0.05, (*) p <0.033, (**) p <0.002, (***) p <0.0002, (****) p <0.0001, alpha= 0.05.* the number of independent experiments (n) is 5 for RA and UP GBMs, 4 for GIN8 and GIN28 GBMs, and 2 for GIN27 and GIN31 GBMs, all in triplicates. Statistical method: two-way ANOVA, and Tukey's and Šídák's multiple comparisons tests. Data presented as mean ± standard error of the mean (SEM).

3.3 Molecular signature of common glioblastoma driver genes in this cohort of primary GBM cells.

GBM are notorious for their genomic instability. Moreover, multiple mutations have been linked to the malignant transformations as mentioned in detail in Chapter 1. Mutations have been analysed by various groups and are summarised at various WEB resources, such as https://www.intogen.org.

As shown in the previous sections, my sample of GBM cell lines is quite diverse in morphology and sensitivity to TMZ. Possibly these differences could be a consequence of different mutations present in these cell lines. Therefore, I decided to assess mutational status of GBM cell lines. Initially I planned to perform a wider screen of larger number of transcripts using Oxford Nanopore sequencing protocol. However, due to a COVID pandemic and loss of time and access to the laboratory, I had to adopt a simplified strategy.

Four well characterised GBM driver genes have been chosen IDH-1, p53, PTEN, and EGFR. A range of primers were generated to cover their protein-coding parts, listed in chapter 2 **Table 2.1**, and RT-PCR was used to amplify products which were then processed individually using Sanger sequencing process.

After RNA extraction, cDNA synthesis (reverse transcription), and PCR with the appropriate primer, PCR products were run in agarose gel electrophoresis to examine the expression of 4 commonly mutated glioma-driver genes, IDH-1, p53, PTEN, and EGFR. All PCR products from all 6 GBM samples were visualised as clear bands of expected sizes on agarose gel electrophoresis. Examples are shown in **Figure 3.3.** Main findings are illustrated in graphic format in **Figures 3.4. to 3.7**. Results of sanger sequencing are summarized in **Table 3.1.**

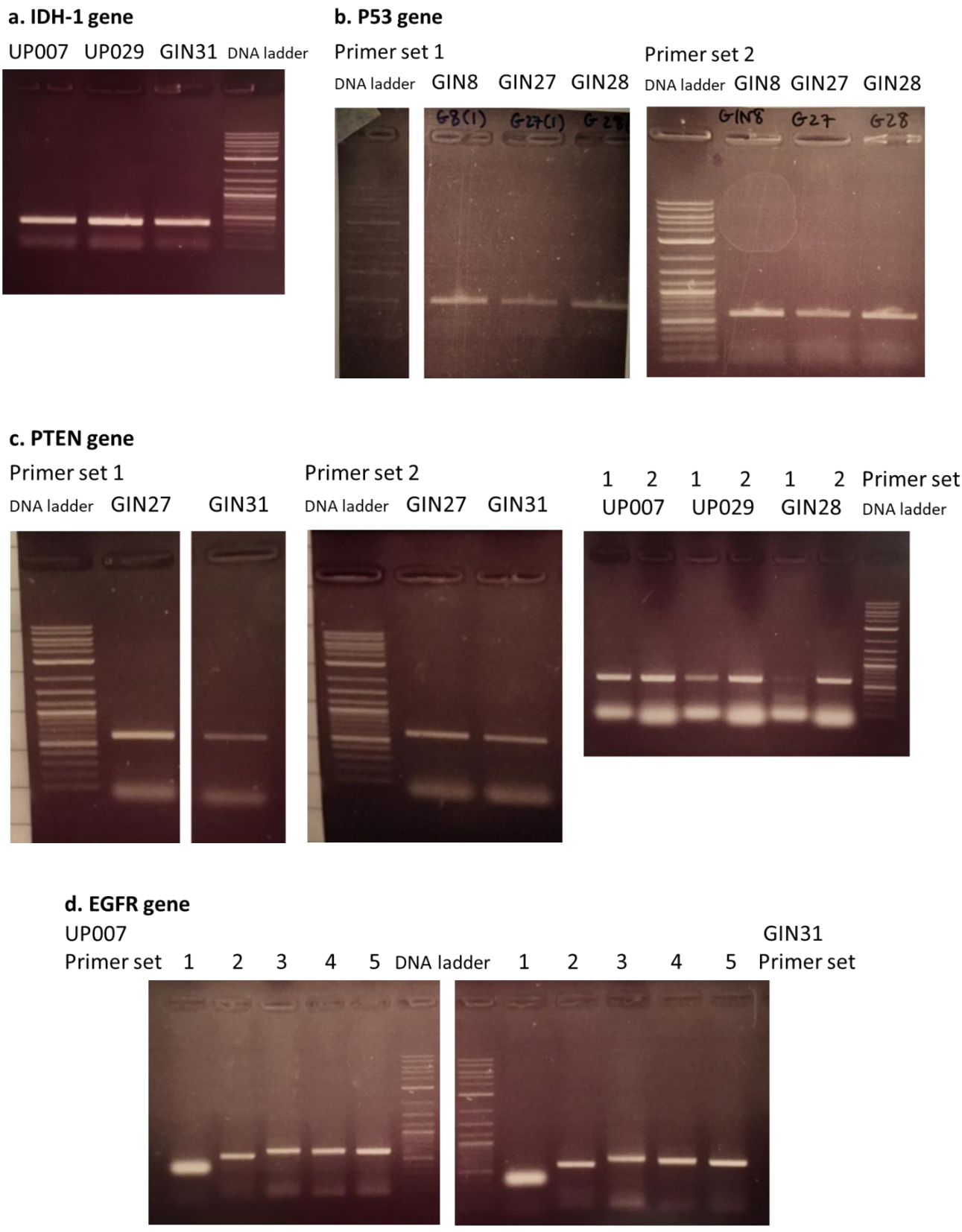

Figure 3.3. Examples of images of agarose gel electrophoresis. PCR products were run in agarose gel electrophoresis in order to examine GBM cells for commonly mutated genes implicated in GBM.

UP007, UP029, and GIN31 are IDH1-wt **(Figure 3.4)**. Sequencing of IDH-1 failed for GIN8 and was not done for GIN27 and GIN28 due to time constraints. UP007 and GIN31 shared a similar mutation in p53 gene: CA to TG substitution at nucleotide position 880 and 881 (only A to G substitution in GIN31), plus T to C substitution at nucleotide position 988 **(Figure 3.5 c and d)**. In UP007, CA to TG substitution produces a histidine to cysteine substitution at amino acid position 273, while in GIN31, A to G substitution results in histidine to arginine substitution. Amino acid position 273 is a known hotspot for mutations in p53 gene (246, 247). Mutations at this site affect DNA binding capacity of p53 protein (246, 247). The T to C substitution at nucleotide position 988 results in serine to proline substitution at amino acid position 309. This mutation was not reported in the top 50 common mutations in p53 gene (246), although serine residues at the carboxy-terminal domain are known targets for phosphorylation for p53 activation (54, 248), and mutations of any of these residues will theoretically disturb p53 response to stress signals. In GIN8 cells, G to C substitution at nucleotide position 735 was found, which results in glutamate to aspartate substitution at amino acid position 224 **(Figure 3.5 b)**. To the best of my knowledge, I couldn't trace any publication reporting this specific mutation in p53 gene. In GIN28, C to T substitution was found at nucleotide position 598, which results in histidine to tyrosine substitution at amino acid position 179 **(Figure 3.5 a)**. This mutation was listed among the top 50 common somatic mutations of p53 gene, with high score for predicted protein misfolding (246).

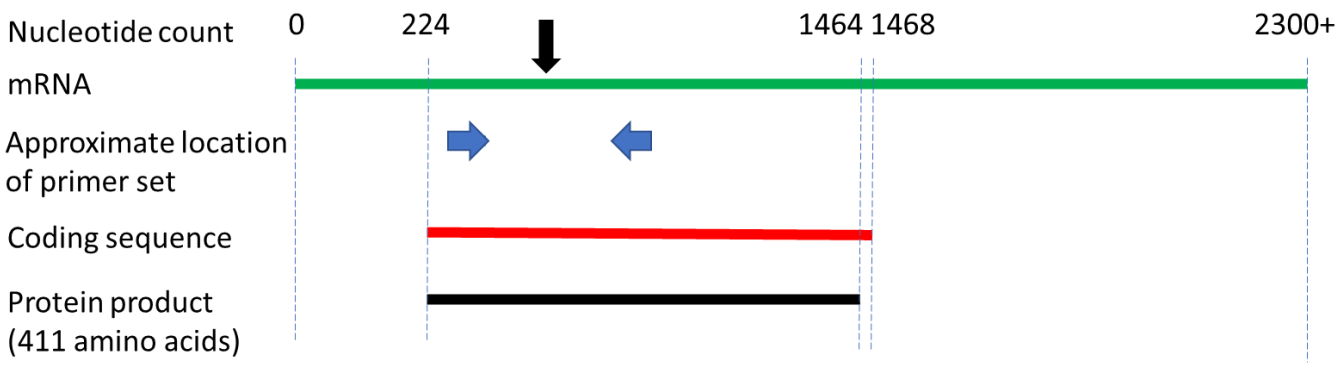

Figure 3.4. Schematic representation of mRNA sequence of human IDH-1 gene. The arrow indicates the common site of mutation of IDH-1 gene at nucleotide position 617-619 resulting in substitution of arginine in the amino acid sequence (>90% are R132H mutation: substitution of arginine with histidine at position 132 of amino acid sequence). UP007, UP029, and GIN31 lacked this mutation.
Reference: https://www.intogen.org/search?cancer=GBM&gene=IDH1#distribution:plot
NCBI sequence reference NM_005896.4
(249) (250)

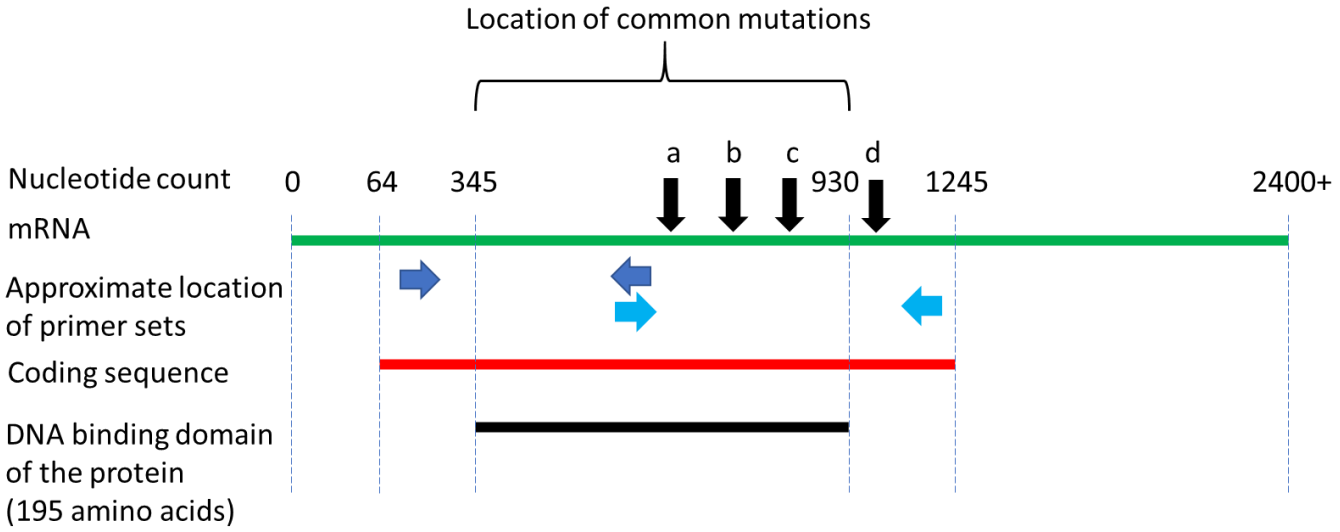

Figure 3.5. Schematic representation of mRNA sequence of human p53 gene. Mutations found in our GBM are mapped as (a) C to T substitution at nucleotide position 598 of mRNA of GIN28 GBM cells, (b) G to C substitution at nucleotide position 735 of the mRNA of GIN8 GBM cells, (c) CA to TG substitution at nucleotide position 880 and 881 of the mRNA in UP007 GBM cells, also noted in GIN31 but only in a form of A to G substitution at position 881, and (d) T to C substitution at nucleotide position 988 of the mRNA noted in UP007 and GIN31.
Reference: https://www.intogen.org/search?cancer=GBM&gene=TP53#distribution:plot
GenBank sequence reference AB082923.1
(249) (250)

Regarding EGFR gene, a common G/A synonymous SNP at nucleotide 2622 (variation ID: rs1050171) is found in UP007, UP029, GIN8, and GIN 31 **(Figure 3.6 a)**. This SNP has been linked to better clinical outcome in colon cancer and small cell carcinoma of the lung (251, 252). To the contrary, this SNP was correlated to worst survival in non-small-cell lung carcinoma (253) and oesophageal cancer patients (254). No published data on this SNP in GBM was found. Thymine insertion at nucleotide position 2770 which was found in UP007 and UP029 results in stop codon at amino acid position 837 within tyrosine catalytic domain **(Figure 3.6 b).** In UP029, T/C synonymous SNP was detected at nucleotide position 2970 as shown in **Figure 3.6 c** (variation ID: rs1140475). This SNP has been identified in colon, bladder, and lung cancer but it was not significantly associated with higher risk of developing these cancers (255, 256). Unfortunately sequencing of products of PTEN gene was unsuccessful. The only results I can report is that UP029 have no mutations in their DSPc **(Figure 3.7)** domain which encodes the tyrosine phosphatase-like catalytic domain in PTEN protein, and that GIN8 is probably wildtype, but no meaningful conclusions could be drawn. I was unable to repeat the sequencing reactions due to time constrains.

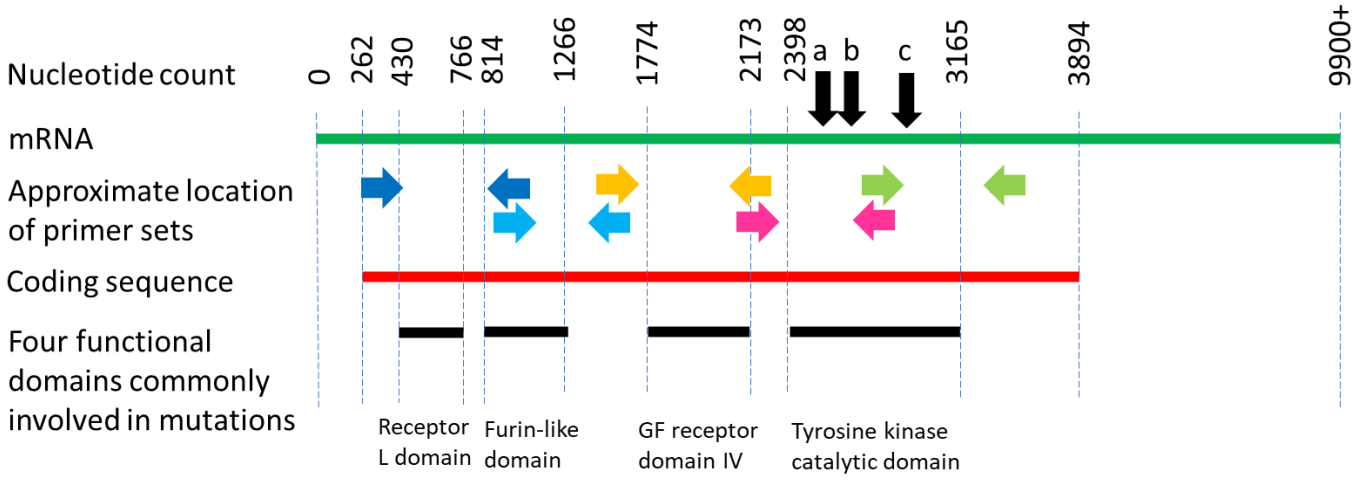

Figure 3.6. Schematic representation of mRNA sequence of human EGFR gene. Common mutations found in our GBM cells are mapped as (a) G to A substitution at nucleotide position 2622 is seen in UP007, UP029, GIN8, and GIN31, (b) Thymine insertion is found at position 2770 in UP007 and UP029, and (c) T to C substitution at nucleotide position 2970 is seen in UP029, GIN8, and GIN31. Other mutations found are listed in table 3.2.
Reference: https://www.intogen.org/search?cancer=GBM&gene=EGFR#distribution:plot
NCBI sequence reference NM_005228.5
(257)

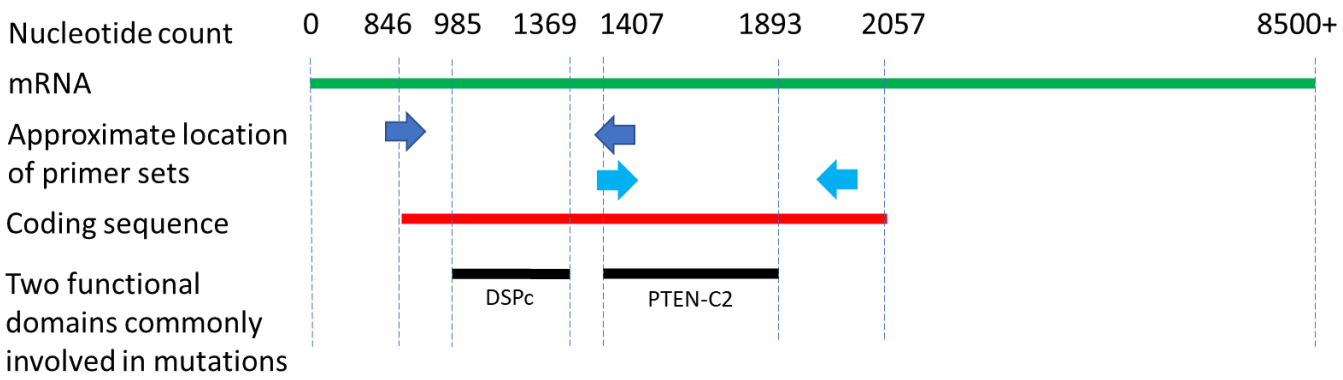

Figure 3.7. Schematic representation of mRNA sequence of human PTEN gene.
Reference: https://www.intogen.org/search?cancer=GBM&gene=PTEN#distribution:plot
NCBI sequence reference NM_000314.8
(258)

Table 3.1. Summary of the results of sequencing of 4 genes implicated in the development of GBM.
WT: wild type, nt: nucleotide, SNP: single nucleotide polymorphism. Similar findings are colour coded.

	IDH-1	p53	EGFR*	PTEN
UP007	WT	Within DNA binding domain of the protein: - CA to TG substitution at nt position 880 and 881 (hotspot for mutations). T to C substitution at nt position 988 (possible site for p53 protein phosphorylation).	Part of the sequencing result is missing (failed sequencing with primer set 1 plus some missing data towards the end of the sequencing reaction). Within Furin-like region: - G to A substitution at nt position 1030 (no published reports). - G to C substitution at nt position 1143 (no published reports). Within Tyrosine kinase catalytic domain: - G to A substitution at nt position 2622 (SNP). - thymine insertion at 2770 (stop codon)	Sequencing failed
UP029	WT	No mutations detected with primer set 1 but sequencing failed with primer set 2.	Part of the sequencing result is missing (small gaps).	Failed sequencing with primer set 2,

			Within Furin-like region: G to C substitution at nt position 876 (no published reports). Within Tyrosine kinase catalytic domain - G to A substitution at nt position 2622 (SNP). - thymine insertion at 2770 (stop codon). - cytosine insertion at 2905 (frameshift- no published reports) - T to C substitution at nt position 2970 (SNP).	otherwise no mutations.
GIN8	Sequencing failed	G to C substitution at nt position 735 (within DNA binding domain of the protein- no published reports). Some of sequencing results are missing.	Part of the sequencing result is missing (small gaps). C to T substitution at nt positions 487 and 507 (within Receptor-L domain- no published reports). Within Tyrosine kinase catalytic domain: - G to A substitution at nt position 2622 (SNP). - T to C substitution at nt position 2970 (SNP).	Small gaps in sequencing results, otherwise no mutations.
GIN27	Not done	Failed sequencing with primer set 2, otherwise no mutations.	Not done	Sequencing failed
GIN28	Not done	C to T substitution at nt position 598 (within DNA binding domain of the protein). Failed sequencing with primer set 2.	Not done	Sequencing failed
GIN31	WT	Within DNA binding domain of the protein: - A to G substitution at nt position 881 (hotspot for mutations). T to C substitution at nt position 988 (possible site for p53 protein phosphorylation).	Failed sequencing with primer set 1. Adenine insertion at 1024 and 1030 (within Furin-like region- frameshift- no published reports). Within Tyrosine kinase catalytic domain: - G to A substitution at nt position 2622 (SNP). - cytosine insertion at 2773 (frameshift- no published reports) - T to C substitution at nt position 2970 (SNP).	Sequencing failed

To conclude this section, it was feasible to assess the mutational status of the 4 driver genes in GBM cells using RT-PCR and Sanger sequencing. I have identified certain key mutations in p53 gene in UP007, GIN28, and GIN31 which most probably resulted in loss of p53 tumour suppressor function and contributed to the development of GBM in the patients from whom these cells were obtained. SNPs in EGFR were documented in UP007, UP029, GIN8, and GIN31 in tyrosine kinase domain which is responsible for the phosphorylation function of the receptor. These mutations are correlated to cancer risk in some cancer types, but no reports could be found on their impact on GBM risk.

This sequencing approach could be improved with the use of parallel sequencing methods such as Oxford nanopore sequencing. This method relies on direct reading of nucleotide sequences rather than the use of DNA synthesis for detection as in Sanger sequencing. As a result, this method has high throughput with no length limit of the sequenced nucleic acid fragments. In future work, Oxford nanopore sequencing protocol should be developed for wide scale genomic analysis of molecular heterogeneity in GBM samples.

Chapter 4: RESULTS-2

Evaluation of the Feasibility and Efficacy of TMRM as a Photosensitizer for Photo-dynamic Therapy of GBM

4.1 GBM cell lines have high basal mitochondrial membrane potential (MMP).

As explained in the introduction, mitochondria has been considered as an important player in the survival of cancer cells including GBM cells. Mitochondria is also the origin and primary trigger of the intrinsic apoptotic cascade (222). In this chapter I have looked further into the properties of the mitochondria in GBM cell lines and investigated the potential use of the technology known as PDT using TMRM as a novel photosensitiser.

Mitochondria accumulate TMRM, which is driven into them by the membrane potential against concentration gradient. TMRM is frequently used for estimation of MMP (241, 242, 259). In these experiments and all others which follow, I used both types of GBM cell lines, including those obtained using conventional approaches (UP007 and UP0029) and more recently derived lines from the GBM leading edge (GIN cell lines).

Cells were loaded with 200nM of TMRM for one hour, then images were obtained using ZOE™ Fluorescent Cell Imager. **Figure 4.1** demonstrates that GBM cells, with only one exception, have MMP which is significantly more polarized (hyperpolarized) than MMP of RA. Indeed, the only exception was GIN27, which has an MMP not significantly different from that of RA.

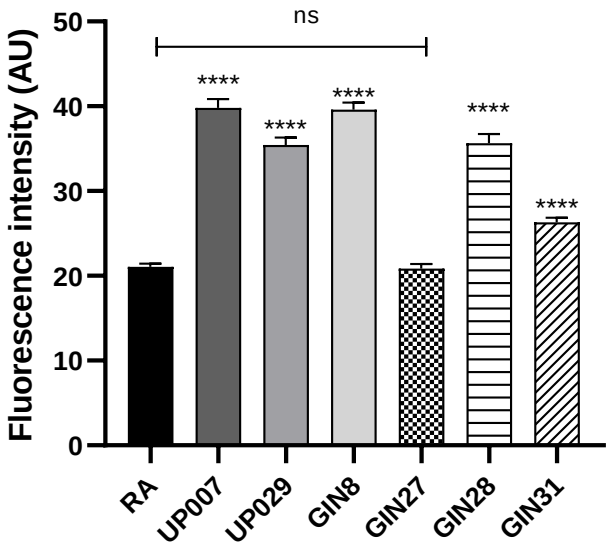

Figure 4.1. Estimation of baseline MMP using TMRM mitochondrial dye. Florescent intensity after TMRM staining was measured, which correlates with MMP. All except one (GIN27) GBM cells have significantly higher baseline MMP than RA. *(ns) p >0.05, (****) p <0.0001. alpha 0.05.* n= RA:155, UP007: 80, UP029:72, GIN8:71, GIN27:77, GIN28:76, and GIN31:82. n is the total number of cells examined from 6 independent experiments on RA, and 3 on GBM cells. Statistical method: one-way ANOVA and Tukey's multiple comparison test. Data presented as mean ± SEM.

These results are consistent with a view, previously expressed in the literature, that mitochondria in tumour cells are hyperpolarised (260-262). It is very interesting to note that here again a striking heterogeneity of GBM cells is observed, which reinforces the need to utilize a wide range of patient derived samples for hypothesis testing rather than employing one or two types of commercial cell lines, often of unclear origin.

By serendipity, while imaging cells for MMP, our laboratory discovered that TMRM could be utilized as an effective PS in PDT against GBM. TMRM localizes almost exclusively in the mitochondria **(Figure 4.2)**. After brief exposure to green light of moderate intensity, TMRM-loaded GBM cells' mitochondria rapidly depolarised. Evident by redistribution of TMRM out of the mitochondria into the cytoplasm. We reasoned that this phenomenon may have therapeutic value. Strong depolarisation is generally thought to lead to irreversible damage to the mitochondria and the release of pro-apoptotic molecules, which eventually should lead to cells death (222).

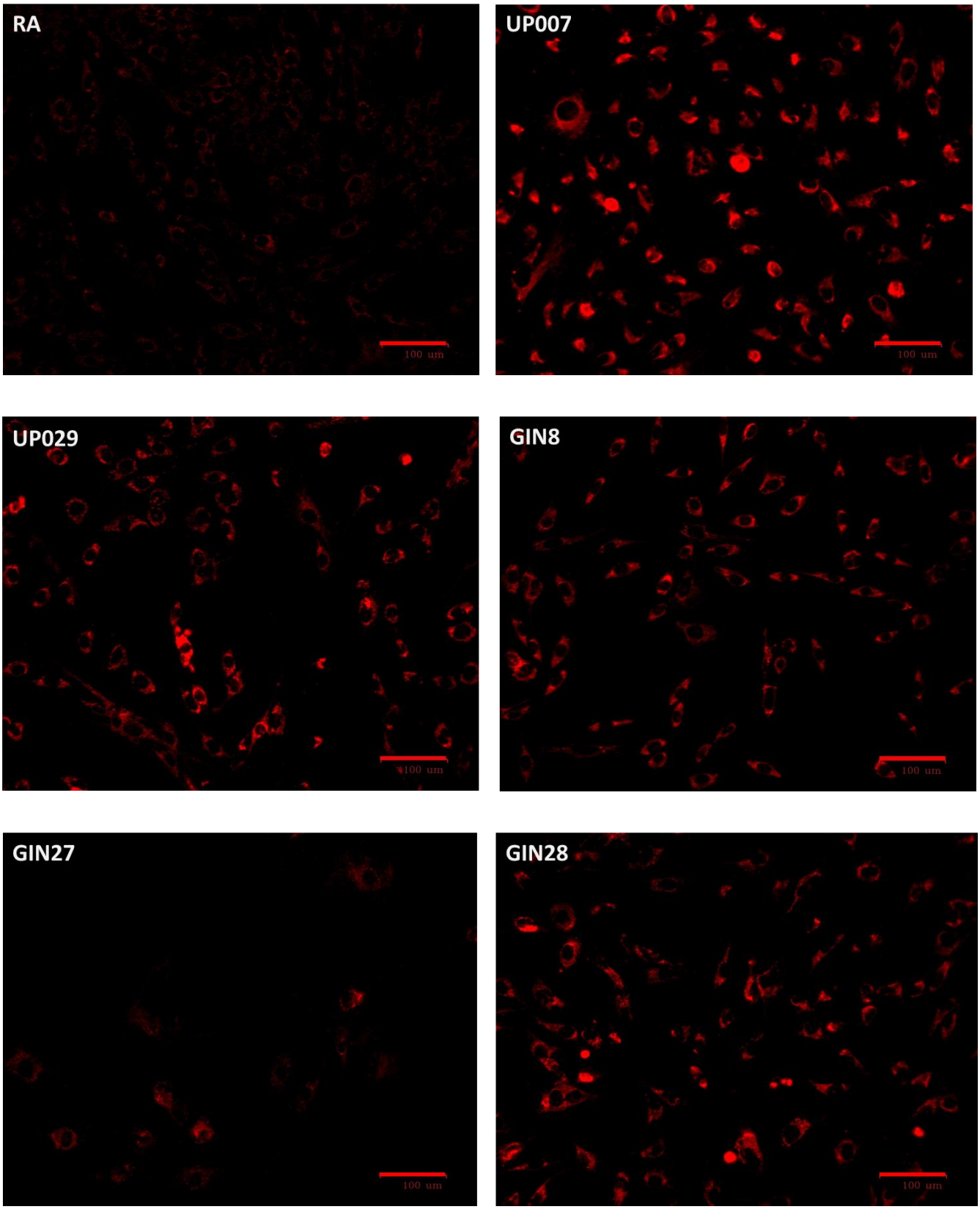
RA
100 um
UP007
100 um
UP029
100 um
GIN8
100 um
GIN27
100 um
GIN28
100 um

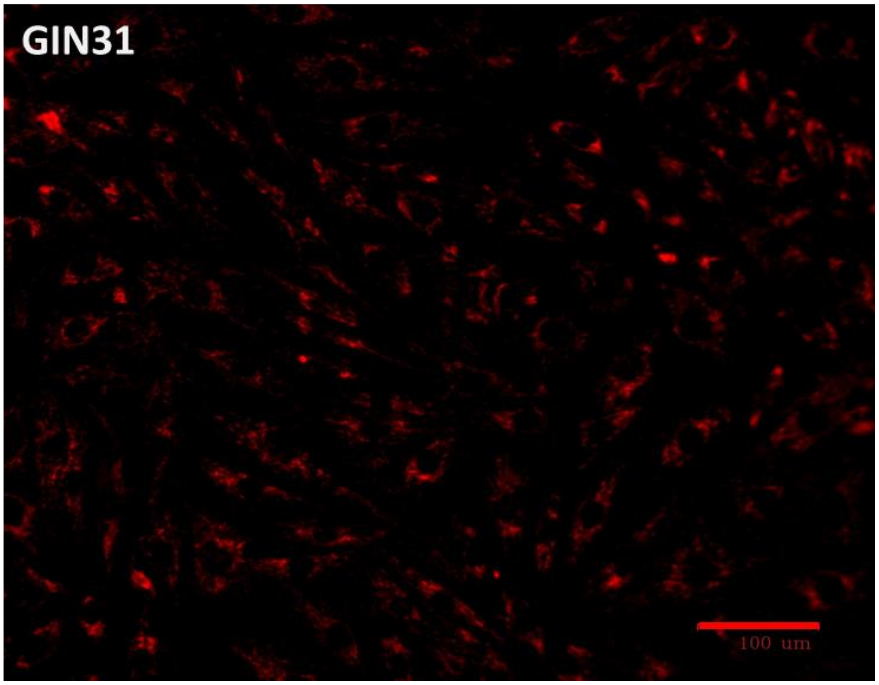

Figure 4.2. Localization of TMRM inside the mitochondria of RA and GBM cells. Cells were loaded with 200nM TMRM for 1 hour prior to imaging. Note the lower uptake of TMRM in RA and GIN27 cells which is consistent with the data in figure 4.1. n=6. Scale bar= 100µm.

4.2 TMRM decay dynamics

To examine the dynamics of TMRM decay after photoactivation, cells were loaded with 100nM TMRM for 1 hour then baseline images were obtained. Exposure time for imaging was 200 ms. As can be seen from **Figure 4.3,** TMRM fluorescence without prolonged light application is very stable. Light illumination then followed using LED-powered green light source. Immediately after 30 seconds of constant light application (1.4mW/mm^2), serial images were obtained every 10 second for 3 minutes. **Figure 4.3** illustrates the dynamics of TMRM decay due to the dissipation of MMP. UP007, UP029, GIN8, GIN28, and GIN31 all experienced a sharp decline in TMRM mitochondrial/ nuclear fluorescence ratio caused by mitochondrial depolarization due to TMRM photoactivation. Interestingly, the trace for GIN27 in **Figure 4.3** is almost a flat line, indicating no effect of light illumination of TMRM on the MMP of these cells. Indeed, they had lower basal fluorescence ratio to start with, which is consistent with data shown in **Figure 4.1** and **4.2**.

This is also seen with RA, which had a lower basal ratio and a mild drop of fluorescence ratio after light illumination.

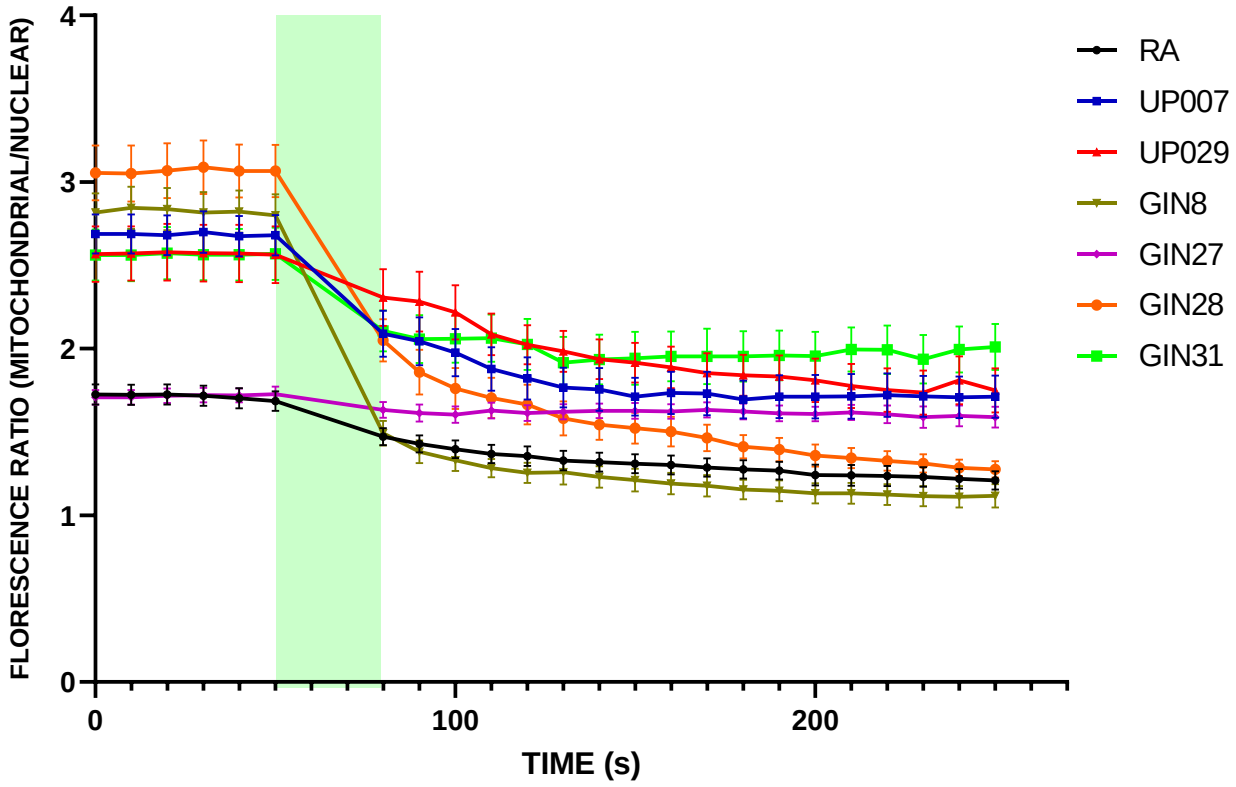

Figure 4.3. The dynamics of TMRM decay after photoactivation in RA and GBM cell lines. After light illumination (1.4mW/mm^2), GBM cells immediately released TMRM which reflects the drop in their MMP. The number of independent experiments is 4 for RA, 3 for UP GBM cells, 2 for GIN GBM cells. The total number of cells examined is 24 for RA, 21 for UP007, 19 for UP029, 11 for GIN8, 16 for GIN27, 14 for GIN28, 10 for GIN31 GBM cells. Data points presented as mean ±SEM.

By comparing initial ratios at time zero to the final ratios at the end of the trace, it may be seen that RA were significantly affected by the photoactivation, but the drop in their MMP is smaller (30.9% ± 3.1 SEM) compared to the GBM cells (with the exception of GIN27: 7.2% ± 2.2 and GIN31: 20.8% ± 4.5) **(Figure 4.4)**. UP007 has lost 36.2% ± 3.5, UP029 has lost 32.2% ± 5.8, GIN8 has lost 59.4% ± 3.1, and GIN28 has lost 57.0% ± 2.4 of their MMP (mean ± SEM). It is overall reasonable to hypothesise that stronger loading of the mitochondria with TMRM as a result of greater MMP could make cells more susceptible to the PDT action of TMRM. **Figure 4.5** is a representative example of the images obtained for this analysis.

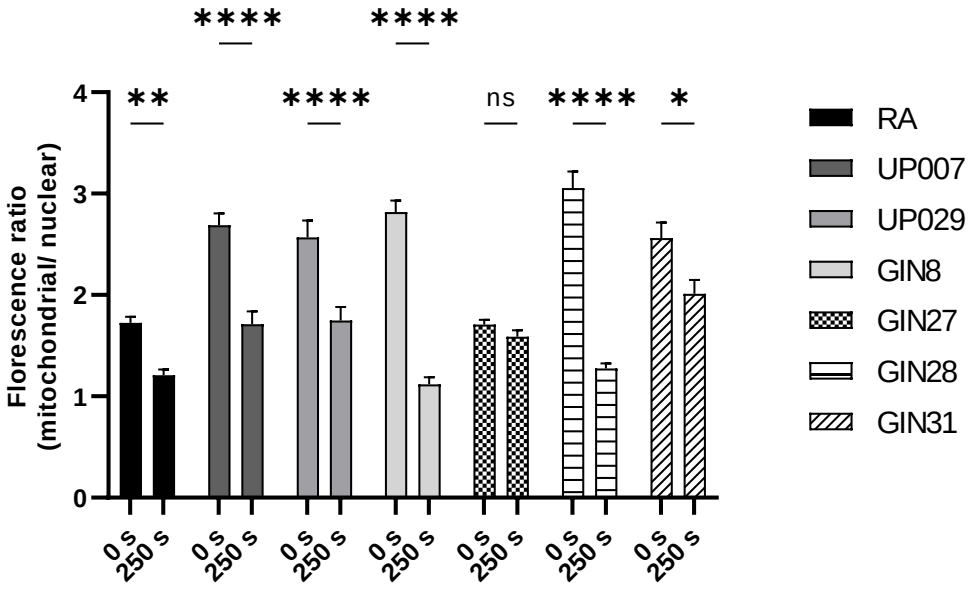

Figure 4.4. Comparison between initial and final fluorescence ratio among GBM cell lines and RA after TMRM photoactivation for 30 seconds. *(ns) p >0.05, (*) p <0.033, (**) p <0.002, (***) p <0.0002, (****) p <0.0001, alpha= 0.05.* Statistical method: two-way ANOVA and Šídák's multiple comparisons test. Data presented as mean ±SEM.

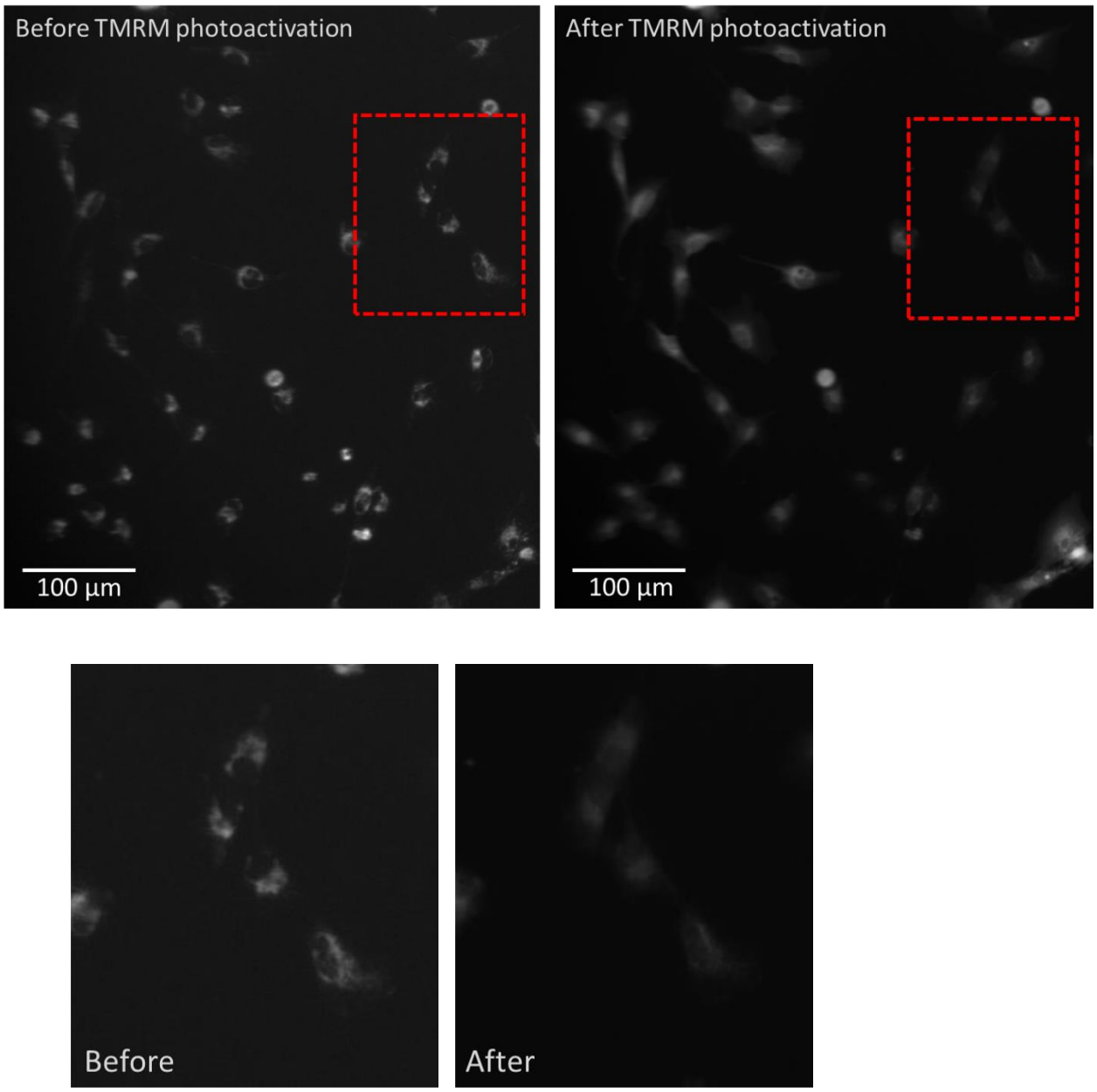

Figure 4.5. TMRM-induced depolarization of UP007 mitochondria. Left panel: images of mitochondria of UP007 GBM cells before photoactivation of TMRM. Right panel: images of mitochondria immediately after photoactivation of TMRM with green light for 30 seconds.

4.3 TMRM up to 1600 nM is not toxic to cells without photoactivation.

Having found that TMRM can be used to trigger powerful depolarising effect on GBM mitochondria, I decided to further investigate its potential as a novel agent for PDT. An ideal photosensitiser should have no toxic effect unless illuminated with appropriate light wavelength. Hence, toxicity of TMRM in absence of illumination was assessed. TMRM proved to be only toxic upon light illumination (**Figure 4.6**). Cells were seeded in 96-well plates and incubated overnight. On the next day, cells were loaded with different concentrations of TMRM for 1 hour then media was replaced with fresh one, and the plates were incubated for 3 days. Measurement of toxicity was carried out using LDH assay. With no light illumination, pre-loading cells with TMRM in concentrations up to 1600nM did not induce toxicity detectable by LDH assay in RA or GBM cell lines. In fact, even a higher concentration (3200nM) did not induce significant toxicity, although a trend may be noticed in **Figure 4.6.**

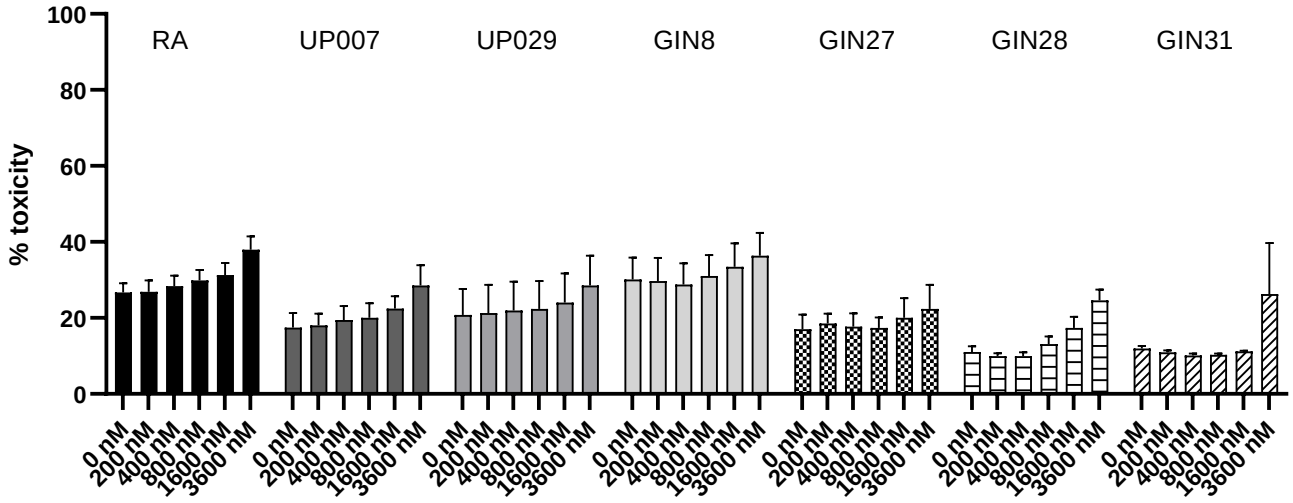

Figure 4.6. TMRM toxicity in absence of illumination assessed using LDH assay. Cells were treated with TMRM in different concentrations for one hour, then were incubated with fresh media for 3 days before LDH assay was carried out. No statistically significant difference in toxicity between

any of the 5 concentrations used in this experiment compared to controls. *alpha= 0.05.* n=6 for RA, n=3 for GBM cells. Data presented as mean ±SEM.

4.4 Photoactivation of TMRM, using green light, induced cell death in primary GBM cells.

The next logical step was to test the efficacy of TMRM-mediated PDT on GBM cells. To achieve equal exposure of cells to light, special seeding protocol was implemented (see chapter 2 section 2.3.2). Briefly, a 4µl drop of cell suspension was placed at the centre of 96-well plate then plates were incubated to allow attachment of the cells to the bottom of the well. After 45 minutes, 100µl of fresh media is added to each well. GBM cells as well as RA preincubated with 200 or 300nM TMRM were subjected to green light illumination for 22 or 40 seconds. Following that, cells were incubated with fresh media for 3 days before fixation and staining with DAPI for nuclear counting. I found that TMRM-mediated PDT resulted in reduced cell count. Cell number reduction was different between different cell lines. Milder treatment (200 nM and 22 sec of light application) reduced proliferation of all cell lines with GIN28 affected the most **(Figure 4.7 a)**. Stronger PDT treatment (300 nM plus 40 seconds light application) almost completely eliminated GIN28 cells and had a powerful effect on all others **(Figure 4.7 b)**. RA were also susceptible to this effect, but it must be reminded that these are cultured astrocytes at a stage when they are still semi-embryonic and dividing, and probably heavily dependent on mitochondrial energy supply as any embryonic cell (263). At the same time, it is well known that postnatal astrocytes are highly glycolytic (264). Thus, it is quite possible that mature postnatal astrocytes are more resistant to this type of PDT.

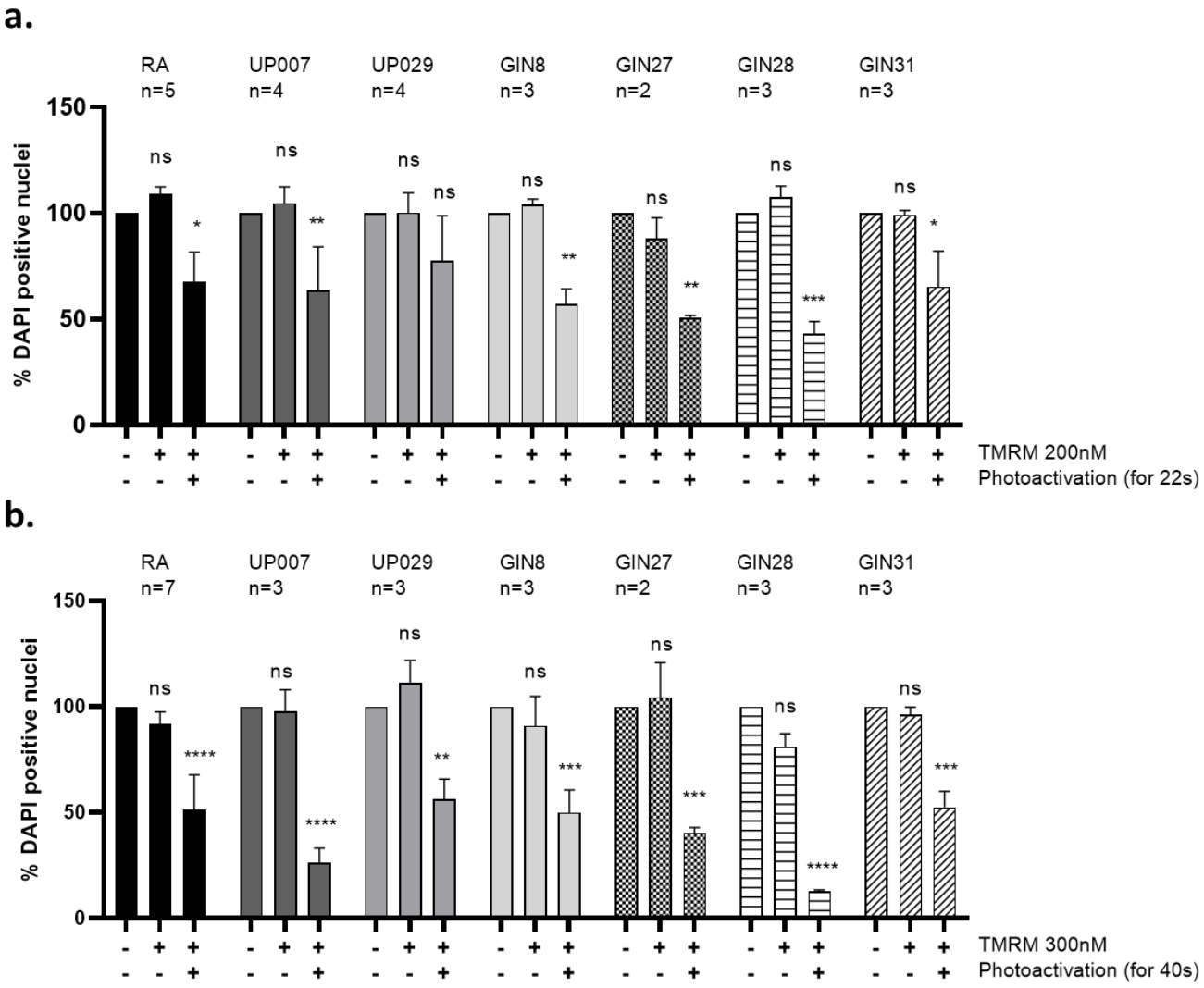

Figure 4.7. Photoactivation of mitochondrial dye TMRM supresses proliferation of GBM cells.
(a) Results obtained with 200nM TMRM and illumination for 22 seconds,
(b) Results with TMRM 300nM and light illumination for 40 seconds.
DAPI stained nuclear count was used. (n) is the number of independent experiments, each one is done in duplicates. *(ns) p >0.05, (*) p <0.033, (**) p <0.002, (***) p <0.0002, (****) p <0.0001, alpha= 0.05.* Statistical method: two-way ANOVA and Tukey's multiple comparisons test. Data presented as mean ±SEM.

4.5 GBM cells, in contrast to normal RA, failed to recover their MMP 24 hours after TMRM photoactivation.

Ideally, TMRM-PDT aims to preferentially affect GBM cells, thus, its effect on GBM cells should be compared to its effect on postnatal differentiated human astrocytes. However, this does not appear to be possible. Therefore, the lack of clear-cut specificity for GBM in the previous experiment cannot be seen as an evidence that healthy cells are affected to the same degree as GBM. I therefore investigated whether RA or GBM cells would recover their normal MMP after TMRM-PDT. Initially all cells were loaded with 300nM TMRM and test group underwent photoactivation with green light for 40 seconds. As shown above this is well enough to trigger the loss of MMP. Media was then replaced with fresh one. Next day, all cells were re-loaded with 300nM TMRM to assess how well mitochondria have recovered their membrane potential. The results show that all GBM cells, except for GIN27, still have significantly lowered MMP (depolarized) 24 hours after TMRM-PDT. Unlike GBM, RA managed to recover their normal MMP within 24 hours as seen in **Figure 4.8**, after having it significantly depolarized by photoactivation **(Figure 4.4).**

Figure 4.9 demonstrates examples of how 24 hours after Photoactivation, GBM cells (b and c) have failed to load with TMRM due to defective MMP, evident by lower intensity staining, in contrast to RA (a).

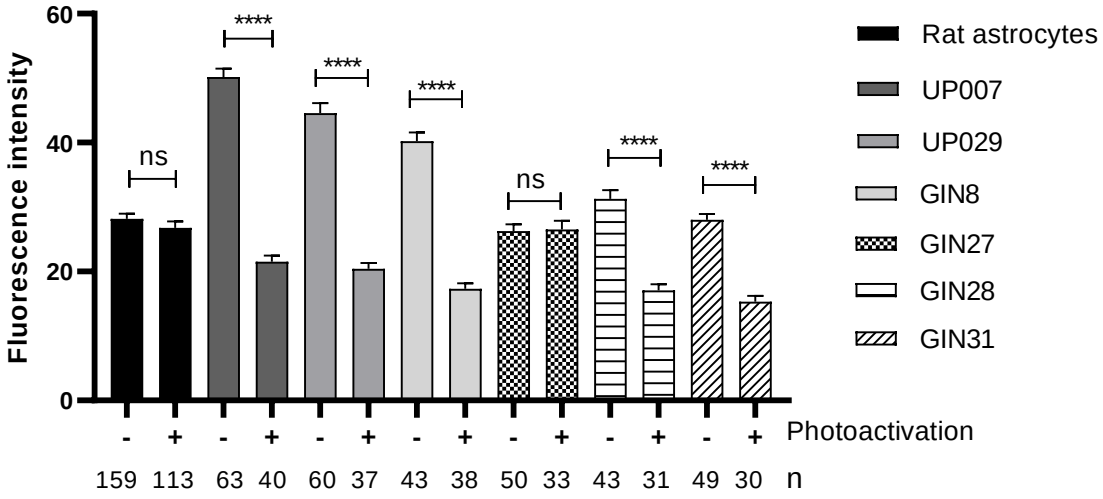

Figure 4.8. MMP of RA and GBM cell lines measured 24 hours after photoactivation. All GBM cell lines (except GIN27) have still had compromised MMP 24 hours after photoactivation, with significant difference in dye loading between test and control groups. Normal RA and GIN27 GBM cells recovered their MMP, with no significant difference in dye loading between test and control groups. *(ns) p >0.05, (****) p <0.0001, alpha= 0.05.* n is the total number of cells examined in 6 independent experiments for RA, and 3 for GBM cells. Statistical method: one-way ANOVA and Tukey's multiple comparison test. Data presented as mean ±SEM.

a. RA

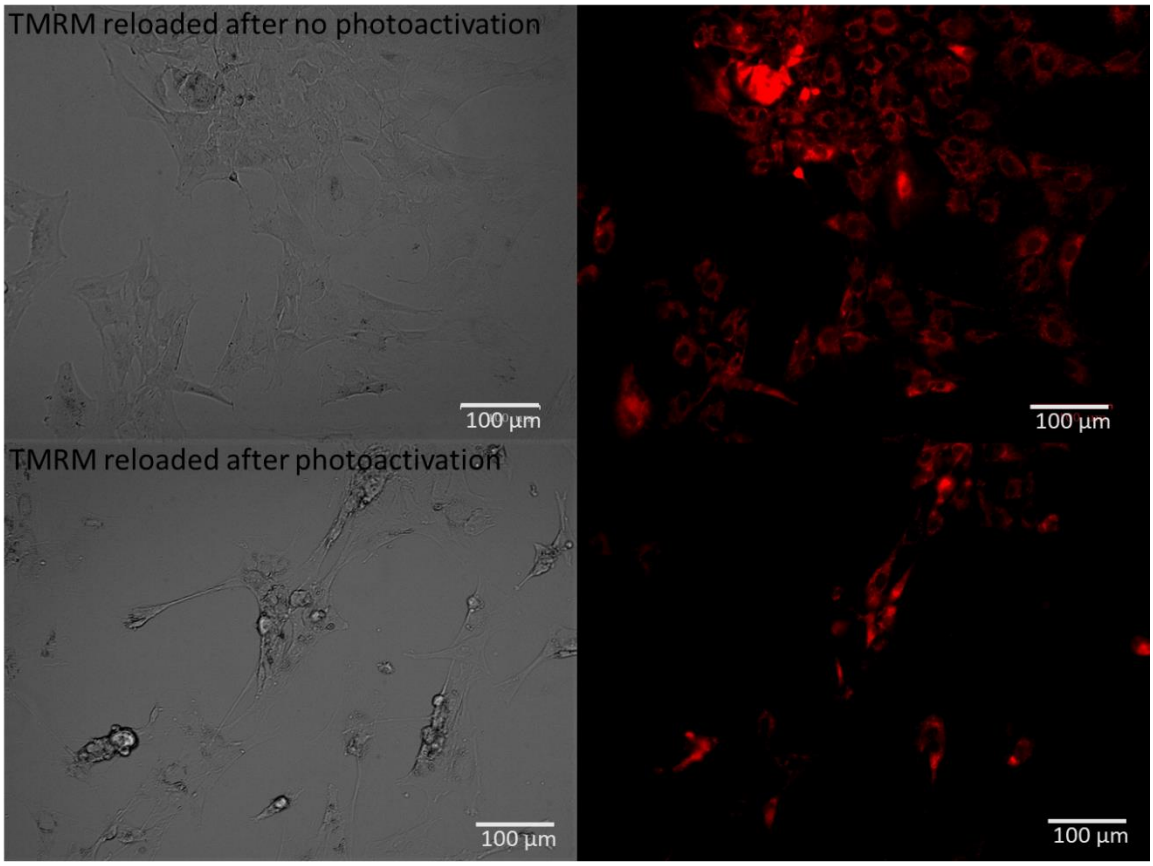

b. UP007 GBM

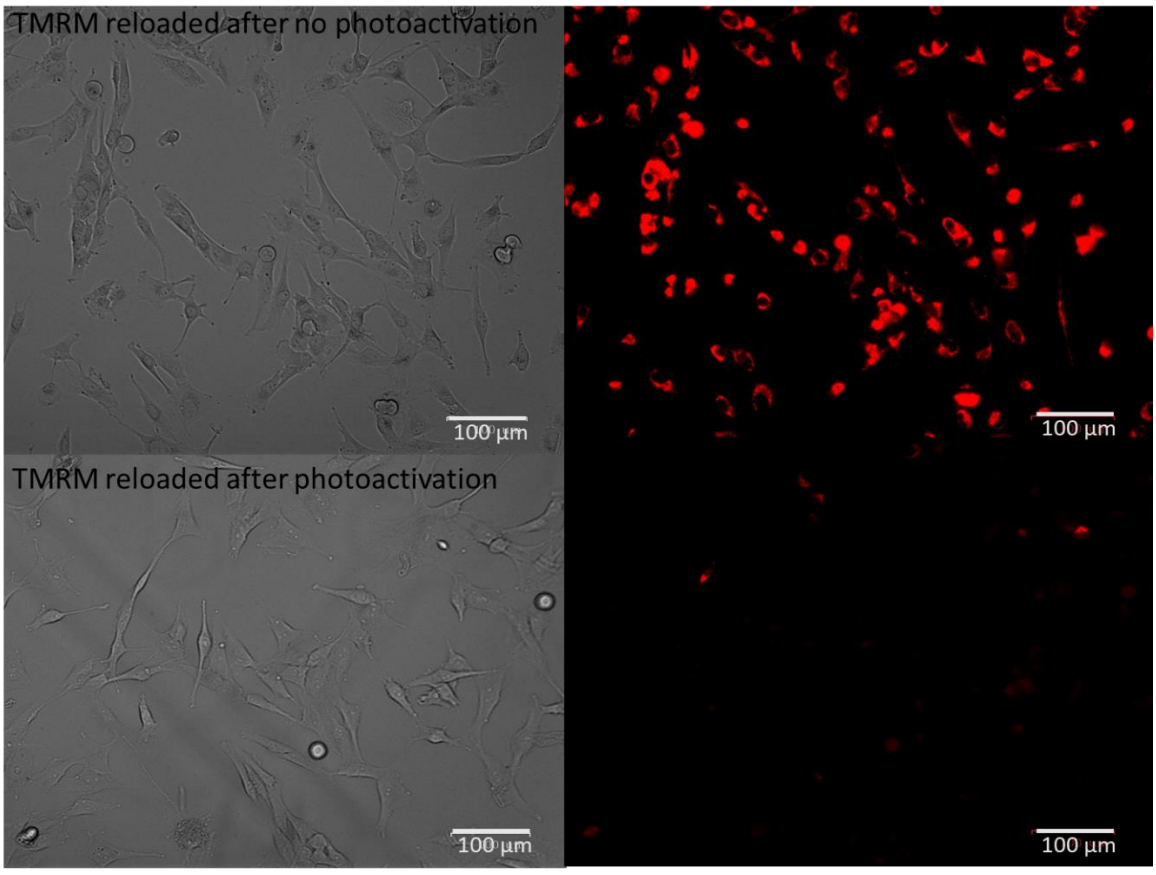

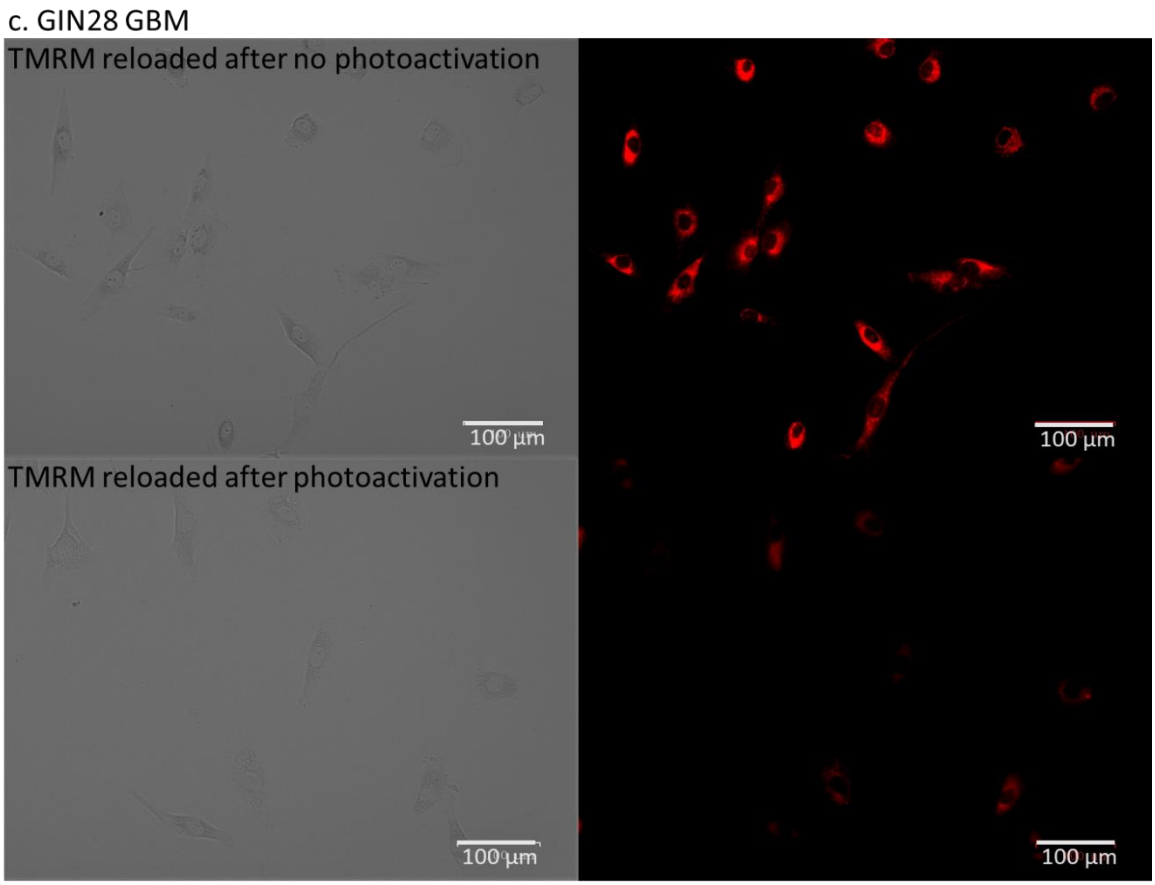

Figure 4.9. Representative images of the MMP recovery (TMRM reloading experiment) after photoactivation. (a) Normal RA: although cell density is affected due to photoactivation, mitochondria in test image (lower right image) are showing same intensity red fluorescence 24 hours after photoactivation compared to controls (upper right image). Mitochondria of **(b)** and **(c)** GBM cells' mitochondria have faint red fluorescence (lower right images) due to disturbed MMP after photoactivation and failure to recover normal mitochondrial potential.

4.6 NKH477, but not clotrimazole, differentially enhanced TMRM-PDT in GBM cells

Milder TMRM-PDT protocol was conducted along with treatment with clotrimazole a glycolysis inhibitor. The rationale was that upon depolarisation, GBM mitochondrial ATP production should be further compromised, making cells more dependent on glycolysis for energy production. This was tested using a PFK inhibitor clotrimazole. In these experiments I employed a mild PDT effect with the assumption that drugs could potentiate it. TMRM was

loaded in concentration of 200nM and photoactivated for 17 seconds only. After that, cells were incubated with 10 µM of clotrimazole for 3 days.

I chose to use 10 µM concentration based on the results of previous publications, which indicated that around 40 µM of clotrimazole alone was enough to induce cell death in GBM cells (265, 266). I did not aim to induce cell death, rather I wanted to mildly inhibit glycolysis to look for synergistic effect with TMRM-PDT if present. First, I tried 20 µM clotrimazole but this concentration was too toxic for all cells (results not shown), therefore, I decided to use 10 µM instead. At this concentration, clotrimazole alone also induced death of RA but did not significantly do so in GBM cells **(Figure 4.10)**. Unfortunately, in cultures treated with TMRM-PDT and clotrimazole, I was unable to reveal a supra-additive effect, possibly with the exception of UP029.

As mentioned previously, increased level of cAMP has been reported by a number of studies to exert negative effects on GBM cells and make them vulnerable for various insults (176, 267). To assess whether an elevated level of cAMP would sensitize GBM cells to TMRM-PDT, cells were pre-incubated with NKH477 for 1 day before TMRM loading (200µM) and photoactivation (17 seconds). Media was then replaced with fresh one and cells were incubated for 3 days before the end point measurement was taken (cell counting using DAPI).

This combined treatment scheme in general was found to bring an additive effect to TMRM-PDT **(Figure 4.10)**. Treatment with NKH477 alone did not induce toxicity in any of GBM cells. Statistical analysis has revealed that in at least two of our cell lines, UP007 and GIN27 **(Figure 4.10 b and e)**, this regime resulted in a supra-additive effect where the suppression of GBM cell number after TMRM-PDT was significantly increased by pre-incubation in NHK477. Thus, in at least some GBM cases this approach could be used to further enhance the efficacy of PDT.

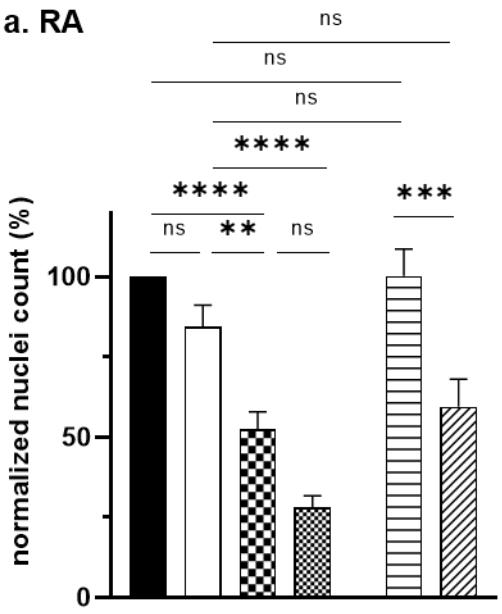
a. RA
ns
ns
ns
****
****
ns
**
ns
***
normalized nuclei count (%)
100
50
0

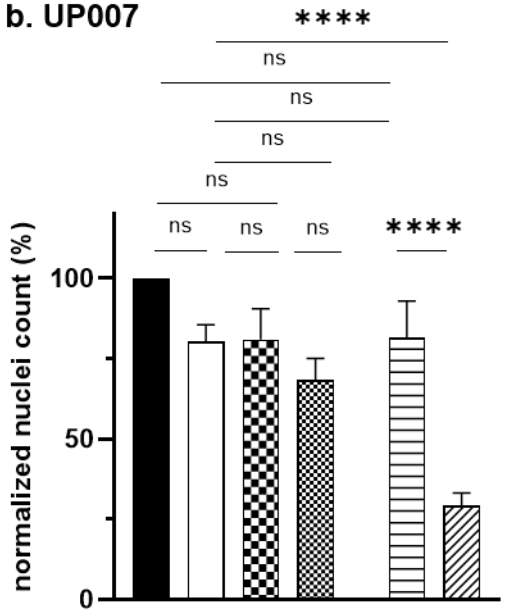
b. UP007
****
ns
ns
ns
ns
ns
ns
ns
****
normalized nuclei count (%)
100
50
0

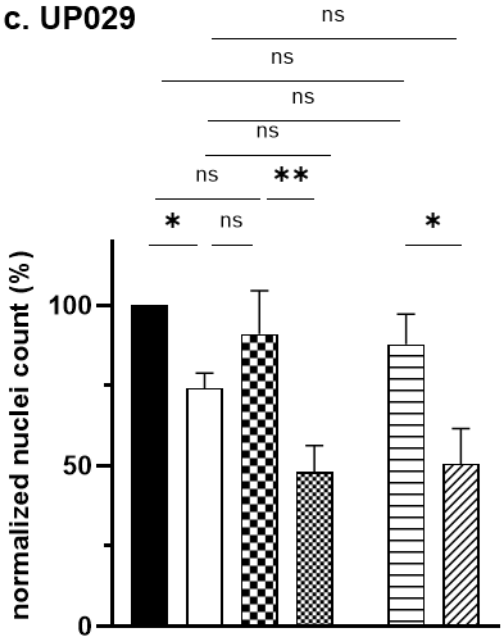
c. UP029
ns
ns
ns
ns
ns
**
*
ns
*
normalized nuclei count (%)
100
50
0

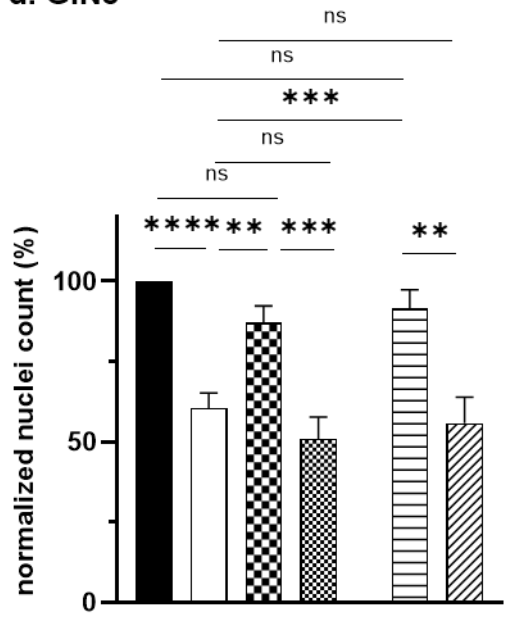
d. GIN8
ns
ns
***
ns
ns
******
***
**
normalized nuclei count (%)
100
50
0

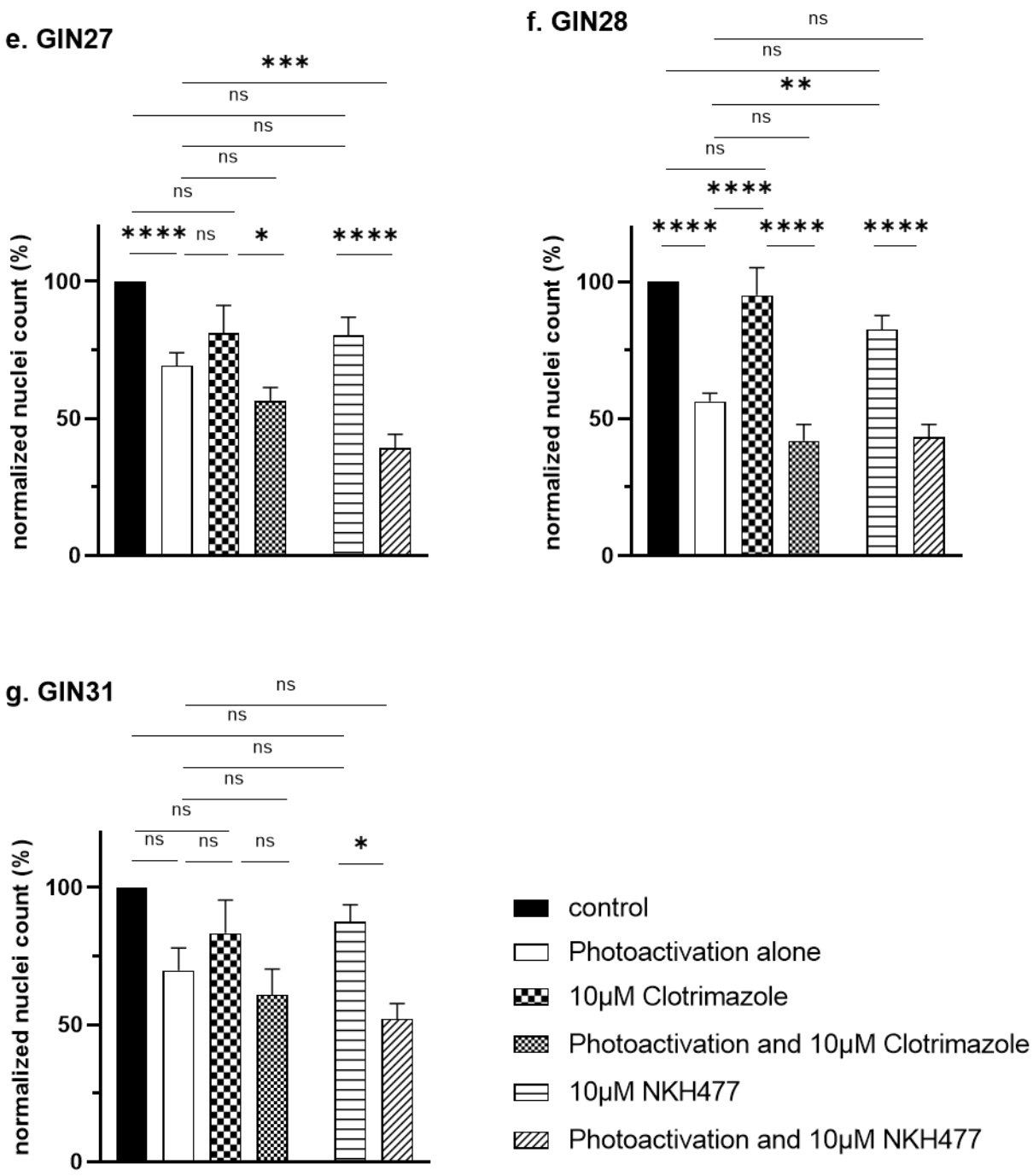

Figure 4.10. Potentiation of TMRM-mediated toxicity on GBM cell lines with glycolytic inhibitor clotrimazole and AC activator NKH477. The number of independent experiments is: 5 for RA, 4 for UP007, UP029, GIN8, and GIN28 cells, and 3 for GIN27 and GIN31 cells, all in duplicates. *(ns) p >0.05, (*) p <0.033, (**) p <0.002, (***) p <0.0002, (****) p <0.0001, alpha= 0.05.* Statistical method: one-way ANOVA and Tukey's multiple comparisons test. Data presented as mean ±SEM.

Chapter 5: Results-3

Re-evaluating the Repurposing of Antidepressants for GBM Therapy

5.1 Antidepressants exert cytotoxic effects on primary GBM cell lines as well as normal RA.

A number of studies reported potential cytotoxic effects of antidepressants on many types of cancer cells including GBM cells **(Table 1.2)**. However, the concentrations used in these experiments often greatly exceed biologically plausible range and concentration-dependence of the effects was often not documented (188-190). Moreover, the use of commercial cell lines makes these results less valid as models to represent GBM cells' behaviour in real life.

Patient-derived primary GBM cell lines UP007 and UP0029 were used in these experiments, as well as normal RA. Cells were grown until 70% confluent then trypsinized and plated in 96-well plates to be treated with different concentrations of antidepressants. After 3 days of drug exposure, LDH assay was performed to assess cell integrity.

All 3 antidepressants IM, CL, and FLX appeared to be toxic to GBM cells as well as normal RA. The results of these experiments are summarised in **Figure 5.1.** Of the 3 drugs, IM effect was fairly concentration-dependent with toxicity becoming evident at ~ 50 µM and then reaching plateau at 100 µM with no further increase at 200 µM. CL and FLX acted in almost all-or-nothing manner. Already with 25 µM cells were severely damaged and the effect essentially did not increase any further up to 200 µM concentrations.

Comparing the degree of toxicity with threshold concentrations of the drugs (50µM for IM, and 25µM for CL and FLX) between astrocytes and GBM cell lines did not reveal statistically significant differences (**Figure 5.1 d**). Moreover, when comparing values of the fitted concentration-response curves (CRC) of the three ADs on the three cell types, no significant differences in EC_{50} was found between GBM cells and RA (**figure 5.2**). These observations indicate that antidepressants do not exhibit selectivity to tested GBM cell lines in comparison to normal RA. Nevertheless, it has to be stated again, that the RA are obtained at the stage when these cells are still not fully mature and are still dividing (230), hence the response of the mature human astrocytes might be different. These observations also help to better understand the range of concentrations required for the anti-GBM actions, unlike some concentrations reported in other studies which are clearly very high and, perhaps exceed what is physically possible *in vivo*.

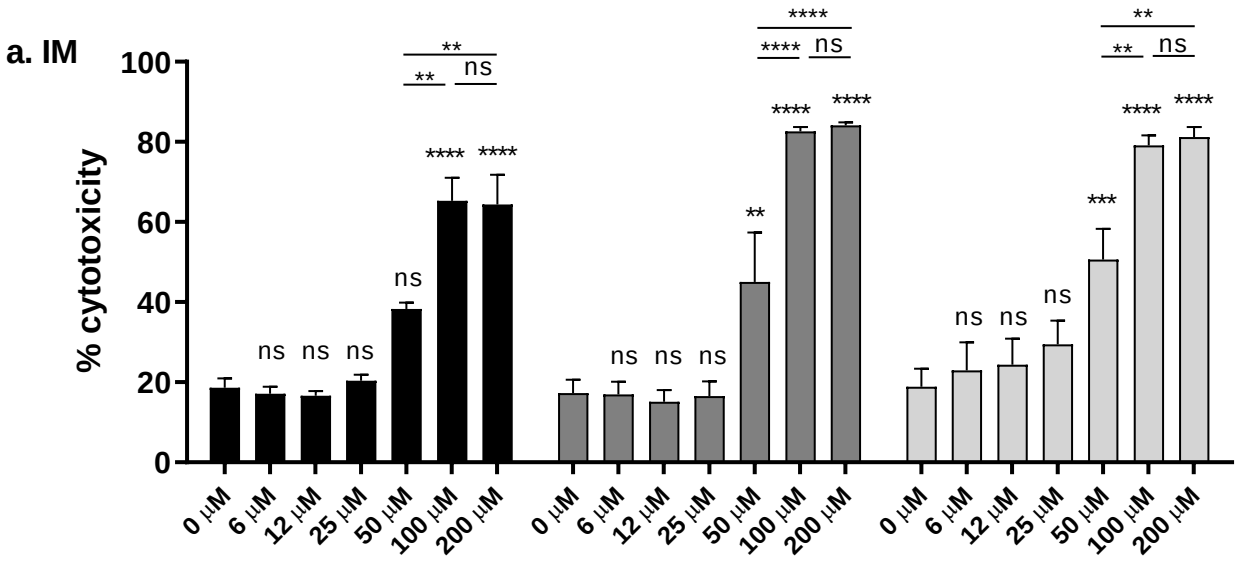

b. CL

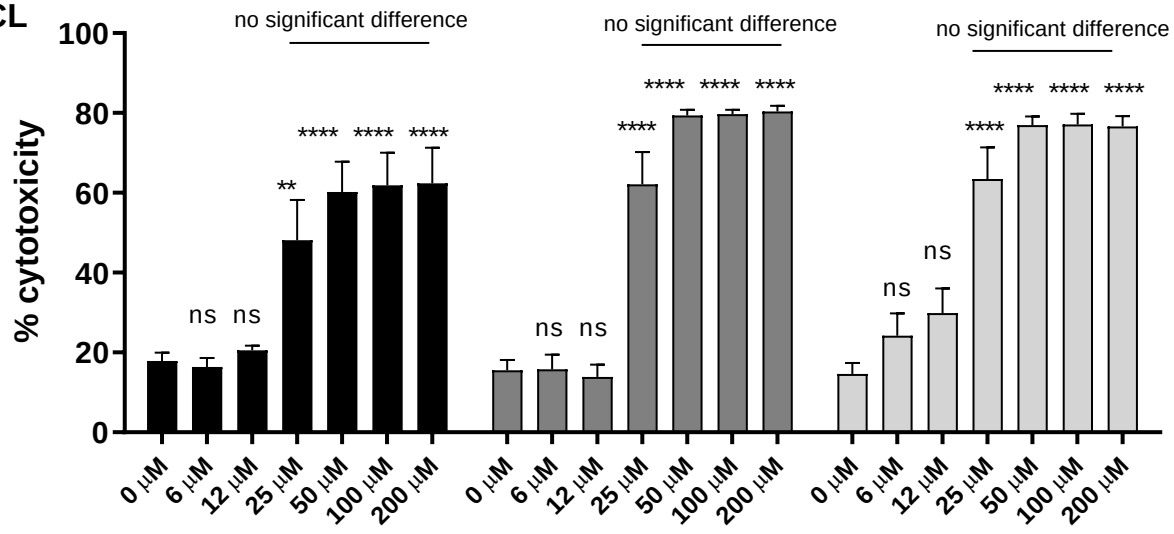
no significant difference
no significant difference
no significant difference
% cytotoxicity
100
80
60
40
20
0
ns
ns
**
****
****
****
ns
ns
****
****
****
ns
ns
****
****
****
0 μM
6 μM
12 μM
25 μM
50 μM
100 μM
200 μM

c. FLX

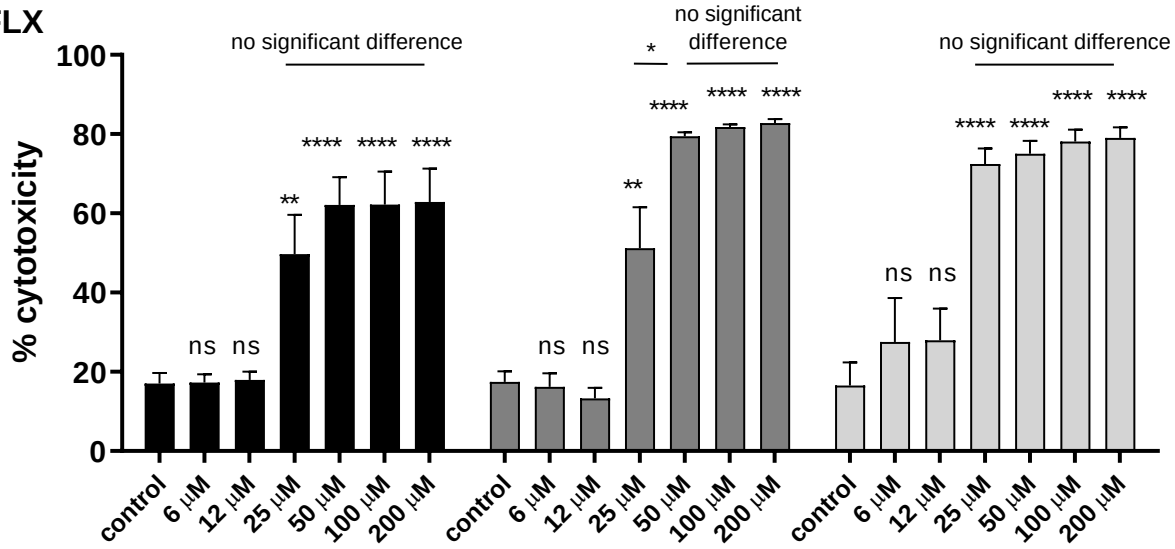
no significant difference
no significant difference
*
no significant difference
% cytotoxicity
100
80
60
40
20
0
ns
ns
**
****
****
****
ns
ns
**
****
****
****
ns
ns
****
****
****
****
control
6 μM
12 μM
25 μM
50 μM
100 μM
200 μM

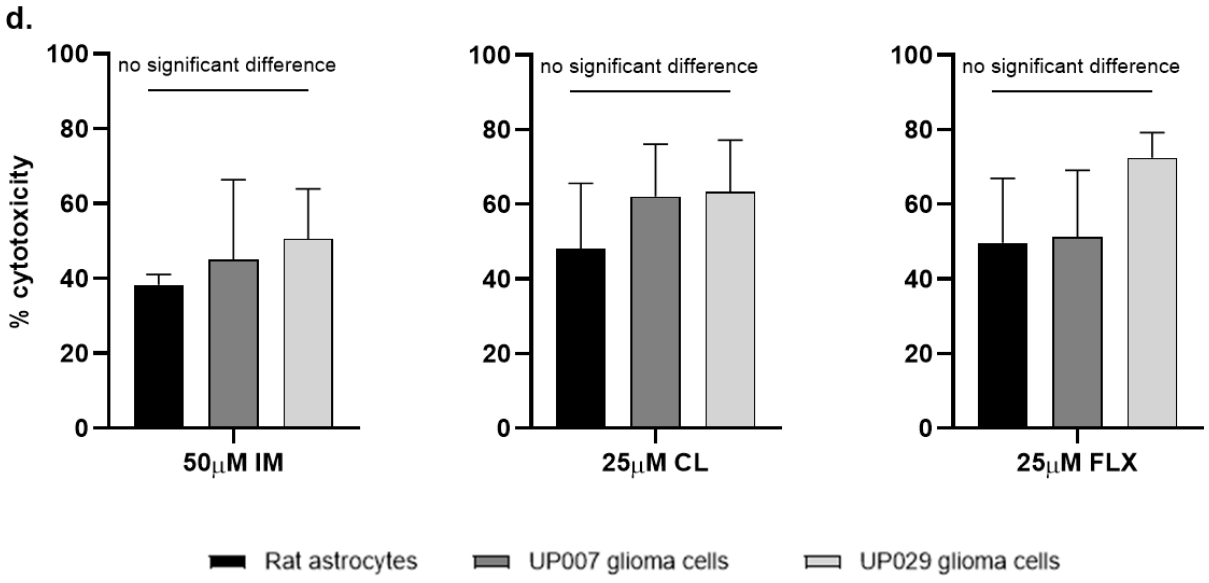

Figure 5.1. Toxicity of antidepressants on normal RA and GBM cell lines assessed using LDH release method. 3-day treatment with (a) imipramine; IM, (b) clomipramine; CL, (c) fluoxetine; FLX, induced toxicity (LDH release) in GBM cells as well as normal RA. Toxic threshold values are 50µM for IM, and 25µM for CL and FLX. Threshold values are the same across the three cell types. (d) % toxicity of threshold values of the three drugs did not differ between RA and GBM cells. *(ns) p >0.05, (*) p <0.033, (**) p <0.002, (***) p <0.0002, (****) p <0.0001. alpha= 0.05. n= 3 independent experiments (in duplicates).* Comparisons are made between each concentration and the control (0 µM) within each cell type. Statistical method: (a-c) two-way ANOVA and Tukey multiple comparison test, (d) ordinary one-way ANOVA. Data presented as mean ± SEM.

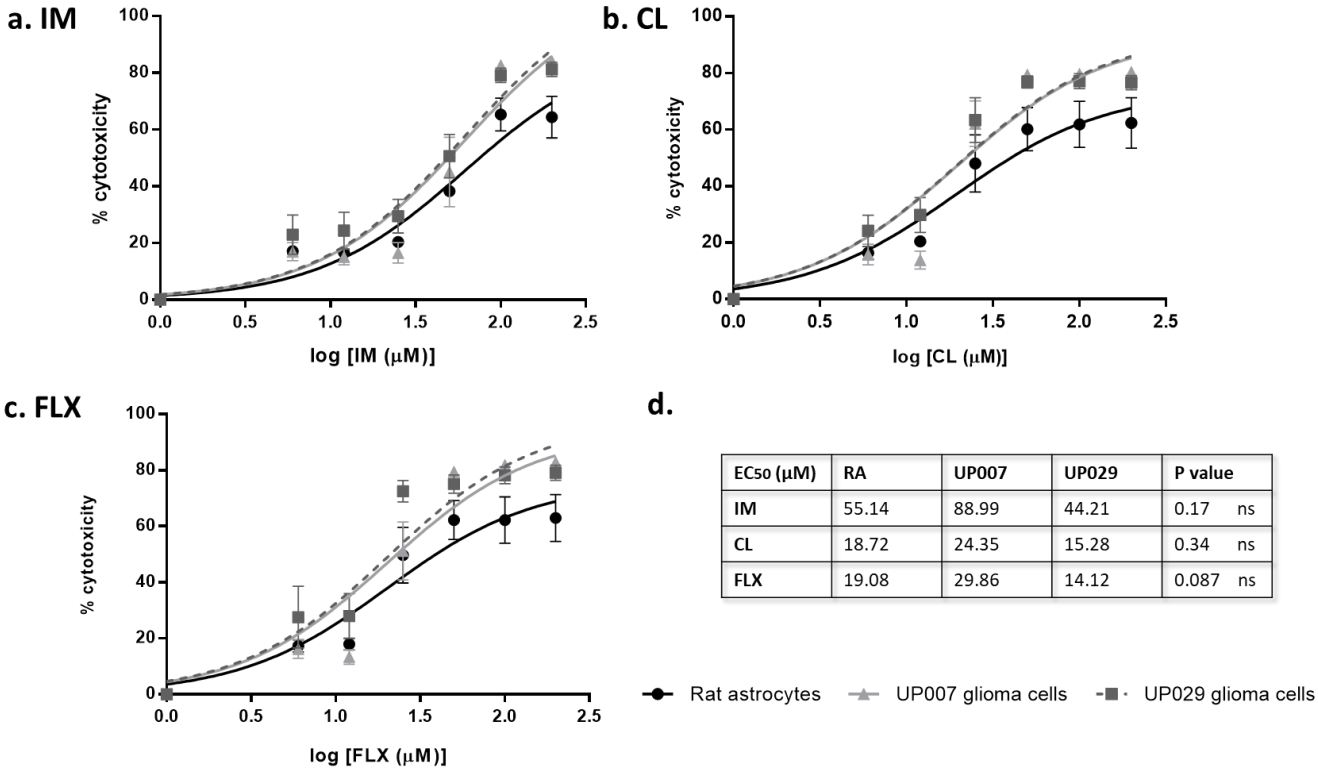

EC50 (μM)	RA	UP007	UP029	P value
IM	55.14	88.99	44.21	0.17 ns
CL	18.72	24.35	15.28	0.34 ns
FLX	19.08	29.86	14.12	0.087 ns

Figure 5.2. Concentration response curve (CRC) for antidepressants toxicity on normal RA and GBM cell lines. (a-c) CRCs were generated in Prism software using the same data as in Figure 1. (d) EC_{50} and p values. No significant differences in EC_{50} between the three cell types was revealed. *(ns) p > 0.05, alpha= 0.05*. Statistical method: nonlinear regression (curve fit). Data presented as mean ± SEM.

5.2 Subtoxic concentrations of antidepressants supress wound healing process in GBM cells but not normal RA.

Scratch wound healing assay was utilized to test whether sub-toxic concentrations of antidepressants, as established in previous section, affect migration and/or proliferation of cancer cells in preference to normal RA. In scratch wound healing assay, filling of the wound gap during the first 24 hours is attributed mainly to cell migration from the edges of the wound (268). After 24 hours, filling of the wound gap continues due to proliferation of cells until the wound is completely healed (268). Overall, time for complete wound healing differs from cell type to another according to motility and cell cycle duration for each cell type (268).

Scratch wound healing assay was carried out as outlined in methods section 2.4.2. IM and CL were tested against UP007 and UP029 GBM cell lines. Normal RA were used as controls. Serial images of the wound healing process plus measurements of relative wound density and wound gap size over time were obtained. I found that sub-toxic concentrations of IM (<50μM) and CL (<25μM) significantly inhibited migration/ proliferation of UP029 GBM cells but not UP007 GBM cell line or normal RA **(Figure 5.3**). CL only inhibited wound healing in UP007 at threshold dose (25μM), but no effect was seen at sub-toxic doses. Representative images of the initial scratch wound and the healing process in UP029 GBM cells is presented in **Figure 5.4.** Interestingly, CL at as low as 12 μM significantly suppressed wound closure in UP029 at both 24 and 48 hours **(Figure 5.3 b and d**). CL was more effective at 25 μM but based on the data from the previous section, I believe that this concentration is already significantly toxic to all cell types. IM was also effective against UP029 although the effect was more obvious at 48 hours when both 12 and 25 μM were effective **(Figure 5.3 a and c)**. Importantly, astrocytes were completely unaffected by antidepressants.

Thus, it appears that the survival benefit reported with antidepressants in mice models in vivo, could be related to the inhibition of GBM infiltrative growth which seem to occure even at lower concentrations in some GBM cell lines (195). It is also clear that the effect is not universal, since UP029 was clearly affected more than UP007.

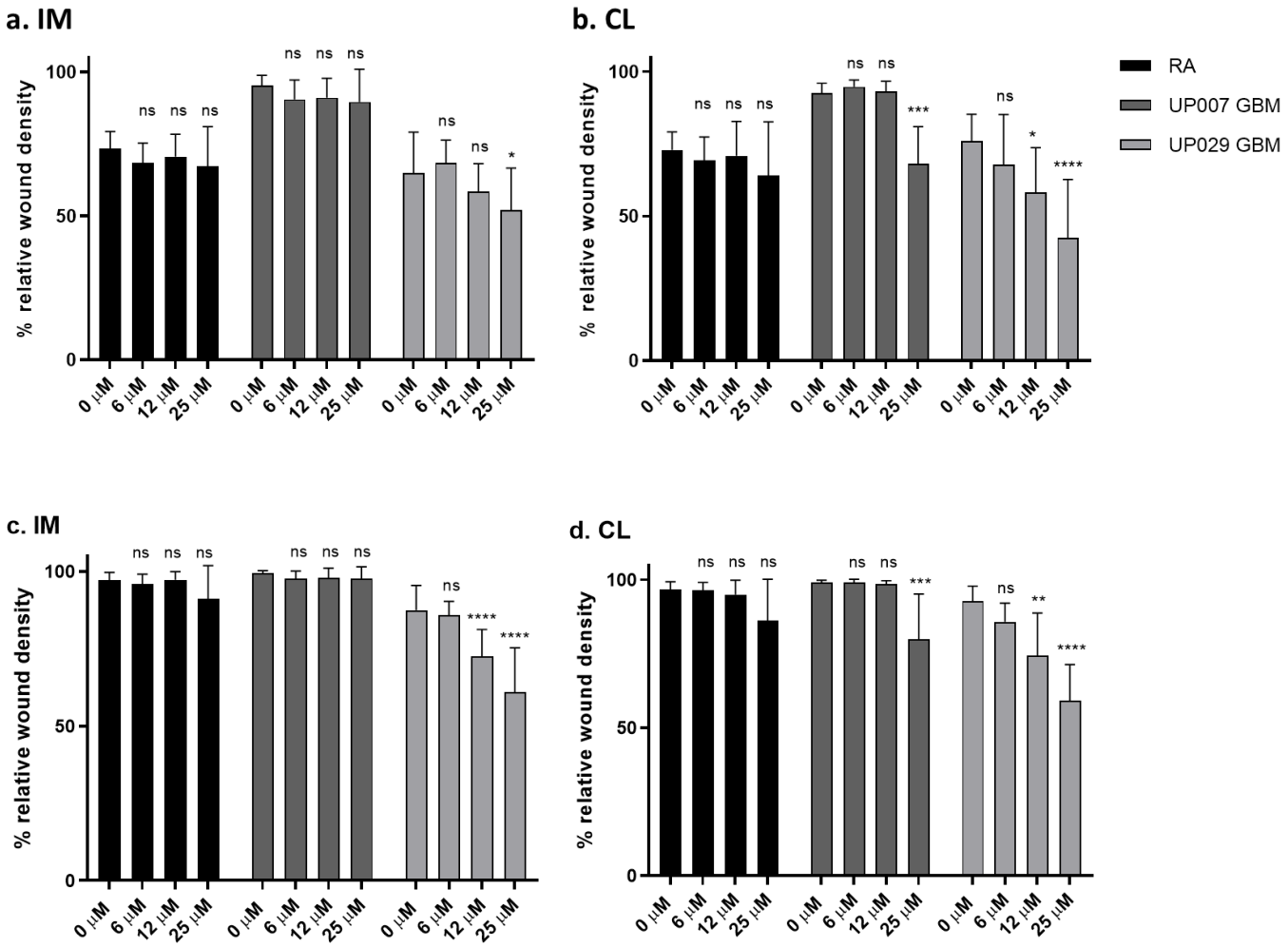

Figure 5.3. The effects of antidepressants on wound healing process. Graphs show relative wound density 24 hours (upper panels a and b) and 48 hours (lower panels c and d) after the scratch with and without drug treatment. The number of independent experiments (n) is (a) 7, 8, and 10, (b) 6, 7, and 5, (c) 7, 7, and 9, (d) 6, 6, and 4, for RA, UP007 GBM, and UP029 GBM respectively. Comparisons were made between different concentrations and the control (0µM) within each group. *(ns) p > 0.05, (*) p <0.033, (**) p <0.002, (***) p <0.0002, (****) p <0.0001. alpha= 0.05.* Statistical method: two-way ANOVA and Dunnett's multiple comparison. Data presented as mean ± SEM.

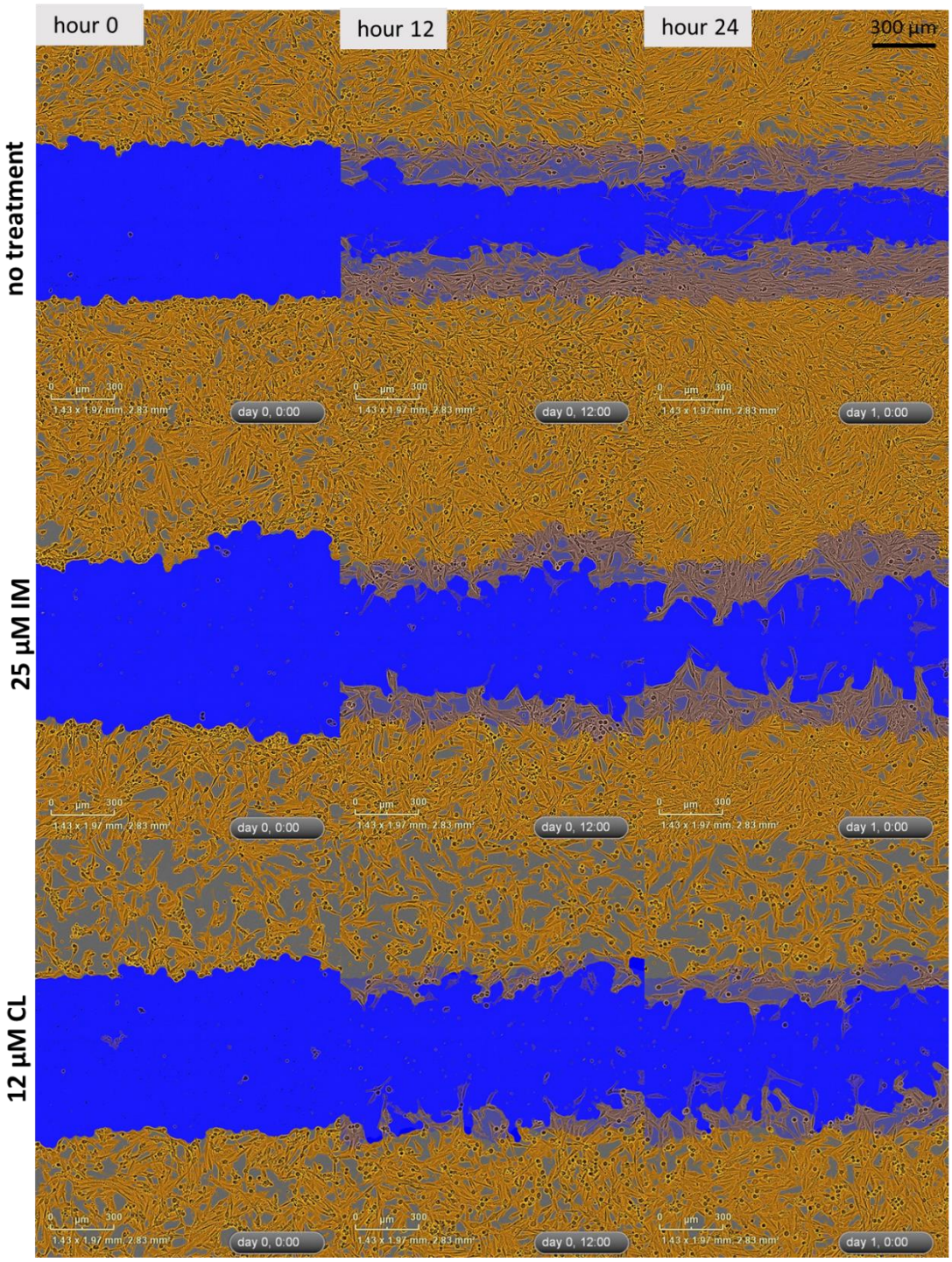

Figure 5.4. Scratch wound assay images of UP029 GBM cells at different time points. IM and CL at sub-toxic concentrations slowed down scratch wound healing in UP029 GBM cells only.

5.3 Antidepressants treatment for 24 hours did not change intracellular cAMP levels in primary GBM cells.

Previously it has been suggested that antidepressants can suppress GBM via elevations in cAMP (176, 192). Elevation of cAMP is generally acknowledged to have a range of negative effects on growth and proliferation of GBM tumours (211, 212). As shown in the previous section, sub-toxic concentrations of ADs affected the ability of UP029 GBM cells to spread and close the scratch in the wound assay. I therefore studied whether intracellular cAMP levels were altered by AD when using similar sub-toxic concentrations. I used Epac-based FRET cAMP sensor, introduced in the Methods section 2.4.3. Images were obtained on SP5 confocal microscope with settings fixed for all series.

Figure 5.5 shows relative intracellular cAMP levels measured after incubation of GBM cells with IM and CL for 24 hours. Interestingly, there was a tendency to an increase in cAMP with IM, but the effect was only significant at IM 25 µM in UP007 GBM cells. Thus, the effect of CL on wound closure mentioned in section 5.2. cannot be explained by elevation of cAMP. Our results are also inconsistent with the concept of cAMP being the primary mediator of antidepressant action on GBM (176).

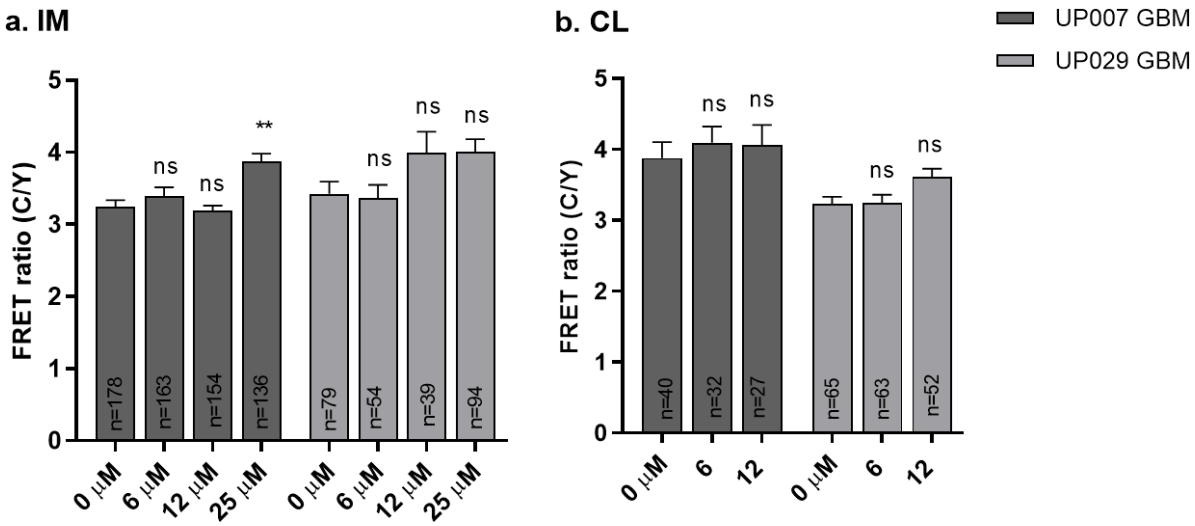

Figure 5.5. The effect of 24-hour imipramine (IM) and clomipramine (CL) treatment on intracellular cAMP levels in GBM cell lines. Treatment with subtoxic concentrations of IM (a) and CL (b) for 1 day had no significant effect on cAMP levels in UP007 or UP029 cells, except for IM at 25µM in UP029 GBM cells. *(ns) p >0.05, (*) p <0.033, (**) p <0.002, (***) p <0.0002, (****) p <0.0001, alpha= 0.05.* n is the total number of cells examined in two independent experiments for UP029 GBM and three independent experiments for UP007 GBM cells. Statistical analysis: one-way ANOVA and Tukey's multiple comparison test. Data presented as mean ± SEM.

5.4 Forskolin analogue NKH477 differentially affected cAMP levels in normal RA and GBM cell lines.

GBM cells are found to generally have a lower basal cAMP level compared to normal brain cells (208, 267). Also, the level of cAMP was found to negatively correlate with GBM tumour growth and aggressiveness (212, 269). Thus, it could be that ADs failed to elevate intracellular cAMP levels in GBM cells because GBM cells have a mechanism of suppressing cAMP rise for their own survival advantage (211). In this case, known cAMP elevating compounds e.g. NKH477 should also be ineffective. NKH477 is a forskolin hydrochloride derivative that is water-soluble, and directly activates AC thus increasing intracellular cAMP (270). It has been previously reported to induce cell cycle arrest and apoptosis in GBM cells (216, 267).

Therefore, I measured the effect of NKH477 on intracellular cAMP levels using Epac-based FRET sensor as outlined in Methods section 2.4.3. NKH477 had differential effect on GBM cells and RA (**Figure 5.6**). 5µM of NKH477 was able to increase cAMP in RA by > 90% of baseline value, in UP007 by > 125% of baseline value **(Figure 5.7).** In contrast, UP029 line showed minimal sensitivity NKH477, with ~10% elevation of cAMP level from baseline value which was not statistically significant. Only 10µM NKH477 was able to increase cMAP significantly in UP029 by 40% from baseline.

Thus, there is a striking difference between UP007 and UP029 cell lines in their sensitivity to NKH477. Given that UP029 was quite more susceptible to AD-induced toxicity, with the lowest EC_{50} among the three cell types (although not statistically significant) (**Figure 5.2**) and with significant inhibition of wound closure **(Figure 5.3**), it appears that the ability to clamp down cAMP does not seem to protect this cell line from damage induced by

these drugs, which again, argues against the idea that cAMP elevation is the principal mechanism of their reported anti-GBM action (176).

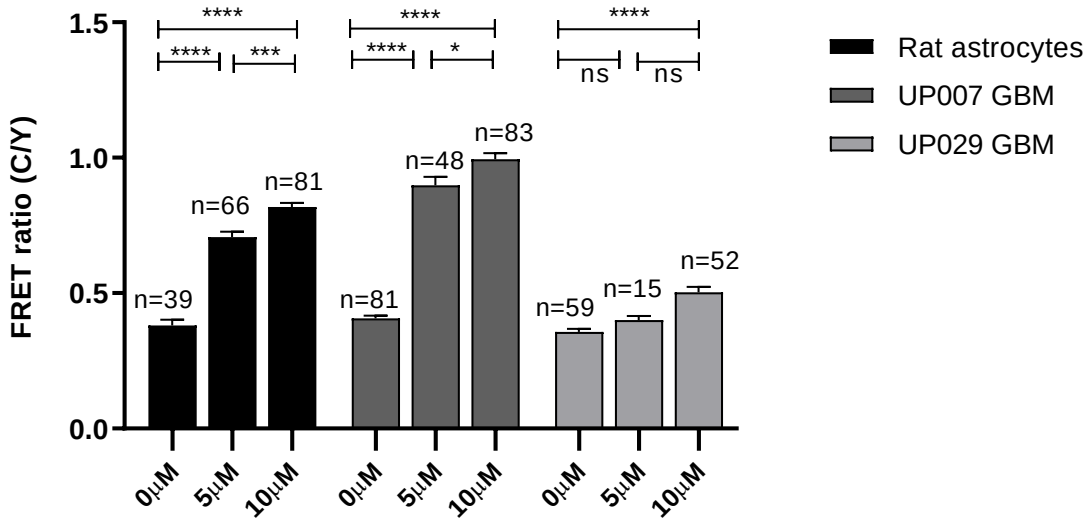

Figure 5.6. The effect of 1-day NKH477 treatment on intracellular cAMP levels in RA and GBM cell lines. Treatment with low concentrations of NKH477 for 1 day significantly increased cAMP level in RA and UP007 GBM cells but not UP029 GBM cells. baseline cAMP levels are not significantly different between the three cell types. *(ns) p > 0.05, (*) p <0.033, (**) p <0.002, (***) p <0.0002, (****) p <0.0001. alpha= 0.05.* n is the total number of cells examined in two independent experiments. Statistical analysis: one-way ANOVA and Tukey's multiple comparison test. Data presented as mean ± SEM.

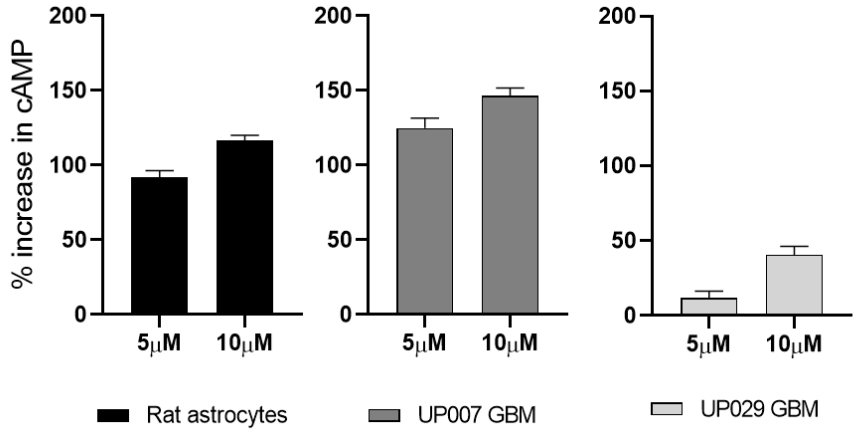

Figure 5.7. The increase in intracellular cAMP level relative to the baseline. Following 1-day incubation with NKH 477. Data presented as mean ± SEM.

5.5 Effects of forskolin analogue NKH477 on cell migration and/or proliferation in scratch wound healing assay.

Given the information about the potential suppressant actions of the elevated cAMP levels on various aspects of GBM survival and proliferation (210, 214, 215), I wanted to test whether NKH447 affects the behaviour of GBM cell lines in the scratch wound assay in light of its ability to differentially cause cAMP elevation in each cell type.

Measurements taken at 24 hours are interpreted mainly as effect on cell migration and motility rather than proliferation (268). As shown in **Figure 5.8 a,** spread of astrocytes was most strongly affected already with 5 µM of NKH 477 while as much as 40 µM was required to achieve a comparable effect in either of the GBM cell lines. Overall, although cAMP treatment had significantly disrupted their motility, it is clear that GBM cells are more resistant to the effects of cAMP on cytoskeleton and motility apparatus and that this may not be mechanistically explained by their inability to raise cAMP because NKH 477 was much more effective in this respect in UP007 than in UP 029 **(Figure 5.6)**.

At 48 hours newly formed cells more significantly aid the closure of the gap but this perhaps is more important for GBM lines, than astrocytes which divide slowly. As shown in panel b on **Figure 5.8**, UP029 line was again, more sensitive (effects significant at 10 and 20 µM) than UP007 at this time point, in spite of its ability to suppress cAMP elevations **(Figure 5.6)**. Therefore, other factors, but cAMP concentration, seem to determine the response of GBM cell lines to antidepressants and NHK477.

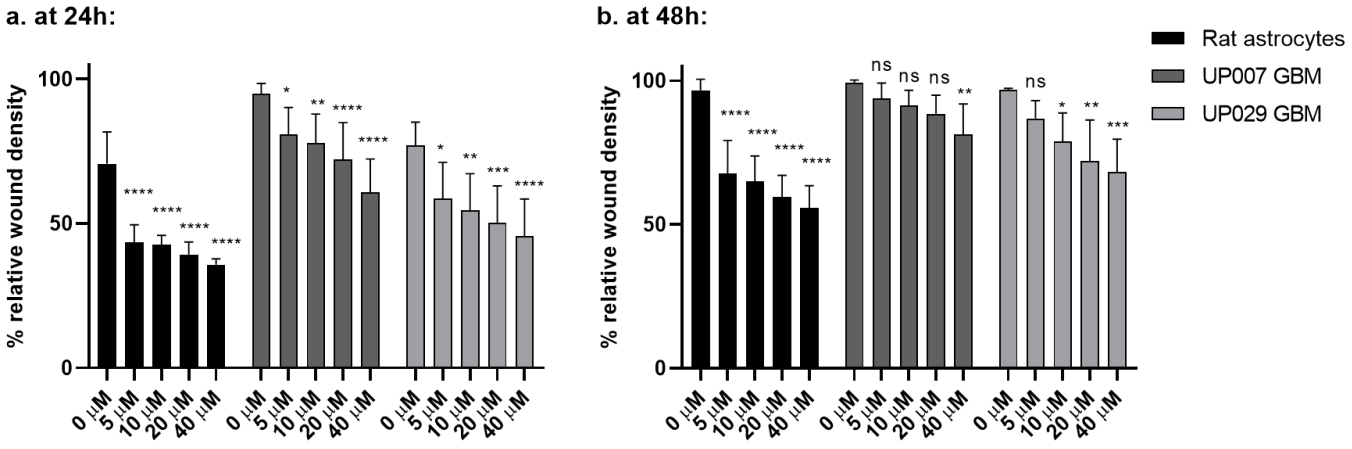

Figure 5.8. The effect of NKH477 treatment on cell proliferation and migration in RA and GBM cell lines. Graphs showing relative wound density 24 hours (a) and 48 hours (b) after scratch wound and NKH477 treatment. The number of independent experiments (n) is (a) 6, 7, and 5, (b) 6, 6, and 3, for RA, UP007 GBM, and UP029 GBM respectively. *(ns) p > 0.05, (*) p <0.033, (**) p <0.002, (***) p <0.0002, (****) p <0.0001. alpha= 0.05.* Statistical method: two-way ANOVA and Dunnett's multiple comparison. Data presented as mean ± SEM.

5.6 Antidepressant treatment for 3 days decreased MMP of primary GBM cells.

One of the theories proposed to explain previously reported effects of antidepressants on GBM, link their actions to their effect on mitochondria (187, 188, 193, 194). Mitochondria are the main source of ATP in cells in presence of oxygen and they are also able to trigger apoptosis via the intrinsic apoptotic pathway. I decided to re-evaluate this hypothesis using mitochondrial membrane potential as a sensitive parameter of mitochondrial health and activity (223, 260).

MMP was assessed using JC-10 MMP assay described in Methods section 2.4.5. Typically, mitochondrial depolarisation is seen as a trigger for release of pro-apoptotic signalling molecules (223). 24-hour treatment did not change MMP with any of the drugs (results not shown). However, after 3 days, MMP in UP007 GBM cells was clearly affected by IM and CL treatment **(Figure 5.9. a and b)**, while UP029 and RA showed some resistance to this effect at lower doses. Regarding FLX, unfortunately, variability was great and I could not

make a solid conclusion, although a trend towards decreasing MMP with increasing concentrations can be noted. This was largely due to small sample size which I was unable to increase for technical reasons. However, the results with IM and CL show that at least some GBM cell lines (exemplified by UP007) are quite sensitive to these drugs and respond with mitochondrial depolarisation while others only show a significant reduction with very high concentrations (50 µM), which however cause general toxicity as seen in **Figure 5.1.** Some representative images of the assay are presented in **Figure 5.10**.

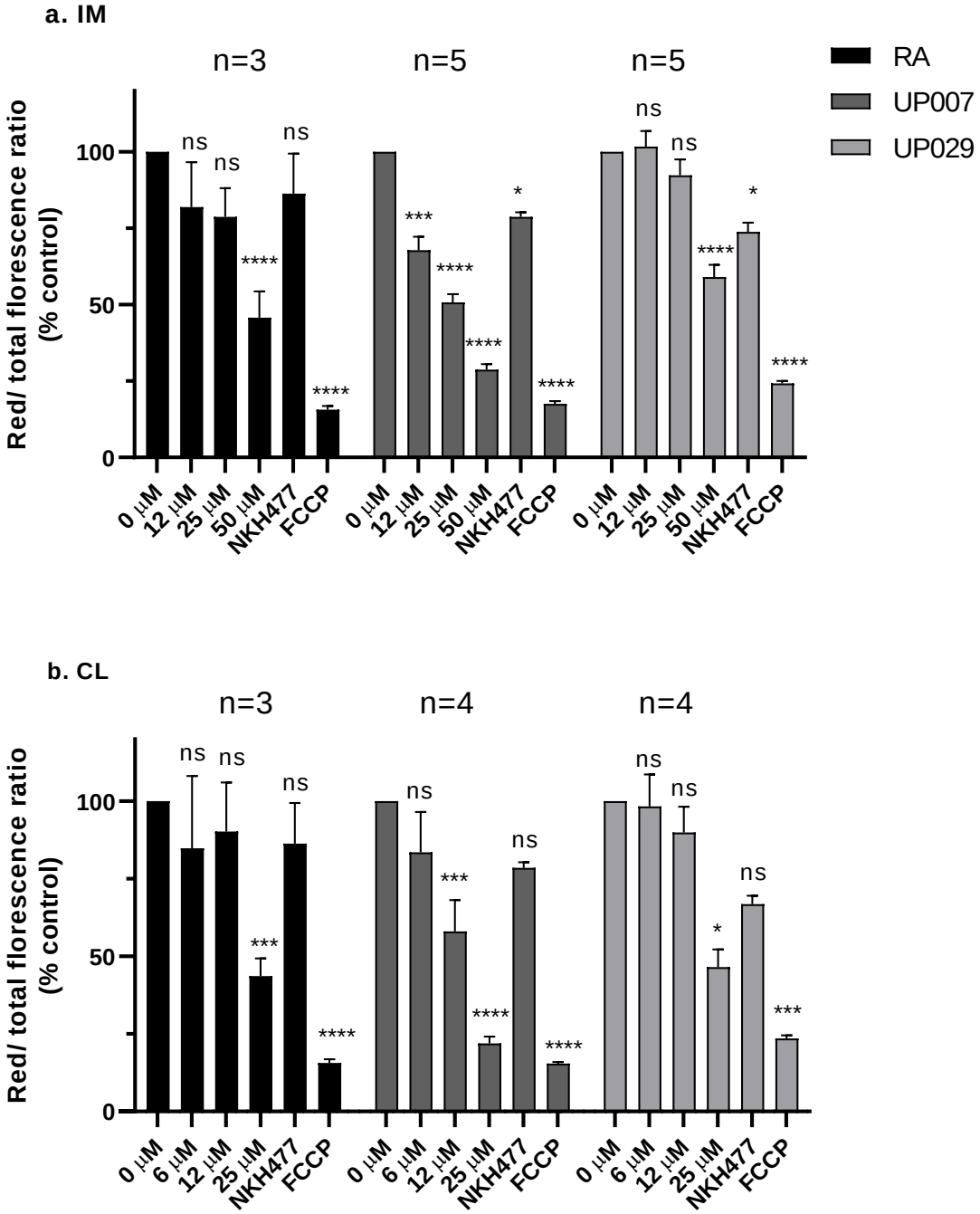

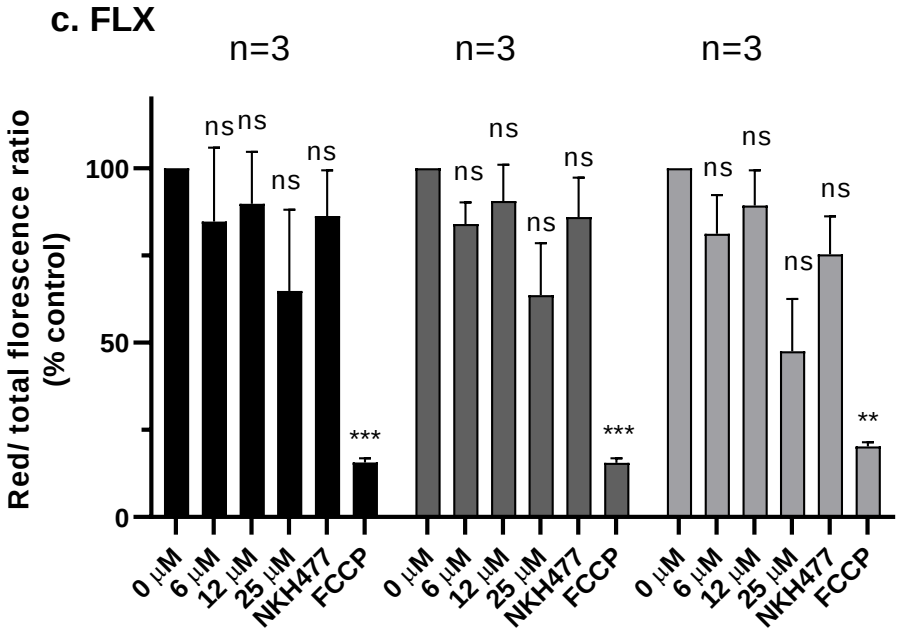

Figure 5.9. The effect of sub-toxic concentrations of IM, CL, and FLX on MMP of normal RA and GBM cell lines. Quantification of the percentage (%) of red to total florescence reflects the percentage of dye driven into the mitochondria based on its membrane potential. Duration of treatment: 3 days. NKH477 is an adenylate cyclase activator. FCCP is an uncoupler of mitochondrial oxidative phosphorylation. *(ns) p > 0.05, (*) p <0.033, (**) p <0.002, (***) p <0.0002, (****) p <0.0001. alpha= 0.05.* n is the number of independent experiments, each one in at least duplicates. Statistical method: two-way ANOVA and Tukey's multiple comparison test. Data presented as mean ± SEM.

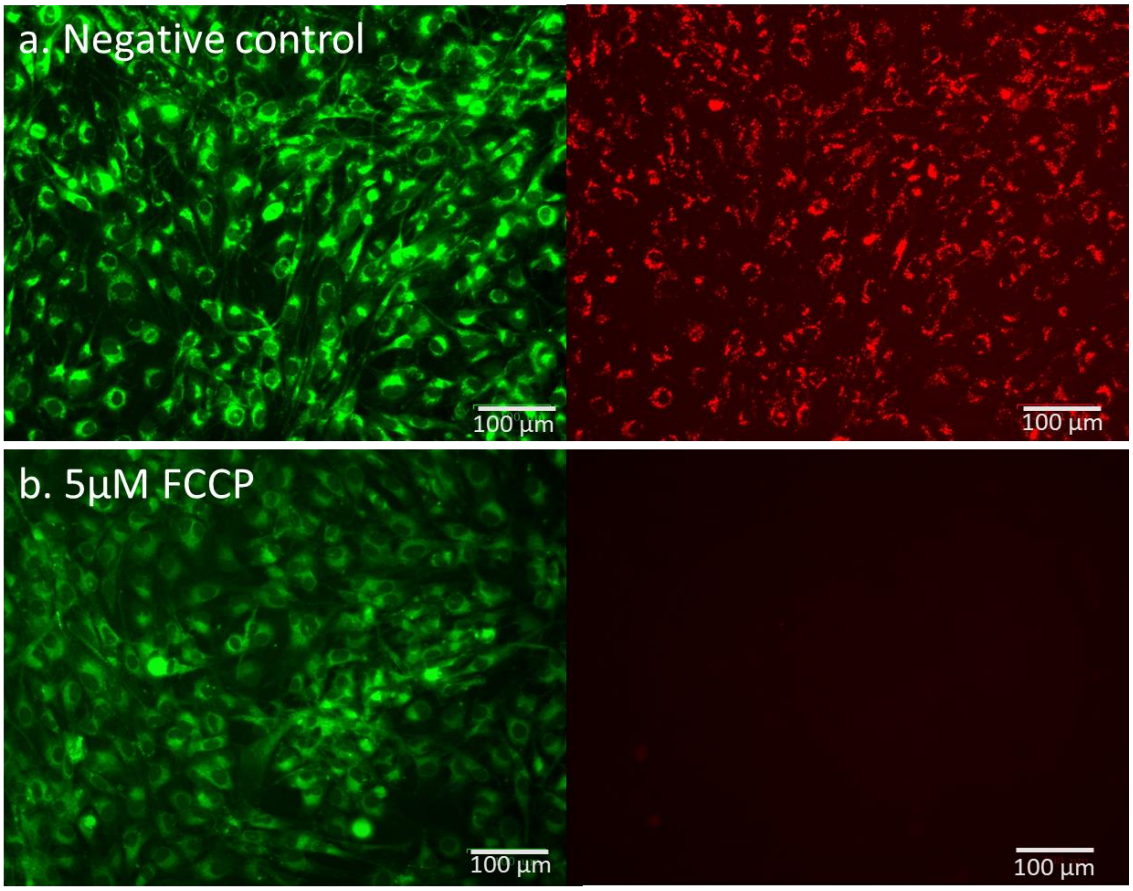
a. Negative control
100 µm
100 µm
b. 5µM FCCP
100 µm
100 µm

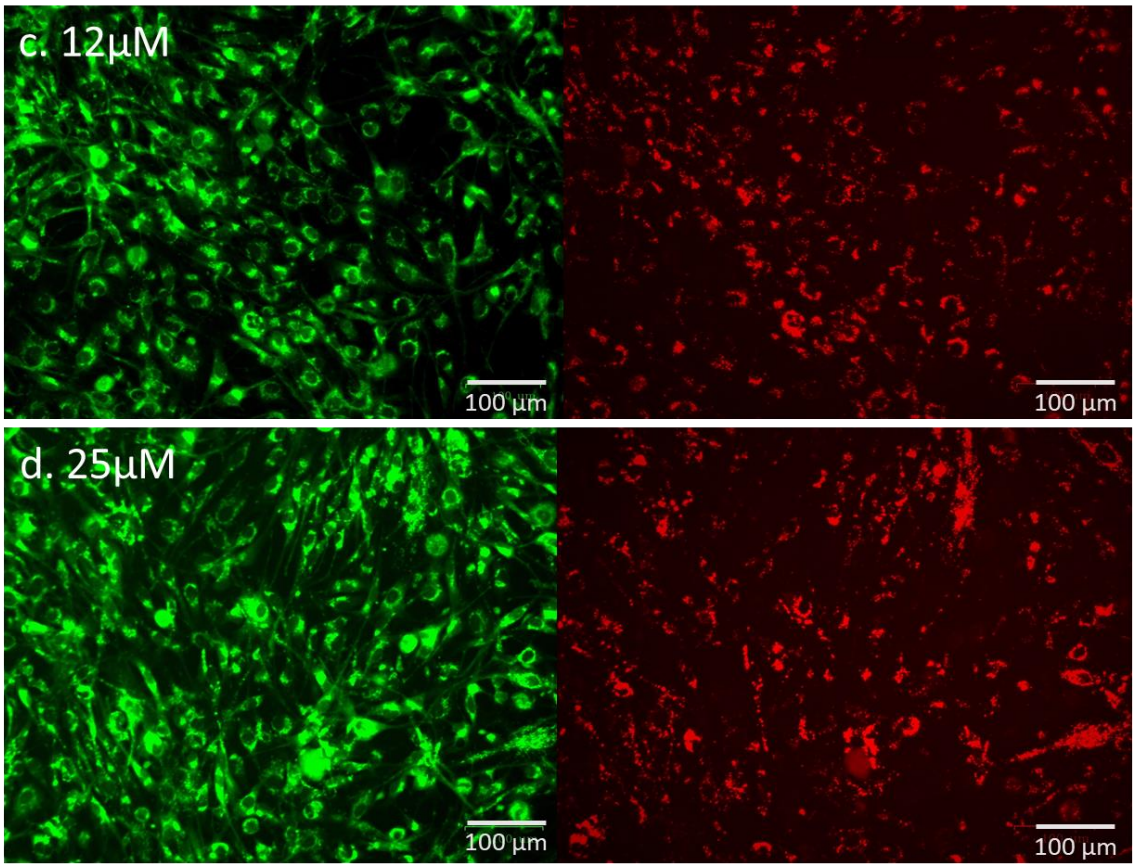
c. 12µM
100 µm
100 µm
d. 25µM
100 µm
100 µm

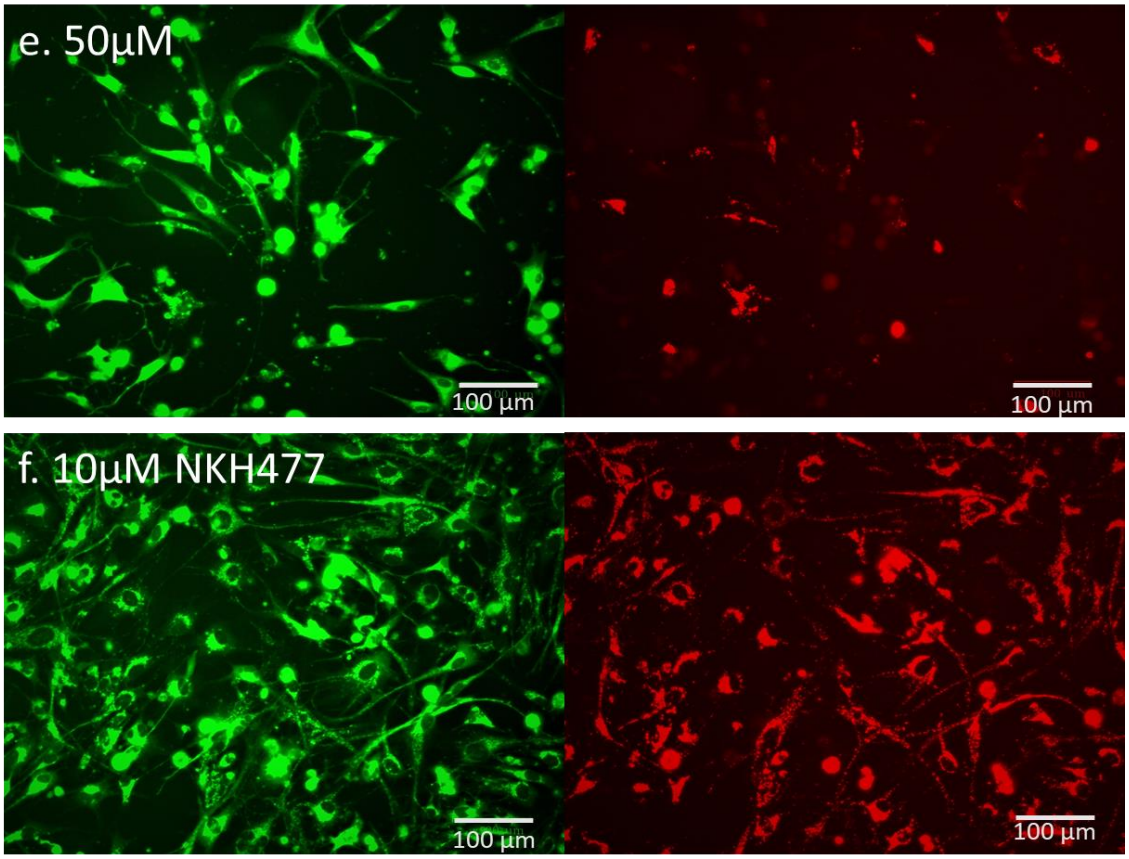

Figure 5.10. Representative images of JC-10 MMP assay on UP007 GBM cells. (a) is the negative control group with no treatment, while **(b)** is the positive control group treated with 5µM FCCP (mitochondrial oxidative phosphorylation inhibitor) for one hour. JC-10 mitochondrial dye fluoresces green when in the cytoplasm (left panels) and red when inside the mitochondria (right panels). Note the disappearance of red fluorescence after FCCP treatment (lower right panel) due to disruption of mitochondrial membrane potential, **(c-e)** The effect of imipramine (IM) treatment for 3 days on UP007 GBM cells' MMP. Note the decrease in red to total fluorescence ratio with increasing IM concentration (best seen with 50 µM IM), indicating MMP depolarization, **(f)** The effect of NKH477 treatment for 1 day on MMP. Stimulation of intracellular cAMP did not change MMP. Note the matched distribution of green fluorescence (cytoplasmic) and red fluorescence (mitochondrial).

In summary, in this chapter I have presented my experiments aimed at re-evaluation of some of the concepts related to potential re-purposing of antidepressants as anti-GBM. AD induced toxicity in GBM cells and RA, which was not accompanied by elevation in cAMP. In fact, using NKH477, cAMP was differentially induced in GBM cells and RA in a way that did not correlate with AD effect on viability or migration. The results presented in this chapter suggest that AD's effect on GBM cells might be mediated by their effects on mitochondria, at least in case of IM and CL.

Chapter 6: Thesis Discussion

In my project I pursued two strategies which potentially could supplement current set of therapies used against GBM. In the first part I have revealed a clear heterogeneity between my samples of GBM cells, in terms of morphology, sensitivity to TMZ, and molecular profile. I planned to do a pilot study to assess the feasibility of using Oxford Nanopore sequencing process to assess their mutational landscape. The plan was then changed to using Sanger sequencing due to time constrains related to COVID-19 national lock down. In the second part, I investigated the possibility of using a serendipitous finding of PDT-inducing effect of a chemical TMRM, via a previously unexplored mechanism, aimed at tumour mitochondria. Finally, I have re-evaluated the therapeutic potential of several AD on GBM cells. In my project I have used 6 GBM lines, including four isolated using a novel technique specifically from the GBM invasive margin.

6.1 The primary GBM cell lines used in this project

In my project, I used 6 different primary patient derived GBM cells: 2 UP cell lines kindly provided by Prof. G. Pilkington from the University of Portsmouth, and 4 GIN cell lines (GIN8, GIN27, GIN28, and GIN31) kindly provided by Dr S. Smith and R. Rahman from the University of Nottingham. UP cell lines were isolated some years ago using traditional process from the tumour mass. In contrast, GIN cells were recently isolated using a novel protocol specifically from the infiltrative margin. In this case patients received 5-ALA to aid visual resection and GBM cells were FACS-sorted from the invasive margin of the tumour to isolate true invasive cells from non-neoplastic parenchyma (65). Prof. Pilkington and his group reported in a previous publication that UP007 cells overexpress Axl receptor, an RTK involved in proliferation and migration signalling (245). Consistent with a number of other groups, my results demonstrate that the use of primary cells is preferable to the use of commercially available cell lines (271). Although genomic and epigenetic alterations,

especially in GBM, are unavoidable with continuous subculturing, chances that primary GBM cells maintain adequate transcriptional similarity to the parent tumour are much higher. This should make them more reliable than commercial cell lines in representing the true biological behaviour of the tumour (271). In fact, in my own experiments, I saw major differences even within the 6 cell lines, although all of them are technically GBM cell lines from patients. This underscores the importance to base any interpretation on an array of GBM samples before making any generalised conclusions. Not all experiments were performed on all 6 cell lines due to time constrains.

6.2 Molecular diversity of GBM

Despite tremendous heterogeneity in GBM, a single agent; TMZ is always prescribed as the first-line chemotherapy for newly diagnosed and recurrent GBM since 2005, following the success of the clinical trial conducted by Stupp R, et al (93). TMZ is a DNA alkylating agent that adds methyl groups to specific locations in the DNA (95). This methylation, if not repaired, usually by the enzyme MGMT in TMZ-resistant GBM, induces DNA base mismatch upon replication and subsequently induces apoptosis (95). Molecular aberrations other than MGMT promoter methylation may also be responsible for determining the sensitivity of GBM to TMZ (119). Reported IC_{50} for TMZ on different GBM cell lines range from 14 µM to 1000 µM (272, 273). This broad range reflects an extreme diversity in molecular set up responsible for TMZ response or resistance.

I examined TMZ sensitivity in my cohort of GBM cell lines. GBM cell lines showed different sensitivity patterns to TMZ treatment. As seen in **Figure 3.2 b, c, and f**, there is a trend for higher sensitivity in GIN28 > UP007 > UP029, with EC_{50} values of 35.92 µM, 41.46 µM, and 149 µM, respectively. While the trend is obvious, EC_{50} values did not differ significantly enough from each other (p= 0.06). Probably a bigger sample size would have revealed the difference. Among the four GIN cell lines, three were resistant to TMZ as seen in **Figure 3.2 d, e, and g**. In these three lines, no additive toxicity of TMZ over DMSO was observed even at 1000 µM TMZ. GIN cells are isolated from the infiltrative edge of the tumour, as described in chapter 2 section 2.1.1. This resistance of GIN cells to TMZ is not

surprising as infiltrative GBM cells are known to resist conventional therapies such as TMZ or radiotherapy (64, 125). The infiltrative nature of these cells is ascribed to a unique molecular profile controlling essential pathways such as proliferation, DNA repair and apoptosis pathways, matrix remodelling, and angiogenesis (274). Besides enabling invasion, these molecular aberrations are implicated in therapy resistance and tumour recurrence (274).

I wanted to relate functional differences of these GBM samples to their mutational profile. To investigate the molecular diversity of GBM cells, I examined them for mutations in four well characterised genes that support development of GBM. These genes are IDH-1, p53, EGFR, and PTEN. Regarding IDH-1, sequencing was successfully carried out for UP007, UP029, and GIN31, and none of them showed a mutation at the hotspot amino acid position 132, which is the site of almost all IDH-1 mutations related to GBM (249).

For the p53 gene, UP007, GIN8, GIN28, and GIN31 were successfully sequenced and mutations within the DNA binding domain were detected in all four of them. Particularly two of these mutations (in UP007 and GIN31) were found in a mutation hotspot at amino acid position 273 (246). These mutations are predicted to disturb the binding of p53 to DNA and prevent the p53-dependent transcription and tumour suppression (246).

Sequencing of the EGFR gene was successful in UP007, UP029, GIN8, and GIN31. UP007, UP029, and GIN31 had similar mutation patterns with mutations detected in furin-like region (within the extracellular domain) and common SNPs found within the tyrosine kinase catalytic domain. Most commonly in GBM, EGFR mutations are found in the extracellular domain of the gene, and these mutations affect mainly the affinity of binding of the ligand and sometimes the response to RTK inhibitors (257). Mutations in the furin-like region in particular, which mediates receptor aggregation and signal transduction, are associated with EGFR amplification (257). In GIN8, a mutation in receptor L-domain (which contains the ligand binding site) was found, as well as a SNP in the tyrosine kinase catalytic domain. Two insertions were found in UP007 and UP029 and generated a stop codon in the tyrosine kinase catalytic domain. More Insertions in the tyrosine kinase catalytic domain were identified in UP029 and GIN31 and would probably cause a frame-shift mutation. Although no report about these particular mutations is found in the literature, insertions in

the tyrosine kinase domain were reported to cause EGFR constitutive activation in some lung cancer patients (275). The impact of the new mutations which we have revealed on the signalling of EGFR is not known.

In summary, GBM cells have shown a range of mutations with known implications on tumour behaviour and prognosis (276). IDH-1 wildtype tumours are known for poor prognosis compared to IDH-1 mutants (83). UP007 and GIN31 carry a very similar mutation profile for p53 and EGFR genes, while each of UP029, GIN8, and GIN28 have distinct mutation types in at least one of these genes. However, regarding response to treatment UP007 and GIN31 are far from similar. In fact, UP007 and GIN28 show similar sensitivity to TMZ and TMRM-PDT as shown in results. Of course, this analysis is not comprehensive, yet it highlights some aspects of similarities and differences among GBM cells.

I initially aimed to utilize Oxford Nanopore sequencing, but due to the unfortunate disruption caused by the COVID pandemic, the decision was made to adopt Sanger sequencing instead. Nanopore sequencing is a third-generation sequencing technology that utilizes electrical current to identify nucleotide base sequence of DNA and RNA, in contrast to other sequencing methods which predominantly rely on DNA synthesis for detection (277). It consists of protein nanopores, embedded in an electrically resistant membrane so when an electrical current is applied, it can only pass through these nanopores (277). A leader enzyme guides the DNA (or RNA) from the applied sample to pass through the pore 1 strand at a time (277). Each nucleotide while passing comes in contact with the membrane once and alter the magnitude of the electrical current in a different way than other nucleotides (277). The sequence of alterations of the electrical current are detected and translated into nucleotide sequence in real time (277). This sequencing method provides high throughput sequencing that is relatively cheap, with no limit for the length of the sequenced DNA (277), and it would have been a great addition to this project. Time permitting, I would have been able to perform a wide scale analysis to include more genes and test for their mutational status in my GBM cells, to obtain a widefield view of the mutational landscape of GBM. Nanopore sequencing is also being increasingly used for detection of copy number variations (CNV), and it is of great value to examine CNV in relation to GBM development.

6.3 TMRM as a potential PS for GBM PDT

In the second part of my project, I decided to pursue an alternative strategy for treatment of GBM, known as PDT. By serendipity in our laboratory, we discovered that a fluorescent agent used to estimate MMP, TMRM, when illuminated with green light of moderate intensity for relatively short periods of time is an efficient PS and decided to further investigate the possibility of using this effect. For this part of the project, I have used all 6 GBM cell lines: UP and GIN GBM cells. GIN cells are representatives of the residual cells usually left behind by surgeons performing debulking surgeries because the infiltration is not visible to eye. These infiltrating cells are the source of recurrences and are the prime target for any local treatment modality. Therefore, results obtained from experiments on GIN cells are particularly valuable in examining potential treatment approaches.

Targeting mitochondria for cancer therapy has been proposed and attempted by previous studies. GBM's mitochondria are compromised by a wide range of aberrations including mtDNA gains or depletion, disturbances of the respiratory chain and dysregulation of apoptosis signalling (222). This makes tumour mitochondria a good target for therapy.

First, I established MMP in my GBM lines. MMP is an indicator of the status of the mitochondrial respiratory chain (223). In cancer cells, MMP is often hyperpolarized compared to normal cells (260). Such hyperpolarized MMP has been suggested to be associated with more aggressive tumour growth (46, 47).

MMP is often inferred from fluorescent intensity readings obtained using potential sensitive florescent dyes (223). TMRM, a rhodamine derivative, is a cationic fluorescent dye that is driven to the inside of the mitochondria proportionally to MMP (259, 278). This process is easily reversible and when mitochondrial membrane potential is lowered, TMRM immediately leaves mitochondria and disperses in the cytoplasm before leaving the cell altogether (241, 278). Thus, changes in florescence directly correspond to changes in mitochondrial membrane potential (278). Moreover, TMRM is reported to have the least non-specific accumulation (outside the mitochondria) and to have minimal interference with mitochondrial respiration among the commonly used mitochondrial fluorescent probes (223, 241). TMRM is distributed in both the inter-membrane space and the matrix due to its

lipophilicity and ability to cross the outer and inner mitochondrial membranes (241), although a recent study has shown that TMRM only accumulates near the surface of the inner mitochondrial membrane (in the inter-membrane space) and not in the matrix (259). TMRM preferably absorbs green light, mainly between 530-560 nm and emits yellow-red light, mainly between 565–592 nm (241, 259).

As shown in **Figure 4.1**, GBM cells had higher MMP (hyperpolarized) compared to RA with the exception of GIN27, which had a MMP not significantly different from that of RA. I do not yet have an explanation for this remarkable difference but once again we see that even at this level, no general conclusions can be made. In all the GBM lines, there was a noticeable heterogeneity of intensity of TMRM fluorescence between individual cells. The distribution of data was examined in order to test for the presence of more than one population (normality test), but in no case it could be confirmed that the distribution was statistically significantly different from the Gaussian. Thus, I believe that my GBM cell lines are statistically homogenous in respect to their MMP (**Figure 4.2.**).

Prolonged (longer than a few seconds) illumination of TMRM induced rapid re-distribution of the dye into the cytoplasm, reflecting a sudden drop in MMP. To further investigate into this observation, I did time lapse imaging of TMRM-loaded GBM cells before and after light illumination (30 sec), in order to track TMRM dynamics. TMRM was stably localized in the mitochondria before light illumination. Immediately after light illumination, a sharp drop in fluorescent intensity in the mitochondria was noted, as well as appearance of the dye in the nucleus and the cytoplasm of the cell. Since TMRM builds up in mitochondria against concentration gradient and is only retained by the MMP, this could only be explained by a sudden mitochondrial depolarization. MMP is critical for the functioning of mitochondria and such depolarization should theoretically lead to induction of intrinsic apoptosis pathways and cell death (223, 260). Thus, the possibility opens to use TMRM as a PS. TMRM was reported previously to induce depolarization upon strong photoactivation in isolated mitochondria and intact cells (279) but conditions in our experiments are much milder and achievable in realistic biological environment. Once again GIN27 cell line behaved differently to the other GBM cells in that it hardly responded to light exposure **(Figure 4.3),** which matched with their poor TMRM loading. At face value, this indicates low basal MMP in GIN27. Interestingly, even RA which had a similar lower MMP

still demonstrated a small decline in fluorescence after illumination. Overall, this experiment demonstrates clearly, that with one specific exemption of GIN27, GBM cells have more polarized potential than normal MMP, which guarantees greater loading of the cell with TMRM, and in theory makes them more susceptible to the PDT effect of TMRM.

One of the fundamental requirements for a PS is lack of toxicity in absence of light, in other words, the photosensitizer must only induce toxicity upon light illumination. The mechanism of the light induced toxicity is detailed in the introduction chapter section 1.2.3. Briefly, a PS molecule localizes to cancer cells and upon light exposure, it absorbs light photons. This brings the molecule to the excited state, and eventually the excited molecule either directly or indirectly triggers photochemical reactions, ROS formation, and induces apoptosis (132). TMRM was tested for its safety in the dark. Concentrations ranging from 0 to 1.6 µM were safe on all GBM cells as well as rat astrocytes in absence of light exposure. In one study, TMRM was reported to induce toxicity independent of light exposure at concentrations higher than 2.5 µM (278), which is ~ 2 orders of magnitude higher than my working concentration where I used concentrations of TMRM typically ranging from 100nM to 300nM (278). Therefore, TMRM is a promising candidate for PS. Firstly, it is driven into the mitochondria by a mechanism which seems to be a common feature of cancer cells, which is the hyperpolarised state of the mitochondria, leading to preferential localization in GBM cells compared to non-malignant cells such as RA. Secondly, it induces no toxicity unless illuminated with light.

The next logical step was to test the efficacy of TMRM-PDT on GBM cells. GBM cells were incubated with 200 or 300 nM TMRM for 45 minutes before illumination with green light for 22 or 40 seconds. The end point measurement of toxicity was carried out by staining the cells with DAPI and counting the number of cells. A novel and unique seeding protocol was employed to ensure reproducibility and reliability of the results obtained from this PDT in-vitro model **(Figure 2.1)**. In a 96-well plate, 4 µl drop of cell suspension containing 350-400 cells was placed at the centre of each well. This seeding protocol ensures that at least 95% of the cells are located at the centre of the well. This was very important to ensure that all cells are subject to equal amount of light and to avoid false negative results due to the re-population of the affected area by the cells from the corners of the well or from the sides where the light was not delivered.

TMRM-PDT was effective against all GBM cell lines. Surprisingly, it also affected GIN27. More toxicity was achieved with stronger TMRM loading and longer duration of light illumination **(Figure 4.7)**. Some degree of selectivity was achieved by milder treatment protocol (using 20nM TMRM and light illumination for 22 seconds) although still RA were significantly affected by both treatment protocols. This again could be attributed to the fact that these rat astrocytes are not post-mitotic, with metabolism and gene expression profile different from mature astrocytes (230). Sensitivity of GBM cells to PDT was different among the 6 cell types. UP007 and GIN28 were the most sensitive, while UP029 and GIN31 were the least sensitive. Comparing this to their ability to build up TMRM, it may be concluded that the impact of TMRM-PDT is determined not only by the quantity of PS but also intrinsic sensitivity of GBM.

It has been suggested that GBM cells generally have a pro-oxidant signature and a higher oxidative stress than normal cells (144). Caverzan et al. reported that patient derived GBM samples had higher basal level of ROS compared to normal brain cells (280). This elevated ROS level was associated with elevated levels of antioxidant enzymes such as superoxide dismutase and catalase (280). This was true for GBM cell lines too. Interestingly, heterogeneity in GBM cells is also reflected at the level of oxidative stress that was found to be different among them (144). Molecular heterogeneity results in different basal ROS levels, different redox balance systems and different antioxidant defence between different GBM tumours (144). This will ultimately result in different response to PDT, presumably higher basal ROS levels associated with higher level of antioxidant defence may indicate a more resistant type of GBM to such treatment. It is also arguable that higher basal ROS level may indicate a more “vulnerable” type of GBM to a further increase in ROS.

Depolarization induced by TMRM-PDT can be expected to lead to the opening of the mitochondria permeability transition pore (MPTP) which opens the gates for the exit of pro-apoptotic signals and at the same time allows Ca^{2+} overflow of the mitochondria, but if this process is not complete, mitochondrial potential may recover (279). Yet, the mechanisms of re-polarization is not fully understood, although a role for normal ETC to regenerate the MMP is highly probable (279). The ability of mitochondria to recover its MMP, which determines the fate of the cell, depends on the time the single mitochondrion stays depolarized (223). Brief depolarization may not be detrimental to normal cells with normal

mitochondria functions (223). “The point of no return” differs from cell type to another (223).

The photoactivation of TMRM in GBM cells induced a lasting depolarization state, evident by low TMRM uptake 24 hours after the initial photoactivation **(Figure 4.8)**. This state of sustained depolarization will ultimately lead to induction of the intrinsic apoptosis pathway. Interestingly, this was not the case for RA. Initially RA had a lower TMRM load and their mitochondria responded mildly to the application of light **(Figure 4.3 and 4.4),** but then, RA recovered this minimal loss of MMP due to normal mitochondrial functions. Looking in contrast, GIN27 had poor TMRM uptake to start with, and there is no evidence of initial depolarization mediated by photoactivation of TMRM in these cells (see **Figures 4.3** and **4.4**). When re-loaded with TMRM 24 hours later, they exhibited a similarly low level of fluorescence demonstrating an apparent resistance of their MMP to this modality of PDT. Nevertheless, PDT was able to suppress their viability. I speculate that there are other factors and mechanisms engaged by TMRM-PDT which have not been revealed here, and which determine the sensitivity of GBM cells to PDT.

In an attempt to enhance the effect of TMRM mediated PDT, combination therapy with either clotrimazole or NKH477 was examined for possible synergy between the two treatment modalities. Clotrimazole (1-α-2-chlorotritylimidazole), is an azole derivative used clinically for treating fungal infections (266). It has been also recognized as an inhibitor of glycolysis acting on phosphofructokinase (PFK), the rate limiting enzyme in glycolysis pathway (266, 281, 282). With Ki of 28 ± 2μM, clotrimazole was reported to inhibit PFK by dissociating the tetrameric structure of the enzyme (282). Clotrimazole has been tested on GBM cells, and it was found to induce cell cycle arrest and consequently cell death at effective concentrations starting from 40μM (265, 281, 283). The reasoning behind using a glycolytic inhibitor to try to potentiate the effect of TMRM-PDT is that with photoactivation and depolarization of mitochondrial membrane, mitochondrial energy metabolism is further disrupted, and cells are solely dependent now on glycolysis, inhibition of which should starve GBM cells of energy and ultimately lead to their demise.

A shorter duration of illumination was employed in this combination therapy experiment to easily identify synergy if present. Cells were loaded with 200 nM TMRM and

after 45 minutes, TMRM was photoactivated for 17 seconds only. They were then incubated with 10 µM clotrimazole for 3 days. At 10µM, clotrimazole was reported to significantly inhibit PFK enzyme without affecting cell viability (281). In my experiments, 10 µM clotrimazole alone was toxic to RA but not to GBM cells, and no additive effect was found in cells treated with combination treatment. Possibly I could have optimised the conditions, but this result suggests that limitation of glycolysis is not an effective approach to potentiate the destruction of GBM after TMRM-PDT.

As mentioned previously, cAMP elevation has been reported to have various detrimental effects on GBM cells (214-216, 267). I therefore examined the effect of pre-incubating GBM cell with AC activator NKH477 for 24 hours before photoactivation of TMRM, reasoning that elevated intracellular cAMP would make the cells more vulnerable to photo-toxicity. NKH477 alone did not induce toxicity in RA or GBM cells. Interestingly, NHK477 potentiated the effect of TMRM-PDT on UP007 and GIN27 GBM cells while in other cell lines there was a trend, but differences were not statistically significant. Here again we see the example of heterogeneity of the biological behaviour of the GBM which highlights the need to work with a range of GBM samples in order to avoid generalised conclusions which may only apply in some cases. Nevertheless, it seems that combination of cAMP potentiators with TMRM-PDT could be a useful approach at least in a sub-set of cases.

Our expanding knowledge about the molecular pathology of GBM is not well reflected yet on patient survival. The Stupp protocol was approved for treatment of GBM based on a 2.5-month benefit in median survival (93), which indicates how devastating is this type of cancer, and highlight the need for novel therapies.

Tumour recurrence in GBM almost always originate from the margins of a resected tumour (132). Infiltrative cells migrate along white matter tracts or grey matter nuclei, and along blood vessels (132). These critical areas often cannot be surgically removed because of the risk of neurological damage, and infiltrative cells are often left behind (132). Therefore, the need for developing local therapies that are directly applied to the resection cavity to eliminate infiltrating cells, such as PDT, might be superior to the need for developing systemic medications (132, 144).

Selectivity of PDT is determined by preferential accumulation of the PS in cancer cells. PS accumulate in cancer cells depending on common criteria that are found in most cancer cells such as aberrant heme metabolism, acidity of the microenvironment, or poor vasculature and lymphatic drainage (132). This contrasts with molecular targeted therapy, when a drug specifically targets cancer cells harbouring a specific molecular abnormality. This aspect of PDT is particularly useful against GBM because of their notorious molecular heterogeneity. Targeting the mitochondria by TMRM-PDT seems an attractive treatment approach, because it targets a common feature of most glioblastoma cells (hyperpolarized MMP) rather than targeting a specific molecular marker that is only present in a fraction of cells. Moreover, a PS which accumulates in the mitochondria has a potential to be particularly powerful in inducing apoptosis (132). This is due to the close proximity of the generated reactive oxygen species to mitochondrial proteins and mtDNA, which has a very limited repair capacity (132).

PDT has shown promising results in therapy of many types of cancers such as oesophageal cancer, bronchial carcer, and skin cancer (see **Figure 1.7**). This treatment modality has been attempted against GBM (117, 145), but many fundamental issues remain, including an effective PS, the optical wavelength for excitation, and the mode of delivery of light. Previously tested PS include HPD porfimer sodium (Photofrin©), 5-ALA (Levulan© or Gleolan©), talaporfin sodium (Laserphyrin©), and chlorin derivative temoporfin (Foscan©) (144).

5-ALA is commonly used for visualising GBM in FGS (284). It has an excitation wavelength of 375-440 nm and emission wavelength range of 640-710 nm (156). A randomized clinical trial demonstrated an increased volume of resection and improved survival with 5-ALA FGS (116). Clinical trials attempted to use 5-ALA for PDT with light at ~630 nm, arguing that it has better tissue penetration than deep blue light (147, 148, 155, 284). While this may be the case, the evidence for ROS generation when using 630nm to excite 5-ALA is lacking and clearly this is very far from optimal wavelength for its excitation. Moreover, high power light used in those studies carries a significant risk of heat injury (132). In fact, almost all studies where PDT in GBM was attempted with deep red light reported side effects such as brain oedema and thromboembolic events (155, 162, 163, 285). Photons of blue and deep blue light (400-500 nm) carry much more energy (132) but

are absorbed in tissue, easily scattered, and poorly propagate further. Therefore, on balance, it is reasonable to say that an optimum excitation wavelength for PDT should be somewhere around 530-550 nm, which is green light. At this wavelength, light photons carry enough energy to excite PS but penetrate tissue better than blue wavelengths (132).

TMRM, which has peak absorption at ~530-540 nm has a promise as a PS, because it demonstrated good tumour cell localization, induced no toxicity in absence of illumination, effectively depolarized mitochondria upon light illumination, and subsequently induced GBM cell death. I envisage a protocol where after de-bulking the risky areas of the brain, where the surgeon suspects infiltrations that are not surgically removable, will be infiltrated by TMRM and after a short period, light will be delivered directly into the brain parenchyma. Importantly, such hardware is already being developed. As an example, Modulight (Finland) have developed a system for interstitial light delivery with fine optical fibres on a comb-like assembly where light is delivered laterally, rather than shining directly straight out of the fibre. More details are found in their website: Medical laser ML7710 - Modulight, Inc. This should ensure even and complete illumination of brain tissue and, hopefully, help to exterminate the remaining infiltrating GBM cells.

6.4 Repurposing of antidepressants for GBM therapy

Obviously, if AD have a convincing and reliable anti-tumour effect on GBM, they would be good candidates for repurposing for GBM therapy because they can cross the BBB and accumulate in brain tissue (164). However, this topic is highly controversial. **Table 1.2** reveals some important weaknesses in the previous research supporting this topic. First, while some studies reported effective anti-tumour effect within physiologically reasonable range of concentrations, many studies have used very high concentrations of AD. Therapeutic plasma concentration of Clomipramine for example is 230-450 ng/ml (286), which is equivalent to 0.65- 1.28 µM. Collective human data indicate that AD can accumulate in high concentrations in the brain, reaching up to 10 µg/ml, which is equivalent to approximately 20–30 µM but it is not known what part of that substance is extracellular and what is inside cells, where it might or might not be biologically relevant (164). It also needs to be stressed that such numbers represent the theoretical maximum, which is

almost certainly not achievable in the real world, especially in a tumour. In any case, even if AD, including CL, are indeed accumulated in brain tissue at higher concentrations than plasma (287-290), the concentrations used in two of the cited studies, 114µM and 250µM; (188, 190), far exceed the feasible concentration range, making these observations clinically irrelevant.

The other problem with the majority of the published studies is that the cells used were commercially available lines that have been around for many decades and might have accumulated mutations and became molecularly too distant to GBM as seen in the clinics. In addition, the origin of these cells is not always known with certainty (291). In fact, 3 out of 39 specifically tested cell lines were found to be misidentified as glioma cells (292). Moreover, when two vials of the commonly used U87MG cell line were purchased from two different sources, only one of them was genotypically identical to U87 genotype published in Cell Lines Service (293). These considerations have motivated me to explore the effect of AD on primary patient derived GBM cells, including GIN lines, and try to assess the concentration-dependency of the effects of these drugs staying closer to clinically and physiologically relevant concentration range. It is reasonable to expect that the effect must be concentration-dependent but, in fact, there are hardly any studies where AD were tested in that way.

TCAs in general have a relatively narrow therapeutic index which means that the range between effective dose and minimum toxic dose is fairly narrow (294). When I examined the impact of IM, CL, and FLX on my GBM cells, a somehow similar pattern was detected. **Figure 5.1** shows no evidence of a classical dose-response relationship between AD concentration and effect on GBM cell lines. With IM, the toxic effect is only statistically significant at 50 µM, but at 100 µM the effect is already maximal. CL and FLX also seem to act in an all-or-nothing fashion. Both drugs exhibited measurable toxicity to the cells at of 25 µM, which seemed to immediately produce the maximum effect with no additional effect seen at higher doses. This is consistent with an earlier observation by Levkovitz et al. who reported a similar pattern of all-or-nothing effect when inducing apoptosis with CL and FLX at 25 µM and 50 µM, respectively (187). Interestingly, they also tested IM and they reported no significant induction of apoptosis with this drug. This could be attributed to GBM heterogeneity, because they have only used a commercial GBM cell line C6 in their

experiment (187), and is a strong argument in favour of my approach of using a panel of patient-derived cell lines.

EC_{50} values of each drug did not differ significantly between RA and GBM cells **(Figure 5.2).** On one hand this might suggest that this treatment fails to preferentially kill tumour cells and therefore is not particularly promising. One the other, the use of neonatal rat astrocytes as controls may also be criticised. Neonatal rat astrocytes are not fully mature and not post-mitotic, they keep dividing in vitro albeit slower than GBM cell lines (230). They exhibit different morphology and protein expression profile than the mature rat astrocytes (230), let alone mature human astrocytes. Lack of perfectly matched in-vitro controls is a known limitation in our work and in brain cancer research in general (164). Researchers typically use either primary neonatal or adult rodent astrocytes, or human embryonic astrocytes as models to evaluate adverse effects on healthy/normal cells (164). But embryonic human astrocytes are no match to mature human astrocytes, and therefore, normal cells' tolerability to treatment cannot be accurately inferred (164). In my work I have also attempted to utilize human embryonic astrocytes NHA (Lonza, #CC-2565), but the results I obtained using this cell line were not reliable because they are extremely different from batch to batch, sometimes fail to expand, must be cultured in a special media and easily die in vitro. In addition, they are extremely expensive. Eventually the decision was then made to use neonatal rat astrocytes as control because of feasibility, reliability, and cost-effectiveness.

In the scratch wound healing experiment, I tried to examine the effect of sub-toxic concentrations (based on LDH assay) of AD on GBM cells' migration and proliferation. My results show that IM and CL in sub-toxic concentrations impaired wound healing process only significantly in one of the two GBM lines tested, UP029. UP007 GBM cells as well as normal rat astrocytes were not significantly affected with the sub-toxic concentrations, although at the toxic concentration of 25µM, which clearly affects cell viability, CL impaired wound closure in UP007 GBM cells **(Figure 5.3)**. This differential effect is obviously attributed to differences in molecular profile between the two GBM cell lines, a very well-known feature of GBM.

The effect of sub-toxic dose of AD on wound healing was significant after only 24 hours, and highly significant after 48 hours as well. This suggests that the effect is mediated by blockade of cell growth as well as cell migration.

Because of the time constrains caused by COVID pandemic, I did not evaluate the GIN cell lines in this paradigm, but it might be that the suppression of infiltration is a more biologically feasible explanation of any detected anti-GBM action of AD, than their direct toxic action of the GBM.

Both IM and CL are taken orally. They are rapidly absorbed from the intestine, strongly bind to plasma proteins, and have a large volume of distribution (295). They undergo extensive first pass hepatic metabolism by hepatic cytochrome P450 (CYP) oxidative enzymes (295). This hepatic metabolism produces metabolites that are as active as the primary drug (295). CYP are a family of enzymes essential for normal hepatic metabolic functions including drug metabolism. They are present in other extra-hepatic tissue as well including the CNS, and localize predominantly in the mitochondria (296). Brain CYP have minimal effect on systemic drug concentration, however, they hugely influence local drug metabolism and concentration in the brain, especially with the preferential increased expression of some CYP enzymes in astrocytes (297). This fact is significant for in vitro experiments. FLX, an SSRI, is metabolized by almost the same hepatic enzymes as IM and CL, and the three of them, plus their metabolites, have the property to inhibit these hepatic enzymes (298). This leads to inhibition of their own metabolism, prolonging their half-life and giving rise to side effects (298). It also causes drug-drug interactions as many drugs rely on hepatic CYP for their metabolism (298). There is also a wide genetic variability, among the population, in the metabolism of TCAs due to different genotypic variants of CYP450 enzymes (299). This leads to inter-individual variability of plasma concentration produced by the same dose of the same drug (298, 299). All this can explain why these AD lack clear dose to plasma concentration relationship. Along with the molecular heterogeneity of GBM, this creates a weak spot in the idea of repurposing AD for GBM therapy, as the calculation of effective safe dose is so complicated. At the same time, in vitro, inhibition of CYP in the mitochondria of GBM could explain their ability to suppress functions and growth of these cells. Moreover, this mechanism could perhaps explain their abrupt concentration-effect

relationship: at some level, mitochondria CYP become overloaded and this triggers apoptosis. It would be interesting to further test this hypothesis.

TCAs and SSRIs were reported by some studies to elevate cAMP in brain cells, the effect that is believed to mediate their therapeutic effect in depression, which may be associated with decreased cAMP level (197). Interestingly, lower levels of cyclic AMP are also associated with more aggressive behaviour of GBM tumours (211, 212). Moreover, stimulation of cAMP signalling pathway resulted in inhibition of tumour growth, metabolic reprogramming, and differentiation of GBM cells (210, 211, 214-216, 267). It has been proposed that the mechanism of anti-cancer effect of some AD on GBM is mediated by cAMP (176, 192).

In light of these considerations, I examined the effect of AD on intracellular cAMP level in GBM cells using a FRET-based cAMP sensor (239). This is a relatively novel approach and allows direct assessment of cAMP level in living cells, in contrast to indirect biochemical assays, such as ELISA. Neither IM nor CL seemed to affect cAMP level in GBM cell lines **(Figure 5.5).** A small increase in cAMP with 25μM IM in UP007 GBM cells is noted, but at this concentration IM did not suppress GBM cells or affected wound healing process in UP007.

Interestingly, AC activator NKH477 differentially affected cAMP in RA and GBM cells. RA robustly responded to 5μM and 10 μM NKH477 by ~90% and ~120% increase in cAMP compared to baseline, respectively. UP007 also responded prominently (~125% and ~140%), but only ~10% and ~40% elevations of cAMP in UP029 were detected **(Figure 5.6 and 5.7)**. This contrasts with the somewhat higher sensitivity of UP029 to AD (the lowest EC_{50} in LDH assay and the most significantly affected wound healing dynamics), yet they are the least sensitive to NKH477. On the other hand, UP007 are much more able to build up cAMP upon stimulation yet wound healing process, for example, was less affected by AD. I reason that this observation further indicates a lack of correlation between AD anti-GBM effects and the cAMP cascade.

Activation of AC by NKH477 resulted in significant impairment of wound healing in RA and GBM cells. However, 10 μM NKH477 which produced profound increase in cAMP level in UP007 only moderately affected wound healing during the first 24 hours, and this effect

was no longer significant after the next 24 hours. In UP029 similar dynamics of the effect are observed **(Figure 5.8).** It is generally considered that the early phases of the wound healing pathway mainly depend on the lateral mobility of the cultured cells, rather than the speed of their division. cAMP is reported in the literature to control a number of signalling pathways involved in wound healing, including cytoskeleton remodelling and cell migration (300-302). Nevertheless, cAMP only minimally affected GBM cells' migratory capacity compared to a profound effect on RA, this suggests a resistance mechanism to cAMP-mediated inhibition of motility in GBM cell lines.

The almost all-or-nothing effect of AD in the LDH test suggests a mechanism which has a certain threshold, such as an overload of the mitochondrial CYP system leading to the destruction of these organelles and apoptosis. It is generally believed that mitochondria in cancer cells are abnormal. They often have more negative (hyperpolarized) basal MMP than normal cells (260-262, 303), and this might be particularly true for the GBM cells, which have been reported to have mitochondria-related disturbances including hyperpolarized MMP, abnormal mtDNA content and morphology (304). Some studies reported a disruptive effect of IM, CL, and FLX on mitochondrial functions in GBM cell lines, with subsequent activation of intrinsic apoptosis pathway (187, 188, 193, 194). I examined changes in MMP in response to AD treatment. IM and CL produced a concentration-dependent decrease in MMP (mitochondrial depolarization) in both GBM cell lines as well as rat astrocytes **(Figure 5.9).** The effect was more significant on UP007 than on UP029. FLX, however, had no statistically significant effect. These observations are generally consistent with the idea that AD, which are oxidised in the mitochondria, at some point overload their CYP and trigger release of the apoptotic signals into the cytoplasm with catastrophic consequences for the cells.

While my data confirm suppressive effect of IM, CL, and FLX on GBM cells viability, migration, and proliferation, their mechanism of action of is not clear. My results suggest that the effects of these AD on GBM cells are mediated by the impact on mitochondria rather than cAMP signalling pathway. It is also very obvious that UP007 and UP029 responses to treatments are often different in terms of the outcomes or effective concentrations, which is a manifestation of different molecular makeup in these two cell lines. This is yet another demonstration that GBM molecular heterogeneity precludes

generalised conclusions based on experiments with one or two cell lines as has been the case with many previous studies.

To conclude, in this thesis I have presented my work aimed at looking for novel and alternative strategies for anti-GBM therapy. I have used a panel of primary patient derived GBM cell lines including novel lines obtained from the GBM leading edge. An initial enquiry into molecular diversity of the GBM cell lines has been made. A novel TMRM-PDT protocol has been proposed and tested in vitro. Anti-GBM potentials previously reported for some AD has been re-evaluated. I hope that my findings will be useful for further development of new therapeutic modalities against GBM.

References

1. Schwartzbaum JA, Fisher JL, Aldape KD, Wrensch M. Epidemiology and molecular pathology of glioma. Nature clinical practice Neurology. 2006;2(9):494-503; quiz 1 p following 16.

2. Ludwig PE, J MD. Histology, Glial Cells. StatPearls. Treasure Island (FL): StatPearls Publishing

3. Louis DN, Perry A, Reifenberger G, von Deimling A, Figarella-Branger D, Cavenee WK, et al. The 2016 World Health Organization Classification of Tumors of the Central Nervous System: a summary. Acta Neuropathologica. 2016;131(6):803-20.

4. Nakada M, Kita D, Watanabe T, Hayashi Y, Teng L, Pyko IV, et al. Aberrant signaling pathways in glioma. Cancers. 2011;3(3):3242-78.

5. Bergles DE, Roberts JD, Somogyi P, Jahr CE. Glutamatergic synapses on oligodendrocyte precursor cells in the hippocampus. Nature. 2000;405(6783):187-91.

6. Venkatesh HS, Morishita W, Geraghty AC, Silverbush D, Gillespie SM, Arzt M, et al. Electrical and synaptic integration of glioma into neural circuits. Nature. 2019;573(7775):539-45.

7. Venkatesh Humsa S, Johung Tessa B, Caretti V, Noll A, Tang Y, Nagaraja S, et al. Neuronal Activity Promotes Glioma Growth through Neuroligin-3 Secretion. Cell. 2015;161(4):803-16.

8. Venkataramani V, Tanev DI, Strahle C, Studier-Fischer A, Fankhauser L, Kessler T, et al. Glutamatergic synaptic input to glioma cells drives brain tumour progression. Nature. 2019;573(7775):532-8.

9. Jiang Y, Uhrbom L. On the origin of glioma. Ups J Med Sci. 2012;117(2):113-21.

10. Holland EC, Celestino J, Dai C, Schaefer L, Sawaya RE, Fuller GN. Combined activation of Ras and Akt in neural progenitors induces glioblastoma formation in mice. Nature genetics. 2000;25(1):55-7.

11. Lindberg N, Kastemar M, Olofsson T, Smits A, Uhrbom L. Oligodendrocyte progenitor cells can act as cell of origin for experimental glioma. Oncogene. 2009;28(23):2266-75.

12. John Lin C-C, Yu K, Hatcher A, Huang T-W, Lee HK, Carlson J, et al. Identification of diverse astrocyte populations and their malignant analogs. Nat Neurosci. 2017;20(3):396-405.

13. Auffinger B, Spencer D, Pytel P, Ahmed AU, Lesniak MS. The role of glioma stem cells in chemotherapy resistance and glioblastoma multiforme recurrence. Expert Rev Neurother. 2015;15(7):741-52.

14. Singh SK, Clarke ID, Terasaki M, Bonn VE, Hawkins C, Squire J, et al. Identification of a cancer stem cell in human brain tumors. Cancer research. 2003;63(18):5821-8.

15. Bourkoula E, Mangoni D, Ius T, Pucer A, Isola M, Musiello D, et al. Glioma-associated stem cells: a novel class of tumor-supporting cells able to predict prognosis of human low-grade gliomas. Stem Cells. 2014;32(5):1239-53.

16. Cheng X, O'Neill HC. Oncogenesis and cancer stem cells: current opinions and future directions. Journal of cellular and molecular medicine. 2009;13(11-12):4377-84.

17. Bradshaw A, Wickremsekera A, Tan ST, Peng L, Davis PF, Itinteang T. Cancer Stem Cell Hierarchy in Glioblastoma Multiforme. Frontiers in Surgery. 2016;3(21).

18. Das PK, Pillai S, Rakib MA, Khanam JA, Gopalan V, Lam AKY, et al. Plasticity of Cancer Stem Cell: Origin and Role in Disease Progression and Therapy Resistance. Stem Cell Reviews and Reports. 2020;16(2):397-412.

19. Hanif F, Muzaffar K, Perveen K, Malhi SM, Simjee SU. Glioblastoma Multiforme: A Review of its Epidemiology and Pathogenesis through Clinical Presentation and Treatment. Asian Pac J Cancer Prev. 2017;18(1):3-9.

20. Ostrom QT, Gittleman H, Truitt G, Boscia A, Kruchko C, Barnholtz-Sloan JS. CBTRUS Statistical Report: Primary Brain and Other Central Nervous System Tumors Diagnosed in the United States in 2011-2015. Neuro Oncol. 2018;20(suppl_4):iv1-iv86.

21. Li QJ, Cai JQ, Liu CY. Evolving Molecular Genetics of Glioblastoma. Chinese medical journal. 2016;129(4):464-71.

22. Ostrom QT, Bauchet L, Davis FG, Deltour I, Fisher JL, Langer CE, et al. The epidemiology of glioma in adults: a "state of the science" review. Neuro Oncol. 2014;16(7):896-913.

23. Goodenberger ML, Jenkins RB. Genetics of adult glioma. Cancer Genet. 2012;205(12):613-21.

24. Brain tumour risk in relation to mobile telephone use: results of the INTERPHONE international case-control study. Int J Epidemiol. 2010;39(3):675-94.

25. Zhang C, Zhu QX. Allergy is associated with reduced risk of glioma: A meta-analysis. Allergol Immunopathol (Madr). 2017;45(6):553-9.

26. Gohar MK, Ammar MG, Alnagar AA, Abd-ElAziz HA. Serum IgE and Allergy Related Genotypes of IL-4R alpha and IL-13 Genes: Association with Glioma Susceptibility and Glioblastoma Prognosis. Egypt J Immunol. 2018;25(1):19-33.

27. Kaur H, Lachance DH, Ryan CS, Sheen YH, Seol HY, Wi C-I, et al. Asthma and risk of glioma: a population-based case-control study. BMJ Open. 2019;9(6):e025746-e.

28. Costanza M, Finocchiaro G. Allergic Signs in Glioma Pathology: Current Knowledge and Future Perspectives. Cancers (Basel). 2019;11(3):404.

29. Anssar TM, Leitzmann MF, Linker RA, Meier C, Becker C, Jick S, et al. Autoimmune diseases and immunosuppressive therapy in relation to the risk of glioma. Cancer Med. 2020;9(3):1263-75.

30. Wiemels JL, Wiencke JK, Patoka J, Moghadassi M, Chew T, McMillan A, et al. Reduced immunoglobulin E and allergy among adults with glioma compared with controls. Cancer research. 2004;64(22):8468-73.

31. Schwartzbaum JA, Huang K, Lawler S, Ding B, Yu J, Chiocca EA. Allergy and inflammatory transcriptome is predominantly negatively correlated with CD133 expression in glioblastoma. Neuro Oncol. 2010;12(4):320-7.

32. Yu JS, Wei MX, Chiocca EA, Martuza RL, Tepper RI. Treatment of glioma by engineered interleukin 4-secreting cells. Cancer research. 1993;53(13):3125-8.

33. Joshi BH, Leland P, Asher A, Prayson RA, Varricchio F, Puri RK. In situ expression of interleukin-4 (IL-4) receptors in human brain tumors and cytotoxicity of a recombinant IL-4 cytotoxin in primary glioblastoma cell cultures. Cancer Res. 2001;61(22):8058-61.

34. Henriksen M, Johnsen KB, Andersen HH, Pilgaard L, Duroux M. MicroRNA expression signatures determine prognosis and survival in glioblastoma multiforme--a systematic overview. Molecular neurobiology. 2014;50(3):896-913.

35. Ostrom QT, Adel Fahmideh M, Cote DJ, Muskens IS, Schraw JM, Scheurer ME, et al. Risk factors for childhood and adult primary brain tumors. Neuro Oncol. 2019;21(11):1357-75.

36. Louis DN, Perry A, Reifenberger G, von Deimling A, Figarella-Branger D, Cavenee WK, et al. The 2016 World Health Organization Classification of Tumors of the Central Nervous System: a summary. 2016;131(6):803-20.

37. Weller M, Reifenberger G. Beyond the World Health Organization classification of central nervous system tumors 2016: what are the new developments for gliomas from a clinician's perspective? Curr Opin Neurol. 2020;33(6):701-6.

38. Brat DJ, Aldape K, Colman H, Figrarella-Branger D, Fuller GN, Giannini C, et al. cIMPACT-NOW update 5: recommended grading criteria and terminologies for IDH-mutant astrocytomas. Acta neuropathologica. 2020;139(3):603-8.

39. Wippold FJ, Lämmle M, Anatelli F, Lennerz J, Perry A. Neuropathology for the Neuroradiologist: Palisades and Pseudopalisades. American Journal of Neuroradiology. 2006;27(10):2037.

40. Delgado-Martín B, Medina MÁ. Advances in the Knowledge of the Molecular Biology of Glioblastoma and Its Impact in Patient Diagnosis, Stratification, and Treatment. Advanced Science. 2020;7(9):1902971.

41. Rodriguez FJ, Vizcaino MA, Lin M-T. Recent Advances on the Molecular Pathology of Glial Neoplasms in Children and Adults. The Journal of Molecular Diagnostics. 2016;18(5):620-34.

42. Perrin SL, Samuel MS, Koszyca B, Brown MP, Ebert LM, Oksdath M, et al. Glioblastoma heterogeneity and the tumour microenvironment: implications for preclinical research and development of new treatments. Biochem Soc Trans. 2019;47(2):625-38.

43. In: De Vleeschouwer S, editor. Glioblastoma. Brisbane (AU): Codon Publications

44. Thon N, Tonn J-C, Kreth F-W. The surgical perspective in precision treatment of diffuse gliomas. Onco Targets Ther. 2019;12:1497-508.

45. Ijzerman-Korevaar M, Snijders TJ, de Graeff A, Teunissen SCCM, de Vos FYF. Prevalence of symptoms in glioma patients throughout the disease trajectory: a systematic review. Journal of neuro-oncology. 2018;140(3):485-96.

46. McGirt MJ, Villavicencio AT, Bulsara KR, Friedman AH. MRI-guided stereotactic biopsy in the diagnosis of glioma: comparison of biopsy and surgical resection specimen. Surgical Neurology. 2003;59(4):279-83.

47. Malzkorn B, Reifenberger G. Practical implications of integrated glioma classification according to the World Health Organization classification of tumors of the central nervous system 2016. Curr Opin Oncol. 2016;28(6):494-501.

48. Comprehensive genomic characterization defines human glioblastoma genes and core pathways. Nature. 2008;455(7216):1061-8.

49. Tuncel G, Kalkan R. Receptor tyrosine kinase-Ras-PI 3 kinase-Akt signaling network in glioblastoma multiforme. Med Oncol. 2018;35(9):122.

50. Venkatesan S, Lamfers ML, Dirven CM, Leenstra S. Genetic biomarkers of drug response for small-molecule therapeutics targeting the RTK/Ras/PI3K, p53 or Rb pathway in glioblastoma. CNS Oncol. 2016;5(2):77-90.

51. Oprita A, Baloi SC, Staicu GA, Alexandru O, Tache DE, Danoiu S, et al. Updated Insights on EGFR Signaling Pathways in Glioma. Int J Mol Sci. 2021;22(2).

52. Zhao HF, Wang J, Shao W, Wu CP, Chen ZP, To ST, et al. Recent advances in the use of PI3K inhibitors for glioblastoma multiforme: current preclinical and clinical development. Mol Cancer. 2017;16(1):100.

53. Duffy MJ, Synnott NC, McGowan PM, Crown J, O'Connor D, Gallagher WM. p53 as a target for the treatment of cancer. Cancer Treat Rev. 2014;40(10):1153-60.

54. Harris SL, Levine AJ. The p53 pathway: positive and negative feedback loops. Oncogene. 2005;24(17):2899-908.

55. Ishii N, Maier D, Merlo A, Tada M, Sawamura Y, Diserens AC, et al. Frequent co-alterations of TP53, p16/CDKN2A, p14ARF, PTEN tumor suppressor genes in human glioma cell lines. Brain Pathol. 1999;9(3):469-79.

56. Zhang Y, Dube C, Gibert M, Jr., Cruickshanks N, Wang B, Coughlan M, et al. The p53 Pathway in Glioblastoma. Cancers. 2018;10(9):297.

57. Giacinti C, Giordano A. RB and cell cycle progression. Oncogene. 2006;25(38):5220-7.

58. Wirsching H-G, Roth P, Weller M. A vasculature-centric approach to developing novel treatment options for glioblastoma. Expert Opinion on Therapeutic Targets. 2021:null-null.

59. Watkins S, Sontheimer H. Unique biology of gliomas: challenges and opportunities. Trends in neurosciences. 2012;35(9):546-56.

60. Boyd NH, Tran AN, Bernstock JD, Etminan T, Jones AB, Gillespie GY, et al. Glioma stem cells and their roles within the hypoxic tumor microenvironment. Theranostics. 2021;11(2):665-83.

61. Evans SM, Jenkins KW, Chen HI, Jenkins WT, Judy KD, Hwang W-T, et al. The Relationship among Hypoxia, Proliferation, and Outcome in Patients with De Novo Glioblastoma: A Pilot Study. Transl Oncol. 2010;3(3):160-9.

62. Osswald M, Solecki G, Wick W, Winkler F. A malignant cellular network in gliomas: potential clinical implications. Neuro Oncol. 2016;18(4):479-85.

63. Alieva M, Leidgens V, Riemenschneider MJ, Klein CA, Hau P, van Rheenen J. Intravital imaging of glioma border morphology reveals distinctive cellular dynamics and contribution to tumor cell invasion. Scientific reports. 2019;9(1):2054.

64. Petrecca K, Guiot MC, Panet-Raymond V, Souhami L. Failure pattern following complete resection plus radiotherapy and temozolomide is at the resection margin in patients with glioblastoma. J Neurooncol. 2013;111(1):19-23.

65. Smith SJ, Rowlinson J, Estevez-Cebrero M, Onion D, Ritchie A, Clarke P, et al. Metabolism-based isolation of invasive glioblastoma cells with specific gene signatures and tumorigenic potential. Neuro-oncology advances. 2020;2(1):vdaa087.

66. Kwiatkowska A, Symons M. Signaling determinants of glioma cell invasion. Advances in experimental medicine and biology. 2013;986:121-41.

67. Artandi SE, DePinho RA. A critical role for telomeres in suppressing and facilitating carcinogenesis. Curr Opin Genet Dev. 2000;10(1):39-46.

68. Lorbeer FK, Hockemeyer D. TERT promoter mutations and telomeres during tumorigenesis. Curr Opin Genet Dev. 2020;60:56-62.

69. Fan HC, Chen CM, Chi CS, Tsai JD, Chiang KL, Chang YK, et al. Targeting Telomerase and ATRX/DAXX Inducing Tumor Senescence and Apoptosis in the Malignant Glioma. Int J Mol Sci. 2019;20(1).

70. Jovčevska I. Next Generation Sequencing and Machine Learning Technologies Are Painting the Epigenetic Portrait of Glioblastoma. Frontiers in oncology. 2020;10:798-.

71. Choi SA, Kwak PA, Park C-K, Wang K-C, Phi JH, Lee JY, et al. A novel histone deacetylase inhibitor, CKD5, has potent anti-cancer effects in glioblastoma. Oncotarget. 2017;8(6):9123-33.

72. Nguyen TTT, Zhang Y, Shang E, Shu C, Torrini C, Zhao J, et al. HDAC inhibitors elicit metabolic reprogramming by targeting super-enhancers in glioblastoma models. J Clin Invest. 2020;130(7):3699-716.

73. Noushmehr H, Weisenberger DJ, Diefes K, Phillips HS, Pujara K, Berman BP, et al. Identification of a CpG island methylator phenotype that defines a distinct subgroup of glioma. Cancer cell. 2010;17(5):510-22.

74. Turcan S, Rohle D, Goenka A, Walsh LA, Fang F, Yilmaz E, et al. IDH1 mutation is sufficient to establish the glioma hypermethylator phenotype. Nature. 2012;483(7390):479-83.

75. Kraboth Z, Galik B, Tompa M, Kajtar B, Urban P, Gyenesei A, et al. DNA CpG methylation in sequential glioblastoma specimens. J Cancer Res Clin Oncol. 2020;146(11):2885-96.

76. Cabrini G, Fabbri E, Lo Nigro C, Dechecchi MC, Gambari R. Regulation of expression of O6-methylguanine-DNA methyltransferase and the treatment of glioblastoma (Review). Int J Oncol. 2015;47(2):417-28.

77. Kitange GJ, Mladek AC, Carlson BL, Schroeder MA, Pokorny JL, Cen L, et al. Inhibition of Histone Deacetylation Potentiates the Evolution of Acquired Temozolomide Resistance Linked to MGMT Upregulation in Glioblastoma Xenografts. Clinical Cancer Research. 2012;18(15):4070.

78. Dunn J, Baborie A, Alam F, Joyce K, Moxham M, Sibson R, et al. Extent of MGMT promoter methylation correlates with outcome in glioblastomas given temozolomide and radiotherapy. British journal of cancer. 2009;101(1):124-31.

79. Lu VM, O'Connor KP, Shah AH, Eichberg DG, Luther EM, Komotar RJ, et al. The prognostic significance of CDKN2A homozygous deletion in IDH-mutant lower-grade glioma and glioblastoma: a systematic review of the contemporary literature. J Neurooncol. 2020;148(2):221-9.

80. Al-Khallaf H. Isocitrate dehydrogenases in physiology and cancer: biochemical and molecular insight. Cell Biosci. 2017;7:37-.

81. Noushmehr H, Weisenberger DJ, Diefes K, Phillips HS, Pujara K, Berman BP, et al. Identification of a CpG island methylator phenotype that defines a distinct subgroup of glioma. Cancer cell. 2010;17(5):510-22.

82. Figueroa ME, Abdel-Wahab O, Lu C, Ward PS, Patel J, Shih A, et al. Leukemic IDH1 and IDH2 mutations result in a hypermethylation phenotype, disrupt TET2 function, and impair hematopoietic differentiation. Cancer cell. 2010;18(6):553-67.

83. Semukunzi H, Roy D, Li H, Khan GJ, Lyu X, Yuan S, et al. IDH mutations associated impact on related cancer epidemiology and subsequent effect toward HIF-1α. Biomedicine & Pharmacotherapy. 2017;89:805-11.

84. Zhang L, Sorensen MD, Kristensen BW, Reifenberger G, McIntyre TM, Lin F. D-2-Hydroxyglutarate Is an Intercellular Mediator in IDH-Mutant Gliomas Inhibiting Complement and T Cells. Clinical cancer research : an official journal of the American Association for Cancer Research. 2018;24(21):5381-91.

85. Böttcher M, Renner K, Berger R, Mentz K, Thomas S, Cardenas-Conejo ZE, et al. D-2-hydroxyglutarate interferes with HIF-1α stability skewing T-cell metabolism towards oxidative phosphorylation and impairing Th17 polarization. Oncoimmunology. 2018;7(7):e1445454.

86. van den Bent MJ, Dubbink HJ, Marie Y, Brandes AA, Taphoorn MJ, Wesseling P, et al. IDH1 and IDH2 mutations are prognostic but not predictive for outcome in anaplastic oligodendroglial tumors: a report of the European Organization for Research and Treatment of Cancer Brain Tumor Group. Clinical cancer research : an official journal of the American Association for Cancer Research. 2010;16(5):1597-604.

87. Li S, Chou AP, Chen W, Chen R, Deng Y, Phillips HS, et al. Overexpression of isocitrate dehydrogenase mutant proteins renders glioma cells more sensitive to radiation. Neuro Oncol. 2013;15(1):57-68.

88. Tran AN, Lai A, Li S, Pope WB, Teixeira S, Harris RJ, et al. Increased sensitivity to radiochemotherapy in IDH1 mutant glioblastoma as demonstrated by serial quantitative MR volumetry. Neuro Oncol. 2014;16(3):414-20.

89. Juratli TA, Cahill DP, McCutcheon IE. Determining optimal treatment strategy for diffuse glioma: the emerging role of IDH mutations. Expert Review of Anticancer Therapy. 2015;15(6):603-6.

90. Appay R, Dehais C, Maurage CA, Alentorn A, Carpentier C, Colin C, et al. CDKN2A homozygous deletion is a strong adverse prognosis factor in diffuse malignant IDH-mutant gliomas. Neuro Oncol. 2019;21(12):1519-28.

91. Liu A, Hou C, Chen H, Zong X, Zong P. Genetics and Epigenetics of Glioblastoma: Applications and Overall Incidence of IDH1 Mutation. Frontiers in oncology. 2016;6(16).

92. Verhaak RGW, Hoadley KA, Purdom E, Wang V, Qi Y, Wilkerson MD, et al. Integrated genomic analysis identifies clinically relevant subtypes of glioblastoma characterized by abnormalities in PDGFRA, IDH1, EGFR, and NF1. Cancer cell. 2010;17(1):98-110.

93. Stupp R, Mason WP, van den Bent MJ, Weller M, Fisher B, Taphoorn MJB, et al. Radiotherapy plus Concomitant and Adjuvant Temozolomide for Glioblastoma. New England Journal of Medicine. 2005;352(10):987-96.

94. Stupp R, Hegi ME, Mason WP, van den Bent MJ, Taphoorn MJ, Janzer RC, et al. Effects of radiotherapy with concomitant and adjuvant temozolomide versus radiotherapy alone on survival in glioblastoma in a randomised phase III study: 5-year analysis of the EORTC-NCIC trial. The Lancet Oncology. 2009;10(5):459-66.

95. Villano JL, Seery TE, Bressler LR. Temozolomide in malignant gliomas: current use and future targets. Cancer Chemotherapy and Pharmacology. 2009;64(4):647-55.

96. Tan AC, Ashley DM, López GY, Malinzak M, Friedman HS, Khasraw M. Management of glioblastoma: State of the art and future directions. CA: A Cancer Journal for Clinicians. 2020;70(4):299-312.

97. Hadjipanayis CG, Stummer W. 5-ALA and FDA approval for glioma surgery. J Neurooncol. 2019;141(3):479-86.

98. Pitter KL, Tamagno I, Alikhanyan K, Hosni-Ahmed A, Pattwell SS, Donnola S, et al. Corticosteroids compromise survival in glioblastoma. Brain. 2016;139(Pt 5):1458-71.

99. Veliz I, Loo Y, Castillo O, Karachaliou N, Nigro O, Rosell R. Advances and challenges in the molecular biology and treatment of glioblastoma-is there any hope for the future? Annals of translational medicine. 2015;3(1):7.

100. Bock HC, Puchner MJ, Lohmann F, Schütze M, Koll S, Ketter R, et al. First-line treatment of malignant glioma with carmustine implants followed by concomitant radiochemotherapy: a multicenter experience. Neurosurg Rev. 2010;33(4):441-9.

101. Ashby LS, Smith KA, Stea B. Gliadel wafer implantation combined with standard radiotherapy and concurrent followed by adjuvant temozolomide for treatment of newly diagnosed high-grade glioma: a systematic literature review. World J Surg Oncol. 2016;14(1):225-.

102. Stupp R, Taillibert S, Kanner AA, Kesari S, Steinberg DM, Toms SA, et al. Maintenance Therapy With Tumor-Treating Fields Plus Temozolomide vs Temozolomide Alone for Glioblastoma: A Randomized Clinical Trial. Jama. 2015;314(23):2535-43.

103. Fabian D, Guillermo Prieto Eibl MDP, Alnahhas I, Sebastian N, Giglio P, Puduvalli V, et al. Treatment of Glioblastoma (GBM) with the Addition of Tumor-Treating Fields (TTF): A Review. Cancers. 2019;11(2):174.

104. Kirson ED, Gurvich Z, Schneiderman R, Dekel E, Itzhaki A, Wasserman Y, et al. Disruption of cancer cell replication by alternating electric fields. Cancer research. 2004;64(9):3288-95.

105. Uhm JH, Ballman KV, Wu W, Giannini C, Krauss JC, Buckner JC, et al. Phase II evaluation of gefitinib in patients with newly diagnosed Grade 4 astrocytoma: Mayo/North

Central Cancer Treatment Group Study N0074. Int J Radiat Oncol Biol Phys. 2011;80(2):347-53.

106. Khasraw M, Lee A, McCowatt S, Kerestes Z, Buyse ME, Back M, et al. Cilengitide with metronomic temozolomide, procarbazine, and standard radiotherapy in patients with glioblastoma and unmethylated MGMT gene promoter in ExCentric, an open-label phase II trial. J Neurooncol. 2016;128(1):163-71.

107. Chinnaiyan P, Won M, Wen PY, Rojiani AM, Werner-Wasik M, Shih HA, et al. A randomized phase II study of everolimus in combination with chemoradiation in newly diagnosed glioblastoma: results of NRG Oncology RTOG 0913. Neuro Oncol. 2018;20(5):666-73.

108. Gilbert MR, Dignam JJ, Armstrong TS, Wefel JS, Blumenthal DT, Vogelbaum MA, et al. A randomized trial of bevacizumab for newly diagnosed glioblastoma. N Engl J Med. 2014;370(8):699-708.

109. Funakoshi Y, Hata N, Kuga D, Hatae R, Sangatsuda Y, Fujioka Y, et al. Update on Chemotherapeutic Approaches and Management of Bevacizumab Usage for Glioblastoma. Pharmaceuticals. 2020;13(12):470.

110. van den Bent MJ, Klein M, Smits M, Reijneveld JC, French PJ, Clement P, et al. Bevacizumab and temozolomide in patients with first recurrence of WHO grade II and III glioma, without 1p/19q co-deletion (TAVAREC): a randomised controlled phase 2 EORTC trial. The Lancet Oncology. 2018;19(9):1170-9.

111. Hainsworth JD, Becker KP, Mekhail T, Chowdhary SA, Eakle JF, Wright D, et al. Phase I/II study of bevacizumab with BKM120, an oral PI3K inhibitor, in patients with refractory solid tumors (phase I) and relapsed/refractory glioblastoma (phase II). J Neurooncol. 2019;144(2):303-11.

112. Puduvalli VK, Wu J, Yuan Y, Armstrong TS, Vera E, Wu J, et al. A Bayesian adaptive randomized phase II multicenter trial of bevacizumab with or without vorinostat in adults with recurrent glioblastoma. Neuro Oncol. 2020;22(10):1505-15.

113. Mozhei O, A GT, Kasparov S. Viral Vectors as Gene Therapy Agents for Treatment of Glioblastoma. Cancers. 2020;12(12).

114. Gill BJ, Pisapia DJ, Malone HR, Goldstein H, Lei L, Sonabend A, et al. MRI-localized biopsies reveal subtype-specific differences in molecular and cellular composition at the margins of glioblastoma. Proc Natl Acad Sci U S A. 2014;111(34):12550-5.

115. Sottoriva A, Spiteri I, Piccirillo SGM, Touloumis A, Collins VP, Marioni JC, et al. Intratumor heterogeneity in human glioblastoma reflects cancer evolutionary dynamics. Proceedings of the National Academy of Sciences. 2013;110(10):4009.

116. Stummer W, Pichlmeier U, Meinel T, Wiestler OD, Zanella F, Reulen HJ. Fluorescence-guided surgery with 5-aminolevulinic acid for resection of malignant glioma: a randomised controlled multicentre phase III trial. The Lancet Oncology. 2006;7(5):392-401.

117. Cramer SW, Chen CC. Photodynamic Therapy for the Treatment of Glioblastoma. Frontiers in Surgery. 2020;6(81).

118. Silbergeld DL, Chicoine MR. Isolation and characterization of human malignant glioma cells from histologically normal brain. Journal of neurosurgery. 1997;86(3):525-31.

119. Arora A, Somasundaram K. Glioblastoma vs temozolomide: can the red queen race be won? Cancer Biol Ther. 2019;20(8):1083-90.

120. Hegi ME, Liu L, Herman JG, Stupp R, Wick W, Weller M, et al. Correlation of O6-Methylguanine Methyltransferase (MGMT) Promoter Methylation With Clinical Outcomes in Glioblastoma and Clinical Strategies to Modulate MGMT Activity. Journal of Clinical Oncology. 2008;26(25):4189-99.

121. Wu P, Cai J, Chen Q, Han B, Meng X, Li Y, et al. Lnc-TALC promotes O(6)-methylguanine-DNA methyltransferase expression via regulating the c-Met pathway by competitively binding with miR-20b-3p. Nat Commun. 2019;10(1):2045-.

122. Yang W-B, Chuang J-Y, Ko C-Y, Chang W-C, Hsu T-I. Dehydroepiandrosterone Induces Temozolomide Resistance Through Modulating Phosphorylation and Acetylation of Sp1 in Glioblastoma. Molecular neurobiology. 2019;56(4):2301-13.

123. Arnold CR, Mangesius J, Skvortsova I-I, Ganswindt U. The Role of Cancer Stem Cells in Radiation Resistance. Frontiers in oncology. 2020;10:164-.

124. Szerlip NJ, Pedraza A, Chakravarty D, Azim M, McGuire J, Fang Y, et al. Intratumoral heterogeneity of receptor tyrosine kinases EGFR and PDGFRA amplification in glioblastoma defines subpopulations with distinct growth factor response. Proc Natl Acad Sci U S A. 2012;109(8):3041-6.

125. Smith SJ, Diksin M, Chhaya S, Sairam S, Estevez-Cebrero MA, Rahman R. The Invasive Region of Glioblastoma Defined by 5ALA Guided Surgery Has an Altered Cancer Stem Cell Marker Profile Compared to Central Tumour. Int J Mol Sci. 2017;18(11).

126. Johnson BE, Mazor T, Hong C, Barnes M, Aihara K, McLean CY, et al. Mutational analysis reveals the origin and therapy-driven evolution of recurrent glioma. Science (New York, NY). 2014;343(6167):189-93.

127. Gillies RJ, Verduzco D, Gatenby RA. Evolutionary dynamics of carcinogenesis and why targeted therapy does not work. Nat Rev Cancer. 2012;12(7):487-93.

128. Pitz MW, Desai A, Grossman SA, Blakeley JO. Tissue concentration of systemically administered antineoplastic agents in human brain tumors. J Neurooncol. 2011;104(3):629-38.

129. Uzdensky AB. The biophysical aspects of photodynamic therapy. Biophysics. 2016;61(3):461-9.

130. Castano AP, Demidova TN, Hamblin MR. Mechanisms in photodynamic therapy: part one-photosensitizers, photochemistry and cellular localization. Photodiagnosis Photodyn Ther. 2004;1(4):279-93.

131. Dolmans DEJGJ, Fukumura D, Jain RK. Photodynamic therapy for cancer. Nature Reviews Cancer. 2003;3(5):380-7.

132. Vasilev A, Sofi R, Rahman R, Smith SJ, Teschemacher AG, Kasparov S. Using Light for Therapy of Glioblastoma Multiforme (GBM). Brain Sci. 2020;10(2).

133. Castano AP, Demidova TN, Hamblin MR. Mechanisms in photodynamic therapy: Part three-Photosensitizer pharmacokinetics, biodistribution, tumor localization and modes of tumor destruction. Photodiagnosis Photodyn Ther. 2005;2(2):91-106.

134. Figge FH, Weiland GS, Manganiello LO. Cancer detection and therapy; affinity of neoplastic, embryonic, and traumatized tissues for porphyrins and metalloporphyrins. Proc Soc Exp Biol Med. 1948;68(3):640.

135. Lipson RL, Baldes EJ, Olsen AM. The use of a derivative of hematoporhyrin in tumor detection. J Natl Cancer Inst. 1961;26:1-11.

136. Kessel D. Photodynamic Therapy: A Brief History. Journal of clinical medicine. 2019;8(10):1581.

137. Ormond AB, Freeman HS. Dye Sensitizers for Photodynamic Therapy. Materials (Basel). 2013;6(3):817-40.

138. Nitta M, Muragaki Y, Maruyama T, Iseki H, Komori T, Ikuta S, et al. Role of photodynamic therapy using talaporfin sodium and a semiconductor laser in patients with newly diagnosed glioblastoma. Journal of neurosurgery. 2018:1-8.

139. Diamond I, McDonagh A, Wilson C, Granelli S, Nielsen S, Jaenicke R. PHOTODYNAMIC THERAPY OF MALIGNANT TUMOURS. The Lancet. 1972;300(7788):1175-7.

140. Dougherty TJ. Photodynamic therapy (PDT) of malignant tumors. Critical Reviews in Oncology/Hematology. 1984;2(2):83-116.

141. Dougherty TJ, Gomer CJ, Henderson BW, Jori G, Kessel D, Korbelik M, et al. Photodynamic therapy. J Natl Cancer Inst. 1998;90(12):889-905.

142. Akimoto J. Photodynamic Therapy for Malignant Brain Tumors. Neurologia medico-chirurgica. 2016;advpub.

143. Dupont C, Vermandel M, Leroy HA, Quidet M, Lecomte F, Delhem N, et al. INtraoperative photoDYnamic Therapy for GliOblastomas (INDYGO): Study Protocol for a Phase I Clinical Trial. Neurosurgery. 2019;84(6):E414-e9.

144. Ibarra LE, Vilchez ML, Caverzán MD, Milla Sanabria LN. Understanding the glioblastoma tumor biology to optimize photodynamic therapy: From molecular to cellular events. J Neurosci Res. 2020.

145. Baskaran R, Lee J, Yang SG. Clinical development of photodynamic agents and therapeutic applications. Biomater Res. 2018;22:25.

146. Dupont C, Mordon S, Deleporte P, Reyns N, Vermandel M. A novel device for intraoperative photodynamic therapy dedicated to glioblastoma treatment. Future oncology (London, England). 2017;13(27):2441-54.

147. Beck TJ, Kreth FW, Beyer W, Mehrkens JH, Obermeier A, Stepp H, et al. Interstitial photodynamic therapy of nonresectable malignant glioma recurrences using 5-aminolevulinic acid induced protoporphyrin IX. Lasers Surg Med. 2007;39(5):386-93.

148. Johansson A, Faber F, Kniebühler G, Stepp H, Sroka R, Egensperger R, et al. Protoporphyrin IX fluorescence and photobleaching during interstitial photodynamic therapy of malignant gliomas for early treatment prognosis. Lasers Surg Med. 2013;45(4):225-34.

149. Mahmoudi K, Garvey KL, Bouras A, Cramer G, Stepp H, Jesu Raj JG, et al. 5-aminolevulinic acid photodynamic therapy for the treatment of high-grade gliomas. Journal of Neuro-Oncology. 2019;141(3):595-607.

150. Wang Y, Gu Y, Zuo Z, Huang N. Choosing optimal wavelength for photodynamic therapy of port wine stains by mathematic simulation. J Biomed Opt. 2011;16(9):098001.

151. Benayoun L, Schaffer M, Bril R, Gingis-Velitski S, Segal E, Nevelsky A, et al. Porfimer-sodium (Photofrin-II) in combination with ionizing radiation inhibits tumor-initiating cell proliferation and improves glioblastoma treatment efficacy. Cancer Biol Ther. 2013;14(1):64-74.

152. van Hillegersberg R, Pickering JW, Aalders M, Beek JF. Optical properties of rat liver and tumor at 633 nm and 1064 nm: photofrin enhances scattering. Lasers Surg Med. 1993;13(1):31-9.

153. Muller PJ, Wilson BC. Photodynamic therapy of brain tumors--a work in progress. Lasers Surg Med. 2006;38(5):384-9.

154. Schipmann S, Müther M, Stögbauer L, Zimmer S, Brokinkel B, Holling M, et al. Combination of ALA-induced fluorescence-guided resection and intraoperative open photodynamic therapy for recurrent glioblastoma: case series on a promising dual strategy for local tumor control. Journal of neurosurgery. 2020:1-11.

155. Eljamel MS, Goodman C, Moseley H. ALA and Photofrin fluorescence-guided resection and repetitive PDT in glioblastoma multiforme: a single centre Phase III randomised controlled trial. Lasers in medical science. 2008;23(4):361-7.

156. Senders JT, Muskens IS, Schnoor R, Karhade AV, Cote DJ, Smith TR, et al. Agents for fluorescence-guided glioma surgery: a systematic review of preclinical and clinical results. Acta Neurochir (Wien). 2017;159(1):151-67.

157. Rulseh AM, Keller J, Klener J, Šroubek J, Dbalý V, Syrůček M, et al. Long-term survival of patients suffering from glioblastoma multiforme treated with tumor-treating fields. World J Surg Oncol. 2012;10(1):220.

158. Schwartz C, Rühm A, Tonn J-C, Kreth S, Kreth F-W. SURG-25INTERSTITIAL PHOTODYNAMIC THERAPY OF DE-NOVO GLIOBLASTOMA MULTIFORME WHO IV. Neuro Oncol. 2015;17(suppl_5):v219-v20.

159. Takahashi M, Arai T. Fluorescence sensing system by Soret-band LED light excitation for estimating relative talaporfin sodium concentration in skin. Photodiagnosis Photodyn Ther. 2014;11(4):586-94.

160. Muragaki Y, Akimoto J, Maruyama T, Iseki H, Ikuta S, Nitta M, et al. Phase II clinical study on intraoperative photodynamic therapy with talaporfin sodium and semiconductor laser in patients with malignant brain tumors. Journal of Neurosurgery JNS. 2013;119(4):845.

161. Sasnouski S, Zorin V, Khludeyev I, D'Hallewin M-A, Guillemin F, Bezdetnaya L. Investigation of Foscan® interactions with plasma proteins. Biochimica et Biophysica Acta (BBA) - General Subjects. 2005;1725(3):394-402.

162. Kostron H, Fiegele T, Akatuna E. Combination of FOSCAN® mediated fluorescence guided resection and photodynamic treatment as new therapeutic concept for malignant brain tumors. Medical Laser Application. 2006;21(4):285-90.

163. Vanaclocha V, Sureda M, Azinovic I, Rebollo J, Cañón R, Sapena NS, et al. Photodynamic therapy in the treatment of brain tumours. A feasibility study. Photodiagnosis Photodyn Ther. 2015;12(3):422-7.

164. Vasilev A SR, Tong L, Teschemacher AG, Kasparov S. In Search of a Breakthrough Therapy for Glioblastoma Multiforme. Neuroglia. 2018;1(2):292-310.

165. Reddy AS, Zhang S. Polypharmacology: drug discovery for the future. Expert Rev Clin Pharmacol. 2013;6(1):41-7.

166. Coogan PF, Strom BL, Rosenberg L. Antidepressant use and colorectal cancer risk. Pharmacoepidemiology and Drug Safety. 2009;18(11):1111-4.

167. Chan HL, Chiu WC, Chen VC, Huang KY, Wang TN, Lee Y, et al. SSRIs associated with decreased risk of hepatocellular carcinoma: A population-based case-control study. Psychooncology. 2018;27(1):187-92.

168. Walker AJ, Card T, Bates TE, Muir K. Tricyclic antidepressants and the incidence of certain cancers: a study using the GPRD. British journal of cancer. 2011;104(1):193-7.

169. Chen Y, Xu R. Drug repurposing for glioblastoma based on molecular subtypes. J Biomed Inform. 2016;64:131-8.

170. Vargas-Toscano A, Khan D, Nickel AC, Hewera M, Kamp MA, Fischer I, et al. Robot technology identifies a Parkinsonian therapeutics repurpose to target stem cells of glioblastoma. CNS Oncol. 2020;9(2):Cns58.

171. Barak Y, Achiron A, Mandel M, Mirecki I, Aizenberg D. Reduced cancer incidence among patients with schizophrenia. Cancer. 2005;104(12):2817-21.

172. Pottegård A, García Rodríguez LA, Rasmussen L, Damkier P, Friis S, Gaist D. Use of tricyclic antidepressants and risk of glioma: a nationwide case-control study. British journal of cancer. 2016;114(11):1265-8.

173. Fayez R, Gupta V. Imipramine. StatPearls. Treasure Island (FL): StatPearls Publishing

Copyright © 2020, StatPearls Publishing LLC.; 2020.

174. Wilson M, Tripp J. Clomipramine. StatPearls. Treasure Island (FL): StatPearls Publishing

Copyright © 2020, StatPearls Publishing LLC.; 2020.

175. Xia Z, Bergstrand A, DePierre JW, Nässberger L. The antidepressants imipramine, clomipramine, and citalopram induce apoptosis in human acute myeloid leukemia HL-60 cells via caspase-3 activation. J Biochem Mol Toxicol. 1999;13(6):338-47.

176. Shchors K, Massaras A, Hanahan D. Dual Targeting of the Autophagic Regulatory Circuitry in Gliomas with Repurposed Drugs Elicits Cell-Lethal Autophagy and Therapeutic Benefit. Cancer cell. 2015;28(4):456-71.

177. Sohel AJ, Shutter MC, Molla M. Fluoxetine. StatPearls. Treasure Island (FL): StatPearls Publishing

Copyright © 2020, StatPearls Publishing LLC.; 2020.

178. Liu K-H, Yang S-T, Lin Y-K, Lin J-W, Lee Y-H, Wang J-Y, et al. Fluoxetine, an antidepressant, suppresses glioblastoma by evoking AMPAR-mediated calcium-dependent apoptosis. Oncotarget. 2015;6(7):5088-101.

179. Ma J, Yang Y-R, Chen W, Chen M-H, Wang H, Wang X-D, et al. Fluoxetine synergizes with temozolomide to induce the CHOP-dependent endoplasmic reticulum stress-related apoptosis pathway in glioma cells. Oncol Rep. 2016;36(2):676-84.

180. Song T, Li H, Tian Z, Xu C, Liu J, Guo Y. Disruption of NF-κB signaling by fluoxetine attenuates MGMT expression in glioma cells. Onco Targets Ther. 2015;8:2199-208.

181. Hosseinimehr SJ, Najafi SH, Shafiee F, Hassanzadeh S, Farzipour S, Ghasemi A, et al. Fluoxetine as an antidepressant medicine improves the effects of ionizing radiation for the treatment of glioma. J Bioenerg Biomembr. 2020;52(3):165-74.

182. Bielecka AM, Obuchowicz E. Antidepressant drugs can modify cytotoxic action of temozolomide. Eur J Cancer Care (Engl). 2017;26(5).

183. Gan H, Zhang Q, Zhu B, Wu S, Chai D. Fluoxetine reverses brain radiation and temozolomide-induced anxiety and spatial learning and memory defect in mice. J Neurophysiol. 2019;121(1):298-305.

184. Dey D, Parihar VK, Szabo GG, Klein PM, Tran J, Moayyad J, et al. Neurological Impairments in Mice Subjected to Irradiation and Chemotherapy. Radiat Res. 2020;193(5):407-24.

185. Spanová A, Kovaru H, Lisá V, Lukásová E, Bohuslav R. Estimation of apoptosis in C6 glioma cells treated with antidepressants. Physiological research / Academia Scientiarum Bohemoslovaca. 1997;46:161-4.

186. Muraoka S, Kamei K, Muneoka K, Takigawa M. Chronic Imipramine Administration Amplifies the Serotonin2A Receptor-Induced Intracellular Ca2+ Mobilization in C6 Glioma Cells Through a Calmodulin-Dependent Pathway. Journal of Neurochemistry. 1998;71(4):1709-18.

187. Levkovitz Y, Gil-Ad I, Zeldich E, Dayag M, Weizman A. Differential induction of apoptosis by antidepressants in glioma and neuroblastoma cell lines: evidence for p-c-Jun, cytochrome c, and caspase-3 involvement. J Mol Neurosci. 2005;27(1):29-42.

188. Daley E, Wilkie D, Loesch A, Hargreaves IP, Kendall DA, Pilkington GJ, et al. Chlorimipramine: A novel anticancer agent with a mitochondrial target. Biochemical and biophysical research communications. 2005;328(2):623-32.

189. Peregrin K, Pilkington G. Apoptosis of human malignant glioma-derived cell cultures treated with clomipramine hydrochloride, as detected by Annexin-V assay. Radiology and Oncology. 2006;40.

190. Higgins SC, Pilkington GJ. The in vitro effects of tricyclic drugs and dexamethasone on cellular respiration of malignant glioma. Anticancer Res. 2010;30(2):391-7.

191. Jeon SH, Kim SH, Kim Y, Kim YS, Lim Y, Lee YH, et al. The tricyclic antidepressant imipramine induces autophagic cell death in U-87MG glioma cells. Biochemical and biophysical research communications. 2011;413(2):311-7.

192. Choi MR, Oh DH, Kim SH, Yang B-H, Lee J-S, Choi J, et al. Fluoxetine Up-Regulates Bcl-xL Expression in Rat C6 Glioma Cells. Psychiatry Investig. 2011;8(2):161-8.

193. Bielecka-Wajdman AM, Lesiak M, Ludyga T, Sieroń A, Obuchowicz E. Reversing glioma malignancy: a new look at the role of antidepressant drugs as adjuvant therapy for glioblastoma multiforme. Cancer Chemother Pharmacol. 2017;79(6):1249-56.

194. Bielecka-Wajdman AM, Ludyga T, Machnik G, Gołyszny M, Obuchowicz E. Tricyclic Antidepressants Modulate Stressed Mitochondria in Glioblastoma Multiforme Cells. Cancer Control. 2018;25(1):1073274818798594.

195. Hsu FT, Chiang IT, Wang WS. Induction of apoptosis through extrinsic/intrinsic pathways and suppression of ERK/NF-κB signalling participate in anti-glioblastoma of imipramine. J Cell Mol Med. 2020;24(7):3982-4000.

196. Varalda M, Antona A, Bettio V, Roy K, Vachamaram A, Yellenki V, et al. Psychotropic Drugs Show Anticancer Activity by Disrupting Mitochondrial and Lysosomal Function. Frontiers in oncology. 2020;10(2148).

197. Marathe SV, D'Almeida PL, Virmani G, Bathini P, Alberi L. Effects of Monoamines and Antidepressants on Astrocyte Physiology: Implications for Monoamine Hypothesis of Depression. J Exp Neurosci. 2018;12:1179069518789149-.

198. Yan K, Gao L-N, Cui Y-L, Zhang Y, Zhou X. The cyclic AMP signaling pathway: Exploring targets for successful drug discovery (Review). Mol Med Rep. 2016;13(5):3715-23.

199. Dorsam RT, Gutkind JS. G-protein-coupled receptors and cancer. Nature Reviews Cancer. 2007;7(2):79-94.

200. McManus MF, Chen LC, Vallejo I, Vallejo M. Astroglial differentiation of cortical precursor cells triggered by activation of the cAMP-dependent signaling pathway. The Journal of neuroscience : the official journal of the Society for Neuroscience. 1999;19(20):9004-15.

201. Zhou Z, Ikegaya Y, Koyama R. The Astrocytic cAMP Pathway in Health and Disease. Int J Mol Sci. 2019;20(3):779.

202. Dugan LL, Kim JS, Zhang Y, Bart RD, Sun Y, Holtzman DM, et al. Differential effects of cAMP in neurons and astrocytes. Role of B-raf. J Biol Chem. 1999;274(36):25842-8.

203. Schubert P, Ogata T, Marchini C, Ferroni S, Rudolphi K. Protective mechanisms of adenosine in neurons and glial cells. Annals of the New York Academy of Sciences. 1997;825:1-10.

204. Gagelin C, Pierre M, Torudelbauffe D. Inhibition of G1 Cyclin Expression and G1 Cyclin-Dependent Protein-Kinases by cAMP in an Astrocytic Cell Line. Biochem Biophys Res Commun. 1994;205(1):923-9.

205. Vardjan N, Kreft M, Zorec R. Dynamics of beta-adrenergic/cAMP signaling and morphological changes in cultured astrocytes. Glia. 2014;62(4):566-79.

206. Paco S, Hummel M, Plá V, Sumoy L, Aguado F. Cyclic AMP signaling restricts activation and promotes maturation and antioxidant defenses in astrocytes. BMC Genomics. 2016;17(1):304.

207. Zhang H, Kong Q, Wang J, Jiang Y, Hua H. Complex roles of cAMP-PKA-CREB signaling in cancer. Exp Hematol Oncol. 2020;9(1):32.

208. Furman MA, Shulman K. Cyclic AMP and adenyl cyclase in brain tumors. Journal of neurosurgery. 1977;46(4):477-83.

209. Sato S, Sugimura T, Yoda K, Fujimura S. Morphological differentiation of cultured mouse glioblastoma cells induced by dibutyryl cyclic adenosine monophosphate. Cancer research. 1975;35(9):2494-9.

210. Moreno MJ, Ball M, Andrade MF, McDermid A, Stanimirovic DB. Insulin-like growth factor binding protein-4 (IGFBP-4) is a novel anti-angiogenic and anti-tumorigenic mediator secreted by dibutyryl cyclic AMP (dB-cAMP)-differentiated glioblastoma cells. Glia. 2006;53(8):845-57.

211. Sengupta R, Sun T, Warrington NM, Rubin JB. Treating brain tumors with PDE4 inhibitors. Trends in pharmacological sciences. 2011;32(6):337-44.

212. Rowther FB, Wei W, Dawson TP, Ashton K, Singh A, Madiesse-Timchou MP, et al. Cyclic nucleotide phosphodiesterase-1C (PDE1C) drives cell proliferation, migration and invasion in glioblastoma multiforme cells in vitro. Molecular carcinogenesis. 2016;55(3):268-79.

213. Kang TW, Choi SW, Yang SR, Shin TH, Kim HS, Yu KR, et al. Growth arrest and forced differentiation of human primary glioblastoma multiforme by a novel small molecule. Scientific reports. 2014;4:5546.

214. Daniel PM, Filiz G, Mantamadiotis T. Sensitivity of GBM cells to cAMP agonist-mediated apoptosis correlates with CD44 expression and agonist resistance with MAPK signaling. Cell Death & Disease. 2016;7(12):e2494-e.

215. Xing F, Luan Y, Cai J, Wu S, Mai J, Gu J, et al. The Anti-Warburg Effect Elicited by the cAMP-PGC1α Pathway Drives Differentiation of Glioblastoma Cells into Astrocytes. Cell Rep. 2017;18(2):468-81.

216. Lv P, Wang W, Cao Z, Zhao D, Zhao G, Li D, et al. Fsk and IBMX inhibit proliferation and proapoptotic of glioma stem cells via activation of cAMP signaling pathway. J Cell Biochem. 2019;120(1):321-31.

217. Donati RJ, Rasenick MM. Chronic Antidepressant Treatment Prevents Accumulation of Gsα in Cholesterol-Rich, Cytoskeletal-Associated, Plasma Membrane Domains (Lipid Rafts). Neuropsychopharmacology. 2005;30(7):1238-45.

218. Erb SJ, Schappi JM, Rasenick MM. Antidepressants Accumulate in Lipid Rafts Independent of Monoamine Transporters to Modulate Redistribution of the G Protein, Galphas. The Journal of biological chemistry. 2016;291(38):19725-33.

219. Singh H, Wray N, Schappi JM, Rasenick MM. Disruption of lipid-raft localized Gα(s)/tubulin complexes by antidepressants: a unique feature of HDAC6 inhibitors, SSRI and tricyclic compounds. Neuropsychopharmacology. 2018;43(7):1481-91.

220. Grobben B, De Deyn P, Slegers H. Rat C6 glioma as experimental model system for the study of glioblastoma growth and invasion. Cell and Tissue Research. 2002;310(3):257-70.

221. Páv M, Kovárů H, Fiserová A, Havrdová E, Lisá V. Neurobiological aspects of depressive disorder and antidepressant treatment: role of glia. Physiol Res. 2008;57(2):151-64.

222. Nagy A, Eder K, Selak MA, Kalman B. Mitochondrial energy metabolism and apoptosis regulation in glioblastoma. Brain Res. 2015;1595:127-42.

223. Zorova LD, Popkov VA, Plotnikov EY, Silachev DN, Pevzner IB, Jankauskas SS, et al. Mitochondrial membrane potential. Analytical Biochemistry. 2018;552:50-9.

224. Pelicano H, Martin DS, Xu RH, Huang P. Glycolysis inhibition for anticancer treatment. Oncogene. 2006;25(34):4633-46.

225. Pilkington GJ, Parker K, Murray SA. Approaches to mitochondrially mediated cancer therapy. Seminars in Cancer Biology. 2008;18(3):226-35.

226. Charles E, Hammadi M, Kischel P, Delcroix V, Demaurex N, Castelbou C, et al. The antidepressant fluoxetine induces necrosis by energy depletion and mitochondrial calcium overload. Oncotarget. 2017;8(2):3181-96.

227. Griguer CE, Cantor AB, Fathallah-Shaykh HM, Gillespie GY, Gordon AS, Markert JM, et al. Prognostic relevance of cytochrome C oxidase in primary glioblastoma multiforme. PloS one. 2013;8(4):e61035.

228. Oliva CR, Markert T, Ross LJ, White EL, Rasmussen L, Zhang W, et al. Identification of Small Molecule Inhibitors of Human Cytochrome c Oxidase That Target Chemoresistant Glioma Cells. The Journal of biological chemistry. 2016;291(46):24188-99.

229. Oliva CR, Zhang W, Langford C, Suto MJ, Griguer CE. Repositioning chlorpromazine for treating chemoresistant glioma through the inhibition of cytochrome c oxidase bearing the COX4-1 regulatory subunit. Oncotarget. 2017;8(23):37568-83.

230. Felix L, Stephan J, Rose CR. Astrocytes of the early postnatal brain. European Journal of Neuroscience.n/a(n/a).

231. Marriott D, Hirst W, Ljungberg M. Neural cell culture: a practical approach. Oxford: Oxford University; 1995.

232. Turovsky E, Theparambil SM, Kasymov V, Deitmer JW, Del Arroyo AG, Ackland GL, et al. Mechanisms of CO2/H+ Sensitivity of Astrocytes. The Journal of neuroscience : the official journal of the Society for Neuroscience. 2016;36(42):10750-8.

233. Vaccari Cardoso B, Shevelkin AV, Terrillion C, Mychko O, Mosienko V, Kasparov S, et al. Reducing l-lactate release from hippocampal astrocytes by intracellular oxidation increases novelty induced activity in mice. Glia. 2021.

234. Chazotte B. Labeling nuclear DNA using DAPI. Cold Spring Harbor protocols. 2011;2011(1):pdb.prot5556.

235. Kralik P, Ricchi M. A Basic Guide to Real Time PCR in Microbial Diagnostics: Definitions, Parameters, and Everything. Front Microbiol. 2017;8:108-.

236. Stoddart MJ. Cell viability assays: introduction. Mammalian cell viability: methods and protocols. 2011:1-6.

237. Liang CC, Park AY, Guan JL. In vitro scratch assay: a convenient and inexpensive method for analysis of cell migration in vitro. Nature protocols. 2007;2(2):329-33.

238. Sekar RB, Periasamy A. Fluorescence resonance energy transfer (FRET) microscopy imaging of live cell protein localizations. J Cell Biol. 2003;160(5):629-33.

239. Klarenbeek J, Goedhart J, van Batenburg A, Groenewald D, Jalink K. Fourth-generation epac-based FRET sensors for cAMP feature exceptional brightness, photostability and dynamic range: characterization of dedicated sensors for FLIM, for ratiometry and with high affinity. PloS one. 2015;10(4):e0122513.

240. Ponsioen B, Zhao J, Riedl J, Zwartkruis F, van der Krogt G, Zaccolo M, et al. Detecting cAMP-induced Epac activation by fluorescence resonance energy transfer: Epac as a novel cAMP indicator. EMBO reports. 2004;5(12):1176-80.

241. Scaduto RC, Jr., Grotyohann LW. Measurement of mitochondrial membrane potential using fluorescent rhodamine derivatives. Biophysical journal. 1999;76(1 Pt 1):469-77.

242. Maldonado EN, Patnaik J, Mullins MR, Lemasters JJ. Free tubulin modulates mitochondrial membrane potential in cancer cells. Cancer research. 2010;70(24):10192-201.

243. Sakamuru S, Li X, Attene-Ramos MS, Huang R, Lu J, Shou L, et al. Application of a homogenous membrane potential assay to assess mitochondrial function. Physiol Genomics. 2012;44(9):495-503.

244. Marcondes NA, Terra SR, Lasta CS, Hlavac NRC, Dalmolin ML, Lacerda LdA, et al. Comparison of JC-1 and MitoTracker probes for mitochondrial viability assessment in stored canine platelet concentrates: A flow cytometry study. 2019;95(2):214-8.

245. Vouri M, An Q, Birt M, Pilkington GJ, Hafizi S. Small molecule inhibition of Axl receptor tyrosine kinase potently suppresses multiple malignant properties of glioma cells. Oncotarget. 2015;6(18):16183-97.

246. Baugh EH, Ke H, Levine AJ, Bonneau RA, Chan CS. Why are there hotspot mutations in the TP53 gene in human cancers? Cell Death Differ. 2018;25(1):154-60.

247. Wright JD, Lim C. Mechanism of DNA-binding loss upon single-point mutation in p53. J Biosci. 2007;32(5):827-39.

248. McKendrick L, Meek DW. A novel system to investigate the phosphorylation of the p53 tumor suppressor protein by the protein kinase CK2. Cell Mol Biol Res. 1994;40(5-6):555-61.

249. Parsons DW, Jones S, Zhang X, Lin JC, Leary RJ, Angenendt P, et al. An integrated genomic analysis of human glioblastoma multiforme. Science (New York, NY). 2008;321(5897):1807-12.

250. Bendahou MA, Arrouchi H, Lakhlili W, Allam L, Aanniz T, Cherradi N, et al. Computational Analysis of IDH1, IDH2, and TP53 Mutations in Low-Grade Gliomas Including Oligodendrogliomas and Astrocytomas. Cancer Inform. 2020;19:1176935120915839.

251. Bonin S, Donada M, Bussolati G, Nardon E, Annaratone L, Pichler M, et al. A synonymous EGFR polymorphism predicting responsiveness to anti-EGFR therapy in metastatic colorectal cancer patients. Tumour Biol. 2016;37(6):7295-303.

252. Ma F, Sun T, Shi Y, Yu D, Tan W, Yang M, et al. Polymorphisms of EGFR predict clinical outcome in advanced non-small-cell lung cancer patients treated with Gefitinib. Lung Cancer. 2009;66(1):114-9.

253. Koh YW, Kim HJ, Kwon HY, Han JH, Lee CK, Lee MS, et al. Q787Q EGFR Polymorphism as a Prognostic Factor for Lung Squamous Cell Carcinoma. Oncology. 2016;90(5):289-98.

254. Kaneko K, Kumekawa Y, Makino R, Nozawa H, Hirayama Y, Kogo M, et al. EGFR gene alterations as a prognostic biomarker in advanced esophageal squamous cell carcinoma. Front Biosci (Landmark Ed). 2010;15:65-72.

255. Poole EM, Curtin K, Hsu L, Kulmacz RJ, Duggan DJ, Makar KW, et al. Genetic variability in EGFR, Src and HER2 and risk of colorectal adenoma and cancer. Int J Mol Epidemiol Genet. 2011;2(4):300-15.

256. Mason RA, Morlock EV, Karagas MR, Kelsey KT, Marsit CJ, Schned AR, et al. EGFR pathway polymorphisms and bladder cancer susceptibility and prognosis. Carcinogenesis. 2009;30(7):1155-60.

257. Liu H, Zhang B, Sun Z. Spectrum of EGFR aberrations and potential clinical implications: insights from integrative pan-cancer analysis. Cancer Commun (Lond). 2020;40(1):43-59.

258. Siew-Kien Mah S-HT. Computational Analysis of PTEN Gene Mutation. International journal on advanced science, engineering, and information technology. 2012;2:4.

259. Ishigaki M, Iketani M, Sugaya M, Takahashi M, Tanaka M, Hattori S, et al. STED super-resolution imaging of mitochondria labeled with TMRM in living cells. Mitochondrion. 2016;28:79-87.

260. Zhang BB, Wang DG, Guo FF, Xuan C. Mitochondrial membrane potential and reactive oxygen species in cancer stem cells. Fam Cancer. 2015;14(1):19-23.

261. Ye X-Q, Li Q, Wang G-H, Sun F-F, Huang G-J, Bian X-W, et al. Mitochondrial and energy metabolism-related properties as novel indicators of lung cancer stem cells. International Journal of Cancer. 2011;129(4):820-31.

262. Bonnet S, Archer SL, Allalunis-Turner J, Haromy A, Beaulieu C, Thompson R, et al. A mitochondria-K+ channel axis is suppressed in cancer and its normalization promotes apoptosis and inhibits cancer growth. Cancer cell. 2007;11(1):37-51.

263. Shyh-Chang N, Daley George Q. Metabolic Switches Linked to Pluripotency and Embryonic Stem Cell Differentiation. Cell Metabolism. 2015;21(3):349-50.

264. Bélanger M, Allaman I, Magistretti Pierre J. Brain Energy Metabolism: Focus on Astrocyte-Neuron Metabolic Cooperation. Cell Metabolism. 2011;14(6):724-38.

265. Liu H, Li Y, Raisch KP. Clotrimazole induces a late G1 cell cycle arrest and sensitizes glioblastoma cells to radiation in vitro. Anticancer Drugs. 2010;21(9):841-9.

266. Sanzey M, Abdul Rahim SA, Oudin A, Dirkse A, Kaoma T, Vallar L, et al. Comprehensive analysis of glycolytic enzymes as therapeutic targets in the treatment of glioblastoma. PloS one. 2015;10(5):e0123544-e.

267. Safitri D, Harris M, Potter H, Yan Yeung H, Winfield I, Kopanitsa L, et al. Elevated intracellular cAMP concentration mediates growth suppression in glioma cells. Biochemical pharmacology. 2020;174:113823.

268. Grada A, Otero-Vinas M, Prieto-Castrillo F, Obagi Z, Falanga V. Research Techniques Made Simple: Analysis of Collective Cell Migration Using the Wound Healing Assay. Journal of Investigative Dermatology. 2017;137(2):e11-e6.

269. Goldhoff P, Warrington NM, Limbrick DD, Jr., Hope A, Woerner BM, Jackson E, et al. Targeted inhibition of cyclic AMP phosphodiesterase-4 promotes brain tumor regression. Clinical cancer research : an official journal of the American Association for Cancer Research. 2008;14(23):7717-25.

270. Morinobu S, Fujimaki K, Okuyama N, Takahashi M, Duman RS. Stimulation of adenylyl cyclase and induction of brain-derived neurotrophic factor and TrkB mRNA by NKH477, a novel and potent forskolin derivative. J Neurochem. 1999;72(5):2198-205.

271. Baskaran S, Mayrhofer M, Kultima HG, Bergström T, Elfineh L, Cavelier L, et al. Primary glioblastoma cells for precision medicine: a quantitative portrait of genomic (in)stability during the first 30 passages. Neuro Oncol. 2018;20(8):1080-91.

272. Murphy SF, Varghese RT, Lamouille S, Guo S, Pridham KJ, Kanabur P, et al. Connexin 43 Inhibition Sensitizes Chemoresistant Glioblastoma Cells to Temozolomide. Cancer research. 2016;76(1):139-49.

273. Perazzoli G, Prados J, Ortiz R, Caba O, Cabeza L, Berdasco M, et al. Temozolomide Resistance in Glioblastoma Cell Lines: Implication of MGMT, MMR, P-Glycoprotein and CD133 Expression. PloS one. 2015;10(10):e0140131.

274. Sciume G, Santoni A, Bernardini G. Chemokines and glioma: invasion and more. Journal of neuroimmunology. 2010;224(1-2):8-12.

275. Jura N, Endres NF, Engel K, Deindl S, Das R, Lamers MH, et al. Mechanism for Activation of the EGF Receptor Catalytic Domain by the Juxtamembrane Segment. Cell. 2009;137(7):1293-307.

276. Ferguson SD, Hodges TR, Majd NK, Alfaro-Munoz K, Al-Holou WN, Suki D, et al. A validated integrated clinical and molecular glioblastoma long-term survival-predictive nomogram. Neuro-oncology advances. 2020;3(1).

277. Crnković A, Srnko M, Anderluh G. Biological Nanopores: Engineering on Demand. Life (Basel). 2021;11(1):27.

278. Monteith A, Marszalec W, Chan P, Logan J, Yu W, Schwarz N, et al. Imaging of mitochondrial and non-mitochondrial responses in cultured rat hippocampal neurons exposed to micromolar concentrations of TMRM. PloS one. 2013;8(3):e58059.

279. Falchi A, Isola R, Diana A, Putzolu M, Diaz G. Characterization of depolarization and repolarization phases of mitochondrial membrane potential fluctuations induced by tetramethylrhodamine methyl ester photoactivation. The FEBS journal. 2005;272:1649-59.

280. Caverzán MD, Beaugé L, Chesta CA, Palacios RE, Ibarra LE. Photodynamic therapy of Glioblastoma cells using doped conjugated polymer nanoparticles: An in vitro comparative study based on redox status. Journal of Photochemistry and Photobiology B: Biology. 2020;212:112045.

281. Penso J, Beitner R. Clotrimazole decreases glycolysis and the viability of lung carcinoma and colon adenocarcinoma cells. Eur J Pharmacol. 2002;451(3):227-35.

282. Marcondes MC, Sola-Penna M, Zancan P. Clotrimazole potentiates the inhibitory effects of ATP on the key glycolytic enzyme 6-phosphofructo-1-kinase. Archives of Biochemistry and Biophysics. 2010;497(1):62-7.

283. Khalid MH, Tokunaga Y, Caputy AJ, Walters E. Inhibition of tumor growth and prolonged survival of rats with intracranial gliomas following administration of clotrimazole. Journal of neurosurgery. 2005;103(1):79.

284. Stepp H, Beck T, Pongratz T, Meinel T, Kreth F-W, Tonn JC, et al. ALA and Malignant Glioma: Fluorescence-Guided Resection and Photodynamic Treatment. 2007;26(2):157-64.

285. Stylli SS, Kaye AH, MacGregor L, Howes M, Rajendra P. Photodynamic therapy of high grade glioma – long term survival. Journal of Clinical Neuroscience. 2005;12(4):389-98.

286. Hiemke C, Baumann P, Bergemann N, Conca A, Dietmaier O, Egberts K, et al. AGNP Consensus Guidelines for Therapeutic Drug Monitoring in Psychiatry: Update 2011. Pharmacopsychiatry. 2011;44(6):195-235.

287. Duncan GE, Paul IA, Fassberg JB, Powell KR, Stumpf WE, Breese GR. Autoradiographic analysis of the in vivo distribution of 3H-imipramine and 3H-desipramine in brain: Comparison to in vitro binding patterns. Pharmacology Biochemistry and Behavior. 1991;38(3):621-31.

288. Kurata K, Kishitani K, Kido H, Kurachi M, Yamaguchi N. A pharmacokinetic study of clomipramine in regions of the brain. Jpn J Psychiatry Neurol. 1986;40(4):631-8.

289. FIŠAR1 Z, RK, KF, SIKORA2 aJ. Imipramine Distribution among Red Blood Cells, Plasma and Brain Tissue Gen Physiol Biophys. 1996;15: 51—64.

290. Henry ME, Schmidt ME, Hennen J, Villafuerte RA, Butman ML, Tran P, et al. A Comparison of Brain and Serum Pharmacokinetics of R-Fluoxetine and Racemic Fluoxetine: A 19-F MRS Study. Neuropsychopharmacology. 2005;30(8):1576-83.

291. Gillet J-P, Varma S, Gottesman MM. The clinical relevance of cancer cell lines. J Natl Cancer Inst. 2013;105(7):452-8.

292. Bady P, Diserens A-C, Castella V, Kalt S, Heinimann K, Hamou M-F, et al. DNA fingerprinting of glioma cell lines and considerations on similarity measurements. Neuro Oncol. 2012;14(6):701-11.

293. Allen M, Bjerke M, Edlund H, Nelander S, Westermark B. Origin of the U87MG glioma cell line: Good news and bad news. Science Translational Medicine. 2016;8(354):354re3.

294. Moraczewski J, Aedma KK. Tricyclic Antidepressants. StatPearls. Treasure Island (FL): StatPearls Publishing

295. Rudorfer MV, Potter WZ. Metabolism of tricyclic antidepressants. Cell Mol Neurobiol. 1999;19(3):373-409.

296. Ghersi-Egea J-F, Perrin R, Leininger-Muller B, Grassiot M-C, Jeandel C, Floquet J, et al. Subcellular localization of cytochrome P450, and activities of several enzymes responsible for drug metabolism in the human brain. Biochemical pharmacology. 1993;45(3):647-58.

297. Ferguson CS, Tyndale RF. Cytochrome P450 enzymes in the brain: emerging evidence of biological significance. Trends in pharmacological sciences. 2011;32(12):708-14.

298. Reis M, Aamo T, Spigset O, Ahlner J. Serum concentrations of antidepressant drugs in a naturalistic setting: compilation based on a large therapeutic drug monitoring database. Ther Drug Monit. 2009;31(1):42-56.

299. Mitchell PB. Therapeutic drug monitoring of psychotropic medications. Br J Clin Pharmacol. 2001;52 Suppl 1(Suppl 1):45s-54s.

300. Howe AK. Cross-talk between calcium and protein kinase A in the regulation of cell migration. Curr Opin Cell Biol. 2011;23(5):554-61.

301. Howe AK. Regulation of actin-based cell migration by cAMP/PKA. Biochim Biophys Acta. 2004;1692(2-3):159-74.

302. Kim MO, Ryu JM, Suh HN, Park SH, Oh Y-M, Lee SH, et al. cAMP Promotes Cell Migration Through Cell Junctional Complex Dynamics and Actin Cytoskeleton Remodeling: Implications in Skin Wound Healing. Stem Cells Dev. 2015;24(21):2513-24.

303. Forrest M. Why cancer cells have a more hyperpolarised mitochondrial membrane potential and emergent prospects for therapy2015.

304. Guntuku L, Naidu VGM, Yerra VG. Mitochondrial Dysfunction in Gliomas: Pharmacotherapeutic Potential of Natural Compounds. Curr Neuropharmacol. 2016;14(6):567-83.